Technical Paper Contest for Women 1992

Space Challenges Earth and Beyond

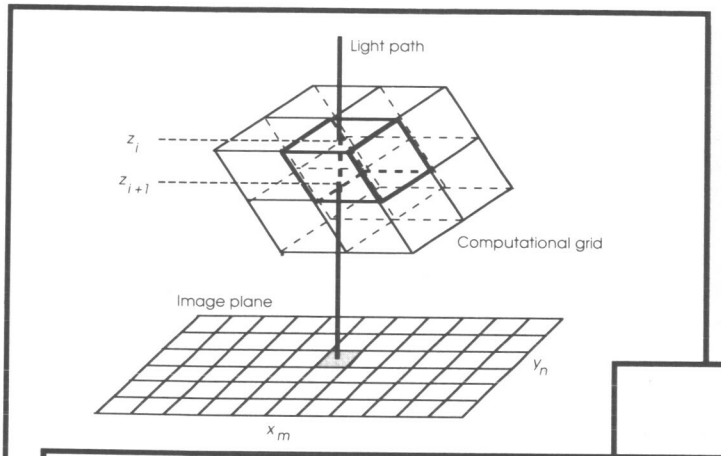

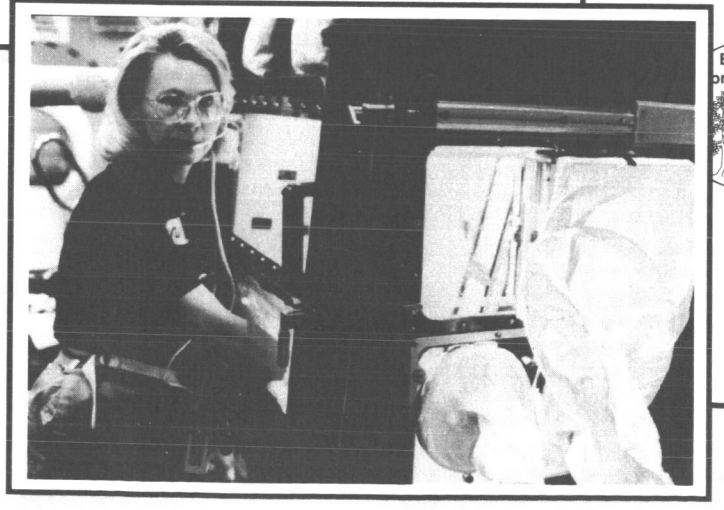

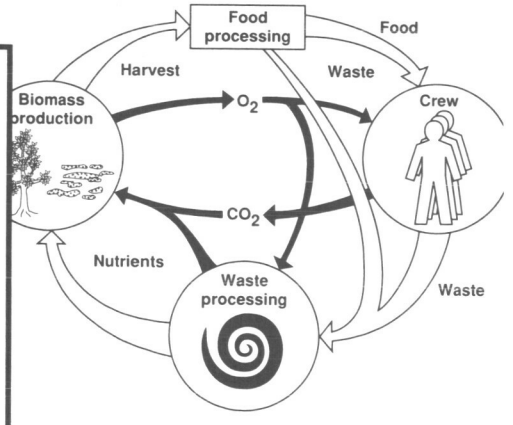

National Aeronautics and Space Administration

Ames Research Center

Technical Paper Contest for Women 1992

Space Challenges Earth and Beyond

Sponsored by
Advisory Committee for Women
Equal Opportunity Council
Ames Research Center

Edited by
Robin Orans
Ames Research Center,
Moffett Field, California

Papers submitted to the first
Technical Paper Contest for Women

National Aeronautics and
Space Administration

Ames Research Center
Moffett Field, California 94035-1000

1993

TABLE OF CONTENTS

LIST OF PARTICIPANTS

Kong Cha Authement
Microsoft, Inc.
Ames Research Center
Moffett Field, California

Carol B. Davies
Ames Research Center
Moffett Field, California

Ewald Denner
Institute of Microbiology and Genetics
University of Vienna
Vienna, Austria

Betsy Dunsky
Ames Research Center
Moffett Field, California

M. A. Farrance
G. E. Government Services
Ames Research Center
Moffett Field, California

Cory Finn
Ames Research Center
Moffett Field, California

Amara L. Graps
Ames Research Center
Moffett Field, California

John W. Hines
Ames Research Center
Moffett Field, California

Soheila Jahromi, Contractor
Bentley Engineering
Ames Research Center
Moffett Field, California

J. W. Jenner
Ames Research Center
Moffett Field, California

Catherine C. Johnson
Ames Research Center
Moffett Field, California

A. Christopher Maese
Ames Research Center
Moffett Field, California

Ann McCormack
Ames Research Center
Moffett Field, California

Cathy Bonifas Parks
Sterling Software, Inc.
Ames Research Center
Moffett Field, California

Annette T. Rodrigues
Ames Research Center
Moffett Field, California

Julie E. Schonfeld
Ames Research Center
Moffett Field, California

Helga Stan-Lotter
Institute of Microbiology and Genetics
University of Vienna
Vienna, Austria
Ames Research Center
Moffett Field, California

Susan Tokarcik
Eloret Institute
Palo Alto, California

Huy Kim Tran
Ames Research Center
Moffett Field, California

Ethiraj Venkatapathy
Eloret Institute
Palo Alto, California

Kimberly Wagenbach
Ames Research Center
Moffett Field, California

Rebecca C. Williamson
Ames Research Center
Moffett Field, California

Leslie A. Yates
Eloret Institute
Palo Alto, California

INTRODUCTION

STRATEGY

Two of the major concerns of the NASA Ames Research Center (NASA ARC) Advisory Committee for Women (ACW) are that recruitment of women scientists, engineers, and technicians needs to increase, and that barriers to advancement need to be removed for improved representation of women in middle and upper management and scientific positions. One strategy that addressed this concern was the ACW sponsorship of a Technical Paper Contest for Women at Ames Research Center. Other sponsors of the Contest were the Ames Equal Opportunity Council and the Ames Contractor Council.

BENEFITS

The Technical Paper Contest for Women greatly increased the visibility of both the civil service women and the women who work for contractors at Ames. The women had the opportunity to hone their written and oral presentation skills. Networking among Ames women increased and a Total Quality Management Spotlight Award was made to Robin Orans from the Center Director, Dale Compton, for her pivotal efforts in organizing the contest.

VISIBILITY

The Technical Paper Contest increased the visibility of NASA ARC women both locally and nationally. The women received recognition in the Center-wide newsletter, the *Astrogram*, and during introductory remarks at the oral presentations of the top eight papers held in February 1992. These introductory remarks included speeches from the NASA ARC Director, Dr. Dale Compton, the Equal Opportunity Council Chairman, Dr. Masayuki Omura, ACW Chair, Deanne Tucker, and a representative from the Ames Contractor's Council, Carolina Blake. National recognition was received when the top eight papers were presented at the 1992 SWE National Convention and Student Conference at a special technical session. Support from Ames also extended to four other Technical Paper Contest participants and their papers were also presented at the Convention. Contest participants attended many of the Convention activities and interacted with both students and regular members. As of the writing of this article we have at least two new SWE members for the Santa Clara Valley Section from among the Ames women who attended the Convention.

OBTAIN MANAGEMENT SUPPORT

Upon approval of the Technical Paper Contest idea by the ACW, the first priority of the Technical Paper Contest Committee was to gain the support of the NASA ARC management. The Committee was formed in July of 1991 and chaired by Robin Orans, P.E., the Wind Tunnel Test Support Coordinator for the Aerodynamics Facilities Branch at NASA ARC. By mid-August presentations of the Technical Paper Contest proposal were made to the Equal Opportunity Council,

comprised of all Deputy Directors of the technical and administrative groups at ARC, and to the Contractor's Council consisting of representatives from all major contractors at ARC.

The presentations included a timeline of activities, a request for funding, a list of the women who had agreed to serve on the Technical Paper Contest Committee, and the men and women who had agreed to serve as judges. Five judges were selected from ARC management, one from the Contractor's Council and two from the Society of Women Engineers. The SWE judges were Kathleen Harrer, Past National President, currently working at Kennedy Space Center, Florida and Esther Williams, SWE Fellow, who works at Lockheed Missile and Space Company in Sunnyvale, California. In addition, arrangements were made with the 1992 SWE Convention Program Chair, Betty Preece, for a three-hour slot at Convention to present the winning papers.

Support of the Technical Paper Contest was obtained. Support included a travel budget for up to five civil service women to attend the 1992 SWE National Convention in Orlando, Florida, for one of the SWE judges to travel to the oral presentations at Ames from Kennedy Space Center, and for reproduction costs of a NASA ARC Technical Memorandum. The Contractor's Council also agreed to encourage its members to support attendance of up to five winners from their organizations at the 1992 SWE National Convention.

TIMELINE

A call for abstracts went out to the women at Ames in August 1991. The same topics as the 1992 SWE National Convention Call for Papers were used. Approximately 600 information packages were sent out to both civil service women and women who work for contractors at Ames. Twenty-five abstracts were received by the Ames Technical Paper Contest Committee at the end of September. Copies of these abstracts were sent to the 1992 SWE Convention Program Chair. Written papers were due in Mid-December to the Technical Paper Contest Committee. Of the twenty-five women who submitted abstracts, sixteen submitted papers for judging. Judging occurred during the later part of December and into early January. In mid-January, the Technical Paper Contest Committee compiled the results and held a judges meeting. Two of the judges joined the meeting via telephone link-up. Eight of the sixteen authors were asked to make oral presentations in February of 1992. All eight oral presenters were judged to have papers meriting ARC sponsorship to the 1992 SWE National Convention and Student Conference. Five of the presenters were civil service women, two were from the Eloret Institute, and one was from Sterling Software. The top three winners were announced at the beginning of the NASA Ames Technical Paper Session at the 1992 SWE National Convention and Student Conference . They were:

Carol B. Davies (Sterling Software) for her paper on "The Development and Application of the Self-Adaptive gridE (SAGE),"

Huy Kim Tran (NASA ARC) for her paper on "Test Model Designs for Advanced Refractory Materials," and

Leslie Yates (Eloret Institute) for her paper titled "Interferograms, Schlieren, and Shadowgraphs Conducted from Real- and Ideal-Gas, Two- and Three-Dimensional Computed Flowfields."

WHAT'S NEXT

The Advisory Committee for Women at NASA Ames Research Center will sponsor a Technical Paper Contest for fiscal year 1993. Ideas for improvement which have come from the continuing networking among the Technical Contest Participants, Technical Paper Committee Members and Judges, and members of the ACW will be incorporated. The women who participated in this year's Technical Paper Contest have been asked to do a series of lunchtime seminars open to all Ames personnel. Some of the women have volunteered to participate in the SWE Santa Clara Valley Section's Speakers Bureau or work on other committees. A number of other NASA Centers across the country will be conducting their own Technical Paper Contests. Winners from these contests will participate in a special NASA technical paper session at the 1993 SWE National Convention and Student Conference in Chicago.

MORE INFORMATION

If you need more information about conducting and managing a technical paper contest please contact me at NASA Ames Research Center, Mail Stop 227-5, Moffett Field, CA 94043. Phone: 415-604-5875. FAX: 415-604-4357. Internet: robin_orans@qmgate.arc.nasa.gov. Contact either of the 1993 Convention Program Chairs, Judy McGoogan or Daryl Farley, about having the winners of your organization's Technical Paper Contest make presentations at the next Convention.

To order copies of this report, contact Teresa Alvarez at (415) 604-6510, MS 241-7, Ames Research Center, Moffett Field, California 94035-1000.

EDUCATION: A SECOND CAREER

Kong Cha Authement
Microcraft, Inc.
Ames Research Center
Moffett Field, California

SUMMARY

Education provides women with the freedom to choose their destiny and forge a life for themselves if desired or necessary. Many women are denied the opportunity of education while growing up and must attempt to achieve such schooling later in life. For most women the decision to pursue this education can represent a very traumatic moment in their lives. Having faced the dilemma and decided to proceed results in a very satisfying feeling when success has been achieved.

Throughout human history, the male has been recognized as the provider and the female has been relegated to the task of caring for the home and the family. Women have been conditioned, over the years, to place responsibility for the economic well being of the household in the hands of the man. Recent history has shown a trend away from male domination in the economic foray as more women prepare themselves for meaningful careers by attending colleges or obtaining vocational training, but there are still many women who are deprived of the opportunity for such career preparation. This lack of opportunity, while institutionalized by societies in the past for all but the elite, need not arise from open denial or exclusion of women. It can result, rather, from a failure of family, teachers and friends to encourage the pursuit of further education by young women. Peer pressure to participate in the social activities which are so much a part of today's secondary school system can also lead to premature termination of further education. Many of these women who have been denied access to career preparation often find themselves suddenly faced with the predicament of becoming single heads of households. As such, they are ill prepared to seek employment which will provide an income which is adequate to provide a comfortable life for themselves and their families.

It is not as bleak as it may seem. There are many positions available in industry which are open to any qualified candidate. These positions can be capably filled by either a woman or a man but generally, the more educationally prepared candidate will be chosen. This leads to exclusion from consideration of women lacking adequate education or career training. Without a college education or other career training, it is extremely difficult to find employment which provides an income which is adequate to support a family. It is even more difficult for a woman to find such employment and this burden is further complicated if there are young children involved. In order to qualify for meaningful careers, such women must obtain the necessary education or skill training and the reality of returning to school in mid-life is difficult to face. These women must continue to struggle to provide the economic support for the family while finding the time to attend classes and study. However, for those women willing to endure these tribulations to continue her education, there is a reward.

It is not impossible to obtain the education and career training necessary to qualify for these positions if the woman is willing and able to attend school. By returning to school, or continuing her

education or career training by attending college, a woman not only learns the skills necessary to qualify for more rewarding positions but also gains self confidence and self esteem. After completing her education, the woman is better prepared to enter the job market and pursue a meaningful career.

Many women faced with the sudden need to support themselves and their families after having been reliant on someone else for a number of years choose not to consider returning to the school environment because of age considerations. The predominant feeling is that it is too late in life to think of beginning a new career or to establish new goals. A hasty review of the educational and training opportunities available to women will rapidly dispel this misconception. In fact, many of the programs being offered by colleges, universities and vocational schools are specifically directed toward the older woman. These programs are available to all interested women irrespective of age. In addition, many four year universities offer fully funded scholarships for degree candidates who wish to apply.

An alarming number of the programs offered are underutilized and scholarships remain unclaimed because of lack of awareness among those women who could benefit the most. In addition, not all programs are offered in the geographical area in which the most good could be provided. This would suggest a need within the educational system for a network through which information about the various programs being offered can be disseminated. Expansion of this concept might include the offering of such programs by correspondence or alternatively, using current technology, video transmission of sessions. Such a program should embrace not only local areas but should extend state-wide and even nationwide.

In support of women who wish to establish a new career for themselves, irrespective of motivation, encouragement should be provided even for the consideration of nontraditional fields of endeavor typically dominated by men. Many women have the ability to perform and also excel in such nontraditional fields but have been historically discouraged from attempting such careers and thus have never realized their full potential. Experience has shown that women who expend the effort and strive for excellence in such nontraditional career fields receive the full support and encouragement of her coworkers. Women who honestly attempt to achieve in such an environment will find that coworkers willingly remove all obstacles in her path toward task accomplishment.

For many years after moving to the United States from Korea with my husband, I remained in the home caring for the household and rearing my children, instilling moral values, providing a role model and attempting to develop in them self confidence and character. With the death of my husband in 1981, 1 found myself facing the dilemma described above. I had no skills other than those learned as a youth and young adult in Korea, skills totally unmarketable at the time and place. Employment opportunities which were pursued included daycare attendant, restaurant work, bartending and janitorial service. None of these jobs offered financial security or held any promise for future advancement. After a great amount of thought and soul searching, a decision was arrived at that led me to return to school to open new career opportunities for my life.

A friend encouraged me to enroll in a Machine Technology Program offered at San Jose City College. Being one of those career fields traditionally dominated by men, the move was taken with more than a small amount of trepidation. Having completed a short basic course in Machine Tool

Technology, I realized that I had identified a challenging and rewarding new career field. Armed with a Certificate of Program Completion from San Jose City College, I set my goal on becoming a Machine Tool Technologist and, possibly, even a Computer Numerical Control Programmer. At this time, I learned of the De Anza/Foothill College-NASA Ames Coop Internship Program and enrolled as a participant.

Having enrolled in the program, I found that I was receiving a tremendous amount of support and encouragement from the program coordinator, practicing apprentices and journeyman machinists. These people, through their encouragement, made me feel comfortable with my objectives and instilled self confidence in my ability to achieve my goals. I was continually assured that my objectives were not unreasonable and were well within my capability. I have now completed the Internship Program and am currently striving to qualify for a State Journeyman Machinist's Certificate.

The De Anza/Foothill College-NASA Ames Co-op Internship Program represents a large portion of the formal education that I have received in my lifetime. My eventual goal is to obtain an Associate Degree from De Anza College that will qualify me to pursue a career in the field of Machine Tool Technology. Having returned to school after seeing all of my children graduate first has demonstrated to me that the time is never too late to establish new personal goals for oneself.

I am extremely grateful that the American educational system has provided me this opportunity to learn new skills and expand my knowledge. I earnestly hope that the various educational programs available will be of benefit to others in the future in the same manner in which this one has provided me with an opportunity to embark on a new and rewarding career.

BIOGRAPHY

Kong Cha Authement:

I was born in Inchon City, Korea, in 1941. With the outbreak of the Korean conflict in the 1950s, my family was forced to evacuate our homestead and flee in many directions. With the arrival of the United States military, I was able to find secure employment as an attendant at the various facilities established by the government to supply the service men and women with goods and services. In this environment, I was able to learn the rudiments of the food preparation and serving business as well a bar and club operation management. I was married to a noncommissioned officer doing a tour of duty in Korea and subsequently returned with him to the United States at the conclusion of his assignment.

I was a contented homemaker until 1981 when my husband passed away. Faced with the grim reality of financially caring for my family of growing children after so many years with limited skills, I sought employment in fields similar to those in which I had previously worked. I found employment alternately as a child daycare attendant, restaurant waitress and manager, and bartender but found no reward in such work. I then sought formal training in the field of Machine Tool Technology and am now employed as an Apprentice Machinist while pursuing an Associate of Arts degree at De Anza College.

THE DEVELOPMENT AND APPLICATION OF THE SELF-ADAPTIVE GRID CODE, SAGE

Carol B. Davies
Ames Research Center
Moffett Field, California

INTRODUCTION

Solution-adaptive grid methods have become an important tool in the field of Computational Fluid Dynamics for accurately computing flow solutions. The adaption procedures are applied to the grid after an initial flow solution has been computed, using the solution to produce a more rational distribution of grid points. There are two basic adaption methods: redistribution and refinement. In redistribution schemes, points are intelligently moved to more appropriate locations; in refinement schemes, points are added to the existing grid. In either case, solution errors are reduced by minimizing grid discretization errors.

The approach used in the development of the Self-Adaptive Grid codE, SAGE, is based on a grid point redistribution scheme. Gnoffo (ref. 1) first introduced a one-dimensional method (1-D) method for the redistribution of grid points based on local flow gradients. This method is analogous to finding the equilibrium position of a system of springs that connect adjacent nodes with spring (or tension) forces that are proportional to the local error or weight function. This spring analogy, with the proper choice of weight function, results in a simple system of algebraic equations. Nakahashi and Deiwert (ref. 2) formulated an appropriate weight function that not only was proportional to local flow gradients but also provided grid control through user-specified minimum and maximum grid spacing, thus introducing the "self-adaptive" nature to the process. This method was extended to two and three dimensions (ref. 3) by approximating the resulting system of equations as a series of 1-D problems. However, the associated adapted grid was not smooth between the adapted lines and Nakahashi and Deiwert therefore introduced grid-smoothing functions which are analogous to torsion springs. This procedure was found to be efficient and fast and it allowed the user to control the quality of the grid while performing the solution adaption.

The user-friendly SAGE has been developed using this method (ref. 4) and applied to a wide variety of 2- and 3-dimensional flow problems (refs. 5 and 6). The present paper describes the development of the basic adaptive procedure as utilized by the code and the application of the code to a variety of flow problems. Results are shown that clearly demonstrate the ability of the adaptive grid scheme to enhance the solutions of both 2- and 3-D flows.

FORMULATION OF THE ADAPTIVE GRID SCHEME

The adaption procedure is analogous to applying tension and torsion spring forces proportional to the local flow gradient at every grid point and finding the equilibrium position of the resulting system. The multidimensional problem of grid adaption is split into a series of 1-D problems along

the computational coordinate lines. The reduced 1-D problem is solved as a tridiagonal system to find the location of grid points along a given coordinate line. Multidirectional adaption is achieved by the sequential application of the 1-D method in each coordinate direction.

The tension forces direct the redistribution of points to the strong gradient regions. The torsion forces relate information between the family of lines adjacent to one another, in order to maintain smoothness and a measure of orthogonality of grid lines. These smoothness and orthogonality constraints are direction dependent, since they relate only the coordinate lines that are being adapted to the neighboring lines that have already been adapted. This implies that the solutions are nonunique and depend on the order and direction of adaption.

The adaption procedure is illustrated in figure 1: three constant k planes of an initial grid are shown in figure 1(a) for which a flow-field solution has been obtained. The points in this grid are now adapted to the computed flow solution, starting on the first line $j = 1$ on the lower plane $k = 1$. In figure 1(b), the first plane has already been adapted and the second plane is the current adaption plane. The current adaption line j is shown, with previous lines already adapted and subsequent lines awaiting adaption. The third plane is still in its original form. Adaption is performed in this line-by-line within a plane-by-plane manner until all requested planes are complete. It is then possible to perform an adaption in a second direction, adapting "on top" of the already adapted grid. The number and order of adaptions are arbitrary and depend on the type of flow problem and the purpose of the adaption. However, for clarity, the analysis in this report assumes that all adaptions are performed in the order shown in figure 1.

Figure 2 shows a segment of the current adaption line in more detail. The lower plane has already been adapted and the upper plane is currently being adapted. Four forces control the redistribution of

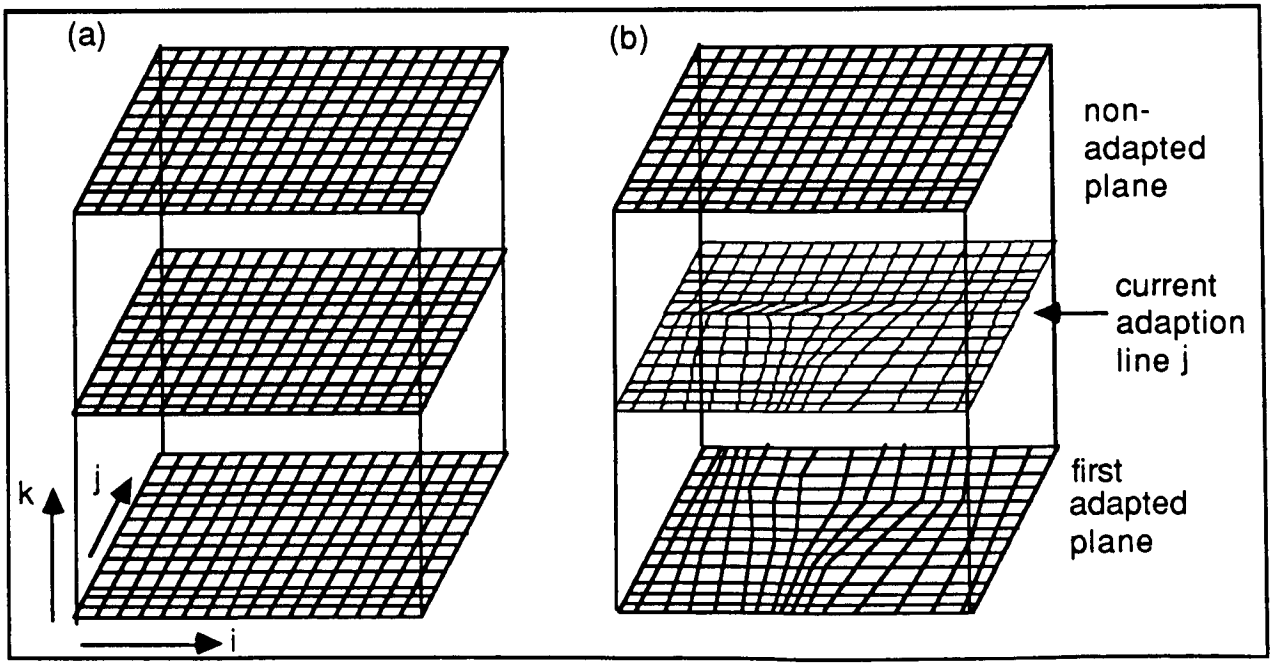

Figure 1. 3-D adaption. (a) Initial grid, (b) first directional adaption.

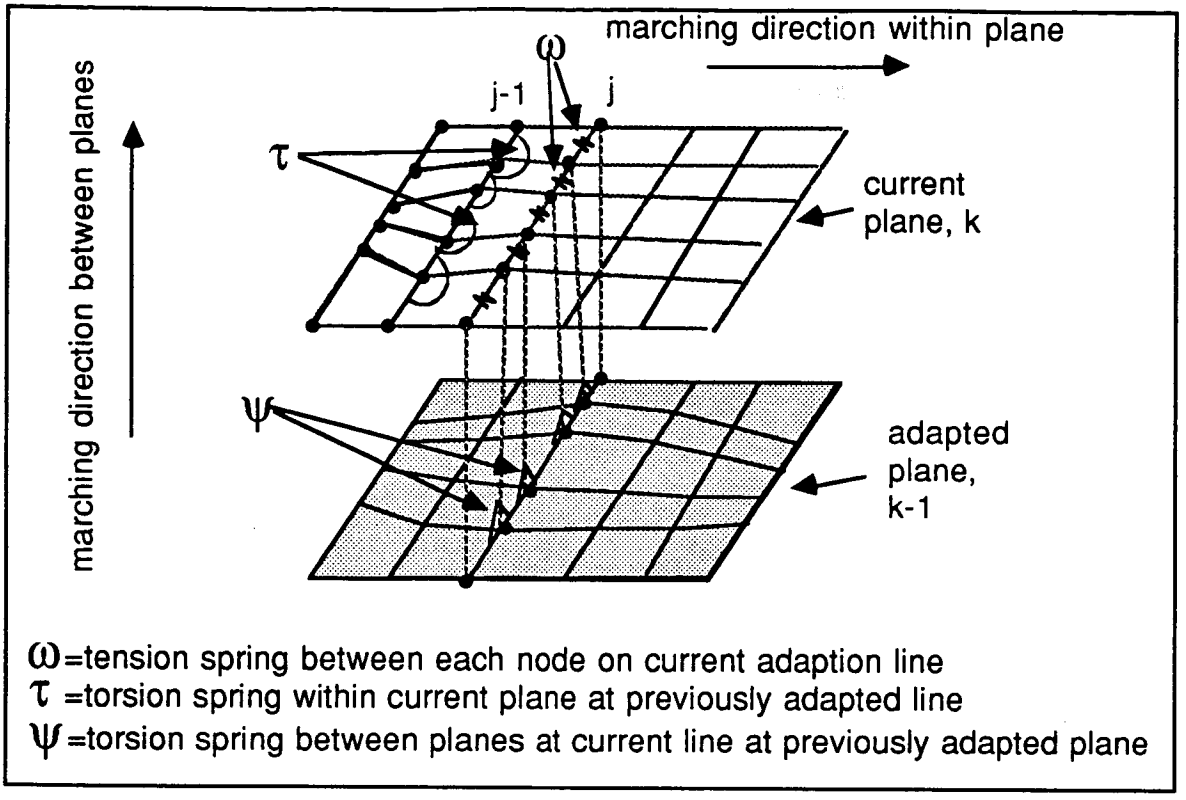

Figure 2. Line-by-line adaption, showing tension and torsion forces.

a point along a line: the two tension springs that act on each side of a node, and the two torsion springs that control the smoothness of the grid. The tension forces, ω, have the effect of clustering the redistributed points into the high gradient regions.The torsion forces (τ and ψ) maintain continuity between sequentially adapted lines. As shown in figure 2, the τ force acts from the previously adapted line within the current plane and the ψ force acts from the previously adapted line in the preceding plane.

The following analysis describes the development of the multi-dimensional adaption from the simple 1-D algorithm, to the added complexities of two and three dimensions. Although the description is segmented for clarity, SAGE is multi-dimensional and can adapt 1-, 2- and 3-D grids.

ONE-DIMENSIONAL ANALYSIS

The first step in the formulation of the adaption algorithm is to consider the adaption of a single line where torsional constraints do not exist. This 1-D analysis and example are given to illustrate the approach; in practice this method is used only along the initial line of a 2- or 3-D problem.

Figure 3 shows a line, where the arc length at P, (i.e. s_i), along the current adaption line, *j*, is defined as

$$s_{i+1} = s_i + \Delta s_i \qquad (1)$$

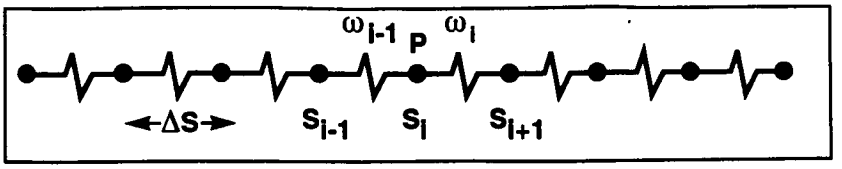

Figure 3. 1-D adaption line, showing initial spacing and tension springs.

A tension force, ω, is defined to act between each node such that

$$\omega_i \Delta s_{i+1} = \text{constant} \tag{2}$$

where ω_i is a function based on the normalized flow gradient $\overline{f}$, and

$$\omega_i = 1.0 + A\,\overline{f}^{\,B} \tag{3}$$

The constants A and B are directly related to the grid spacing and maintain the grid intervals to within the requested minimum and maximum limits (Δs_{MIN} and Δs_{MAX}). Put simply, equation (2) states that the larger the flow gradient, the denser the mesh spacing. This equation is written for each node on the line, giving a 1-D formulation that can be solved directly for Δs_i. Taking the sum of both sides of equation (2) gives

$$\sum \Delta s_i = s_{max} = K \sum 1/\omega_i \text{ giving } K = s_{max}/\sum 1/\omega_i \tag{4}$$

Substituting back in equation (2), we obtain

$$\Delta s_i = s_{max} / \left(\omega_i \sum 1/\omega_i\right) \tag{5}$$

and from equation (1), we can obtain the value of each s_i using an iterative procedure.

One-Dimensional Application

Example 1. 1-D sine wave– Figure 4 shows a simple example of this 1-D process. The flow function is given as a sine wave with 51 points on the initial line that are equally spaced and displayed by the filled symbols. The user-requested spacing-control parameters, Δs_{MAX} and Δs_{MIN}, are given to be 0.1 and 0.002 respectively (i.e., a ratio of 50/1). The 1-D adaption algorithm intelligently redistributes the points so that clustering occurs in the high gradient regions. These redistributed points are presented as the open symbols on the constant line in the figure.

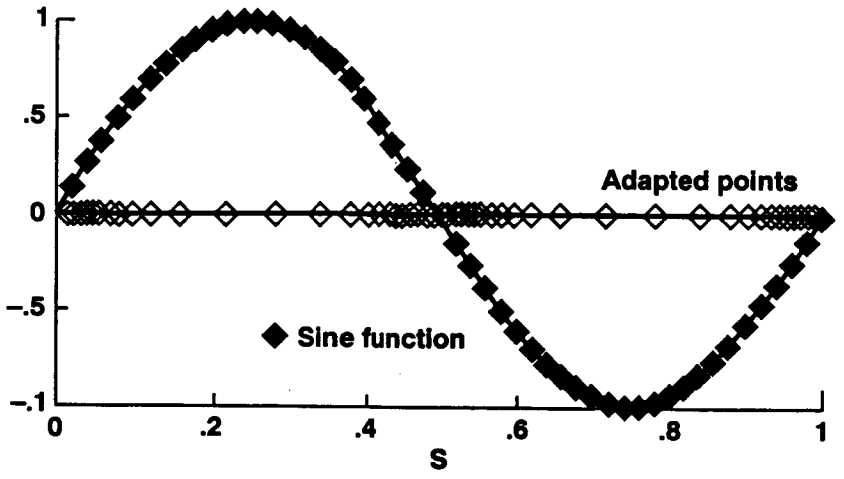

Figure 4. Adaption of a 1-D sine wave.

TWO-DIMENSIONAL ANALYSIS

The continuation of the 1-D approach for successive line-by-line adaptions does not create a mesh that is sufficiently smooth for input into computational flow-field codes. To ensure a more reasonable grid, the redistribution of points (driven by tension springs) is constrained by torsion springs. Within a 2-D plane, a torsion parameter τ is defined that represents the magnitude of the torsion force that maintains smoothness and orthogonality between the node *(i,j,k)* and the nodes *(i,j – 1,k)* and *(i,j – 2,k)*. This torsion force is evaluated as $\tau_i(s'_i - s_i)$ where τ defines the magnitude and s' the direction (i.e., orthogonality and smoothness) of the torsion force. To introduce the torsion forces to the system of equations, equation (2) can be rewritten to represent the force balance, i.e.,

$$\omega_i(s_{i+1} - s_i) - \omega_{i-1}(s_i - s_{i-1}) = 0 \tag{6}$$

Adding the torsion term gives

$$\omega_i(s_{i+1} - s_i) - \omega_{i-1}(s_i - s_{i-1}) + \tau_i(s'_i - s_i) = 0 \tag{7}$$

which can then be rearranged to give

$$\omega_{i-1}\, s_{i-1} - (\omega_i + \omega_{i-1} + \tau_i)\, s_i + \omega_i s_{i+1} = -\tau s'_i \tag{8}$$

This equation is written for each interval along the adaption line, producing a system of n – 1 equations that can be expressed as a tridiagonal matrix.

Two-Dimensional Applications

To maintain the integrity of the adapted grid, the user has the choice of several grid quality control variables. These include: the extent of the adaption domain; the maximum and minimum

mesh spacings; the proportion of straightness to orthogonality of the grid lines and the magnitude of the torsional effect. In addition, boundary spacing and grid matching controls are available to accommodate patched, zonal and multiple grids. Finally, there is the choice of stepping direction. As described earlier, the adaption process is a line-by-line stepping process and for 2-D applications, there will be four choices of adaption direction: stepping in the *i* direction, the *j* direction, or both (in either order). Each of these options will produce a different adapted grid, however there is no way to quantify which of these will produce the "best" adapted grid. It has been shown (ref. 6) that limiting the adaption to only one direction can produce adequately adapted grids. However, for problems with distinct two-directional flow features, experimenting with the order of adaption may be necessary.

The following two examples of 2-D adaption demonstrate both these cases: the supersonic inlet problem, despite the cross-flow nature of the features, is adequately adapted in one direction only. The more complex case of an axisymmetric nozzle plume flow requires a limited adaption in the second direction.

Example 2: Supersonic inlet– The first 2-D illustration of the adaption procedure is a supersonic channel flow with shock reflection and expansion features. Supersonic viscous flow through a variable-width channel was simulated by Abrahamson (ref. 7) using the thin-layer Navier-Stokes equations. The initial grid is shown in Figure 5(a) and the resulting density contours in Figure 5(b). Initial clustering has been imposed in the streamwise direction at the corners of the upper wall and in the transverse direction near the channel walls. Flow is from left to right, creating a shock from the upstream upper wall corner that reflects off the lower wall. An expansion fan emanates from the downstream upper wall corner and interacts with the reflected shock downstream.

The initial grid is adapted to the density flow gradients, stepping in one direction only, producing the adapted distribution shown in figure 6(a). The adaption procedure has moved the grid points so that the dense mesh spacing now closely follows the high gradient regions across the shocks. This adapted grid, along with the interpolated flow variables, were re-input to the flow solver, producing a new flow-field solution shown in figure 6(b). The improvement in the resolution of the incident and reflected shocks is considerable when compared to the initial solution.

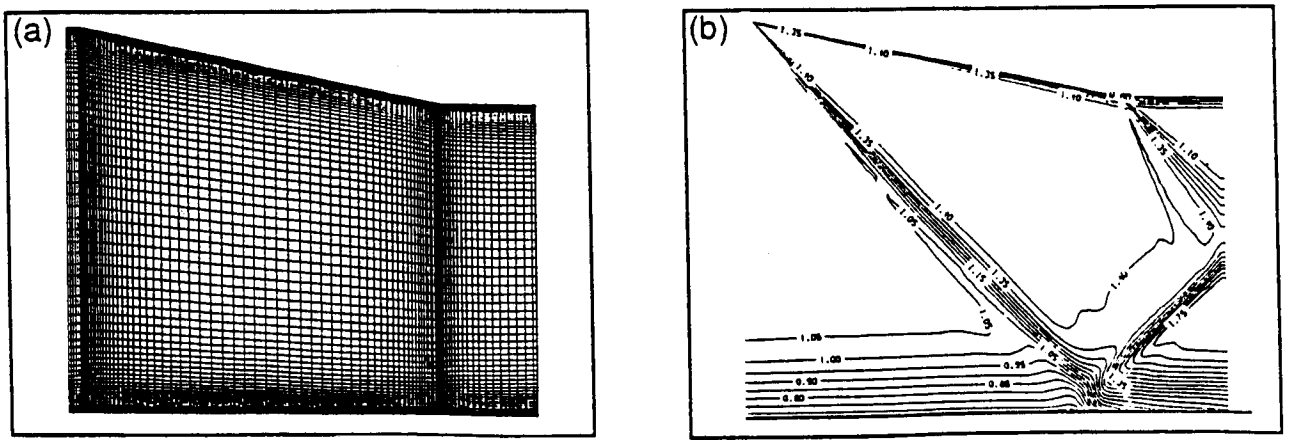

Figure 5. 2-D flow through a supersonic inlet. (a) Initial grid, (b) density contours.

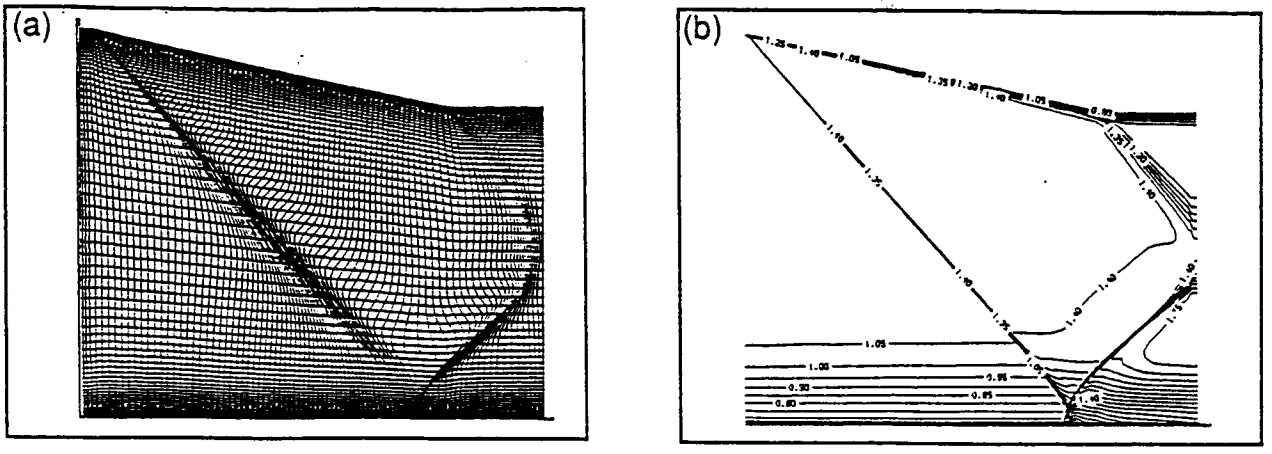

Figure 6. 2-D supersonic inlet. (a) Adapted grid, (b) solution computed on adapted grid.

Example 3: Axisymmetric plume flow– The second 2-D example is an axisymmetric nozzle plume flow (ref. 8). Supersonic flow exits from the nozzle on the lower left side of the grid and interacts with the surrounding quiescent air, causing complex plume features to develop. The upper part of figure 7(a) shows the initial grid used to compute this flow; below, in mirror image, are the Mach contours computed using this initial grid. Because of the lack of grid points in the appropriate regions, this solution does not clearly capture the flow features seen in the experimental results (ref. 8).

Several iterations through the grid solver and SAGE were required to create the final adapted grid and the significantly improved flow solution shown in figure 7(b). Two-directional adaption was required in order to capture the Mach disk whose gradient is in the opposite direction to the other features. The accuracy of the solution is illustrated with a comparison to experimental data: the picture in figure 7(c) is a shadowgraph of the actual experiment and is almost mirrored by the computed solution shown below.

THREE-DIMENSIONAL ANALYSIS

For the extension of the algorithm to three dimensions, a second torsion parameter, ψ is introduced to constrain the movement between the current node *(i,j,k)* and the nodes *(i,j,k – 1)* and *(i,j,k – 2)* on adjoining computational planes. This second torsion term is defined as $\psi_i(s^*_i - s_i)$ and is added to equation (7). After rearrangement, the final equation becomes

$$\omega_{i-1}s_{i-1} - (\omega_i + \omega_{i-1} + \tau_i + \psi_i)\, s_i + \omega_i s_{i+1} = -\tau s'_i - \psi s^*_i \qquad (9)$$

In SAGE, this is the final equation that is solved for all cases. When a 2-D grid is indicated, the ψ terms are simply set to zero. The full details of the solution method can be found in reference 4.

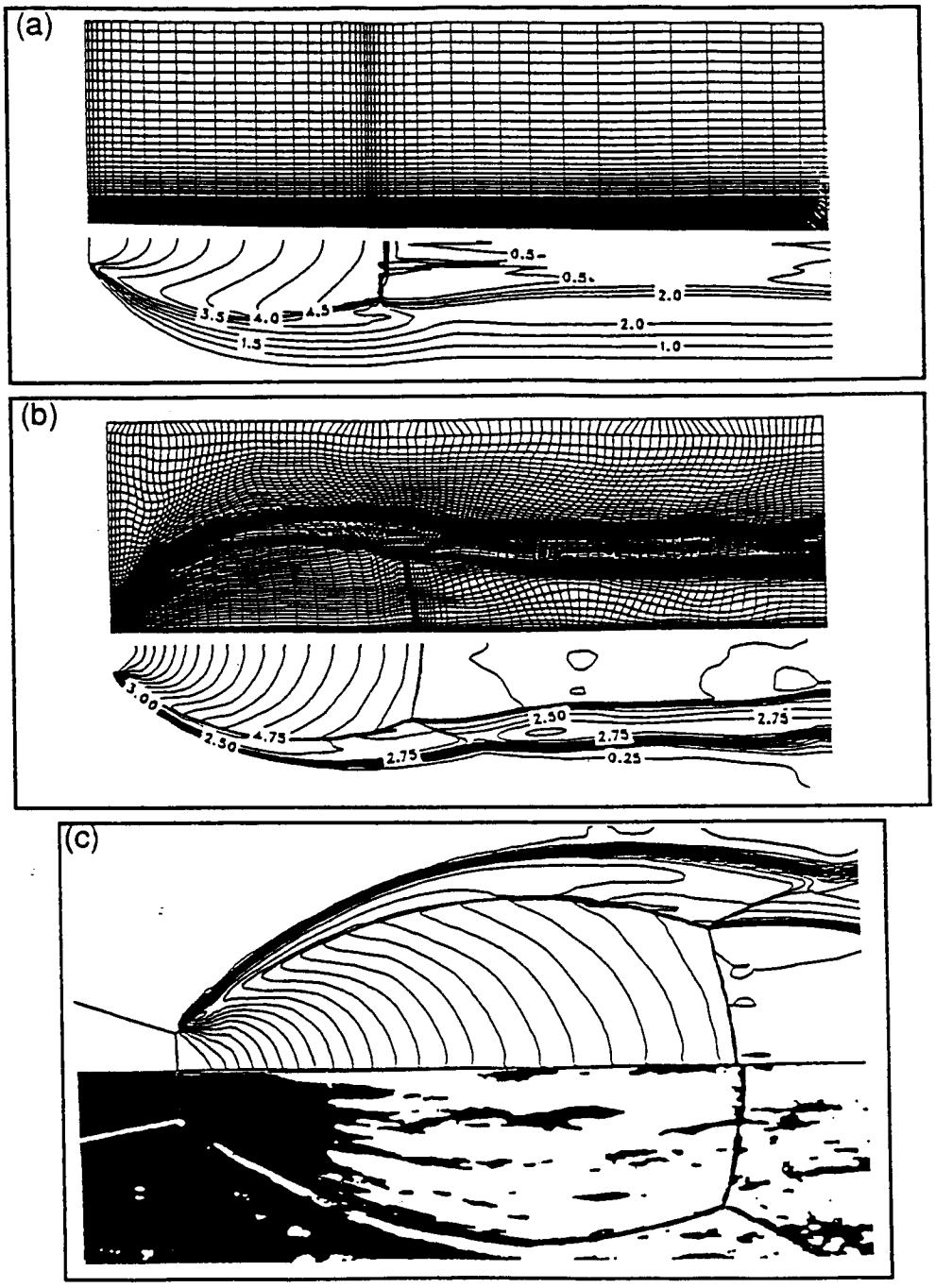

Figure 7. Axisymmetric plume flow. (a) Initial grid and undeveloped solution, (b) final adapted grid and solution, (c) comparison of computed axisymmetric plume flow with experimental shadowgraph result.

Three-Dimensional Applications

For 3-D adaption, the choice of adaption control parameters is expanded to include the direction and magnitude of the torsion force acting between planes. However, the most difficult of the

expanded choices is that of the direction, number and order of adaptions. With more complex flow structures, the apparent need for two- or even three-directional adaption increases. However, even a one-directional adaption will significantly change the grid in all three directions as demonstrated by this first example.

Example 4: Supersonic air injection– The problem shown in figure 8 is the University of Virginia combustor-flow experimental test (ref. 9). The figure shows a Mach 2 flow over a backward-facing step, with two sonic transverse air jets behind the step. An outline of the grid used for this computation is shown in the figure by dotted lines. The flow data was provided by Dr. Jong H. Wang of Rockwell International. Figure 8(b) shows three selected planes *i,j,k* from the initial grid that have been separated for clarity in the remaining figures. Figure 8(c) shows the corresponding Mach contours from the initial flowfield solution that were used as the adaption variable. Adaption takes place on constant *j* planes with marching in the *i* direction within the plane. This implies that the points were redistributed along *k* lines. Figure 8(d) shows the adapted planes, and although only one adaption pass has been made, both the *i* and *j* planes are adapted with respect to Mach number, with these planes retaining their original "flat" 3-D surfaces. However, the *k* plane shows a different effect; points have not moved within the plane, but the 3-D surface has deformed, since points have shifted in the *k* direction through the adaption.

It is also interesting to look at the effect of two-directional adaption. Figure 8(e) shows the result of a second adaption, this time adapting in the *i* direction and marching in *k* lines, "on top" of the adaption already shown in figure 8(d); points have been redistributed in the *i* direction as well as the *k* direction and both the *i* and *k* planes are now curved surfaces. This *i* redistribution can also occur by marching in *j* within the constant *k* planes. This alternate adapted grid (not shown) gives a very similar redistribution on the *j* plane, even though that was not the adaption plane. Other combinations were also tested that confirmed that the choice of adaption order may not be crucial to the creation of an acceptable adapted grid. In addition, we have seen that both one- and two-directional adaptions can produce an adapted grid that sufficiently represents the complex 3-D flow features.

Example 5: Supersonic flow over a 3-D swept ramp– The geometry of a 3-D ramp is shown in figure 9(a), where the dotted lines outline the computational grid. The recompression shock at the ramp corner and the viscous-inviscid interaction with the boundary layer results in a large separation that is three-dimensional in nature. Solutions have been computed for two ramp angles, 15° and 30°, and compared to experimental oil flow patterns (ref. 10). For the 15°-ramp-angle case, the experimental and the computed results agreed well. However, the results obtained for the 30° case, computed on the initial grid shown in figure 9(b), were not as close. This is demonstrated in figure 9(c), where the computed oil-flow patterns along the ramp surface show a significant difference in the size of the separation zone from the experimental values (shown by the open symbols). This discrepancy was suspected to be caused by local grid inaccuracies, which suggested utilizing the adaption procedure. The adapted grid, shown in figure 9(d), was able to more accurately capture the interaction between the shocks from the separated region and the wall boundary layer. This improved interaction generated a larger separation zone than before, which is seen in the recomputed oil-flow patterns shown in figure 9(e). This example demonstrates how a one-directional adaption pass influences the entire 3-D flow solution. The ramp surface plane was not adapted directly, but nevertheless, the flow on this surface changed considerably.

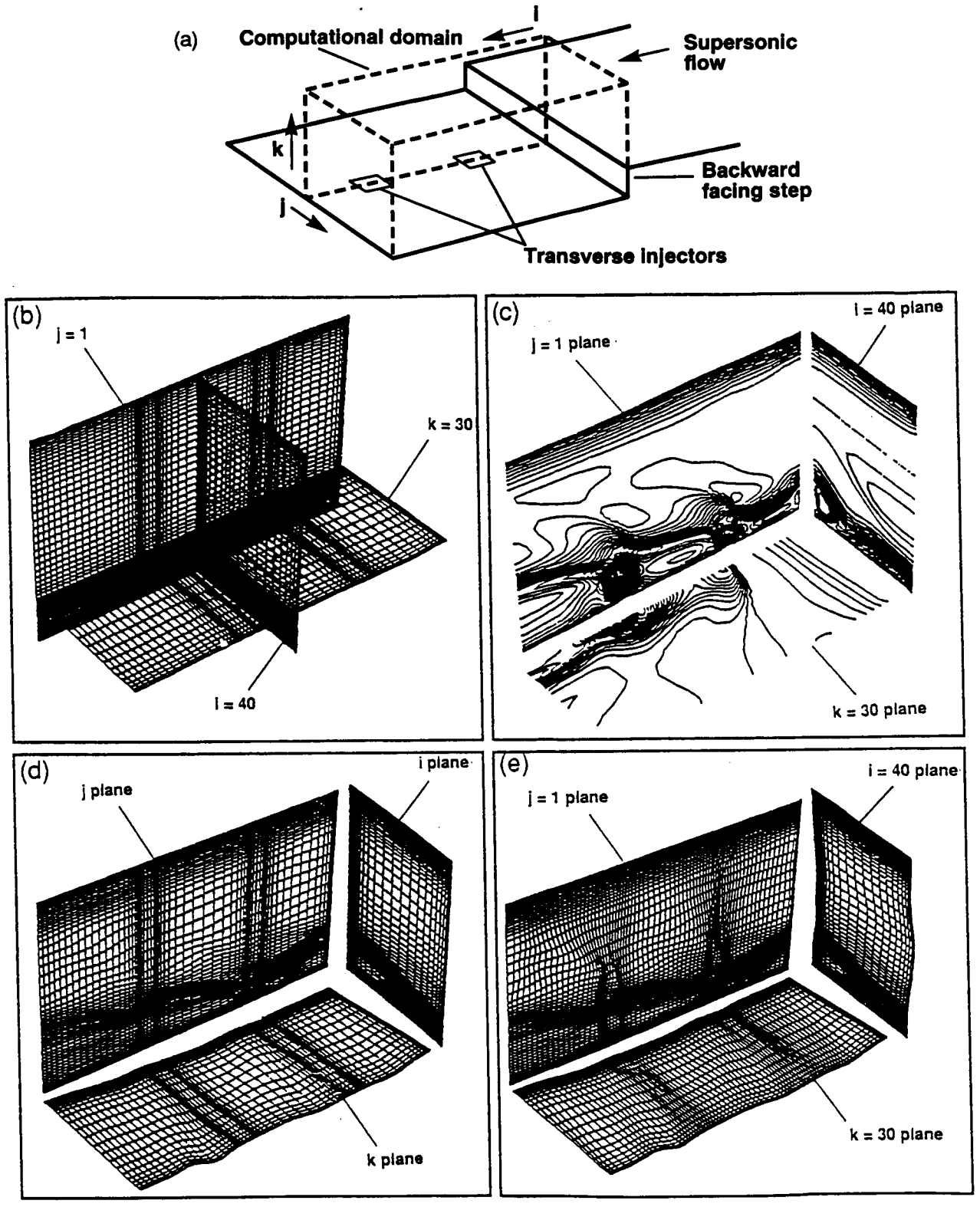

Figure 8. Supersonic air injection model. (a) Computational grid.(b) three planes from the initial grid, (c) mach contours on same three planes, (d) one-directional adapted grid, (e) two-directional adapted grid.

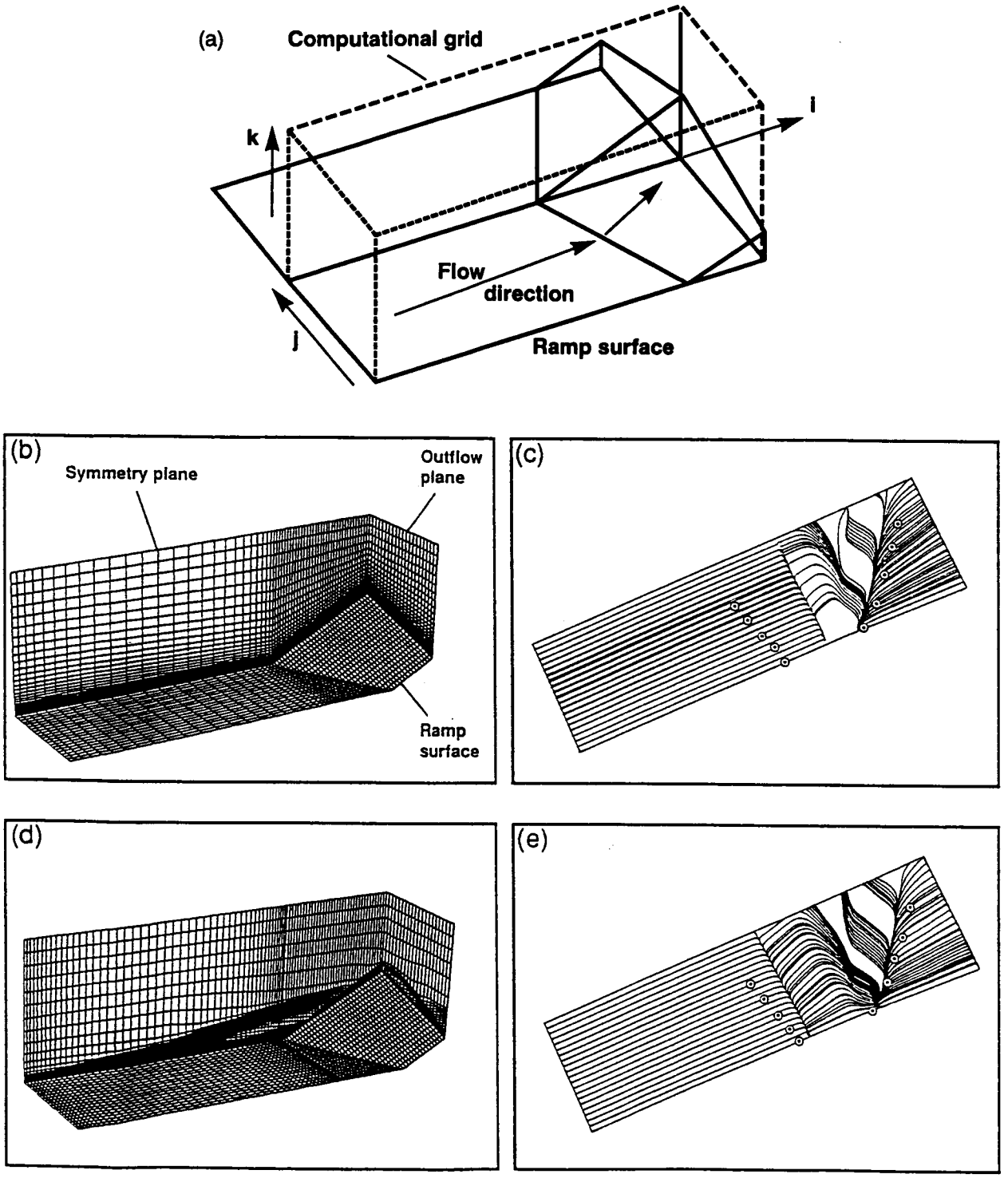

Figure 9. 3-D 30° swept ramp. (a) Experimental model, (b) initial grid, (c) oil-flow patterns, comparing computed and experimental separation regions, (d) adapted grid, (e) oil-flow patterns from adapted solution.

Example 6: Hypersonic NASP nozzle-plume flow– Ideal gas solutions have been obtained using a multiple, 3-D grid topology for the supersonic flow around a generic National Aero-Space Plane (NASP) nozzle configuration known as the single exhaust ramp nozzle (SERN) (ref. 11). The 3-D model is shown in figure 10 along with an outline of the computational zone in the plume region. This grid is one of the eight separate overlapping grids that were required to model this problem and this example demonstrates the flexibility of using SAGE for adapting segments of multiple grids. Figure 11(a) shows three planes (the symmetry plane, the outflow plane and the plane containing the ramp surface) from the original grid that covered the plume region. Figure 11(b) shows the Mach contours from the flow-field solutions obtained on this grid (ref. 11). It is clear that the interaction of the plume shocks with the ramp and the edge flow is complex and three-dimensional in nature. Although most of the flow features were observed, they were not all well-defined and thus the adaption procedure was invoked. The initial grid was adapted in two stages: first the points were redistributed in two directions, based on Mach number; then points were moved from the outer, constant region to the more complex interior flow region.

The resulting adapted grid is shown in figure 11(c). The inflow plane (not shown) and the lower ramp plane were not adapted, to maintain continuity between this grid and the unadapted grids surrounding it. Smoothness between the nonadapted planes and the internal adapted planes was maintained by the merging process described in reference 4. The flow solver used this adapted grid to obtain the result shown in figure 11(d). It can be seen that the flow features have sharpened considerably. Figure 12 compares the experimental shadowgraph (ref. 12) to the computed Mach contours along the symmetry plane downstream of the nozzle exit. The external and internal plume shocks are captured well and the agreement between the computation and the experiment is seen to be good.

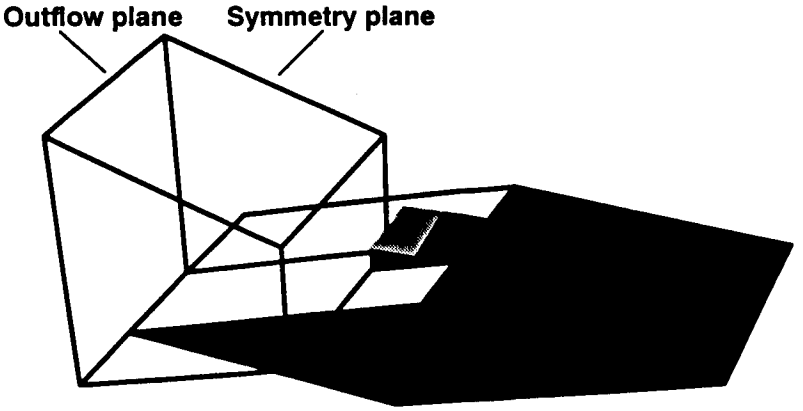

Figure 10. SERN experimental model showing computational grid in plume region.

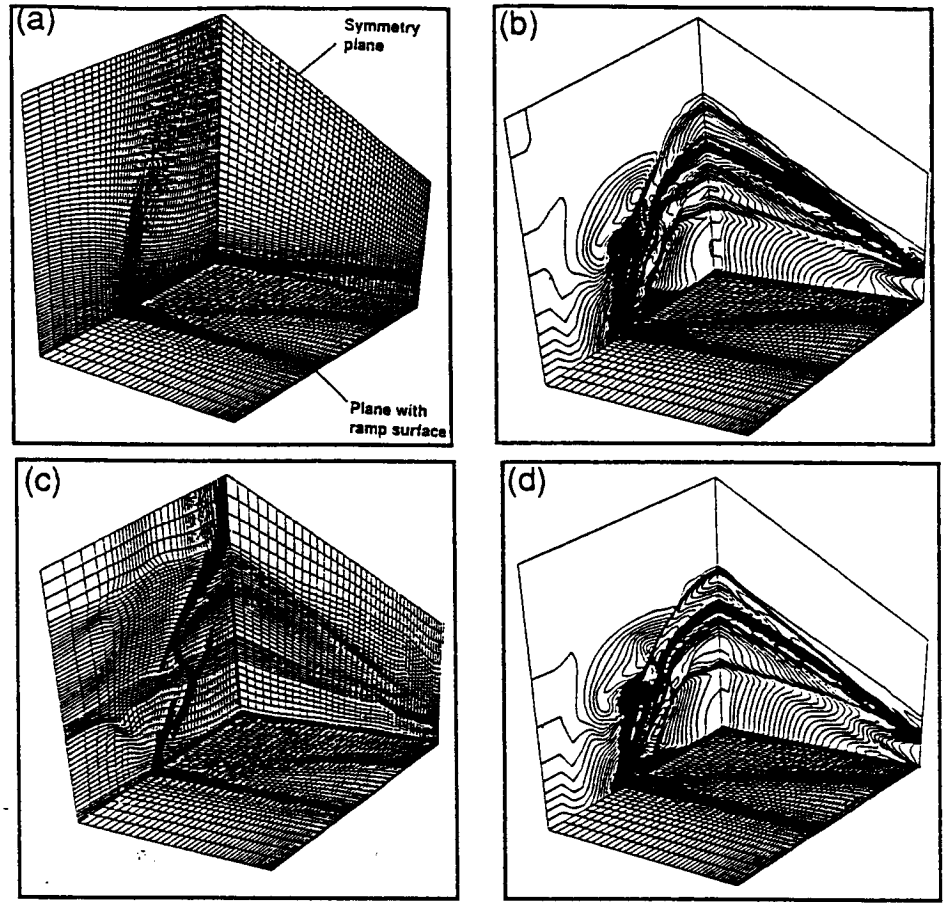

Figure 11. Nozzle plume flow. (a) Initial grid showing symmetry plane, outflow plane, and ramp surface, (b) initial Mach contours, (c) adapted grid, (d) adapted Mach contours.

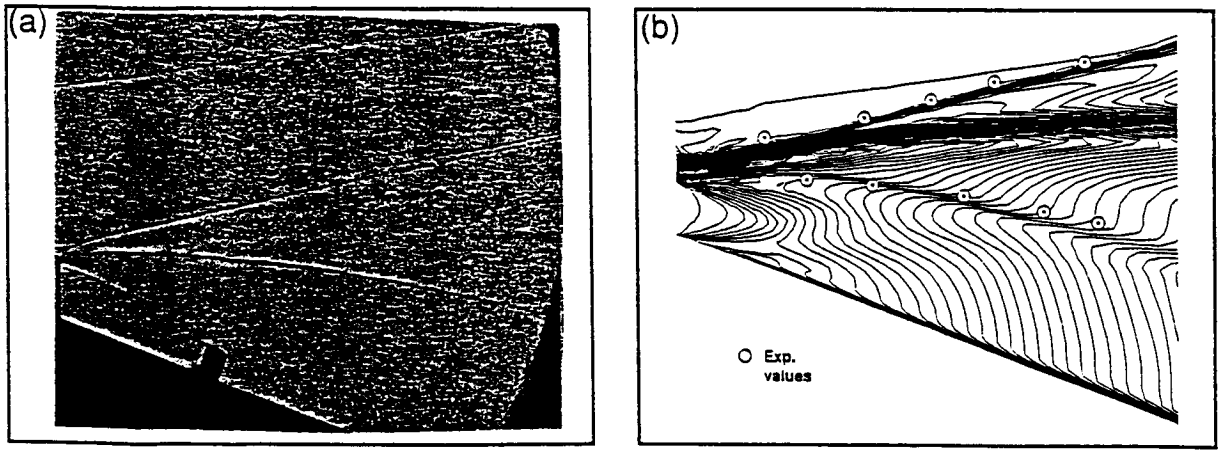

Figure 12. Comparison along the symmetry plane of the SERN nozzle flow. (a) Experimental shadowgraph, (b) computed Mach contours.

CONCLUSIONS

The multidimensional self-adaptive grid code, SAGE, has proven to be a flexible and useful tool in the solution of complex flow problems. Both 2- and 3-D examples given in this report show the code to be reliable and to substantially improve flowfield solutions. Since the adaptive procedure is a marching scheme the code is extremely fast and uses insignificant CPU time compared to the corresponding flow solver. The SAGE program is also machine and flow solver independent. Significant effort was made to simplify user interaction, though some parameters still need to be chosen with care. It is also difficult to tell when the adaption process has provided its best possible solution. This is particularly true if no experimental data are available or if there is a lack of theoretical understanding of the flow. Another difficulty occurs if local features are important but missing in the original grid; the adaption to this solution will not result in any improvement, and only grid refinement can result in an improved solution. These are complex issues that need to be explored within the context of each specific problem.

REFERENCES

1. Gnoffo, P.: A Vectorized, Finite-Volume, Adaptive Grid Algorithm Applied to Planetary Entry Problems. AIAA Paper 82-1018.

2. Nakahashi, K. and Deiwert, G. S.: A Practical Adaptive Grid Method for Complex Fluid Flow Problems. NASA TM-85989, 1984.

3. Nakahashi, K. and Deiwert, G. S.: A Three-Dimensional Adaptive Grid Method. AIAA Paper 85-0486.

4. Davies, C. B. and Venkatapathy, E.: The Multi-Dimensional Self-Adaptive Grid Code, SAGE. NASA TM-103905, 1992.

5. Davies, C. B. and Venkatapathy, E.: Application of a Solution Adaptive Grid Scheme, SAGE, to Complex Three-Dimensional Flows. AIAA Paper 91-1594, 10th Applied Computational Fluid Dynamics Conference, Honolulu, 1991.

6. Deiwert, G. S.; Venkatapathy, E.; Davies, C. B.; Djomehri, J.; and Abrahamson, K.: Application of a Self-Adaptive Grid Method to Complex Flows. NASA TM-102223.

7. Abrahamson, K. W.: Numerical Investigation of a Mach 3.5 Axisymmetric Inlet with Multiple Bleed Zones. AIAA Paper 88-2588, 6th Applied Aerodynamics Conference, June 1988, Williamsburg, Va.

8. Venkatapathy, E. and Feiereisen, W. J.: Computational Studies of Hard-Body and 3-D Effects in Plume Flows. AIAA Paper 89-0129, 1989.

9. Fletcher, D. G. and McDaniel, J. C.: Quantitative Characterization of a Non-Reacting, Supersonic Combustor Using Laser-Induced Iodine Fluorescence. AIAA Paper 89-2565.

10. Venkatapathy, E., "Computational Results for 2-D and 3-D Ramp Flows with an Upwind Navier-Stokes Solver," to appear in the Proceedings of the Hypersonic Workshop, Springer-Verlag.

11. Ruffin, S. and Venkatapathy, E., "Computational Design Aspects of a NASP Nozzle/Afterbody Experiment," AIAA Paper 89-0446, 1989.

12. Ruffin, S. M., Venkatapathy, E., Lee, S. H., Keener, E. R., and Spaid, F. W., "Single Expansion Ramp Nozzle Simulations," AIAA Paper 92-0387, Reno, Jan. 1992.

BIOGRAPHY

Carol B. Davies was born and educated in England. She attended Reading University and received her B.S. in Mathematics in 1966. After postgraduate studies in Meteorology she emigrated to the USA and started work at NASA Ames as a contractor in 1968. From 1968 to 1976 she worked on a variety of projects, including analyzing experimental data from the Pioneer Space Project and the development of an Inlet Boundary Layer code. In 1976, she moved to the Republic of Singapore and joined the University of Singapore. There, she taught Statistics and was a consultant in the Computer Science Dept. On her return to the USA in 1980, she rejoined NASA Ames as a contractor with Sterling Software. She has since worked on several projects including particle spallation from the Galileo Space Probe and the development of Aero-assisted Space Transfer Vehicles (ASTV), for which she received a patent and a Space Act Award.

ENGINEERING THE FUTURE WITH AMERICA'S HIGH SCHOOL STUDENTS

M. A. Farrance
G. E. Government Services
Ames Research Center
Moffett Field, California

J. W. Jenner
Ames Research Center
Moffett Field, California

SUMMARY

The number of students enrolled in engineering is declining while the need for engineers is increasing. One contributing factor is that most high school students have little or no knowledge about what engineering is, or what engineers do.

To teach young students about engineering, engineers need good tools. This paper presents a course of study developed and used by the authors in a junior college course for high school students. Students learned about engineering through independent student projects, in-class problem solving, and use of career information resources.

Selected activities from the course can be adapted to teach students about engineering in other settings. Among the most successful techniques were the student research paper assignment, working out a solution to an engineering problem as a class exercise, and the use of technical materials to illustrate engineering concepts and demonstrate "tools of the trade."

INTRODUCTION

The United States is facing a serious threat to our economic, social, and environmental well-being. Problems include a fiercely competitive global economy, energy shortages, depletion of natural resources, degradation of the environment, and deterioration of infrastructure, all complicated by shrinking federal budgets. Because these problems have substantial technical components, engineers are well qualified to contribute significantly to their solutions. Although some see the present employment market for engineers as weak, we believe that this country's future depends on engineering talent in all disciplines to provide cost effective, innovative, and permanent solutions to these interdisciplinary, national problems.

Future engineers are students attending elementary and high schools today. The number of high school graduates enrolling in undergraduate engineering programs, however, is declining. At the university level nationwide, the number of new college freshmen enrolling in engineering programs

declined, with a corresponding decline in the number of Bachelor of Science degrees in engineering awarded, from almost 80,000 in 1986 to 66,000 in 1990.

There are many ways to encourage more young people to choose engineering as a career. *Engineering Careers*, the course described in this paper, was developed as one means to do so. Figure 1 illustrates some complementary ways in which a growing number of programs today, including *Engineering Careers*, are contributing to an overall solution to our national dilemma.

Some of these programs help to *inspire* young people to pursue scientific and technical study by drawing on the very powerful images provided by space exploration. The use of such imagery to inspire students to pursue technical careers is an excellent technique. Inspiration alone, however, is not sufficient. We also need to *inform* students about engineering. Many students face the difficulty of deciding what career to choose without the benefit of some very basic information about engineering.

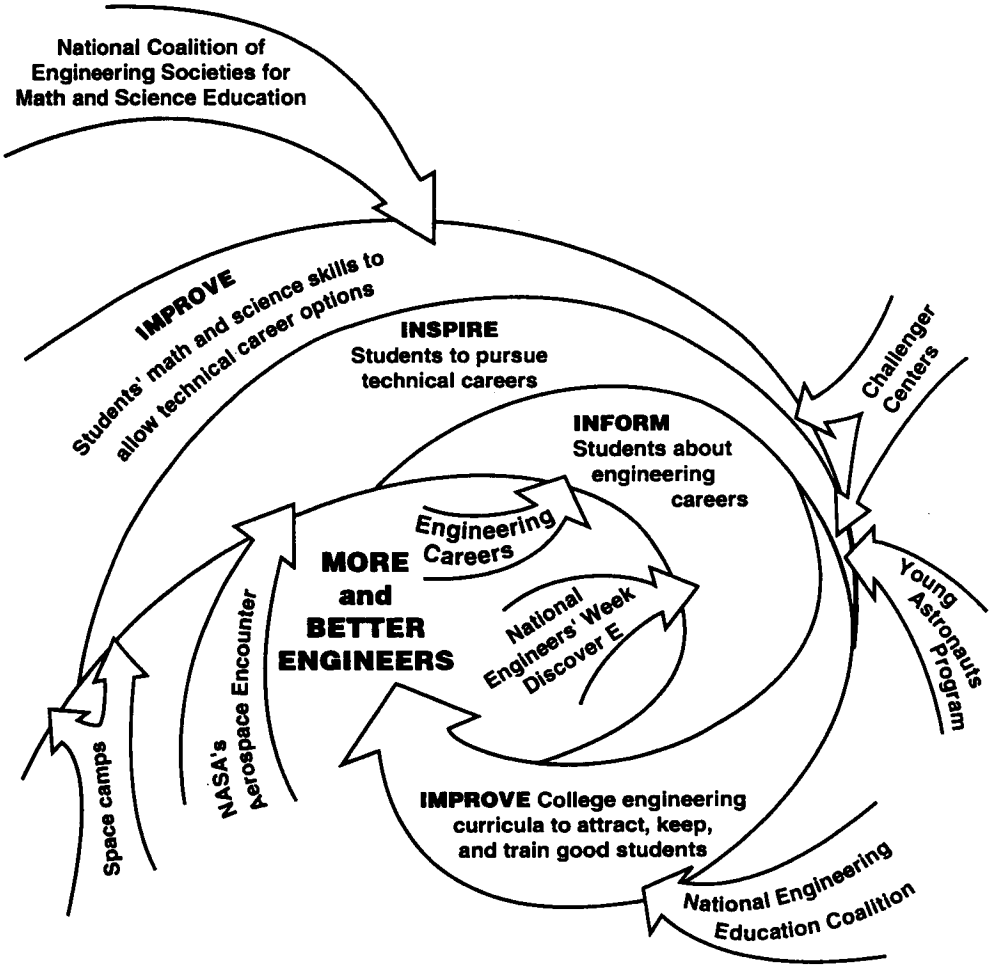

Figure 1. Engineering Careers and other programs target students in complementary ways along the path to producing more and better engineers.

The authors have twice taught an engineering careers course to high school students in California's "Silicon Valley." Nearly every student gave as the reason they took the course: "I *might* be interested in being an engineer...but first I want to find out what engineering is all about." Because our Silicon Valley students (many of whom had an engineer parent) lacked this information, we suggest that high school students in less technology-oriented areas in this country are even less able to make an informed decision to choose a career in engineering.

Across the country, engineers can balance the intangibility of "inspiration" with the substance of "information." Engineers can teach--*uniquely*--what engineering is and who engineers are. Today's engineers need good tools to inspire and inform tomorrow's engineers. This paper describes the tools the authors used in a self-contained, integrated course of study that we developed and taught in a junior college program for high school students.

LEARNING ABOUT ENGINEERING

Engineering Careers at Foothill College

Engineering Careers, the course described in this paper, is part of the Foothill Summer Youth Programs. These programs provide 8th through 12th grade students with academic challenge in a college environment; all classes offered in the Summer Youth Programs are part of the college curriculum and supply college credit. A proposal for a course entitled *Engineering Careers* was developed by M.A. Farrance and accepted by Program Director Janice Carr in 1989. In the summers of 1990 and 1991, Foothill College offered the course as part of the Space Sciences Youth Program, co-sponsored by the Mathematics and Applied Science Department, and taught by Farrance. Both authors have worked on course improvements. We expect to offer the course again in 1992. The course syllabus is shown in figure 2.

Engineering Careers is a 12-hour course offered for one college quarter unit of credit. In 1990 the class met twice a week in two-hour sessions for three weeks; in 1991 we changed to four one-hour sessions each week for three weeks. Class size and grade levels of students are shown in figure 3.

Course objective(s)– Objectives for the course are stated in terms of what we expected students to accomplish. They were told that by the end of the course, they would be able to:

1. identify a variety of engineering career disciplines;

2. identify what kinds of work can be performed by engineers in different disciplines;

3. understand by example how engineers typically approach physical engineering problems (that is, by setting up a problem model and using algebra, trigonometry, calculus and physics as tools for problem solution);

4. identify some college course work necessary to obtain an engineering degree;

Engineering Careers

Session	Topics Covered	Assignment
1	Introduction "A job" vs "a career" Making career choices; the significance of doing work that one enjoys "Engineering" and "science"	Complete Strong Interest Inventory[2]
2	Engineering disciplines Engineering functions Video: "Turning Ideas into Reality"[4] Confirm research paper topics	Read "Proud to be an Engineer"[3]
3	Engineering Disciplines Where engineers work	Deadline to return Strong Interest Inventory
4	Guest speaker	
5	Problem solving in engineering The engineer's toolbox Video: "Techniques for Visualizing Flight Dynamics"[5]	Deadline to return orientation completions
6	Problem solving in engineering	
7	Guest speaker or field trip	Read "Earning the Title of "Professional Engineer"[5]
8	Academic preparation for an engineering career The Professional Engineer The entrepreneurial engineer	
9	Guest speaker	Read "The Coming Crisis in Aerospace Employment?"[7] and "The Interdisciplinary Team"[8]
10	The engineering roles of the technical team The future of engineering Video: "Journey into Tomorrow"[9]	
11	Guest speaker	
12	Engineering a science satellite system Video: "Fast Forward to the Future"[10]	Deadline to turn in research papers and book reports

[2]Strong, E.K., Jr.; Hansen, J.C.; and Campbell, D.P., *Strong Interest Inventory*, 1991.
[3]Gardner, Dana, Design News Magazine, 11 June 1990.
[4]National Engineers Week DiscoverE, 1991.
[5]NASA Ames Research Center, 1989.
[6]Jenner, J.W., and Farrance, M.A., 1991.
[7]Supplement to *Aerospace Engineering Magazine*, January 1990.
[8]Jenner, J.W., and Farrance, M.A., 1991.
[9]Lockheed Missiles and Space Company, 1990.
[10]NASA Ames Research Center, 1990.

Figure 2. *Engineering Careers* course syllabus.

5. understand that different engineering disciplines work together in engineering projects; and

6. use newly acquired research skills to learn about *any* career choice that might interest them.

Students were evaluated for a grade based on their independent research papers, book reports, class attendance, and class participation. The instructor determined if the students met the course

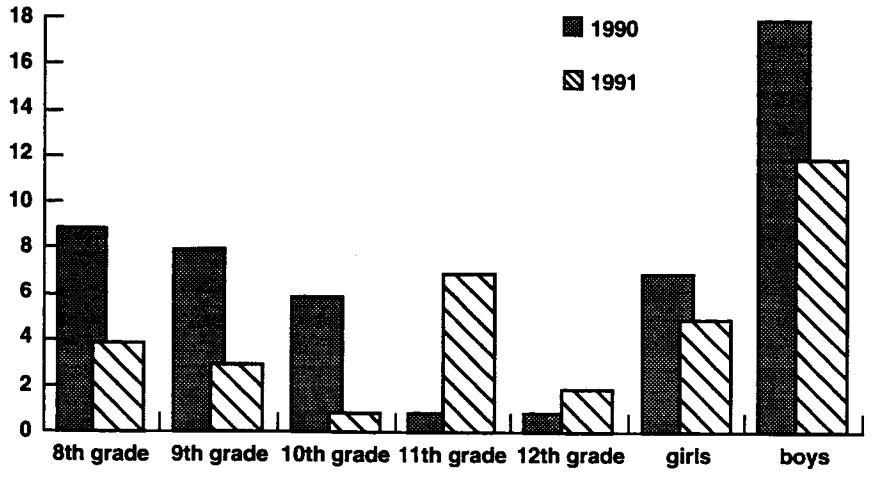

Figure 3. *Engineering Careers* class composition.

objectives by evaluating their papers and reports, in-class question-and-answer sessions, class discussions, and individual student interviews. We intentionally structured the class to avoid requiring students to memorize information that is easily available in references.

Criteria for success– Our criteria to determine the success of the course were the following.

1. More than 15 students would sign up for the course;

2. At least 90% of students would indicate an increased awareness of what engineering is, and what engineers do, at the conclusion of the course;

3. At least one student would indicate an interest in pursuing an engineering career after the class;

4. More than one-half of the students would indicate a willingness to recommend this course to their peers.

Tools for Teaching/Means for Learning

Students learned about engineering through lectures, reading materials, video, in-class activities, and independent assignments, described below.

Lectures/reading materials/video– The instructor presented lectures, some with supplemental reading assignments and videos, on topics as shown in figure 2.

The instructor used videotapes to stimulate class discussions about how the engineers featured represented their profession in various disciplines. Another short, technical tape was used with a lecture about "the engineer's toolbox" to illustrate how computer-generated graphics can be used by engineers.

In-class activities– There were two types of in-class group activities. The first was designed for self-discovery. The second provided a glimpse of how engineers use math and physical science to solve real-world problems, that is, "what engineers do."

Self-discovery exercises: One self-discovery exercise was used to help students place "education" and "work" into the context of their projected lifetimes. "This is Your Lifeline" was used to represent students' lifetimes graphically on a timeline (fig. 4). After students completed their individual lifelines, the class discussed the relationship between education and employment options, how fast technology changes, and how technology changes might affect the need for continuing education. We particularly stressed the significance of how much of the lifeline graph was filled by working years. A typical person is likely to spend 30 years—or more—working. This was compared with the 17 years that one might ultimately spend in school before earning a bachelor's degree. This comparison proved to be especially meaningful to students, who have already spent the majority of their years in school, some of whom expressed feeling "as if it will never end!" In that context, the importance of spending 30 years doing things that one enjoys becomes significant.

The authors feel strongly that self-knowledge is a prerequisite for a sound career choice. The *Strong Interest Inventory* was used to help students learn more about their own interests, and to compare their individual patterns of likes and dislikes to those of a wide variety of working adults. An in-class discussion about the individual results of the *Strong Interest Inventory* gave students an opportunity to discuss some possible reasons behind some of the correlations to professionals' profiles, and interpret their results in the context of career planning.

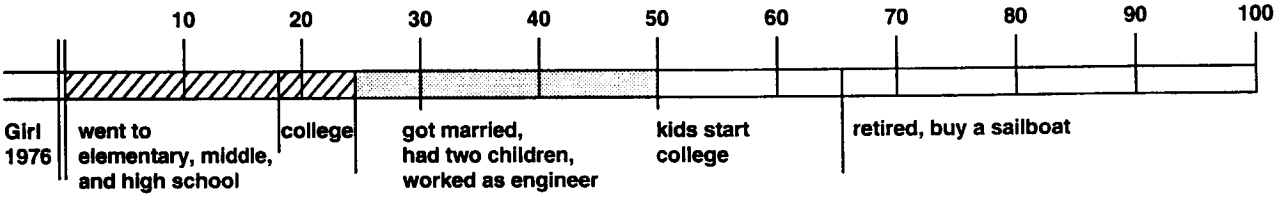

Figure 4. "This is Your Lifeline" student graph.

Engineering exercises: To learn about the use of mathematics and physical science as engineering tools, the class worked out a solution to a problem based on one posed by Smith, Butler, and LeBold, shown in figure 5. All students were unfamiliar with one or more of the techniques demonstrated. As each new element of the problem was introduced, the instructor explained the basic math and physics principles behind it. Students who had already learned the algebra, trigonometry, or physics were called on to help explain how each was being applied.

Independent assignments– Independent assignments helped students learn about various aspects of engineering and gave them a chance to practice written communication skills that engineers use in their work environments. The importance of communication in engineering was heavily stressed.

These assignments included a research paper about an engineering discipline (see fig. 6), and two letters of inquiry. Each student sent one inquiry to a university offering an appropriate engineering degree, and the other to a company or agency that employs engineers in the discipline selected.

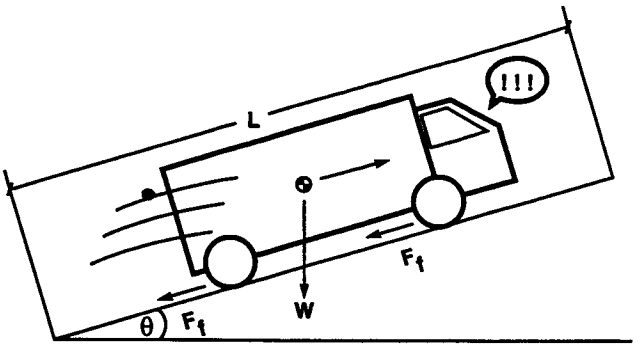

PROBLEM (Part 1): The potential for expensive damage caused by runaway trucks on a particular long, steep downgrade is high. What is a simple and effective way to minimize damage that might be caused by runaway trucks?

POSSIBLE SOLUTIONS: (suggested by students)
- **design new trucks**
- **design new brakes**
- **redesign highway slope**
- **put center divider in road**
- ***put in up-ramp next to highway**

PROBLEM (Part 2): How long does the up-ramp have to be so that the speeding truck will roll to a stop?

ASSUMPTIONS

15% grade = 8.5 deg
gravel-covered, coefficient of friction for gravel = 0.20
initial velocity of truck = 100 m/hr

Figure 5. To solve this basic physical engineering problem, the students learned to apply some universal techniques of engineering problem-solving, such as drawing free-body diagrams, making assumptions, calculating forces, and checking solutions.

A report on a book about engineering was also assigned. Students selected a book from the course bibliography (fig. 7).

To assist them with their research, students were introduced to the Foothill College Library and the Career Center through required individual orientations with the reference librarians. These

TOPIC OF PAPER

Name the engineering discipline or field you have chosen.

DESCRIPTION OF FIELD

Describe this field of engineering. What does it include? Are there specializations within this field of engineering? What kind of work do people in this field do? Describe the kinds of products these engineers produce in the various specializations.

EDUCATION

What education is required for a degree in this field? How many years of college does it usually take to get the appropriate degree? Give two required technical courses needed for a degree in this major. Describe what these courses are meant to teach. Why do you think they are required? What high school classes are helpful for preparing for college course in this major? Name two colleges or universities that offer a degree in this field.

EMPLOYMENT

For what kinds of companies, government agencies, or institutions are people in this field likely to work? Name two companies, agencies, and institutions that might hire an engineer who has just graduated with a degree in this field.

PROFESSIONAL DEVELOPMENT

Find an article from a journal or periodical publication that might be of interest to this type of professional engineer. Give its title, author, name of the publication, and date of issue. Explain why a professional engineer might find this article interesting. Include a copy of the article with your paper.

PERSONNEL OBSERVATIONS

Does this field appeal to you as a career choice, or not? If yes, why is it interesting? If no, what do you find unappealing, and what field would you research next? How does this field match with the results of your interest inventory? Does the interest inventory indicate that you might like working in this field? Why, or why not?

REFERENCES

Use the Foothill College Semans Library, Career Center, and any other resource you want. List the sources of your information (books, encyclopedias, periodicals, college catalogues, Eureka database, etc.)

Figure 6. Research paper outline.

The Civilized Engineer, Florman, Samuel; St. Martin's Press, 1987
Structures, or Why Things Don't Fall Down, Gordon, J.E.; Plenum Press, 1978
Freedom to Soar, Kimball, J.B.; Kimball Publishing, 1989
Ethics and Professionalism in Engineering, Mantell, M.I.; MacMillan, 1964
Psychology of Everyday Things, Norman, D.A.; Basic Books, 1988
Beyond Engineering, Petroski, Henry; St. Martin's Press, 1986
Women in Engineering, Posner, Alice; Career Horizons, 1981
Engineering as a Career, Smith, R.J., McGraw Hill, 1983
The Encyclopedia of How It's Built, Clarke, D., A&W Publishers, 1979

Figure 7. *Engineering Careers* course bibliography.

assignments gave them practice in using research resources: the on-line catalogue, the reserve library, college and university catalogues, newspaper want ads, the periodicals index, and the Eureka careers information database.

Guest speakers – We invited engineers from the local area to talk to the class. We made a deliberate effort not only to have the speakers represent a variety of engineering disciplines, but also

to introduce students to enthusiastic, articulate engineers of both sexes, with varied backgrounds. To increase the chances of a successful interaction with the students, both the guest speakers and the students were prepared in advance by the instructor. Students were reminded that part of their class grade was based on "class participation," including interaction with the guests, and some class time was spent before speakers' visits to generate some questions to ask each of them. Guest speakers were provided with some orientation material supplied by the instructor. A sample is shown in figure 8.

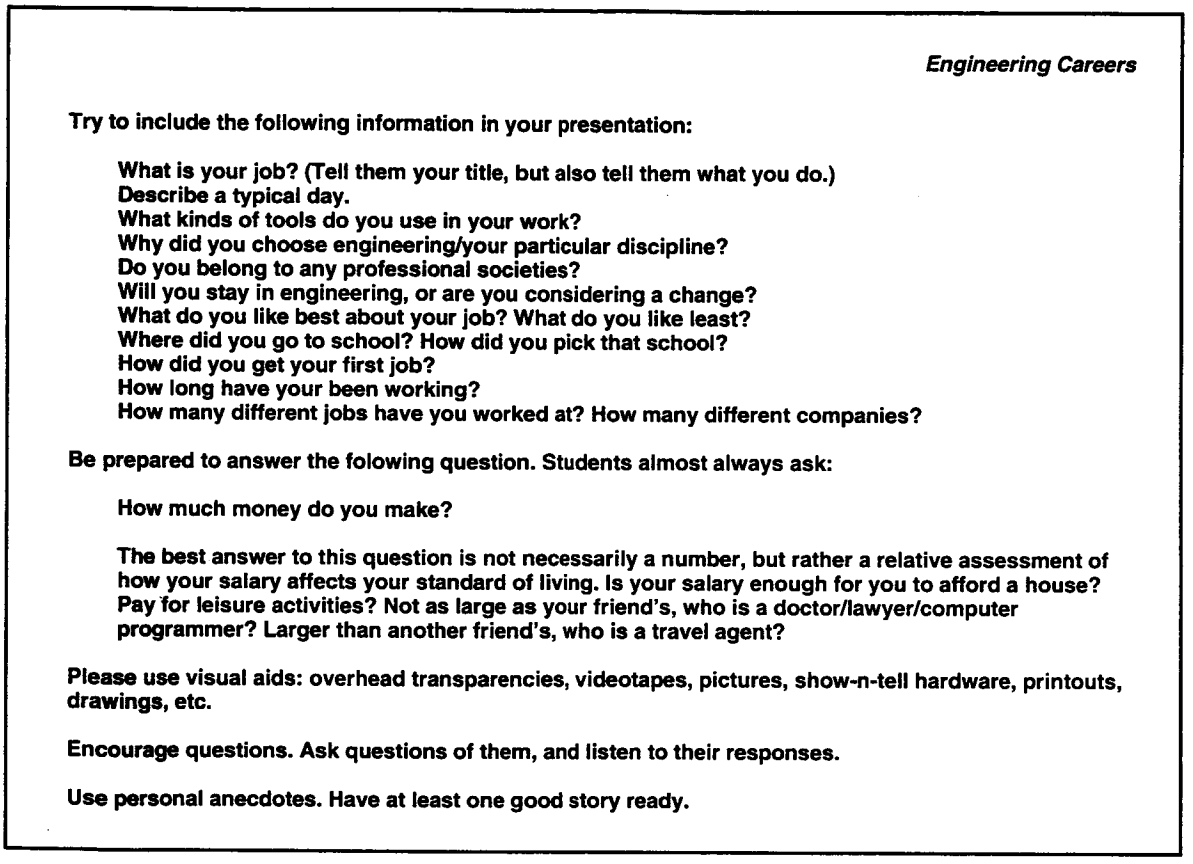

Engineering Careers

Try to include the following information in your presentation:

What is your job? (Tell them your title, but also tell them what you do.)
Describe a typical day.
What kinds of tools do you use in your work?
Why did you choose engineering/your particular discipline?
Do you belong to any professional societies?
Will you stay in engineering, or are you considering a change?
What do you like best about your job? What do you like least?
Where did you go to school? How did you pick that school?
How did you get your first job?
How long have your been working?
How many different jobs have you worked at? How many different companies?

Be prepared to answer the folowing question. Students almost always ask:

How much money do you make?

The best answer to this question is not necessarily a number, but rather a relative assessment of how your salary affects your standard of living. Is your salary enough for you to afford a house? Pay for leisure activities? Not as large as your friend's, who is a doctor/lawyer/computer programmer? Larger than another friend's, who is a travel agent?

Please use visual aids: overhead transparencies, videotapes, pictures, show-n-tell hardware, printouts, drawings, etc.

Encourage questions. Ask questions of them, and listen to their responses.

Use personal anecdotes. Have at least one good story ready.

Figure 8. Suggestions made to guest speakers.

CONCLUSIONS

Meeting the Success Criteria

We obtained student feedback from a course evaluation (fig. 9) and student interviews. From this information we determined that this course had met our success criteria.

1. We had 25 students in 1990 and 17 students in 1991 complete the course;

2. 100% of students indicated an increased awareness of what engineering is and what engineers do at the conclusion of the course;

Engineering Careers

Was this a worthwhile course for you? Why or why not?

Was the level of work required appropriate?

too much	about right	too little

Was the lecture and class material appropriate?

too much detail	about right	not enough detail

Was the number of guest speakers appropriate?

too many	about right	not enough

Was the variety of guest speakers appropriate?

too many	about right	not enough

What did you like BEST about the course?

What did you like LEAST about the course?

I would like to improve this course. What do you recommend that I do to make it better?

Would you recommend this course to a friend? Why or why not?

Figure 9. Course evaluation form.

3. 44% of students indicated that the course helped them decide to pursue an engineering career (one former student is currently working as an intern at NASA Ames Research Center and plans to major in engineering next year);

4. 88% of students (100% of the students who answered this question) indicated a willingness to recommend this course to their peers.

Additional student feedback about the course is given in figure 10. We are making improvements to the course based on both feedback from students and our own observations.

What Worked

From the student's point of view– The activities that students liked most were those that required student involvement, in particular, the self-discovery exercises and the engineering problem. Frequently mentioned were the guest speakers. Guest speakers who brought items for show-and-tell had good student involvement. (See fig. 11.)

No student actually claimed to have liked doing the book report, but several students reported that they had read a book they would not have found or read otherwise, and enjoyed it. Most books met with the students' approval. *The Civilized Engineer*, by Samuel Florman, was the most popular.

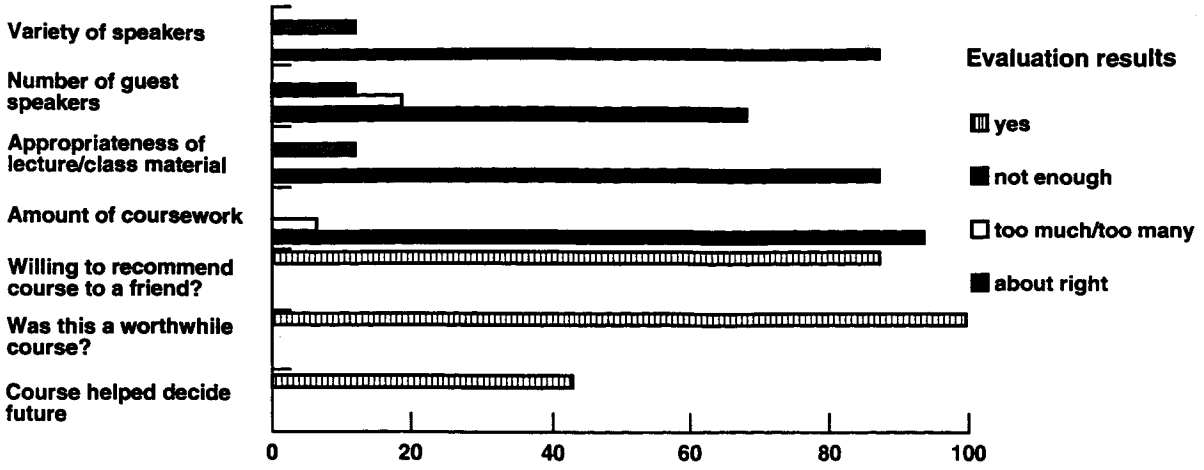

"The guest speakers gave us a good idea about what engineers do."

"I probably wouldn't have done as much research and reading about [engineering] as I've done here."

"This course let me learn more about the different career choices in engineering."

"I would recommend this course because it helps a person have a better perspective on whether he/she wants to become an engineer."

"[This course] helped me make up my mind to go into software engineering."

"Now I have a better idea of what the different types of engineers do so I can better decide what area I want to major in."

"[This course] showed me what kinds of careers there are, and what I might be good at."

"This class was very worthwhile, even to get up at 6:30 for. It helped me decide what I want to major in once I go to college."

"[This class] really taught me a lot about engineering. I learned more than I ever could back at high school. It really broadened my horizons. I think I've finally decided what I'm going to do with my life: become an aerospace engineer!"

"I learned what I wanted to and I know about the fields of engineering now. I'm seriously considering a career in engineering."

Figure 10. Student evaluation results.

From the instructor's point of view– The learning value of the engineering exercise was not *what* problem we worked, but *how* we worked through it. The explanations of each element of the problem helped illustrate how engineers approach problem-solving.

The judicious use of selected technical materials such as videotapes and drawings was found to be highly effective for teaching. The access to such material, along with the ability to explain in basic terms what it is and how it's used, is unique to the engineer-as-teacher.

Student orientations with the library and career center worked well. This requirement was added in the second year of the course, because many students in the first course did not take advantage of

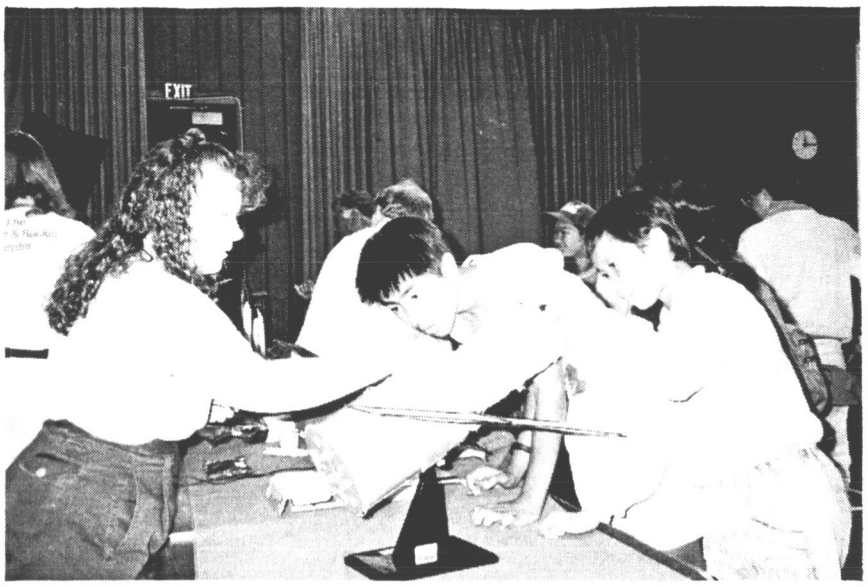

Figure 11. Students particularly enjoyed guest speakers who brought items for "show-and-tell" and encouraged student involvement.

these resources when they were not required. The cooperation of the librarians at Foothill College reminded us that librarians in general are happy to help people learn to use resources and need only to be asked.

We found that the value of the self-discovery exercise is primarily in the discussion about the results. The *Strong Interest Inventory* is not the only self-discovery exercise appropriate for high school students; others are available or can be developed. Our first year students completed a different inventory based on an exercise from SPACES.

What Didn't Work—Room for Improvement

The student's inquiry letters to companies that employ engineers did not always produce a satisfactory response; many replies were form letters. Student evaluations indicated that straight lectures (those without student reading preparation or exercises) were uninteresting and did not involve them enough.

Recommendations

Engineering Careers 1992

We are making the following changes to the course, consistent with suggestions by students.

1. Develop more written material for student reading assignments, especially on engineering disciplines and functions, and shorten lectures.

2. Add at least one class engineering project as an extension of the problem solving exercise. For example, in the case of the truck-ramp exercise, the class might test their chalkboard solution by rolling vehicles down a ramp of the same slope as the hill in the problem and determining (after scaling the distances) how far up the second ramp the vehicle will travel after it has accelerated down the "hill."

3. Increase class duration to six weeks (a total of 24 hours of class time) to allow time for in-class engineering projects.

4. Retain the one-hour-session format. Students and instructor both found the shorter sessions easier for their attention spans.

5. Add options from which to choose for a second project. We hope to provide students with more opportunity for communication practice. Options will include book reports and presentations to the class on some engineering topics.

6. Send the inquiry letters early and have students bring in the replies to share with the class.

Adapting Engineering Careers to Other Settings

Based on our own observations and feedback from students who have taken *Engineering Careers*, this course appealed to a range of ages, from 8th to 12th grade level. That is, it was not too difficult for the youngest class members nor too simplistic for the older class members. Eighty-eight percent of the student evaluations indicated "I would recommend this course to a friend." Our plan is to continue to offer the course through Foothill College, and we would also like to encourage others to use what has worked for us. We feel, however, that this course is appropriate for students who are already interested in math, science, and technical subjects. Without major changes, it is not likely to appeal to "at risk" students who are already uninterested in school, or with students below an 8th grade level.

Engineering Careers might be used in slightly modified form for programs in which students meet regularly and explore an interest in science and technology, such as Young Astronauts or Scouts. It might also be adapted to a regular high school class setting with a well-motivated class, such as an honors course in physics.

Individual exercises from *Engineering Careers* can be used in other contexts. The chalkboard engineering exercise might be used to illustrate engineering problem-solving techniques, but we emphasize that this exercise should be reinforced with hands-on activity. The independent assignments can be used in almost any setting where students meet at least twice and can earn some type of reward for their effort (such as a grade, a merit badge, or an award).

Finally, our techniques for preparing both students and guest speakers have provided good results. We encourage teachers to invite engineers into their classes, and we encourage fellow engineers—especially women and minority engineers—to volunteer to speak to students. Engineers who both inspire and inform young people about engineering literally are helping to "engineer the future."

BIBLIOGRAPHY

1. Curry, David: Engineering Schools Under Fire. *Machine Design*, Penton Publishing, Inc., Cleveland, OH, October 1991.

2. Fraser, Sherry; et al.: SPACES: Solving Problems of Access to Careers in Engineering and Science. Lawrence Hall of Science, 1982.

3. Strong, E. K., Jr.; Hansen, J. C.; and Campbell, D. P.: Strong Interest Inventory. 1991.

4. Smith, R.; Butler, B.; LeBold, W.: Engineering as a Career. 4th Ed., 1983.

5. *Eureka* California Career Information Systems. Richmond, CA, 1991.

6. Fraser, Sherry; et al.: Do You Want to be an Engineer? *SPACES: Solving Problems of Access to Careers in Engineering and Science*, Lawrence Hall of Science, 1982.

BIOGRAPHIES

Michelle (Mickey) Farrance is a mechanical systems engineer developing Space Station *Freedom* environmental science research payloads for NASA Ames Research Center as an employee of G.E. Government Services. She has previously worked on *Freedom* design and mechanical interface coordination for Lockheed Missiles and Space Co. Since 1982, she has taught space science and engineering courses for the California Academy of Sciences, Girl Scouts, Young Astronauts, and most recently Foothill College. She is currently completing an M.S.M.E. at Santa Clara University.

Jeffrey Jenner is a mechanical engineer responsible for development of biological research equipment for Space Station *Freedom* and is employed by NASA Ames Research Center. For the past ten years, he has worked on several NASA and Air Force spaceflight programs, designing ground support facilities and testing spaceflight hardware. He has worked with high school and college students in various internship programs. He is currently completing an M.S.M.E. at Stanford University.

USING EMERGENT ORDER TO SHAPE A SPACE SOCIETY

Amara L. Graps
Ames Research Center
Moffett Field, California

INTRODUCTION

A fast-growing movement in the scientific community is reshaping the way that we view the world around us. The short-hand name for this movement is "chaos." Chaos is a science of the global, nonlinear nature of systems. The center of this set of ideas is that simple, deterministic systems can breed complexity. Systems as complex as the human body, ecology, the mind or a human society. While it is true that simple laws can breed complexity, the other side is that complex systems can breed order. It is the latter that I will focus on in this paper.

In the past, nonlinear was nearly synonymous with nonsolvable because no general analytic solutions exist. Mathematically, an essential difference exists between linear and nonlinear systems. For linear systems, you just break up the complicated system into many simple pieces and patch together the separated solutions for each piece to form a solution to the full problem. In contrast, solutions to a nonlinear system cannot be added to form a new solution. The system must be treated in its full complexity.

While it is true that no general analytical approach exists for reducing a complex system such as a society, it can be modeled. The technique involves a mathematical construct called phase space. In this space stable structures can appear which I use as analogies for the stable structures that appear in a complex system such as an ecology, the mind or a society. The common denominator in all of these systems is that they rely on a process called feedback loops. Feedback loops link the microscopic (individual) parts to the macroscopic (global) parts. The key, then, in shaping a space society, is in effectively using feedback loops. This paper will illustrate how one can model a space society by using methods that chaoticists have developed over the last hundred years. And I will show that common threads exist in the modeling of biological, economical, philosophical and sociological systems.

PHASE SPACE VISUALIZATION OF DYNAMICAL SYSTEMS

In nonlinear science, modeling is performed on what are called "dynamical systems." This is a physical system that evolves in time according to well-defined rules. It is characterized by the rate of change of its variables as a function of the values of the variables at that time. Examples are Maxwell's equations, the Navier-Stokes equations, and Newton's equations of motion for a particle with suitably specified forces. Modeling of dynamical systems are done in "phase space." This mathematical space that has position (x) as one axis and velocity (v) as the other axis. However, sometimes scientists represent the phase space with just the spatial coordinates of the system to better visualize the dynamics. Each point in this space represents the complete behavior of the

system. For example, the position and velocity of a pendulum with one degree of freedom at any instant in time is in a two dimensional phase space. Notice that if we have a more complicated system the number of dimensions of the phase space is enormous. The reason being that the space is constructed by assigning coordinates to every independent variable (every degree of freedom requires 2 more dimensions in phase space). In fact, the dimension is taken to be infinite in the general hydrodynamic description.

Since all of the information about a system is stored in a point at one instant in time, the evolution of a system can be charted by the moving point tracing its path through phase space. The time evolution is often called a "trajectory" or an "orbit." The set of orbits originating from all possible initial conditions generates a "flow" in this space governed by a set of $2n$ first-order coupled differential equations:

$$\frac{dx_i}{dt} = F(x_1, x_2, \ldots, x_n; v_1, v_2, \ldots, v_n), \quad i = 1, \ldots n$$

$$\frac{dv_i}{dt} = F(x_1, x_2, \ldots, x_n; v_1, v_2, \ldots, v_n), \quad i = 1, \ldots n$$

where n is the number of degrees of freedom and F is the rate of change in position and velocity. This change is added to the previous values of the position and velocity to get a new x, v point in phase space, i.e.:

$$x_{t+1} = x_t + F(x_1, x_2, \ldots, x_n; v_1, v_2, \ldots, v_n)$$

for position and

$$v_{t+1} = v_t + F(x_1, x_2, \ldots, x_n; v_1, v_2, \ldots, v_n)$$

for velocity, where t represents a particular time.

One advantage of thinking of states as points in space is that it makes *change* easier to watch. If some combination of variables never occur, then a scientist can simply imagine that that part of space is out of bounds. If a system behaves periodically, then the point will move around in a loop, passing through the same position in phase space again and again. The motion of a point in phase space must *always* be non-self-intersecting. This arises from the fact that a point in phase space representing the state of a system encodes all of the information about the system, including its future history, so that there cannot be two different pathways leading out of one and the same point.

Since scientists are usually interested in the long-term behavior of dynamical systems, what will be the nature of the motion after all of the short-lived motions have died out? For dynamical systems with friction or some other form of dissipation (i.e., a nonconservative system), the system will eventually approach a restricted region of the phase space called an attractor. This is the solution set of the dynamical system. If we know the structure of the attractor, then we can sensibly claim that we know all the important things about the solution of our differential equation.

WHAT IS AN ATTRACTOR?

As the name implies, nearby initial conditions are "attracted;" the set of points that are attracted form the *basin of attraction*. A dynamical system can have more than one attractor, each with its own basin, in which case different initial conditions lead to different types of long-term behavior. The region in the $2n$ -dimensional phase space occupied by the attractor, its "volume," is, in general, very small relative to the amount of phase space.

The simplest attractor in phase space is a fixed point. Figure 1 shows the damped harmonic oscillator (Shaw, 1981):

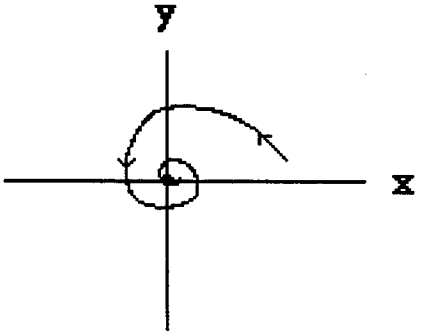

Figure 1. Damped harmonic oscillator. The equations describing motion are:

$$\frac{dx}{dt} = -y, \quad \frac{dy}{dt} = x - y$$

With fixed points, motion in phase space eventually stops; the system is attracted toward one point and stays there. Regardless of its initial position, the pendulum will eventually come to rest in a vertical position. Similarly, if a glass of water is shaken and then placed on a table, the water eventually approaches a state of uniform rest as its solution set. This is true despite the fact that the water's phase space is initially virtually infinite in dimension.

Another example of an attractor is a periodic cycle called a limit cycle. Limit cycles represent a spontaneous sustained motion that is not often explicitly present in the equations describing the dynamical system. One example where this happens is the predator-prey system used in ecological models (Prigogine, 1980):

$$\frac{dX}{dt} = k_1AX - k_2XY$$

$$\frac{dY}{dt} = k_2XY - k_3Y$$

The variable X represents a prey population that uses product A, Y represents a predator population that propagates at the expense of the prey, and k_i are constants. This relationship is usually referred

to the "Lotka-Volterra" equations. In phase space this system yields an infinite variety of close concentric orbits, as seen in figure 2. The different orbits, or periodic trajectories, correspond to different initial conditions and arise from the dynamics of the predator and prey reducing each other's populations continuously.

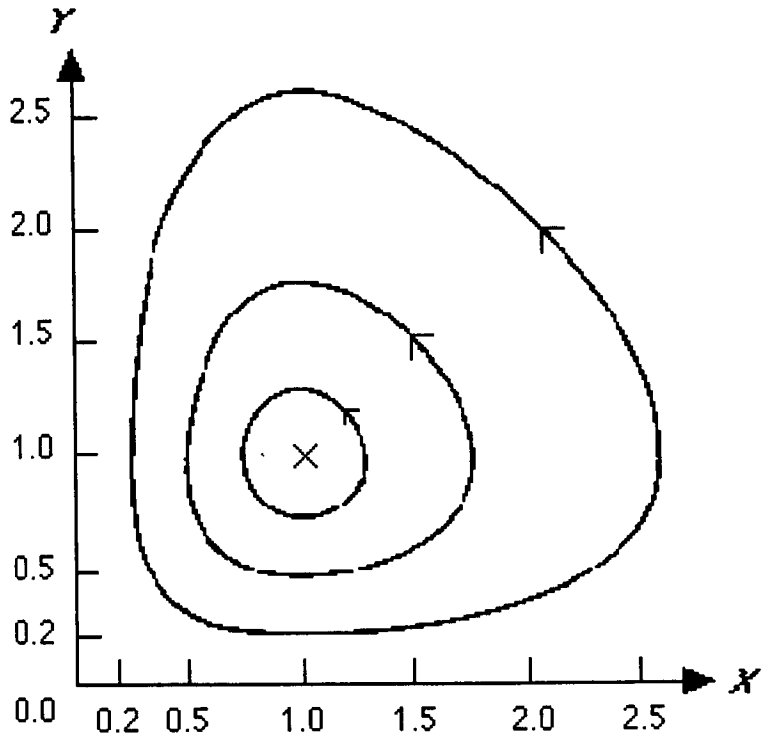

Figure 2. Periodic (Limit) cycle solutions of the Lotka-Volterra system for different initial conditions (Prigogine, 1980).

STRANGE ATTRACTORS AND CHAOTIC BEHAVIOR

In dissipative systems, one can find attractors such as the two examples just mentioned (fixed and periodic). However, one can also find a *strange attractor* . The two examples just cited are oscillating systems without any forcing. When a forcing oscillator is added to the system, one has more dimensions in the phase space and the orbits converge to an object that is neither a fixed point nor a limit cycle. It is a strange attractor. Figure 3 is an example. This strange attractor depicts the chaotic behavior of a rotor, a pendulum swinging through a full circle, driven by an energetic kick at regular intervals.

A trajectory on a strange attractor exhibits most of the properties intuitively associated with random functions, although no randomness is ever explicitly added. The equations of motion are purely deterministic; the random behavior emerges spontaneously from the nonlinear system. This is often referred to as "deterministic chaos." Over short times it is possible to follow the trajectory of

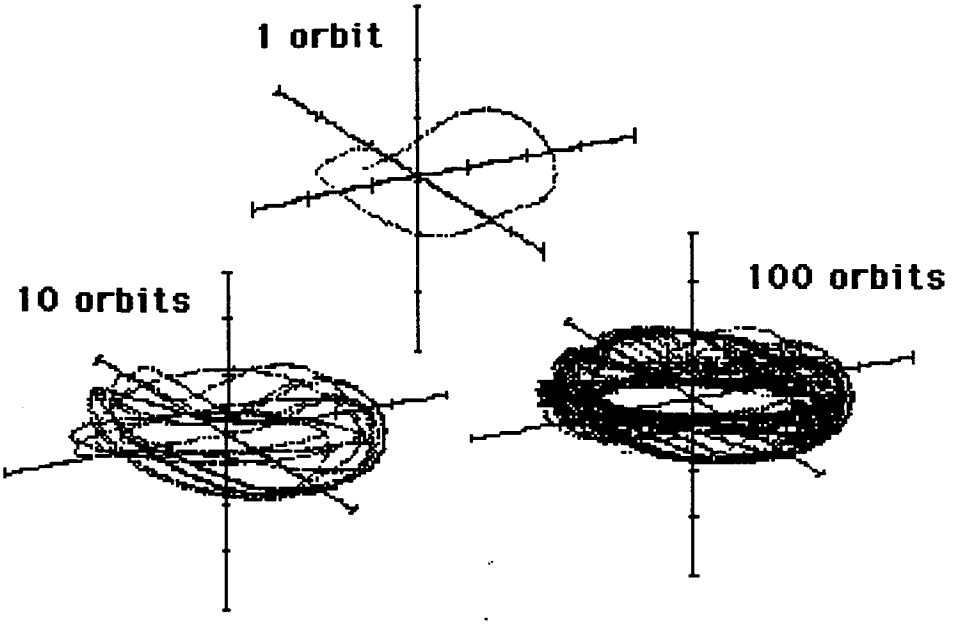

Figure 3. Snapshots in time of the Rotor strange attractor (Gleick, 1987).

each point, but over longer periods small differences in position are greatly amplified, so predictions of long-term behavior are impossible.

BIFURCATIONS AND FEEDBACK LOOPS

I've now introduced phase space, attractors, strange attractors, and chaos. I will tie these ideas with what I call "emergent order" in this section.

In many dynamic systems there will be an instant in time when something as small as a slight fluctuation in density or a slight rise in temperature will be amplified by the iteration function F to a size so great that the system takes off in a new direction. This behavior is called a bifurcation, and it is the beginning of a qualitatively different solution of the underlying mathematical model. There are different types of bifurcations. In addition, bifurcations can combine with each other to produce a new state (steady, periodic, quasi-periodic, or chaotic) of the dynamic system. Figure 4 diagrams bifurcations. This figure was derived using a relationship for population growth called the "logistic map," which was first investigated by P. F. Verhulst in 1845. The Verhulst relationship is:

$$X_{n+1} = kX_n(1 - X_n)$$

where X represents the size of population, and k is a constant called the birthrate. As k increases, the system undergoes a bifurcation where there are two possible outcomes for population size and, therefore, the system periodically oscillates between them. When the birthrate increases again, we have four, eight, sixteen different population sizes. Finally, when k increases again, the total population size becomes chaotic. The chaotic zones are the dark regions filled with points. The bands of white are windows of stability where the system becomes stable and predictable again.

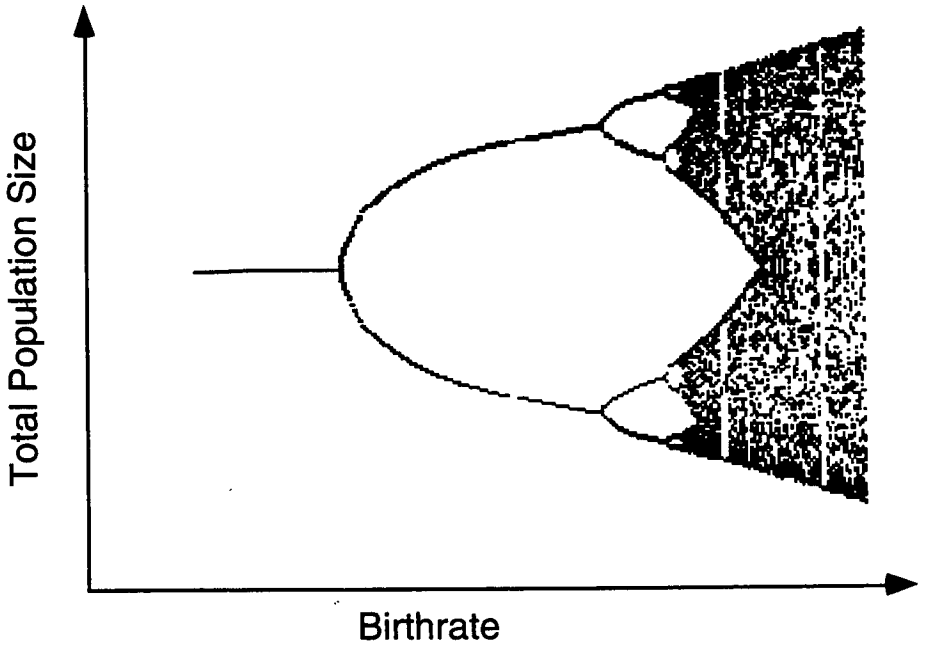

Figure 4. A model describing population growth called the Logistic Map (Stewart, 1989).

Over the course of time cascades of bifurcation points either cause the system to fragment itself, in what is called "period doubling toward chaos," or it causes the system to stabilize a new behavior through a series of feedback loops. How are bifurcations and feedback loops related in a nonlinear model such as the one above?

To see how feedback loops are related, we can separate the Verhulst equation into two terms: kx_n and $(1\text{-}X_n)$. View the first as a "stretching" term and the other as a "folding" term. A property specific to all dissipative systems is that the volume of any set of initial conditions in phase space diminishes on the average in time. Chaoticists express this property by saying that "the flow contracts volumes in phase space." The folding term is the reason for this property in the above nonlinear system. *The folding term is our feedback loop.*

The net result of bifurcations and feedback loops in a nonlinear and dissipative system is a process that links microscopic behavior with macroscopic behavior into an unpredictable, often symmetrical, beautiful form that can be characterized in phase space by a strange attractor. Strange attractors exhibit fractal microstructure. The most beautiful aspect of fractals is a quality of self-similarity which means that any section of the fractal, when blown up, reveals itself to be just as exquisitely detailed as was the larger picture from which it was taken.

Philosophically, this process means that we have a world that is interconnected, unpredictable, but with a subtle order present. Even what appears on the surface as disorder contains a high degree of implicit correlation. Sometimes this below-the-surface correlation can be triggered and it emerges to shape the system. I call this correlation *emergent order*. The following are some common ideas that I've noticed in systems exhibiting emergent order.

COMMON THREADS IN SELF-ORGANIZED SYSTEMS

Self-organization operates on a wide range of levels. The three that I find most obvious are Minds, Ecologies/Evolution, and Free Markets. Common threads that run through all three are:

1) The order that emerges is unplanned and unpredictable.

2) Millions of things are operating under a simple set of rules while also operating in unique local conditions.

3) The rules evolve.

4) The individuals involved don't have to have knowledge or understanding of the whole system.

5) The systems regulate themselves by feedback loops.

6) The systems are as much *processes* as they are *systems* because they are continuously adapting to the fluctuations produced by the environment and as a result, matter/ life/ information is created and destroyed.

7) The systems are irreversible.

8) Intervention and attempts to control the systems will fail.

SOCIAL AND ECONOMIC EVOLUTION

Since emergent order is unpredictable and unplanned, the best we can hope for in designing a society of productive people is to create relevant elements let the elements interact. If we try to control the detailed workings of these systems, we will interfere with its own logic and obstruct its self-ordering, rather than intelligently guiding it (Lavoie, 1989). What elements can we create?

The elements we can create are rules. These rules coordinate cooperation and agreement between unknown individuals (or companies) pursuing unknown purposes. Voluntary consent between the individuals is imperative (DiZerega, 1989). All participants within the system are equal in relationship to the rules. New rules may arise out of the self-organizing process in response to changes in the environment. The rules must be general and abstract and therefore, the particular details must be left to the individuals. (Hayek, 1975). Some rules could be the rules of property, the rules of contract, and the rules of law. In addition, the individuals could agree to certain rules of morals and rules of social convention. In a society based on division of labor and exchange, all individuals work to earn an income. So another rule could be that one's productivity (and hence their income) increases if one's effort increases.

The following are two social simulations with a resulting emergent order. Both simulations use very simple rules.

EXAMPLE 1– EVOLUTION OF COOPERATION

In the early 1980's Robert Axelrod asked himself the question: Under what conditions will cooperation emerge in a world of egoists without central authority? In other words, in situations where each individual has an incentive to be selfish, how can cooperation ever develop (Barlow, 1991)? He framed this in a game that he called the "Prisoner's Dilemma." The game is that two accomplices to a crime are arrested and questioned separately. Either can renege against the other by confessing and hoping for a lighter sentence. However, if both confess, their confessions are not as valuable. If, on the other hand, both cooperate with each other by refusing to confess, then the district attorney can only convict them on a minor charge. In a collective sense it would be best for both of them to cooperate with each other. But if one has no conscience at all toward the other, and he confesses while the other one does not, then he still wins.

This game was quantified in a computer simulation and studied with methods of game theory. The problem was extended to apply to the same situation in sequential rounds so points were accumulated for each round. A computer tournament was staged in which participants sent in entries of their best strategies. The winning strategy was submitted by Professor Anatol Rapoport of the University of Toronto and was called: "Tit-for-Tat." The basic strategy was that each prisoner starts with one of the cooperative choices and then thereafter does what the other prisoner did on the previous round. The success of the strategy lies on its combination of being nice, retaliatory, forgiving and clear. These are good concepts to base any set of rules in setting up a space society. The feedback loop inherent in this strategy is a response to what the other prisoner did in the previous round.

EXAMPLE 2– URBANIZATION

Another example of a simulation with very simple rules is that of urban evolution (Prigogine, 1980). One can use a variation of the logistic equation, mentioned previously, to characterize an urban region in terms of economic functions which are located at places called cities. The economic functions are dependent on populations. The efficiency of the feedback loop in which functions and populations relate depend on the increase of the population and the competition from other rival production units. When this model is run the appearance of an economic function works to destroy the initial uniformity of the population distribution by creating employment opportunities that concentrate the population at a point. These may be destroyed by the competition from similar but better developed economic functions. Some economic functions may develop in coexistence.

Figure 5 is a temporal sequence of an urbanization using the above model of an initial uniform region, in which four economic functions try to develop at each point in a network of fifty localities.

This type of model permits an estimation of the long-term consequences of decisions concerning elements such as transportation, investments, etc.

We see, that a model such as the above offers one an understanding of emergent order resulting from the choices of the many agents operating under similar constraints and pursuing their own goals. A complex structure such a space society can be shaped in this way.

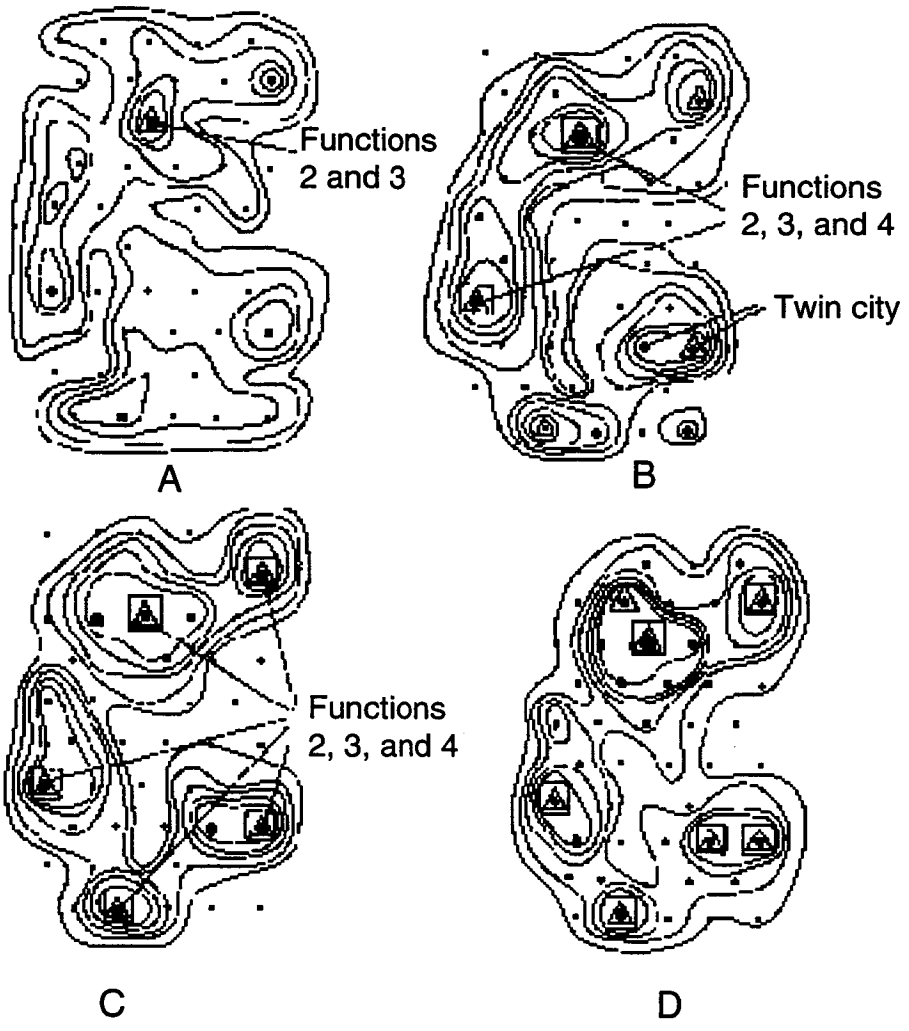

Figure 5. Urban evolution based on the logistic equation (Prigogine, 1980).

REFERENCES

Barlow, Connie; ed.: From Gaia to Selfish Genes: Selected Writings in the Life Sciences, (MIT Press: Cambridge, MA), pp. 122-129.

DiZerega, Gus: Democracy as a Spontaneous Order. Critical Review, Spring 1989, pp. 206-240.

Gleick, James: Chaos: Making a New Science. (Viking: New York, NY), 1987, p. 143.

Hayek, F. A.: Kinds of Order in Society. (Institute for Humane Studies: Menlo Park, CA), 1975, pp. 11-16.

Lavoie, Don: Economic Chaos or Spontaneous Order? the Cato Journal, Winter 1989, p. 621.

Prigogine, Ilya: From Being to Becoming. (W. H. Freeman: San Francisco, CA), 1980, pp. 96-97, pp. 124-128.

Shaw, Robert: Strange Attractors, Chaotic Behavior, and Information Flow. Z. Naturforsch., vol. 36a, 1981, pp. 80-112.

Stewart, Ian: Does God Play Dice? (Blackwell: Oxford, England), 1989, p. 323.

BIOGRAPHY

Amara L. Graps currently works at NASA Ames Research Center writing data reduction software for infrared astronomers and atmospheric scientists. Her specialties are in computational physics, computer graphics, and scientific data analysis. Her experience was gained from her current job at Ames, which she has held for six years, her previous job at the Laboratory for Atmospheric and Space Physics at the University of Colorado, and her job prior to that at the Jet Propulsion Lab.

At these jobs, she has analyzed data from NASA's Kuiper Airborne Observatory, the Voyager 2 spacecraft, the Pioneer Venus spacecraft, the Dutch's Infrared Astronomical Satellite (IRAS), and ground-based telescopes in Hawaii, California, and Arizona. The data are from Comet Halley, Supernova 1987a, Venus, Mars, Io, Saturn's and Uranus' rings, the Moon, Mercury, asteroids, Earth's atmosphere, protostars, galaxies and main-sequence stars. She got her first job (at JPL) in this field by volunteering her help to a woman who conducts a systematic search at Palomar Observatory to find asteroids. During her first trip there, she met several JPL scientists, who soon after offered her a job.

Ms. Graps earned her B.S. in Physics in 1984 from the University of California, Irvine while she was working at JPL, and her M.S. in Physics (with a Computational Physics option) in 1991 from San Jose State University while she has been at Ames.

ARCHITECTURAL DESIGN OF THE SCIENCE COMPLEX AT ELIZABETH CITY STATE UNIVERSITY

Soheila Jahromi, Contractor
Bentley Engineering
Ames Research Center
Moffett Field, California

This paper gives an overall view of the architectural design process and elements in taking an idea from conception to execution. The project presented is an example for this process. Once the need for a new structure is established, an architect studies the requirements, opinions and limits in creating a structure that people will exist in, move through and use.

Elements in designing a building include factors such as volume and surface, light and form changes of scale and view, movement and stasis. Some of the other factors are functions and physical conditions of construction. Based on experience, intuition and boundaries, an architect will utilize all elements in creating a new building.

In general, the design process begins with studying the spatial needs which develop into an architectural program. A comprehensive and accurate architectural program is essential for having a successful building. The most attractive building which does not meet the functional needs of its users has failed at the primary reason for its existence. To have a good program an architect must have a full understanding of the daily functions that will take place in the building.

The architectural program along with site characteristics are among a few of the important guidelines in studying the form, adjacencies and circulation for the structure itself and also in relation to the adjacent structures. Conceptual studies are part of the schematic design, which is the first milestone in the design process. The other reference points are design development and construction documents. At each milestone is established review and coordination with all the consultants and the user is essential in refining the project. In design development phase conceptual diagrams take shape, architectural, structural, mechanical and electrical systems are developed. The final phase construction documents convey all the information required to construct the building.

The design process and elements described were applied in the following project.

SCIENCE COMPLEX

The Science Complex at Elizabeth City State University in North Carolina was constructed in 1989 and houses the major undergraduate Science curricula at the university. Primarily, the programs include Biology, Geo-Science, Physics, and Chemistry. The entire instructional program includes classrooms, laboratories, support facilities, and faculty and administrative space. In addition, the complex features a Science theatre/planetarium and a lecture hall to be used by the community.

The following is the architectural program as approved by the university planning committee for the science complex:

		No. of Rooms	Capacity (persons)
A.	General Purpose Instructional Fac.		
1.	Lecture Hall	1	180
2.	Science Theatre/Planetarium	1	60
3.	General Purpose Classrooms	3	35
4.	Lecture Classrooms (Tiered)	2	60
5.	Seminar Rooms	4	20
6.	Micro-Computer Laboratory	1	25
7.	Library/Enrichment Center	1	—
B.	Laboratories		
1.	Biology	2	35
2.	Chemistry	2	35
3.	Physics	2	30
4.	Geo-Science	2	30
5.	Research Laboratories	16	8-10
6.	Cartography Room	1	—
7.	Animal Room	1	—
8.	Greenhouse	1	—
9.	Electron Microscope Room	1	—
C.	Support Spaces (Instructional)		
1.	Storage and Preparation Rooms	8	—
2.	Central Supply Rooms	2	—
3.	Balance Room	1	—
4.	Walk-In Freezer (Cold Room)	1	—
5.	X-Ray/Dark Room	1	—
D.	Faculty and Administrative		
1.	Department Chairpersons Office	3	1
2.	Secretary/Department Chairpersons	3	1
3.	Faculty Offices	20	1
4.	Secretarial Pool (Faculty)	1	4
5.	Faculty Lounge	1	—
6.	Conference Room	1	25
E.	Student Facilities		
1.	Student Lounge	1	—
2.	Student Organization Offices	5	—
F.	Unassigned Space		
	Mechanical Space, Circulation, Storage, Restrooms, and Other Miscellaneous Space - Approximately 35% of Net		

The gross area for the building is programmed at 56,413 square feet.

SITE DESCRIPTION

The site, located at the northeastern end of the Elizabeth City State University campus is primarily flat, typical for that region of the state. Very little vegetation existed on the site. Storm drainage, water/sewer utilities, and electrical service were all available to the site from the campus and/or from Elizabeth City.

SITE DEVELOPMENT

The site was developed in order to provide an anchor building to the northeastern end of the campus, where most of the buildings are at least 30 years old or more. The challenge in master planning this site resided in creating a landmark that would symbolize the community of Elizabeth City. Another design criteria was the harmonization of the science complex within the low-key campus atmosphere.

To stay in scale with the existing two and three story buildings, the mass of the new science complex graduates from a one-story structure closest to the existing structures to a four-story building adjacent to Hoffler Street. Figure 1 shows the layout of the site plan.

Because of its location, the site design sought to create a promenade of trees from the existing campus to the science complex plaza area.

This promenade continues through the building, creating a bifocal entrance, with visitors from off-campus having access via the Hoffler Street entrance and students and faculty gaining access from the plaza. Outdoor classrooms, science exhibits, and other university events are scheduled at this plaza. A new parking lot adjacent to the building will provide space for faculty and visitors arriving to use the complex.

DESIGN SOLUTION

The main spine of this complex is an interior pedestrian atrium (Science Boulevard) extending the campus entrance promenade (south) through the building and leading to the community entrance (north). This atrium also connects the four story laboratory classroom building to high-use spaces housing the lecture hall and the science theatre/planetarium. The primary reason for creating the science boulevard was to provide interaction among students from all veins of science, faculty and at times, community.

The four-story graduates from a one-story structure of the southeastern end of the building to a four-story structure adjacent to Hoffler Street (city street). Each successive floor houses a smaller number of functions commensurate and consistent with the program requirements. On the first floor (fig. 2) are housed general purpose classrooms, lecture halls, the science theatre, library and the laboratories for the Biology department. In addition, a connecting structure houses the animal room and greenhouse spaces, which are primarily used by the Life Sciences, and other support spaces.

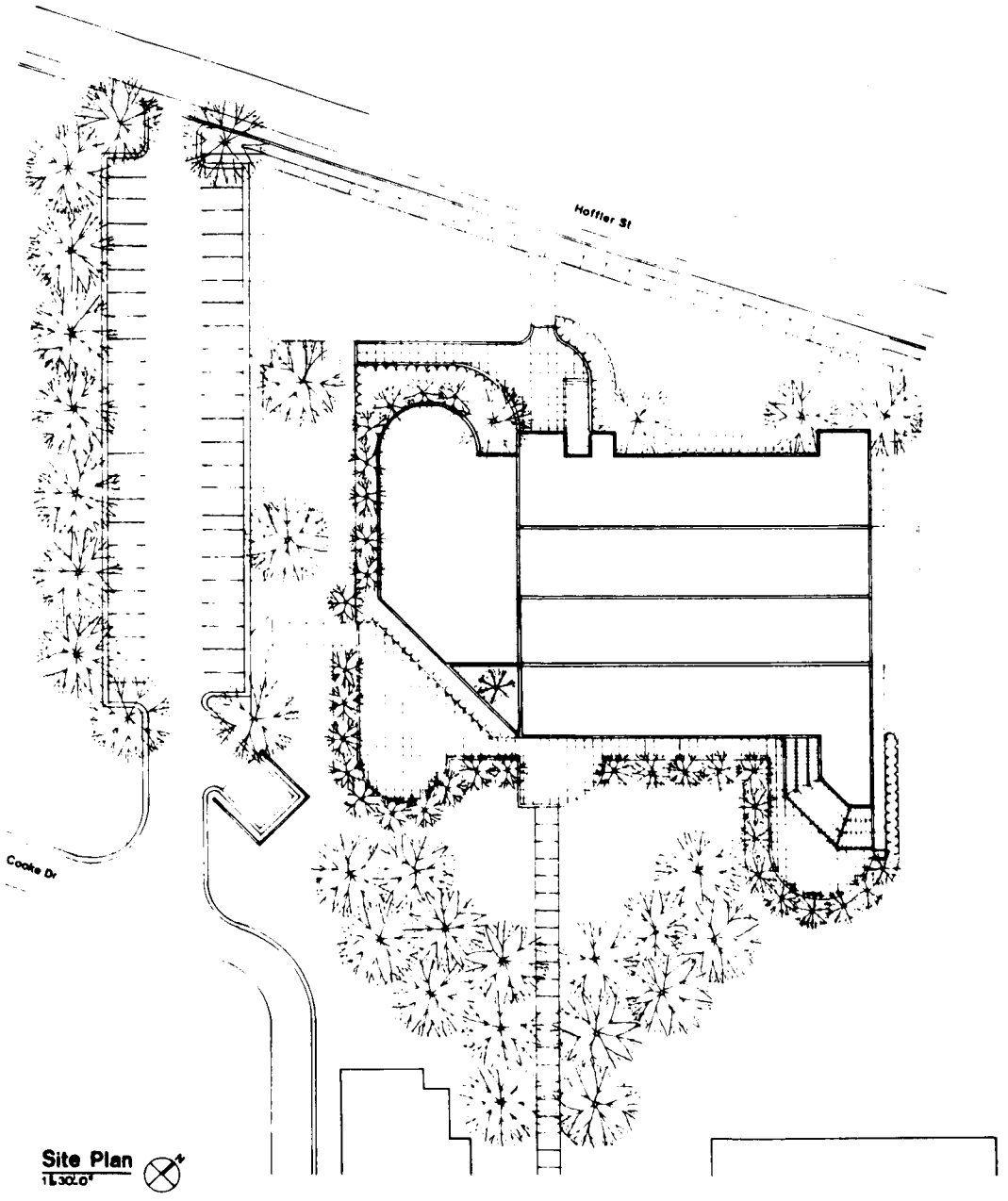

Figure 1. Site plan.

The second floor (fig. 3) houses physics and chemistry facilities, student offices, and other support spaces. The third floor, (fig. 4) the Geo-Sciences with its corresponding support area, in addition to administrative offices for department chairman. The fourth floor (fig. 5) is primarily faculty offices. The central circulation system is a large atrium corridor connecting all floors by an open stairway system (fig. 6). The form of this building followed the functional requirements. Figures 7 and 8 show model studies and elevations for this building.

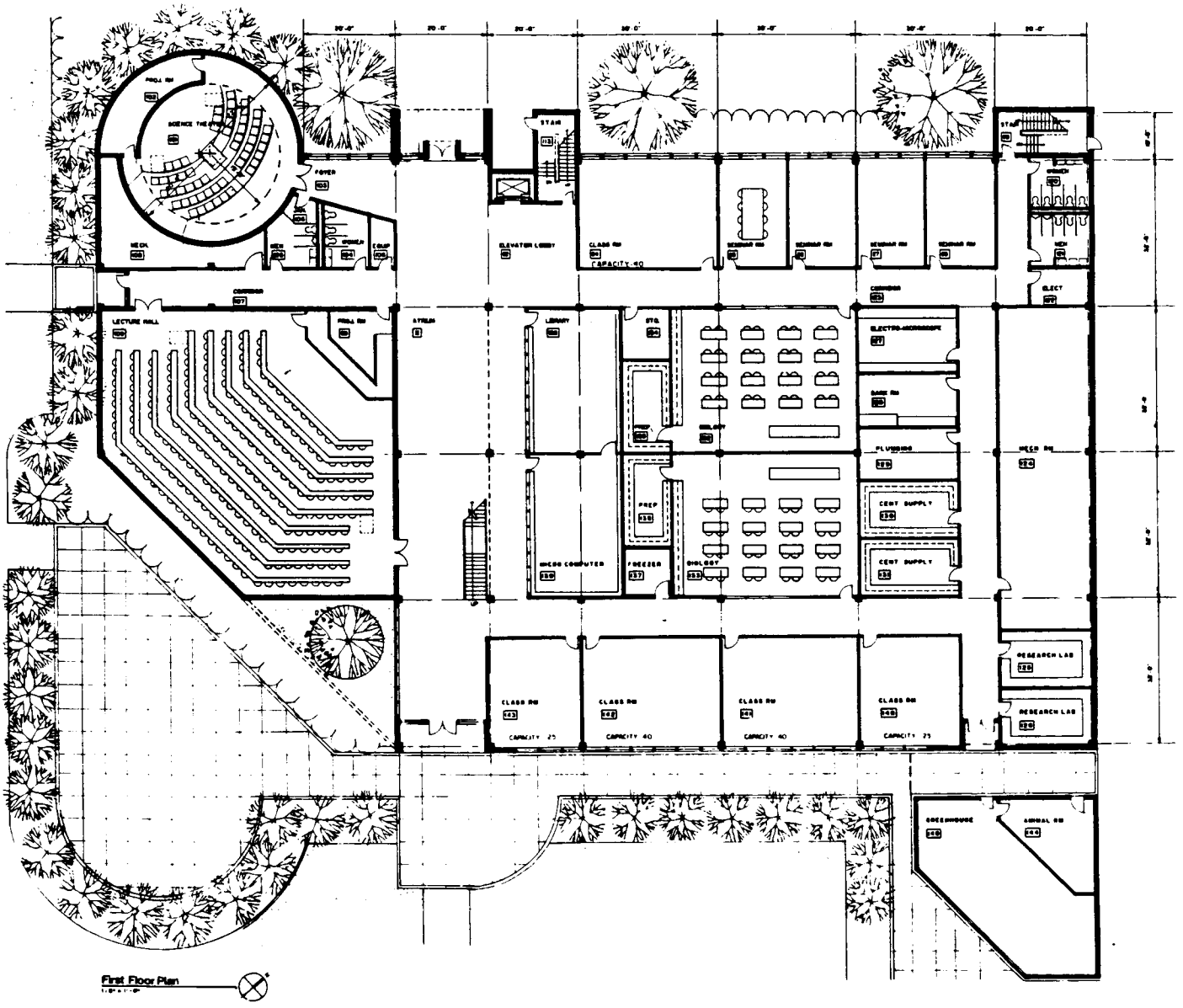

Figure 2. First floor plan (design).

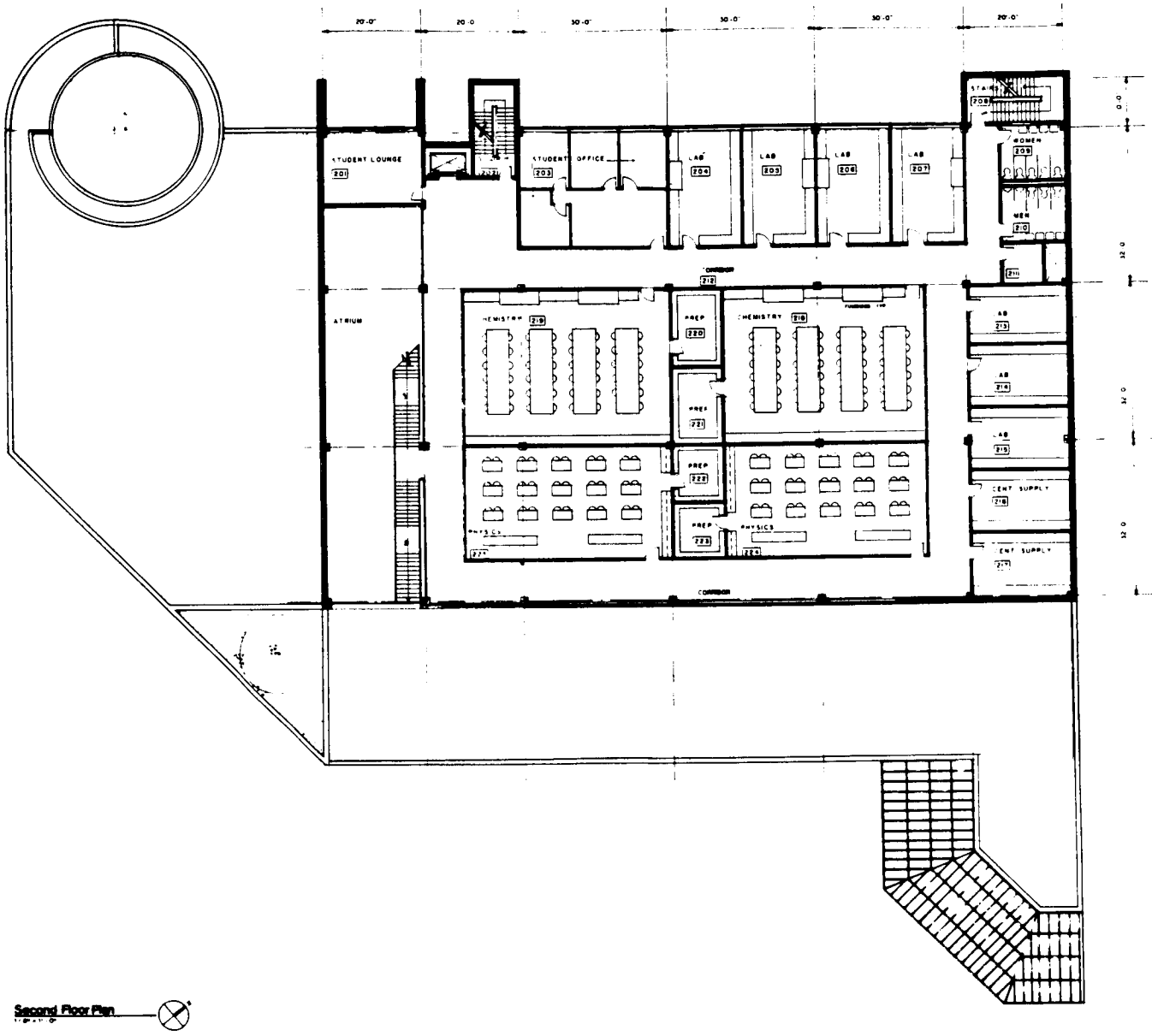

Figure 3. Second floor plan.

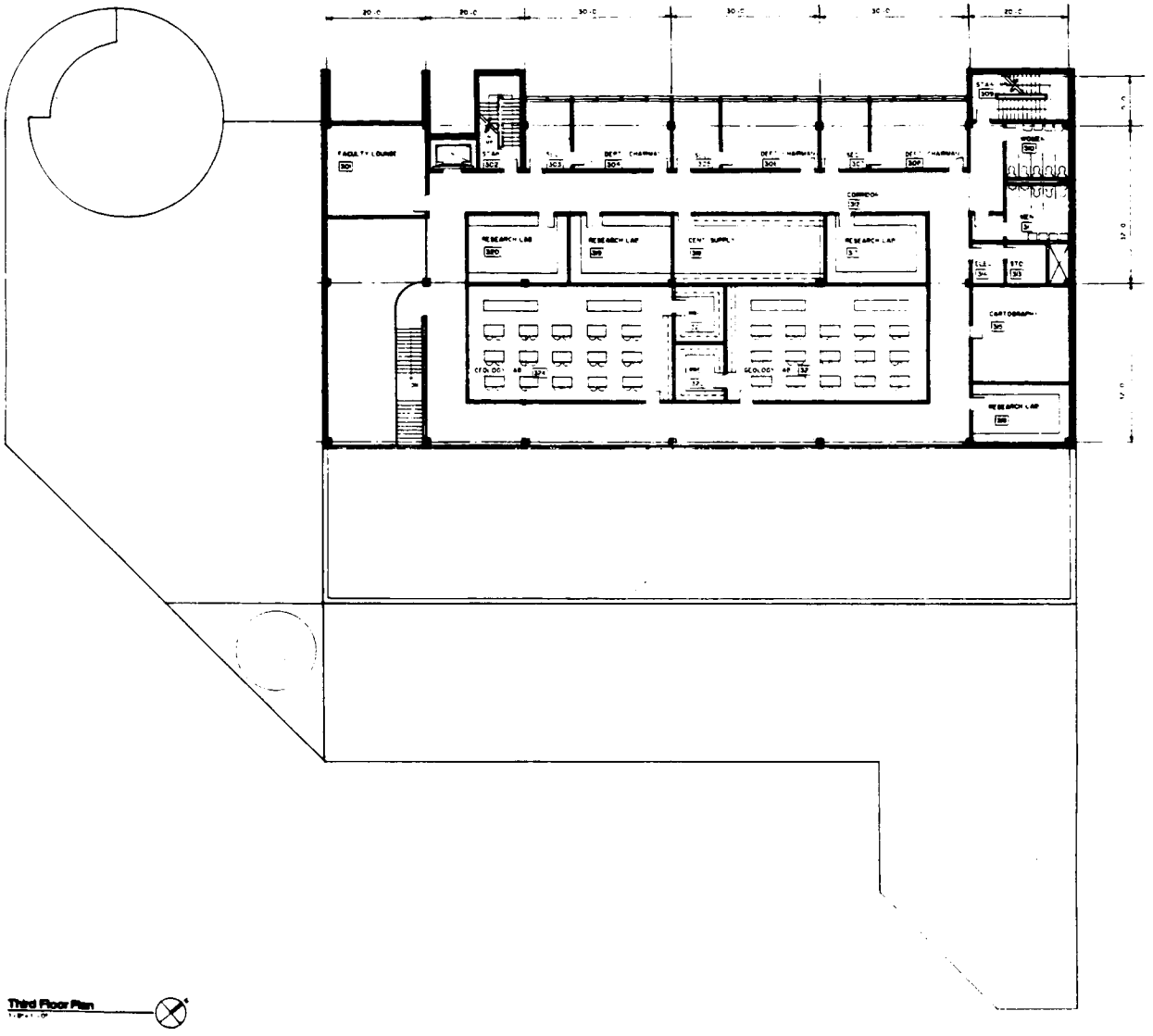

Figure 4. Third floor plan.

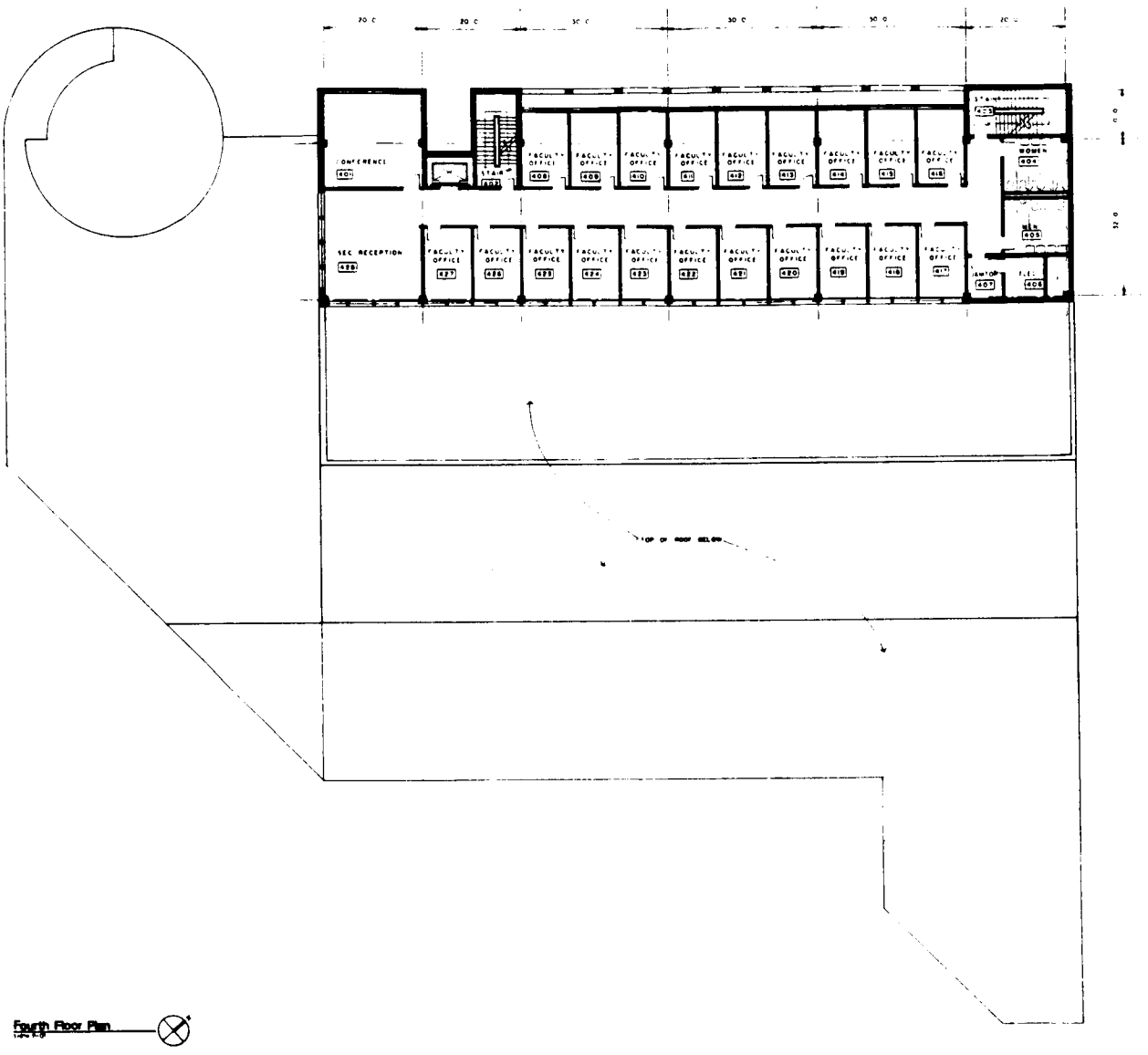

Figure 5. Fourth floor plan.

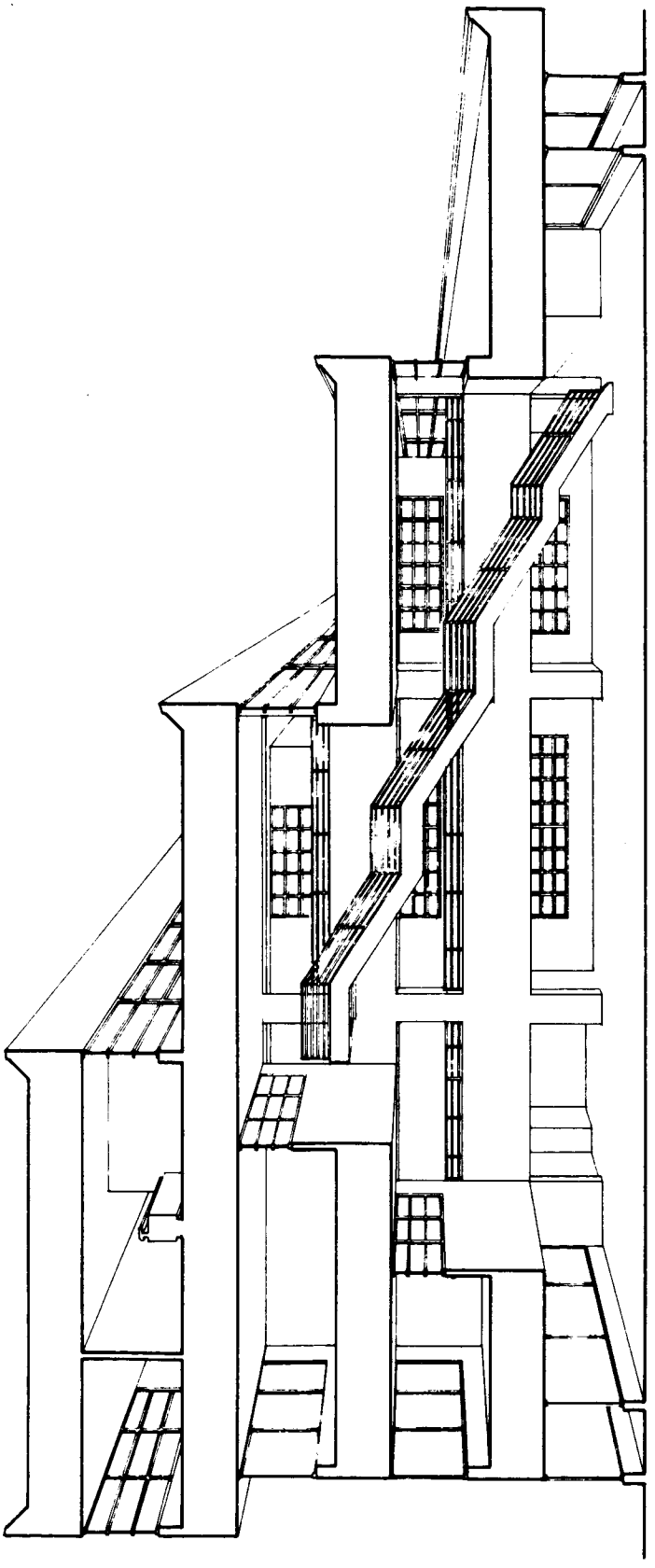

Figure 6. Sectional perspective through the atrium.

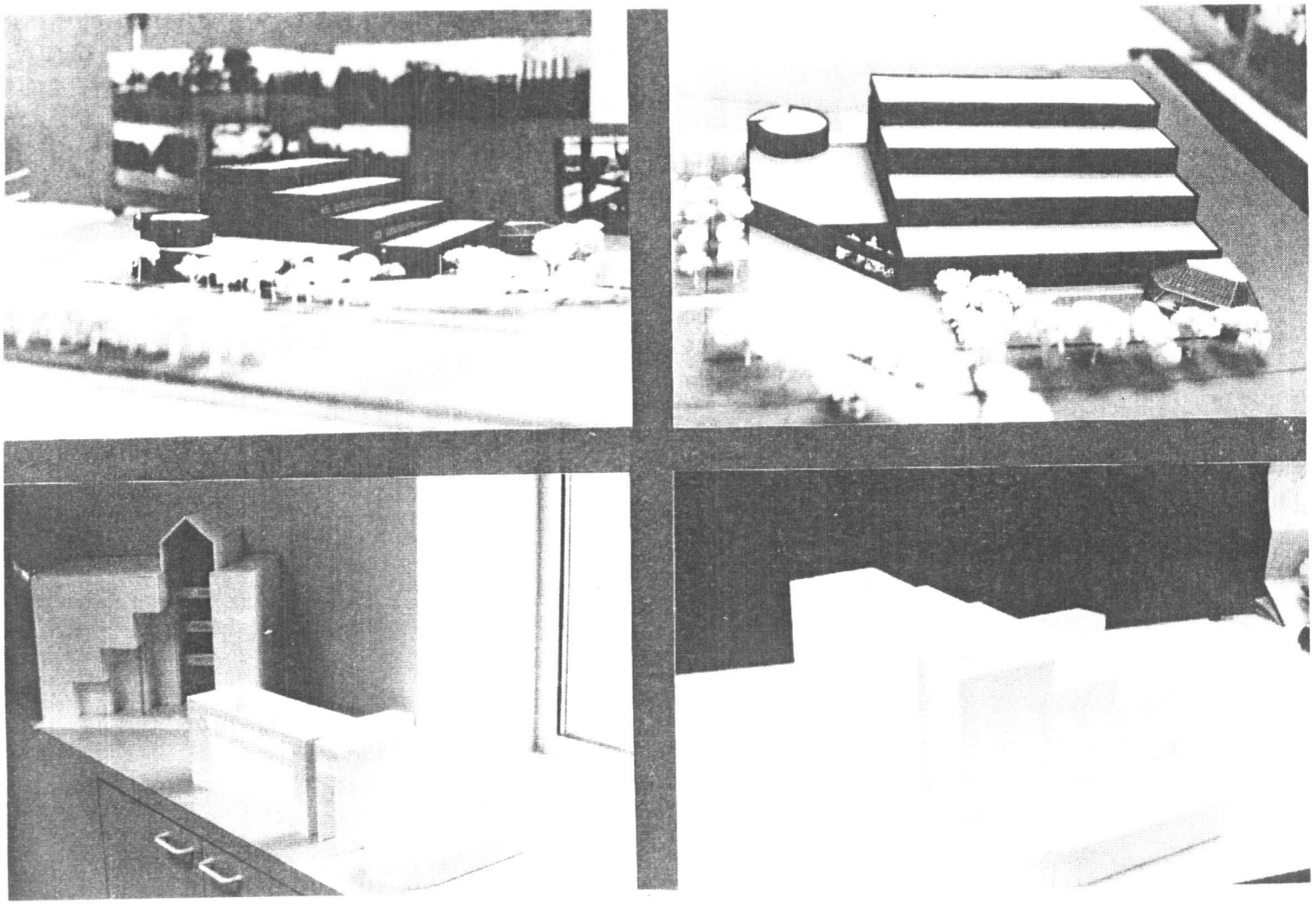

Figure 7. Model studies.

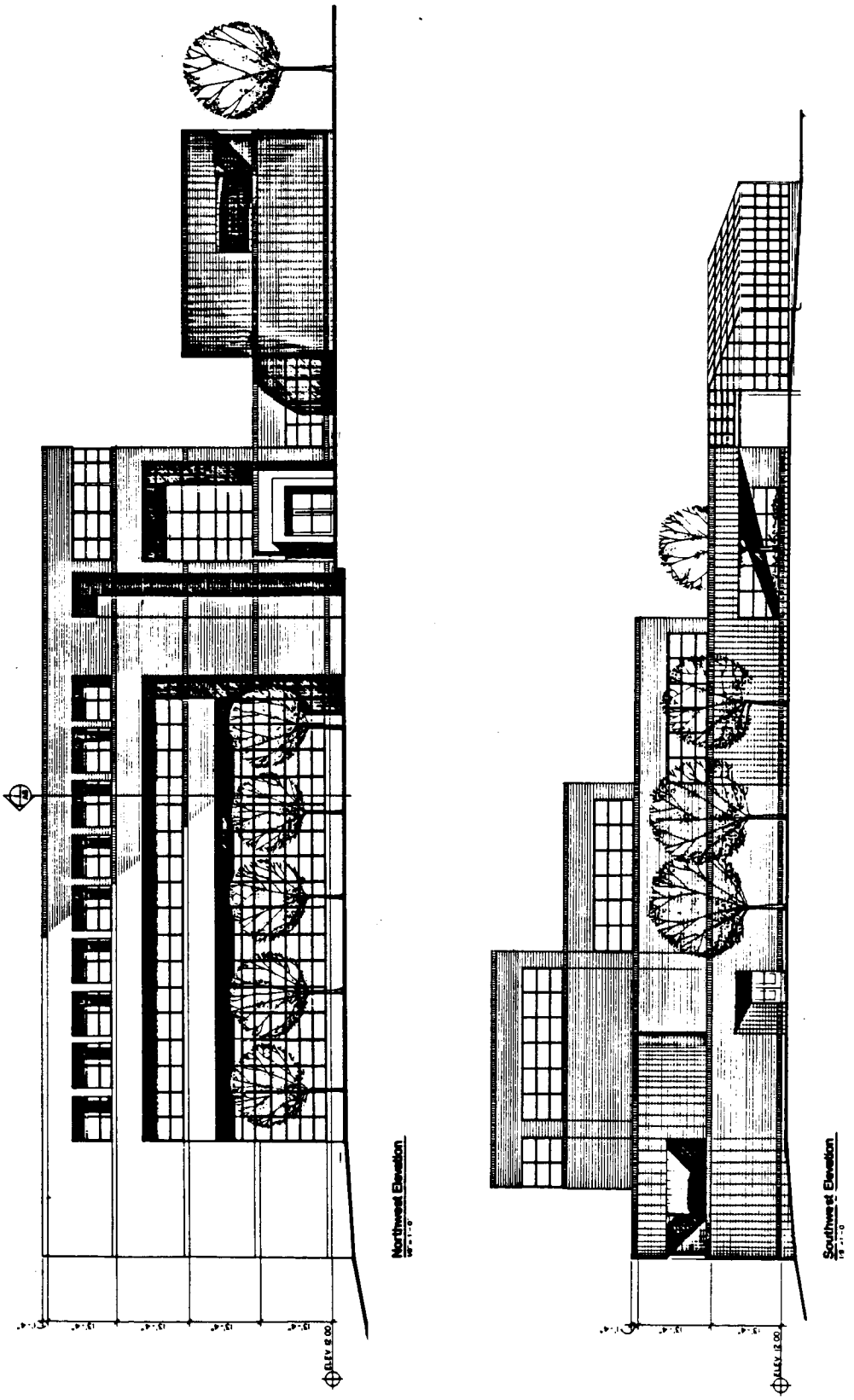

Figure 8. Elevations.

ARCHITECTURAL MATERIALS

The exterior walls are composed of 4-inch face brick (the common material for this region), 1-inch air space, 1-inch rigid insulation, and batt insulation between studs, 6-inch metal stud and gypsum board finish. All labs will have epoxy painted gypsum board. Figure 9 shows the wall section cut through the north wall.

Materials used in the building will consist of the following:

Exterior glazing consists of 1-inch tinted insulated glass and spandrel glass in aluminum frames, with fixed and operable units for ventilation and emergency egress.

Interior partitions are painted gypsum board on metal studs. Interior partitions are detailed to meet the required fire protection requirements. Doors are stave-core wood units in hollow metal frames. Exterior doors are aluminum framed with tempered glazing.

Ceilings in most areas are acoustical tile ceilings. As an alternate, the 30' 0" diameter projection dome over the Science Theatre is fuse bonded vinyl on aluminum. The dome surface is 23% perforated for acoustical purposes. The Lecture Hall has reflective panels to direct sound evenly throughout the space.

Single-ply roofing over rigid insulation is used on most roof areas. The Greenhouse is specially skylighted to meet the requirements of that space. All roofing assemblies are designed to meet a "U" value of 0.10.

Finish flooring in most areas is vinyl composition tile, with the exception of sheet rubber on all lab areas and ceramic tile floors in the toilets. The Lecture hall, Planetarium, all offices, conference room, and student and faculty lounge areas are carpeted.

Miscellaneous fixed equipment will include the following:

1. Science Theatre/Planetarium: Fixed seating; desk and special projection equipment.
2. Lecture Hall: Fixed desks and seating, chalkboard and projection screen.
3. Seminar and Classrooms: Chalkboard and tackboards.
4. Library: Library shelving, casework.
5. Labs: Most labs include a fixed experiment station.
6. Support Areas: Storage and shelving, casework, and lockers.

STRUCTURAL SYSTEM

The structural system for the four-story science complex is structural steel frame. The roof structural system is 1 1/2-inch-metal roof deck supported by H-series steel joist framed into wide flange section steel beams. The floor structural system is 2 inch composite metal floor deck with a 3 1/4-inch light weight concrete topping. Steel beams and steel girders provide support to the composite metal deck floor system.

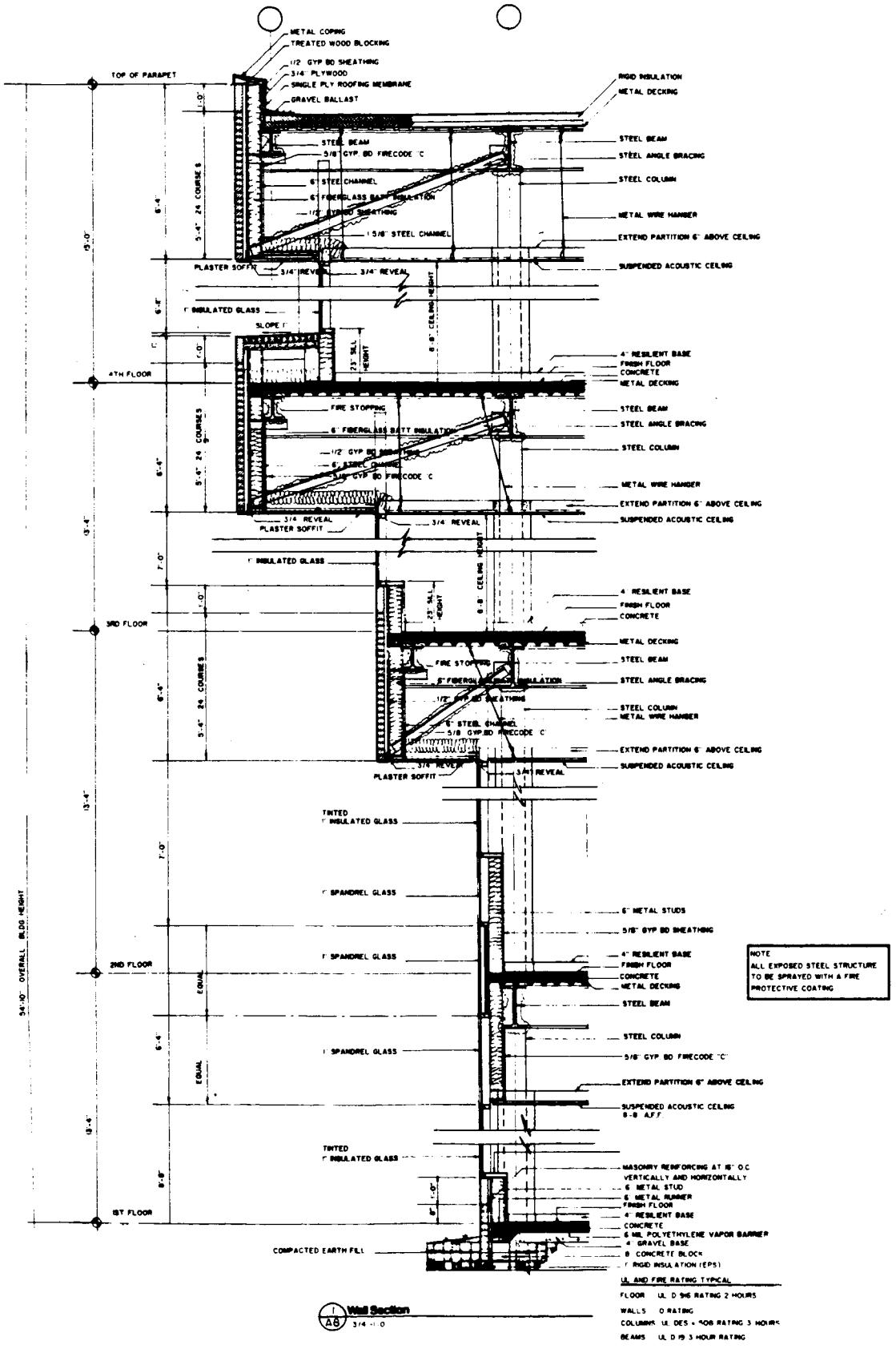

Figure 9. Wall section.

The foundation system is prestressed concrete piling driven into the dense to very dense sand.

MECHANICAL SYSTEM

Based on the data provided by a life cycle cost analysis of six mechanical system alternatives, the following was selected. The cooling system consists of two reciprocating water cooled chillers. Heat is provided by a fuel oil fired boiler. Exhaust systems: All laboratory spaces are furnished with laboratory hood and exhaust system. The laboratories are also capable of being 100% exhausted for odor and fume control.

The entire plumbing system was designed in accordance with all local, state and national plumbing codes.

FIRE PROTECTION

An automatic sprinkler system was required throughout this building.

ELECTRICAL SYSTEM

Electrical systems included the following:

1. A complete system of power distribution equipment and wiring, power connections to equipment, etc. Electrical service to the building is from a utility company padmounted transformer.
2. A complete lighting system, primarily utilizing fluorescent fixtures for interior spaces and high pressure sodium fixtures for exterior areas.
3. A system of raceways, outlets, and equipment space to accommodate the installation of telephone and other communications equipment.
4. A complete fire alarm system.

All systems—architectural, structural, mechanical and electrical—were selected in the design development phase. In the construction document phase all the details were established for conveying the information to all the prime contractors figures 10 through 12 show some examples of the construction documents. Figure 13 presents the final image of the new Science Complex for the Elizabeth City University at Elizabeth City, North Carolina.

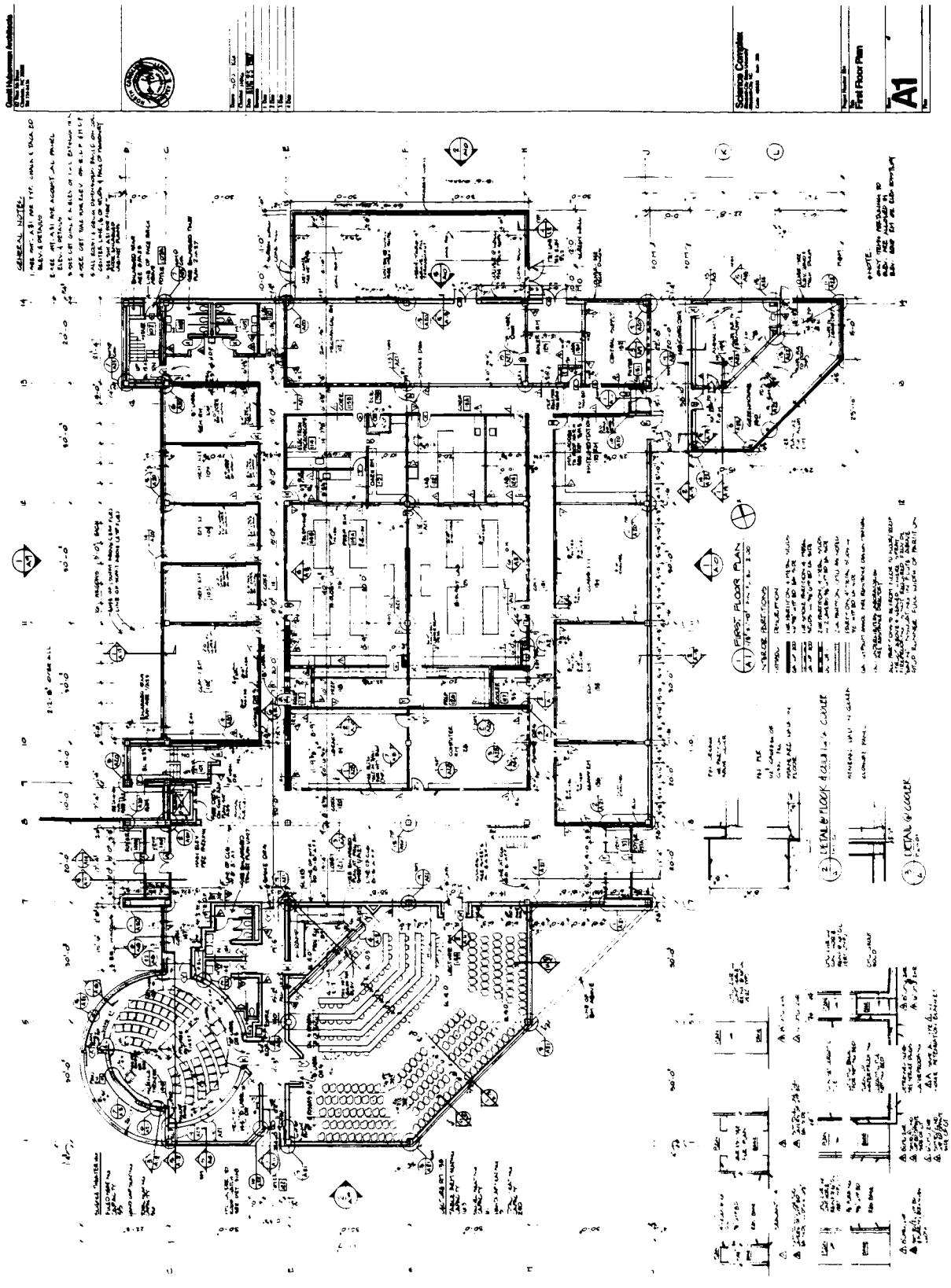

Figure 10. First floor plan (construction document).

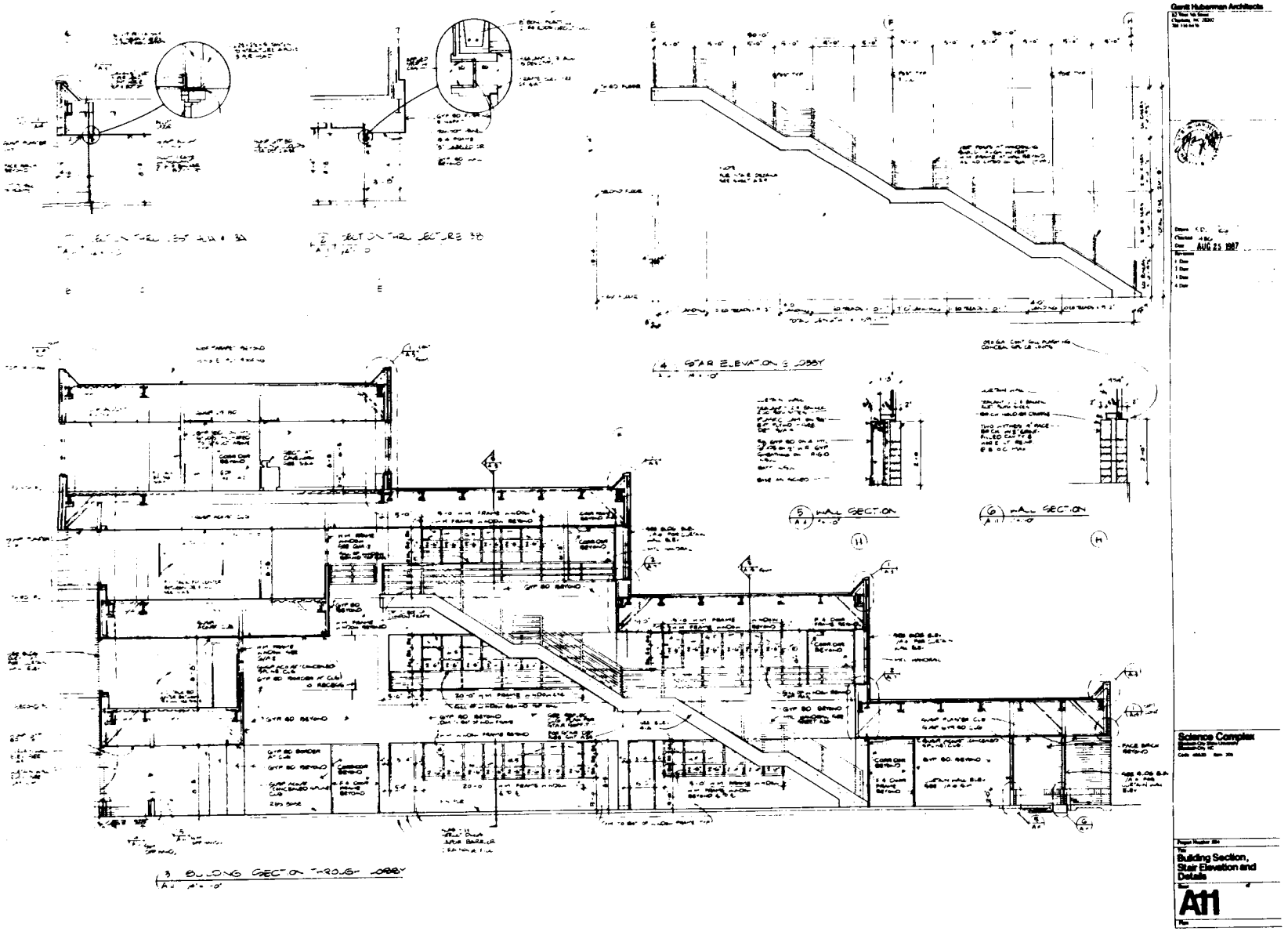

Figure 11. Section (construction document).

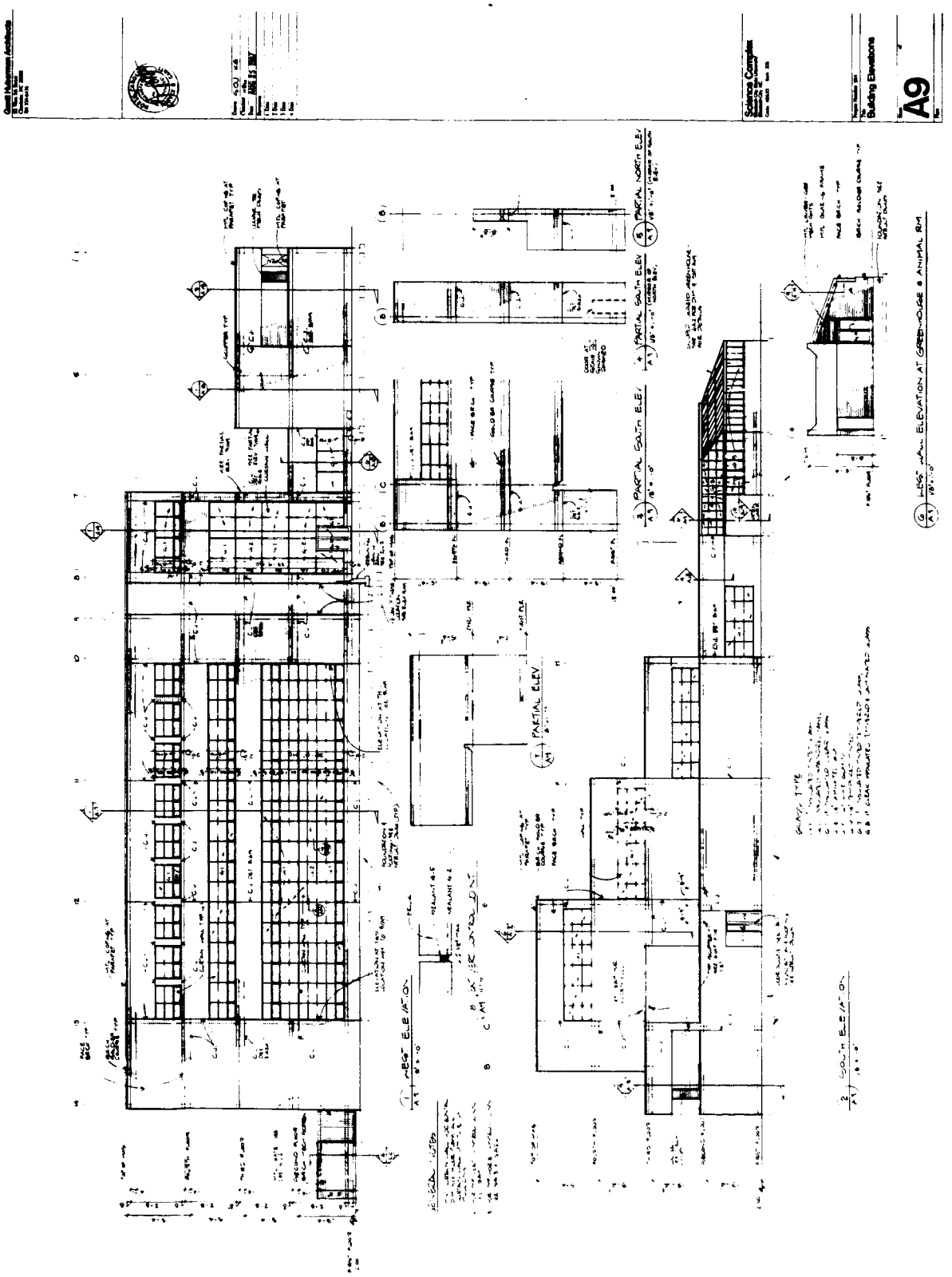

Figure 12. Elevation (construction document).

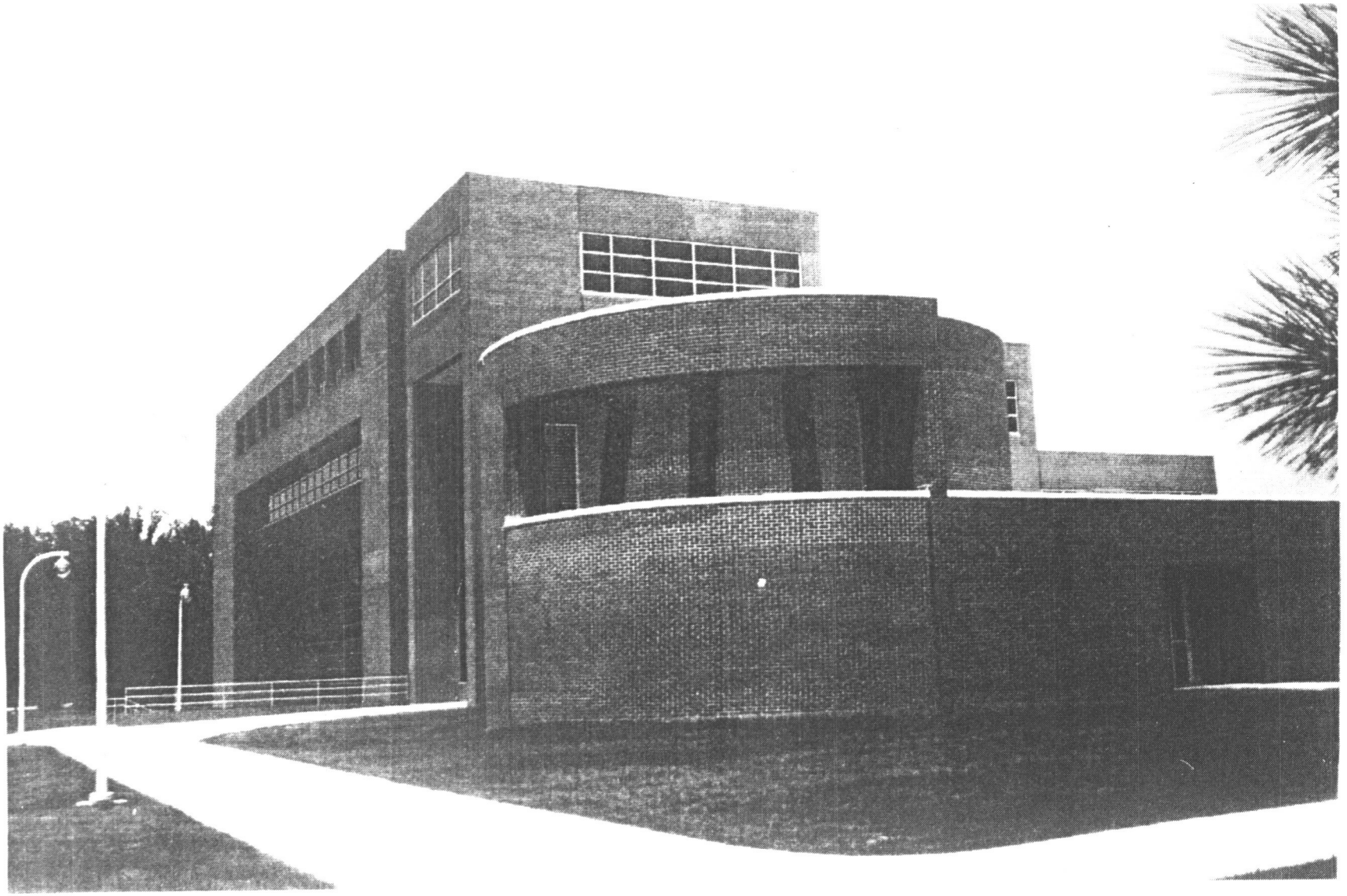

Figure 13. The Science Complex.

BIOGRAPHY

Soheila Jahromi:

I was born in 1955 in Tehran, Iran. After finishing high school, I came to the United States to attend Clemson University in Clemson, South Carolina. At Clemson I studied architecture and worked for Overstreet Architectural Co. In 1982 I completed my studies at Clemson receiving a Masters degree in Architecture. From 1982 to 1985 I worked for Overstreet Architectural and also was involved as a volunteer with "Habitat for Humanity," an organization providing architectural and construction labor services.

In 1985 I moved to Charlotte, North Carolina to work at the Architectural office of Harvey Gantt (Mayor of Charlotte, North Carolina). The project presented in my technical paper was my assignment at Gantt Huberman Architects. While in Charlotte I served on the committee board for "The Guild of Charlotte Artist." I was married in 1985 and my son was born in 1987. In 1988 we moved to the Bay Area. I am currently employed with Bentley Engineering working as a contract employee for Ames Facilities Engineering Branch. I am also a volunteer member of Disaster Assistance Response Team (DART).

THE BIOLOGICAL FLIGHT RESEARCH FACILITY

Catherine C. Johnson
Ames Research Center
Moffett Field, California

SUMMARY

NASA Ames Research Center (ARC) is building a research facility, the Biological Flight Research Facility (BFRF), to meet the needs of life scientists to study the long-term effects of variable gravity on living systems. The facility will be housed on Space Station Freedom and is anticipated to operate for the lifetime of the station, approximately thirty years. It will allow plant and animal biologists to study the role of gravity, or its absence, at varying gravity intensities for varying periods of time and with various organisms. The principal difference between current Spacelab missions and those on Space Station Freedom, other than length of mission, will be the capability to perform on-orbit science procedures and the capability to simulate Earth gravity. Initially the facility will house plants and rodents in habitats which can be maintained at microgravity or can be placed on a 2.5 meter diameter centrifuge. However, the facility is also being designed to accommodate future habitats for small primates, avian and aquatic specimens. The centrifuge will provide 1 g for controls and will also be able to provide gravity from 0.01 to 2.0 g for threshold gravity studies as well as hypergravity studies. Included in the facility are a service unit for providing clean chambers for the specimens and a glovebox for manipulating the plant and animal specimens and for performing experimental protocols. The BFRF will provide the means to conduct basic experiments to gain an understanding of the effects of microgravity on the structure and function of plants and animals, as well as investigate the role of gravity as a potential countermeasure for the physiological changes observed in microgravity.

INTRODUCTION

The microgravity environment represents an important research tool for the life sciences. Its strategic use offers unprecedented opportunities to enhance our understanding of basic biological processes. Space Biology seeks to understand how living organisms, which have evolved in Earth's gravitational field, adapt both acutely and chronically to a microgravity environment. An extension of this type of research includes the development of countermeasures to maintain physiological responses at an appropriate level. Gravitational Biology seeks to understand the role that gravity plays in all biological processes as it affects form and function. Both Space Biology and Gravitational Biology require a laboratory in the microgravity environment with a centrifuge.

An inflight centrifuge which can provide controlled acceleration (artificial gravity) between 0 and 1-g is necessary if NASA is to take full advantage of the unique research resources of spaceflight. The capability to provide varying g-levels between 0 and 1 is not possible on Earth and an inflight centrifuge fills this critical gap in the fields of Space Biology and Gravitational Biology.

Moreover, the capability of the inflight centrifuge to produce artificial gravity to levels of 2.0 g will enable hypergravity studies. The major reasons for including an inflight centrifuge in the BFRF are to provide: (1) a 1-g control; (2) a means of examining gravity threshold effects; (3) a supply of gravity-conditioned specimens; and (4) development of intermittent hypergravity countermeasures. The rationale for these capabilities are:

1-g Control

A major use of the inflight centrifuge is to satisfy the need for a 1-g control environment in order to separate the effects of microgravity from those of other environmental factors. Rigorous research standards dictate the use of adequate controls to ensure that the variable of interest is the causal factor in any observed response. To date, ground-based controls have been used as the control for spaceflight biological experiments. However, spaceflight produces far more perturbations in the environment than simply an alteration in the g-field, e.g., varying radiation, atmospheric contaminants, vibration, illumination, magnetic field, and launch/reentry stress. Only through the use of an inflight 1-g control can the effect of microgravity be isolated from these other variables.

Gravity Threshold Effects

Life has always existed under a 1-g field. Therefore, a reasonable and important scientific question is how much can the normal gravity field be reduced or increased before significant changes are seen? Or, asked from a slightly different perspective, what is the minimum or maximal intensity and duration of gravity stimulus required to elicit a gravitational response? In order to determine gravitational effects satisfactorily, it is essential that the inflight centrifuge be capable of providing different gravity levels between 0-g and 1-g. Understanding threshold gravity levels is essential to the coherent development of gravitational biology as a more exact science.

Supply of 1-g Conditioned Specimens

The centrifuge can also be used as a specimen holding facility from which 1-g conditioned animals and plants can be obtained. The transition of biospecimens to microgravity can be made in a controlled manner permitting careful and repeated observations of the acute responses to a 1-g change in the ambient acceleration field. Similarly, biospecimens can be maintained under conditions of weightlessness and then transferred to the 1-g centrifuge to simulate the return to Earth's gravity. Readaptation to 1-g often occurs so quickly that Spacelab-flown animals cannot be retrieved soon enough to allow adequate study.

Intermittent Hypergravity Countermeasures

It is anticipated that within the next few decades space travel will involve long-duration manned missions to other planets. Both the United States and the Soviet Union have relied on physical exercise as a countermeasure for the crew to ameliorate the effects such as musculoskeletal loss and

cardiovascular deconditioning caused by exposure to the microgravity environment. However, another approach may be the use of hypergravity at intermittent intervals to prevent microgravity deconditioning. The centrifuge will allow the initial systematic study of the effect of g intensity versus duration as a countermeasure in rodents.

HARDWARE

The major hardware items within the BFRF comprise a suite of hardware known collectively as the Centrifuge Facility and it is that suite of hardware which will be described in this paper. The Centrifuge Facility (CF), shown in figure 1, includes a micro-g habitat holding unit, a large diameter centrifuge, a glovebox, a specimen chamber service unit and the modular habitats which are housed either in the holding unit or the centrifuge. NASA Ames has just concluded a competitive Phase B design concept study with McDonnell Douglas Space Systems Division, Huntington Beach, CA and with Lockheed Missiles and Space Company, Inc., Sunnyvale,CA which demonstrated that it is possible to build the facility and remain within the power, volume and weight constraints of Space Station Freedom. Because these design concepts are proprietary, the discussion of the hardware will be restricted to functional and scientific uses of the hardware. The facility is an integrated suite of equipment which must function together. A key element is the modular habitat. The habitat is designed to fit either within the holding unit or on the centrifuge, and to mate with the glovebox. Hence, interfaces must be compatible between the holding unit, the centrifuge and the glovebox. Furthermore, the habitat may also be used to transport specimens to and from orbit.

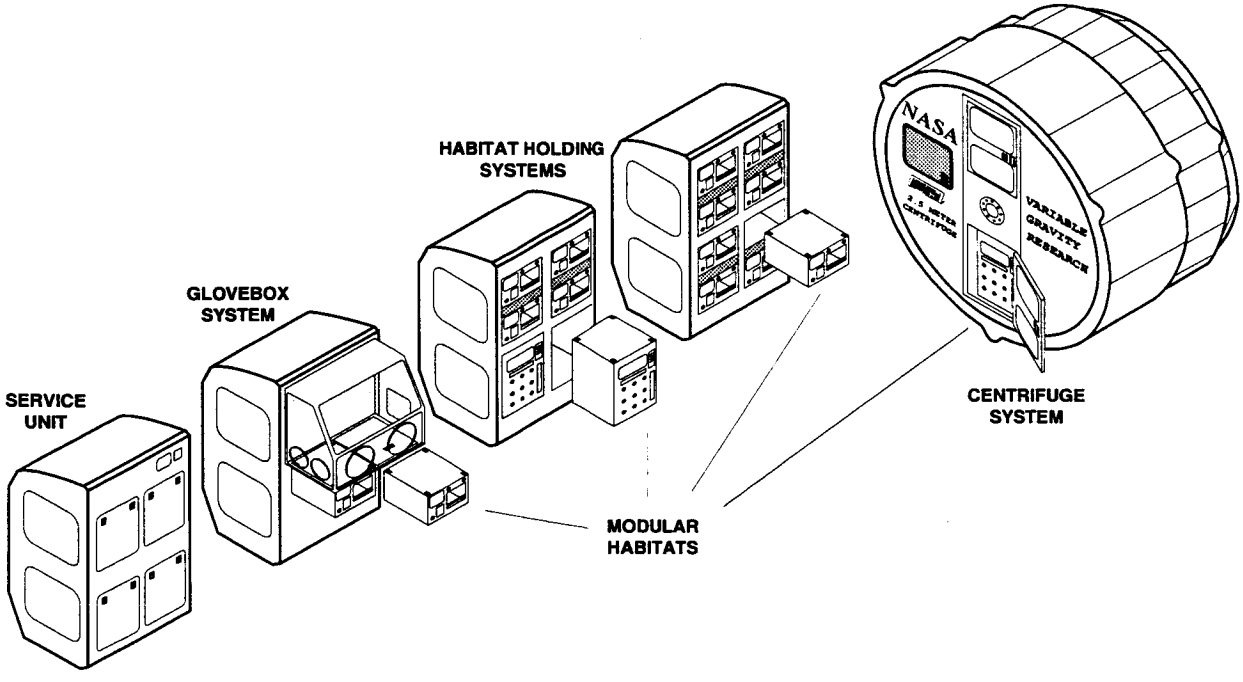

Figure 1. Centrifuge facility.

Centrifuge

A 2.5 meter diameter centrifuge has been baselined for Space Station Freedom. Initially, a 1.8 meter diameter centrifuge was proposed since that was the largest diameter centrifuge which could be mounted in a rack in the science laboratory module. However, when the decision was made to place the centrifuge in a node of SSF rather than in the science laboratory module, it was possible to enlarge the diameter to approximately 2.5 meters by mounting it in the end-cone of the node. The increased diameter of the centrifuge enhanced science capability as well as relieved engineering packaging constraints. The increased diameter of the centrifuge significantly reduced the gravity gradient across the specimens, increased the number of specimens which could be accommodated on the centrifuge and permitted the inclusion of an inner concentric row of habitats on the centrifuge rotor allowing two gravity levels to be run simultaneously. An ARC concept of the 2.5 meter diameter centrifuge mounted in a node is shown in figure 2.

The centrifuge will provide a 1-g control environment, and varying levels of g for threshold and other studies, and allow the development of countermeasures/artificial gravity techniques, including intermittent hypergravity exposures. The centrifuge will be capable of gravity levels from 0.01 to 2 g with a nominal spin-up rate which limits the acceleration experienced by the specimens to less than

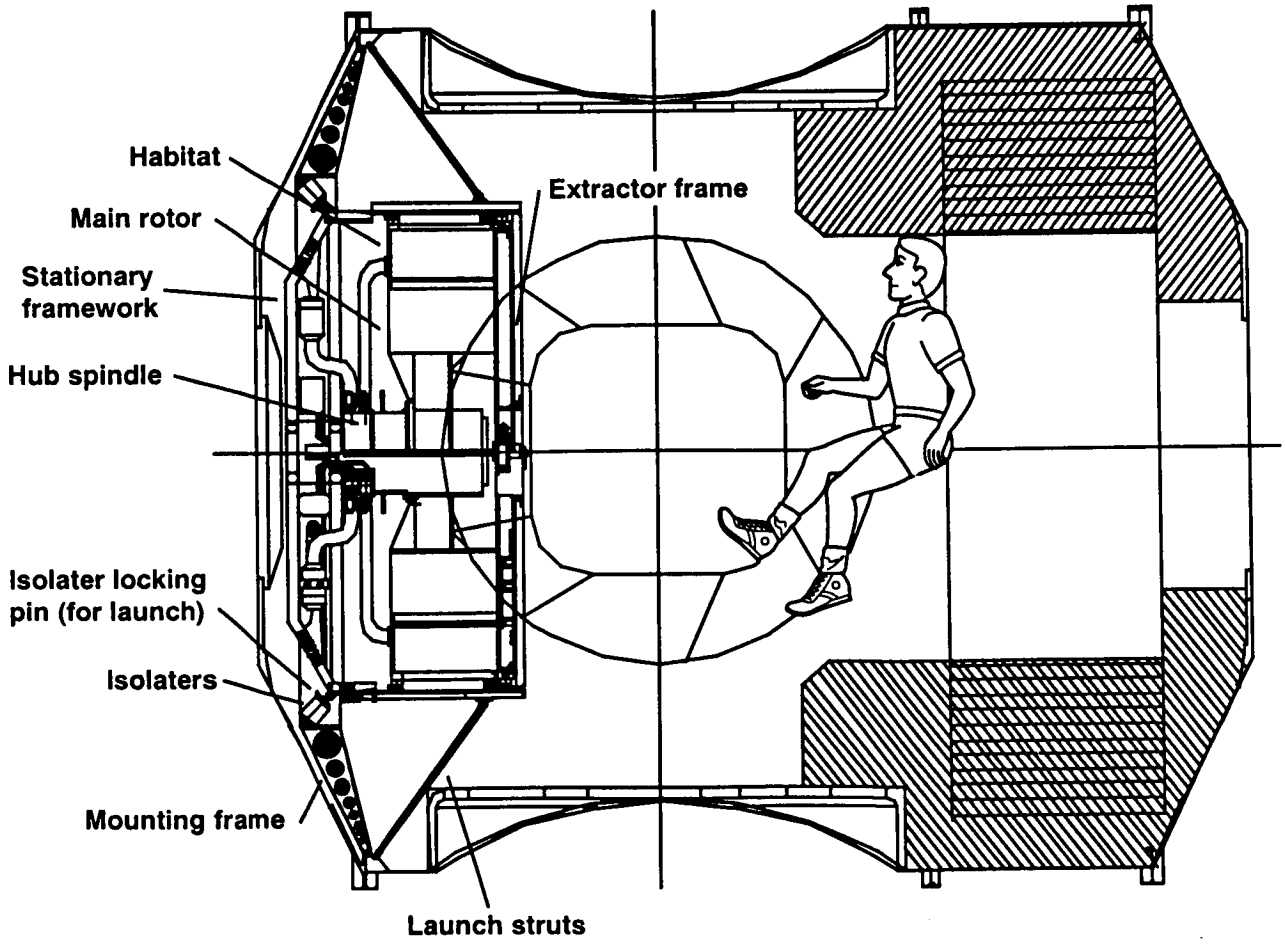

Figure 2. ARC concept of the 2.5 meter diameter centrifuge mounted in a node.

0.01 g per second. It will provide life support for both plants and animals. The control accuracy of the g level is 0.01 g at the higher g levels with less than 0.001 g vibration imparted to the specimens in the habitat in the range of 5 to 100 Hz. A momentum compensation mechanism will be incorporated into the design of the centrifuge to minimize attitude changes of Freedom during centrifuge starts and stops and the very small torque (2-5 ft-lb) due to gyroscopic effects. Several approaches have been studied, the simplest being no additional mechanism and use of the Control Moment Gyros (CMGs) of the station itself. Most cases studied show this to be a viable approach.

A unique feature strongly endorsed by the science community is a service rotor which can extract habitats from the centrifuge without having to stop the main rotor. This feature will minimize the disturbance to other habitats on the centrifuge during routine servicing of the habitats, including waste tray changeout and food replenishment. In addition to enhancing the science capability of the centrifuge, the service rotor also has some engineering benefits. It significantly reduces the mass which must be spun up and spun down for access to the specimens and hence reduces momentum compensation activity and the power required for that operation. Conversely, it increases the engineering complexity of the centrifuge by adding a subsystem which must have the capability to spin up and precisely match the speed of the main rotor, engage and extract or insert habitats and spin down.

During centrifuge operation there may be a dynamic mass balancing system to compensate for variations in mass distribution along the rotor over the life of an experiment. The balance system and vibration isolation system are expected to limit forces coming from the centrifuge to less than about 0.1 pound in the frequencies near the centrifuge spin rate. This value was derived from a preliminary analysis which attempted to determine the magnitude of a sole disturbance force that would create g-jitter in the US laboratory exceeding 10^{-6} g. The NASA Office of Space Science and Application requires this ultra quiet environment for the performance of material science's experiments. However, one must keep in mind that nominal crew movement and SSF operations may impart as much as 10^{-3} g.

Life support functions not directly incorporated into the habitat are placed on the centrifuge. In the ARC study these include air thermal conditioning and distribution, condensate collection, and specialized gas supply. The life support functions on the centrifuge are analogous to those in the habitat holding unit and are shown in figure 3.

Habitat Holding Unit

The habitat holding unit occupies a International high double rack and is capable of holding either rodent habitats, plant habitats or a combination of both. Since the habitats must be accommodated on the centrifuge, in the habitat holding unit, and the glovebox, the interface plate on each must be identical and the partitioning of services between the holding systems and the habitats must be the same.

A block diagram showing the ARC concept for life support of a habitat and the habitat holding unit is show in figure 3. The habitat holding unit and the centrifuge condition the inlet cabin air by HEPA and charcoal filtration and temperature and humidity regulation. Air enters the system

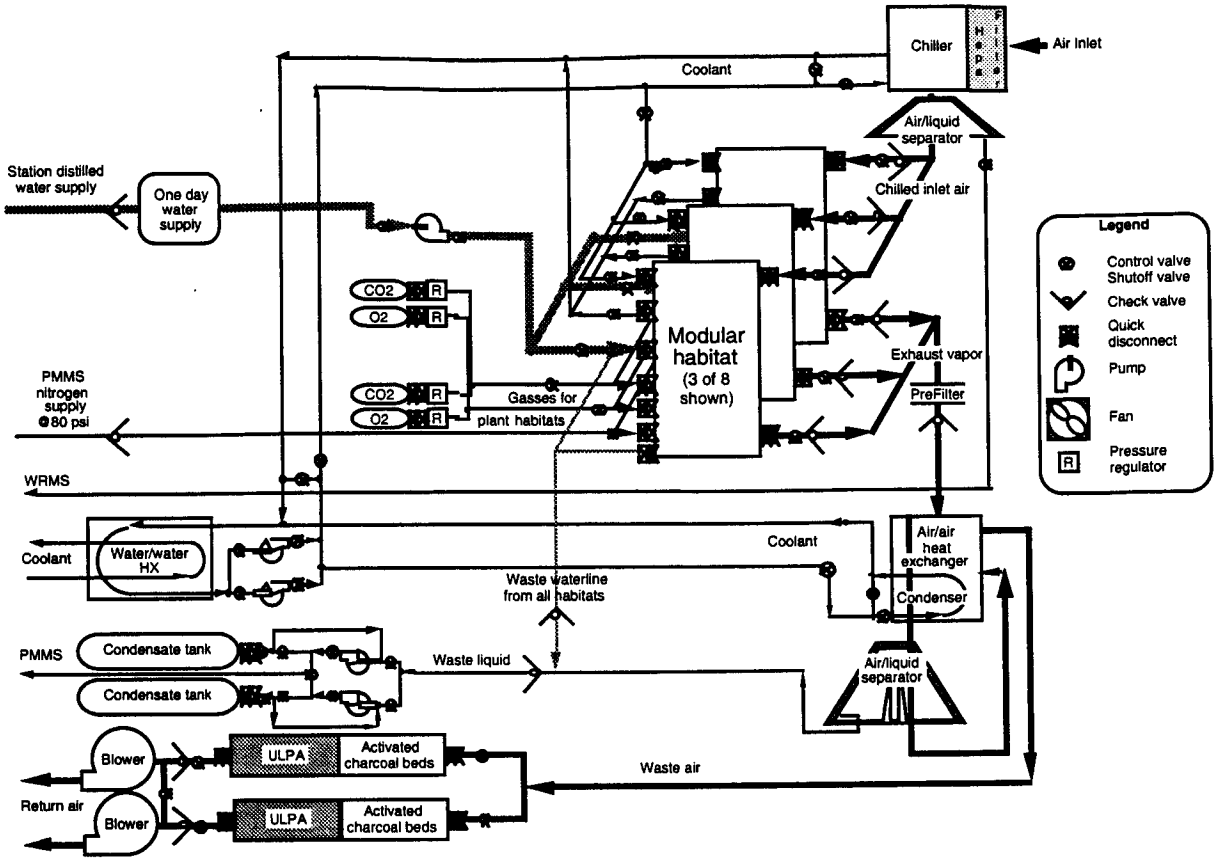

Figure 3. ARC life support block diagram for the habitat holding unit and habitats.

through a heat exchanger and an air-liquid separator which conditions it to the lowest temperature and humidity level required by the habitats. Heaters and humidifiers within the habitats adjust the temperature and humidity to the required values. Air exiting the habitats passes through an air-to-air heat exchanger and an air/liquid separator to reduce moisture content and finally through a charcoal bed and HEPA filter before returning to the cabin. This meets Freedom's particulate and ECLSS requirements of not contributing to the bioburden in the cabin or adding excess heat and humidity to the cabin atmosphere.

In addition to the life support systems mentioned above, both the holding unit and the centrifuge include a data management system and display panel for monitoring the environmental parameters of the habitats. The data management system accommodates hard-wired, telemetered data and video. The data signals are processed by the habitat holding unit subsystems to meet Freedom data network requirements prior to transferring the data to Freedom's Data Management System (DMS) which transmits the data to the ground either in real time, near real time or as time permits. The data system will have limited data storage capacity and may have data compression capability. A representative list of the types of rodent data which will be collected in the facility is shown in table 1. The system is being designed to anticipate future needs and not limit the type of data to be generated by investigators in the decades to come.

Table 1. Representative data requirements for rodents

Sensor	Sample Rate/Channel
EMG	4000
ECG	600
Tendon Force	200
Brain μelectrode	20,000
EEG	300
EOG	250
Cardiac Dimension	250
Blood Flow	300
Core Temperature	0.02

Modular Habitats

Two types of habitats are being designed for biospecimens, one for rodents and one for plants. A third habitat is under consideration for small primates but was not part of the scope of the recently completed Phase B contract. The two contractors considered the design implications of having to accommodate a larger primate habitat and designed the habitat holding unit and centrifuge in such a way as not to preclude a small primate habitat as a growth option.

Rodent habitat– The rodent habitat is to house both rats and mice either in a group or individually. The habitats differ significantly from the Research Animal Holding Facility (RAHF) currently flown on Spacelab. The major differences are level of containment (ref. 1), range of temperature, video capability both in the light and dark cycle, adjustable light level, on orbit refurbishment of cages, and hard-wired data collection system (ref. 2).

Although some of these features are mandated by the necessity to maintain biospecimens on orbit in a closed environment, others will provide greater scientific return and range of experiments than currently possible with the RAHF. Because Freedom is a long duration facility with planned increments of 90 days between resupply visits, the habitats must be designed to be cleaned on orbit efficiently and without releasing contaminants into the cabin environment. The animal habitats will provide two levels of containment. The habitat itself provides a physical barrier and is also maintained at a negative pressure (minimum 0.5" water gauge) with respect to the cabin atmosphere. Thus, if the physical integrity of the habitat should fail, the leak would be into the habitat rather than into the cabin environment. All servicing of the habitat will be performed at the glovebox. No servicing will be done at the rack front as is done on Spacelab. The habitats will be provided with an auxiliary fan for air circulation while the habitats are being transported from the habitat holding unit or the centrifuge to the glovebox. The habitats will mate with the glovebox in such a manner as to prevent particulates from escaping into the cabin. Two methods of cleaning the specimen chambers were investigated—washing of the soiled chambers and replacement with disposable chambers. The latter method was chosen because it did not require any power and because it was felt that the technology for recycling water from a cage washer was not sufficiently mature.

The temperature within the rodent habitats will be controllable over the range of 18-27° C ±1° C in increments of 1° C. Precise control of this parameter will extend the range of experiments to be performed on orbit to include study of the thermoregulatory system and the use of compromised rodents, e.g., hypothymectomized rats. The inclusion of a video system to monitor animals during both the light and dark cycle will permit behavioral studies as well as provide needed activity data to further elucidate observed changes in the musculoskeletal and cardiovascular systems attributed to the microgravity environment. The habitats will also provide control of the illuminance and the photoperiod. The illuminance will be controllable over the range of 5-100 lux in increments of 5 lux and the photoperiod will be controllable to within ± 1 minute with independent adjustable light and dark periods without being constrained to a 24 hour cycle. This will permit controlled experiments to determine the effect of the microgravity environment on response to light levels, on circadian rhythms and on the thermoregulatory system.

Plant habitat– The science requirements for the plant habitat are ambitious and may be difficult to achieve, especially during the early phases of Space Station Freedom . If achievable, they will provide a unique facility in which to conduct basic plant physiology and far surpass the environmental control achievable with the Plant Growth Unit (PGU) currently used in the Shuttle middeck (ref. 3). Some of the science requirements are: temperature control in the range of 15-30° C ±1° C; independent atmospheric control of O_2 (5-27% ± 0.5%) and CO_2 (300-5000 ppm ± 1%), ethylene <5 ppb, air velocity 0-10 changes/hour ±5%, photon flux 0-600 μmole/m^2/s ±5%, solid or liquid growth matrix, and field or subdividable growing area. Engineering studies by the Phase B contractors suggest that it is not possible to meet all of the science requirements simultaneously and that it will be necessary to restrict the range in which they can be met. For example, at high flux levels it is not possible to meet the current temperature uniformity requirement at low air velocity. Hence one must either relax the temperature requirement or relax the requirement to provide low air flow at high flux. Nevertheless, even if the above requirements cannot be fully met, the flux level and control of atmospheric conditions in the plant habitat will be a significant improvement over the PGU (75 μmoles/m^2/s and open loop to cabin environment). The plant habitat provided for the BFRF will provide sufficient control of the necessary parameters to advance Space Biology and Gravitational Biology, particularly in the areas of photosynthesis, metabolism and nutrient transport. It will also provide much needed information on how to design the next generation plant habitat for use in the microgravity environment.

Other habitats– Although the CF is only providing rodent and plant habitats, the habitat holding unit and centrifuge are being designed with sufficient capability and flexibility to accommodate advanced habitats, i.e., metabolic, avian, aquatic, provided that these habitats can meet the interface requirements These include compatible air, water, thermal control, data, and power connectors. Accurate temperature and atmospheric control and monitoring capability within the advanced habitats would be within the habitats themselves, as they are in the rodent and plant habitats.

Specimen Chamber Service Unit

Initially, the specimen chamber service unit (SCSU) was envisioned as a cage washer capable of washing and sterilizing specimen chambers for reuse and of recycling the water required for that process. However, an ARC study concluded that it would be more feasible and resource-effective to

provide disposable specimen cages than to wash the cages on orbit and to recycle the dirty water (ref. 4). The SCSU is essentially a storage unit which will supply clean specimen chambers, waste management trays, and food for the rodent habitats as well as storing the spent units. Because dirty specimen chambers and waste trays will also be stored in the SCSU, it will be necessary to incorporate into the design of the SCSU a waste management subsystem to limit and control the release of biologically produced gasses. The waste management subsystem will have to meet Freedom's requirements for particulate, microbial, and odor control.

Glovebox

The glovebox, in which all servicing and experiment protocols will be performed, is classified as a modified Class III Biological Cabinet because it does not have a dunk box or an airlock and vents to an interior space. Instead, the habitats and equipment transfer boxes will mate in a fully sealed manner with the glovebox to meet Freedom particulate containment requirements. Moreover, because Freedom is a closed environment, sufficient contamination control will be included in the glovebox air exchange system to prevent the release of chemicals which could exceed the Spacecraft Maximum Allowable Concentration (SMAC) levels. The current Space Station volume allocation limits the glovebox to an International standard double rack but that volume may constrain the performance of life sciences experiment tasks. In order to accommodate two workers simultaneously, a glovebox which can be deployed into the aisle is proposed. The ARC concept is shown in figure 4.

Data and electrical ports to support experiment unique equipment and general laboratory support equipment will be provided in the work volume. Also included will be a video system for recording/transmitting operations within the glovebox. In addition to performing the functions normally associated with a Class III Biological Cabinet, the glovebox will provide some life support to the habitats while they are connected to it for servicing and performance of experiment protocols. The glovebox will have an interface plate identical to that in the habitat holding unit and centrifuge which will provide power and air to maintain the specimens at nominal conditions. While connected to the glovebox, the specimens will be maintained at approximately cabin temperature and humidity.

CONCLUSION

The pieces of hardware described above are the major elements of the Centrifuge Facility. The centrifuge occupies the equivalent of two standard double racks but will be mounted in the end cone of a node or in a specialized module to take advantage of the full diameter of the Space Station structure. The habitat holding unit, specimen chamber service unit and glovebox each occupy a standard double rack bringing the volume of the Centrifuge Facility to approximately five double racks or six double racks if two habitat holding units are included. The power requirements of each of the standard double rack elements is within the 3 kW supplied to each rack by Station.

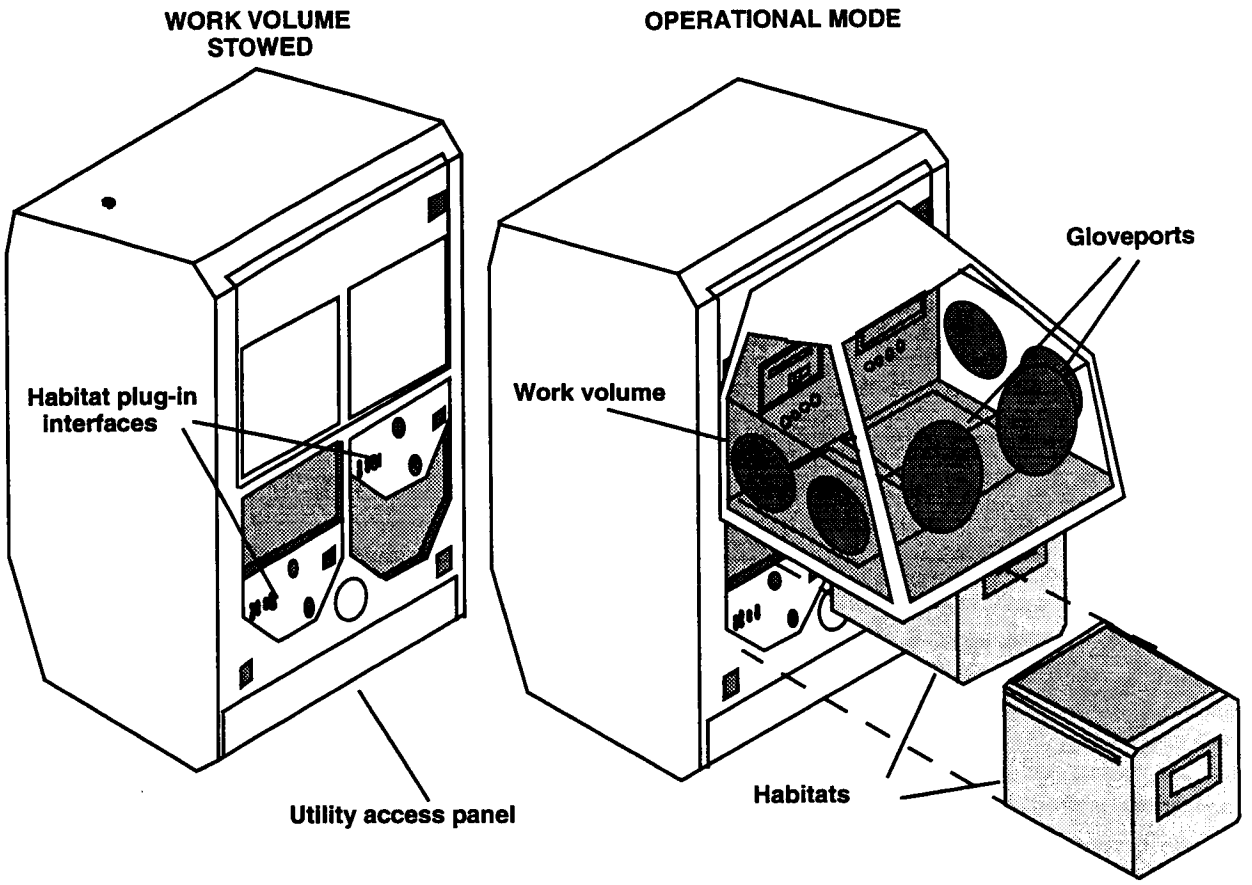

Figure 4. ARC concept for a deployable glovebox.

The Centrifuge Facility represents a major commitment to the performance of Life Sciences research on Space Station Freedom by the NASA Office of Space Science and Applications. It will continue the investigations begun on Spacelab and greatly expand the capability to perform onboard analyses. The Facility will permit the life sciences community to fully exploit the microgravity environment and use gravity as a research tool to understand basic biological processes and the response of both plants and animals to the lack of gravity. Information learned from understanding the mechanism by which plants and animals adapt will provide the foundation for designing effective countermeasures for man's eventual exploration and habitation of the moon and Mars.

REFERENCES

1. Funk, G. A. and Johnson, C. C.: Bioisolation Concepts for Life Sciences Research on Space Station Freedom. SAE Paper No. 911475, presented at the 21st International Conference on Environmental Systems, July 15-18, 1991, San Francisco, CA.

2. Synnestvedt, R., ed.: Centrifuge Facility Conceptual System Study. NASA TM-102860, October 1990.

3. Cowles, J. R.; Scheld, H. W.; Lemay, R.; and Peterson, C.: Growth and Lignification in Seedlings Exposed to Eight Days of Microgravity. Annals of Botany 54, Supplement 3, 1984, pp. 33-48.

4. Calvisi, M. L. and Sun, S. C.: Trade Study Comparing Specimen Chamber Servicing Methods for the Space Station Centrifuge Facility. SAE Paper No. 911597, presented at the 21st International Conference on Environmental Systems, July 15-18, 1991, San Francisco, CA.

BIOGRAPHY

Catherine C. Johnson received a Bachelor of Arts in Biology from Stanford University in 1963 and has been employed at NASA Ames Research Center since 1964. She analyzed lunar samples from the Apollo 11 Mission both in the lunar quarantine facility at Johnson Space Center and at Ames Research Center for evidence of biologically significant compounds and microbial life. She also worked on the development of the gas exchange experiment which flew on the Viking lander to Mars and on the Solar Sail for a proposed rendezvous with Halley's Comet. She joined the Biological Flight Research Projects Office (BFRPO) in 1985 where she is the science task manager. The BFRPO is responsible for developing hardware to support non-human life sciences research on Space Station Freedom. Prior to joining the BFRPO she worked in the area of Advanced Life Support specializing in water reclamation and solid waste management using reverse osmosis, wet oxidation and supercritical water oxidation technology. She is a member of the American Institute of Aeronautics and Astronautics and of the American Society of Gravitational and Space Biology. She has published over 40 papers, holds a patent, edited two NASA Technical Memorandum, and served on several technical committees. She is the recipient of two NASA Achievement Awards and three NASA Certificates of Recognition. She is married to Richard D. Johnson and has two sons, Eric 20 and Greg 12.

TECHNIQUES FOR OPTIMAL CROP SELECTION IN A CONTROLLED ECOLOGICAL LIFE SUPPPORT SYSTEM

Ann McCormack, Cory Finn, and Betsy Dunsky
Ames Research Center
Moffett Field, California

SUMMARY

A Controlled Ecological Life Support System (CELSS) utilizes a plant's natural ability to regenerate air and water while being grown as a food source in a closed life support system. Current plant research is directed toward obtaining quantitative empirical data on the regenerative ability of each species of plant and the system volume and power requirements. Two techniques were adapted to optimize crop species selection while at the same time minimizing the system volume and power requirements. Each allows the level of life support supplied by the plants to be selected, as well as other system parameters. The first technique uses decision analysis in the form of a spreadsheet. The second method, which is used as a comparison with and validation of the first, utilizes standard design optimization techniques. Simple models of plant processes are used in the development of these methods.

INTRODUCTION

To date, life support technology is based solely on physical/chemical processes, and this is likely to remain true for the initial phases of the Space Exploration Initiative. However, for long-duration missions, such as a trip to Mars or long-term habitats on the Moon or Mars, a CELSS has the potential to provide human life support with significant cost and safety benefits over the currently envisioned physical/chemical systems. In particular, food resupplied from Earth may be significantly diminished, higher plants can accomplish both air revitalization (through the release of oxygen and uptake of carbon dioxide) and water processing (through transpiration), and some waste disposal may be accomplished biologically. Figure 1 shows an example of an integrated biological and physical/chemical life support system (CELSS) as conceived by Dr. John Rummel, a NASA scientist/administrator. Other studies have resulted in variations on this conceptual design (refs. 1-3).

Normally, a trade study is conducted to determine advantages and disadvantages of various design options. Trade-study techniques can be developed in parallel with research on basic performance parameters, so that when reliable data become available, the analysis tool is also ready to perform trades. These tools will become increasingly important as we begin to address the complexities involved in integrating biological components with physical/chemical life support system components.

To date, most research in the use of plants for life support has concentrated on productivity levels and the effects of environmental parameters on productivity. Little work has been done in evaluating the air and water regeneration and waste management capabilities, which would be the next logical

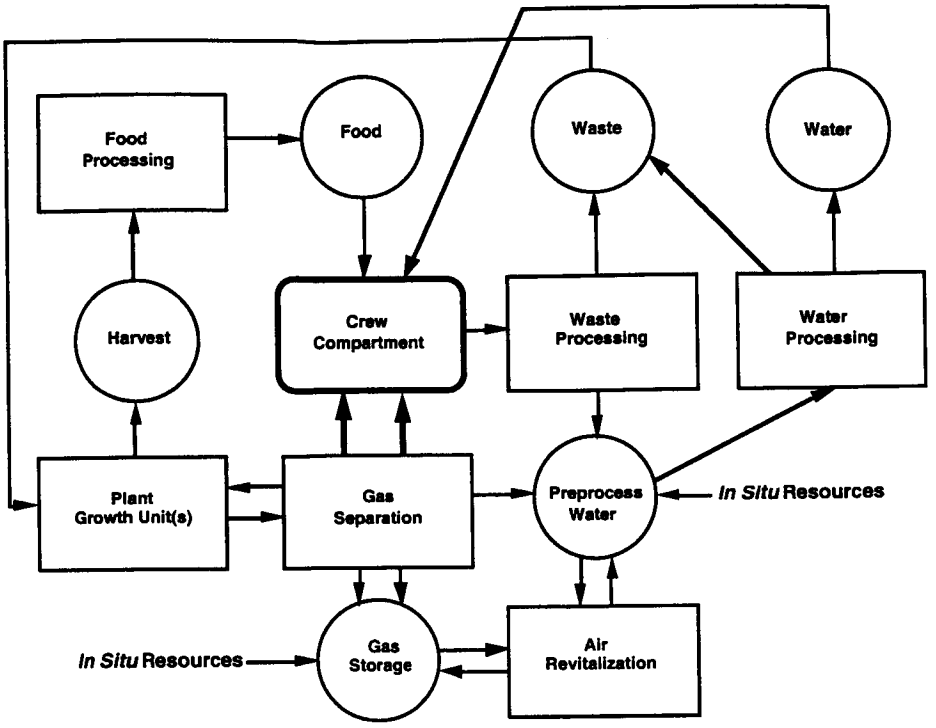

Figure 1. Conceptual design for a controlled ecological life support system.

step towards developing an integrated life support system. The techniques outlined herein transform newly acquired plant performance data into parameters describing a CELSS system for use in trade studies, thus providing the link between generating data and developing an optimal CELSS design.

We are adapting two techniques to optimize crop selection for minimum power and volume penalties. The first technique involves the use of decision analysis which implements a decision tree. The second method, intended to be both a comparison with and a validation of the first, involves the use of standard design optimization (linear programming) techniques. Previously, design optimization techniques have been applied to crop mix selection to select the minimum crop area which satisfies human nutritional requirements (ref. 4). While the results of that study do not account for power penalties, nor do they allow for air and water regeneration constraints, some comparisons can be made with our own data. These comparisons are reported in the results section of this paper.

A spreadsheet is used as an interface with the user and to generate plant and system parameters. The user specifies the level of life support to be supplied by the plants for each life support function, oxygen generation, carbon dioxide uptake, water regeneration, and nutrient (carbohydrate, lipid, and protein) production. Plant parameters are generated both directly from input, empirical data and from models of plant processes. However, the techniques are intended to be generic and applicable to other plant parameter generation schemes.

APPROACH

Derivation of Plant and System Parameters for Input to Analyses

Parameters specifying system requirements are input into the spreadsheet section shown in table 1. Here the user can input which crops of those whose performance data has been entered into table 2 should be considered. Up to five crops can be chosen. If variety in the crop mix is desired, a minimum number of crops can be entered (a number greater than one will force multiple crops to be chosen). Currently this feature only applies to the decision analysis method. The level of life support to be fulfilled by plants and the daily life support requirements (ref. 5) are input into table 1, as well as the power and volume penalties (refs. 6 and 7) and end-to-end lighting efficiency.

Table 2 lists parameters which were obtained from the literature and other sources of plant data (refs. 8-12). These parameters include each species' rate of transpiration and biomass growth as well as diet composition, edible fraction, and chamber height requirement. The lighting level and photoperiod under which these rates have been measured are also recorded and used for the power requirement calculations. There are a myriad of other factors that influence plant productivity, transpiration rates, edible fraction, and even diet composition, such as carbon dioxide level, oxygen level, nutrient solution composition, temperature, and humidity. These influences could be added in a more sophisticated effort to derive the parameters for the analyses input, but are not necessary for our purposes of technique development and demonstration.

Table 3 lists the parameters describing plant species performance required by the optimization methods. Generation of these parameters can be accomplished in many different ways, from using empirical data to employing modeling techniques. We have elected to use a combination of these two methods, largely because gas exchange data for plant species are limited. Parameters which are more readily available from empirical data are used directly and as the basis for some simplified relations used to generate the remaining parameters.

Transpiration rate and biomass production rate are taken directly from the empirical data recorded in table 2. The fat, carbohydrate, and protein production rates are products of the biomass generation rate, $\dot{m}_{bio}$, the edible fraction, and the fraction of the total biomass generation, which is fat, carbohydrate, and protein, respectively.

$$\begin{bmatrix} \text{fat generation} \\ \text{carbo. generation} \\ \text{protein generation} \end{bmatrix} = \dot{m}_{bio} * (\text{edible fraction}) * \begin{bmatrix} \text{fat fraction} \\ \text{carbo. fraction} \\ \text{protein fraction} \end{bmatrix}$$

Carbon dioxide and oxygen generation rates are difficult to find in the literature, but are products and reactants of photosynthesis and respiration, as is biomass production. This link between biomass production and gas exchange rates is described by the photosynthetic equation, assuming respiration is ignored. The chemical reaction of photosynthesis varies with the biomass type being formed, whether it is fat, carbohydrate, or protein. For simplicity, here it is assumed that carbohydrate is the substance formed. The photosynthetic equation describing carbohydrate formation is (ref. 13).

$$6CO_2 + 6H_2O \rightarrow C_6H_{12}O_6 + 6O_2$$

Table 1. CELSS specifications input

CELSS Specifications Input Table

Species to choose between (upto 5)	
1	LETTUCE
2	POTATOES
3	WHEAT
4	Y
5	SOYBEANS
Minumum number of species required	1

Portion of Life Support Requirments Fullfilled by Plants	
% Oxygen	100
% Carbon Dioxide	100
% Water	40
% Lipids	25
% Carbohydrates	100
% Protein	25

Penalties	
Cost/kW power	1.44
Cost/m3 volume	1.56

System Parameters	
Lighting System Efficiency	0.3

Life Support Requirements for 1 Person	
Oxygen [Kg/day]	0.84
Carbon Dioxide [Kg/day]	1.00
Water [Kg/day]	31.26
Lipids [gm/day]	105
Carbohydrates [gm/day]	633
Protein [gm/day]	76

Table 2. Plant performance data for model input[a]

Plant Model Input Table (Species listed in Alphabetic order)	1 Plant Species	2 Trans. Rate [Kg/m2 day]	3 Biomass Growth Rate [Kg/m2 day]	4 Biomass Edible Fraction	5 Lipids [% Tot. Bio.]	6 Carbohydrates [% Tot. Bio.]	7 Protein [% Tot. Bio.]	8 PPF Level [umol/m2 s]	9 Lighting Photoperiod [hr/day]	10 Height Required [m]
	LETTUCE	1.02	0.6	0.8	5	58	22	485	18	0.3
	POTATOES	6.41	0.136	0.8	0.5	85	10	725	20	0.11
	SOYBEANS	7.7	0.3	0.4	35	20	40	532	12	0.2
	WHEAT	9.98	0.4	0.5	2	82	14	534	20	0.6
	X	3	0.3	0.7	15	65	5	400	20	0.2
	Y	5	0.7	0.5	3	87	2	600	20	0.3

[a]Crops X and Y have been added to enlarge the database. These two "species" are not real; the data from them merely illustrates the development of this tool.

Table 3. Plant performance data for analyses input

Analyses Input Table	1	2 Plant Species	3 Transpir. Rate* [Kg/m2]	4 Biomass Growth* [Kg/m2]	5 Lipids Produced* [gm/m2]	6 Carbohydrates Produced* [gm/m2]	7 Protein Produced* [gm/m2]	8 CO2 Taken up* [Kg/m2]	9 O2 Produced* [Kg/m2]	10 Power Required [kW/m2]	11 Total Cost* [$/m2]
	1	LETTUCE	1.02	0.6	24	278.4	105.6	0.88	0.64	0.207	0.7666
	2	POTATOES	6.41	0.136	0.544	92.48	10.88	0.20	0.15	0.344	0.6675
	3	WHEAT	9.98	0.4	4	164	28	0.59	0.43	0.254	1.3013
	4	Y	5	0.6	9	261	6	0.88	0.64	0.285	0.8784
	5	SOYBEANS	7.7	0.3	42	24	48	0.44	0.32	0.152	0.5303

*production rates are per day

This equation gives the ratio of moles of carbohydrate produced to the moles of carbon dioxide taken up and oxygen released. Converting these mole fractions to mass fractions (using the corresponding molecular weights) the oxygen generation rate, $\dot{m}_{O_2}$, and the carbon dioxide take-up rate, $\dot{m}_{CO_2}$, are related to the biomass production rate, $\dot{m}_{bio}$, by

$$\dot{m}_{O_2} = 1.0667\ \dot{m}_{bio}$$

$$\dot{m}_{CO_2} = 1.4\ \dot{m}_{bio}$$

The power requirement is determined using the lighting level recorded in table 2 measured as Photosynthetic Photon Flux (PPF, the radiation given off by the lights in the wavelength band useful for photosynthesis), the photoperiod which is the hours each day that light is supplied to the plants, and the lighting system efficiency, η, which is the end-to-end efficiency of the lighting system. The equation used to calculate the required power, P_{REQ}, is

$$P_{REQ} = \frac{PPF * photoperiod}{\eta}$$

We have not incorporated optimum lighting levels for crops in this study. For a legitimate application of these techniques, either data representing crops at optimal conditions must be entered into table 2 or a more sophisticated, compensating model must be devised. Alternatively, multiple entries of the same crop species could be made with parameters reflecting the crops' performance when optimized for biomass production, transpiration, power, or volume conservation.

The final calculation is the total cost. This is the sum of the power and volume (height times $1m^2$) times their corresponding penalties as given in table 1.

$$\text{Total cost} = (P_{REQ})(\text{Power Penalty}) + (\text{Volume})(\text{Volume Penalty})$$

Note that this function could be made more sophisticated by weighting the relative importance of the two requirements or by adding mass as an additional cost. While mass penalties could easily be incorporated into the cost function, current understanding of mechanically optimized plant chamber mass is sufficiently limited to defer incorporating mass penalties into this study.

DECISION ANALYSIS METHOD

Decision analysis methods (ref. 14) provide a tool for making decisions based on a single principal value (in our case, we have chosen to express everything in terms of cost). Most often, the tool used in decision analysis is a decision tree, where all possible outcomes and all possible paths to these outcomes are diagrammed. Many decision-tree analyses also have expected values or probabilities attached to each branch stemming from a decision or node. In our case, we are merely minimizing cost at each decision node, with equal probability that any particular pathway will be followed. The decision tree (fig. 2) is constructed such that the initial decision determines which crop selection is the cheapest for all permutations of solutions having the same number of crops. A

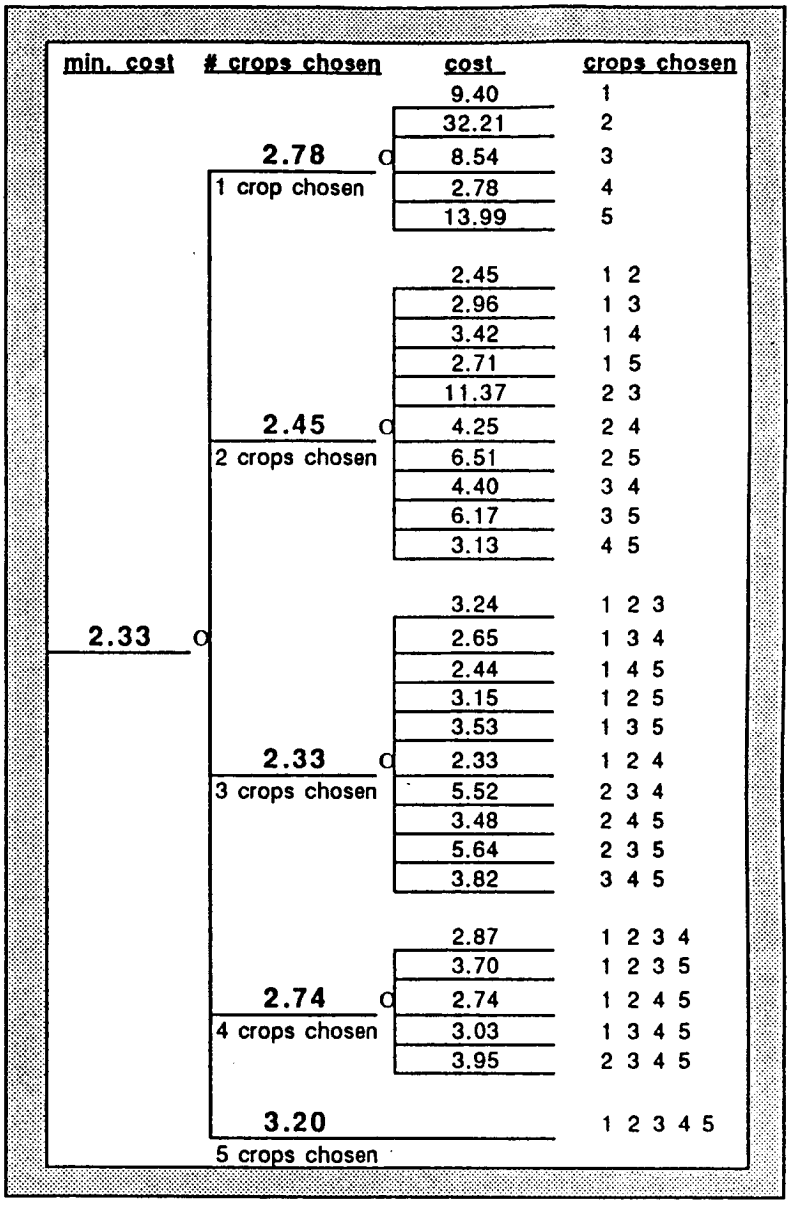

Figure 2. Decision tree.

second round of decision-making is then done to determine the most economical number of crops one could use.

Computation of the cost values is shown in table 4. The assumption is made that an equal area is allotted to each crop in a crop mix. Thus the generation/dissipation rates of the plant products, power, volume, and cost are averages of the individual crops in a crop mix computed on a per-m^2 basis. The penalties incurred by this assumption are shown through the comparison of results with the results from the design optimization method, where this assumption is not required. The required generation/dissipation rates (calculated from the human requirements and the degree of support specified in table 1) are divided by the productivity of each crop mix to obtain the scaling factor (planting area in m^2) required to meet the specified level of life support. The largest scaling factor

Table 4. Crop mix cost calculation

Mixed Crop Calculations

crops chosen	Production per m2/Scale Factors (X's)												Power	Volume	Cost	Max
	water	X	O2	X	CO2	X	Lipids	X	Carbo's	X	Protein	X	[kW/m2]	[m3]	[per m2]	X
1	1.0	12.3	0.6	1.3	0.9	1.1	24.0	1.1	278.4	2.3	105.6	0.2	0.2	0.3	0.767	12.3
2	6.4	2.0	0.1	5.8	0.2	5.0	0.5	48.3	92.5	6.8	10.9	1.7	0.3	0.1	0.668	48.3
3	10.0	1.3	0.4	2.0	0.6	1.7	4.0	6.6	164.0	3.9	28.0	0.7	0.3	0.6	1.301	6.6
4	5.0	2.5	0.6	1.3	0.9	1.1	9.0	2.9	261.0	2.4	6.0	3.2	0.3	0.3	0.878	3.2
5	7.7	1.6	0.3	2.6	0.4	2.3	42.0	0.6	24.0	# #	48.0	0.4	0.2	0.2	0.530	26.4
1 2	3.7	3.4	0.4	2.1	0.5	1.9	12.3	2.1	185.4	3.4	58.2	0.3	0.3	0.2	0.717	3.4
1 3	5.5	2.3	0.5	1.6	0.7	1.4	14.0	1.9	221.2	2.9	66.8	0.3	0.2	0.5	1.034	2.9
1 4	3.0	4.2	0.6	1.3	0.9	1.1	16.5	1.6	269.7	2.3	55.8	0.3	0.2	0.3	0.822	4.2
1 5	4.4	2.9	0.5	1.7	0.7	1.5	33.0	0.8	151.2	4.2	76.8	0.2	0.2	0.3	0.648	4.2
2 3	8.2	1.5	0.3	2.9	0.4	2.5	2.3	11.6	128.2	4.9	19.4	1.0	0.3	0.4	0.984	11.6
2 4	5.7	2.2	0.4	2.1	0.5	1.9	4.8	5.5	176.7	3.6	8.4	2.3	0.3	0.2	0.773	5.5
2 5	7.1	1.8	0.2	3.6	0.3	3.1	21.3	1.2	58.2	# #	29.4	0.6	0.2	0.2	0.599	10.9
3 4	7.5	1.7	0.5	1.6	0.7	1.4	6.5	4.0	212.5	3.0	17.0	1.1	0.3	0.5	1.090	4.0
3 5	8.8	1.4	0.4	2.2	0.5	1.9	23.0	1.1	94.0	6.7	38.0	0.5	0.2	0.4	0.916	6.7
4 5	6.4	2.0	0.5	1.7	0.7	1.5	25.5	1.0	142.5	4.4	27.0	0.7	0.2	0.3	0.704	4.4
1 2 3	5.8	2.2	0.4	2.1	0.6	1.8	9.5	2.8	178.3	3.6	48.2	0.4	0.3	0.3	0.912	3.6
1 3 4	5.3	2.3	0.6	1.5	0.8	1.3	12.3	2.1	234.5	2.7	46.5	0.4	0.2	0.4	0.982	2.7
1 4 5	4.6	2.7	0.5	1.6	0.7	1.4	25.0	1.1	187.8	3.4	53.2	0.4	0.2	0.3	0.725	3.4
1 2 5	5.0	2.5	0.4	2.3	0.5	2.0	22.2	1.2	131.6	4.8	54.8	0.3	0.2	0.2	0.655	4.8
1 3 5	6.2	2.0	0.5	1.8	0.6	1.6	23.3	1.1	155.5	4.1	60.5	0.3	0.2	0.4	0.866	4.1
1 2 4	4.1	3.0	0.5	1.8	0.7	1.5	11.2	2.3	210.6	3.0	40.8	0.5	0.3	0.2	0.771	3.0
2 3 4	7.1	1.8	0.4	2.1	0.6	1.8	4.5	5.8	172.5	3.7	15.0	1.3	0.3	0.3	0.949	5.8
2 4 5	6.4	2.0	0.4	2.3	0.5	2.0	17.2	1.5	125.8	5.0	21.6	0.9	0.3	0.2	0.692	5.0
2 3 5	8.0	1.6	0.3	2.8	0.4	2.4	15.5	1.7	93.5	6.8	29.0	0.7	0.2	0.3	0.833	6.8
3 4 5	7.6	1.7	0.5	1.8	0.6	1.6	18.3	1.4	149.7	4.2	27.3	0.7	0.2	0.4	0.903	4.2
1 2 3 4	5.6	2.2	0.5	1.8	0.6	1.6	9.4	2.8	199.0	3.2	37.6	0.5	0.3	0.3	0.903	3.2
1 2 3 5	6.3	2.0	0.4	2.2	0.5	1.9	17.6	1.5	139.7	4.5	48.1	0.4	0.2	0.3	0.816	4.5
1 2 4 5	5.0	2.5	0.4	1.9	0.6	1.7	18.9	1.4	164.0	3.9	42.6	0.4	0.2	0.2	0.711	3.9
1 3 4 5	5.9	2.1	0.5	1.7	0.7	1.4	19.8	1.3	181.8	3.5	46.9	0.4	0.2	0.4	0.869	3.5
2 3 4 5	7.3	1.7	0.4	2.2	0.5	1.9	13.9	1.9	135.4	4.7	23.2	0.8	0.3	0.3	0.844	4.7
1 2 3 4 5	6.0	2.1	0.4	1.9	0.6	1.7	15.9	1.7	164.0	3.9	39.7	0.5	0.2	0.3	0.829	3.9

encountered for a particular crop mix is multiplied by the cost of the crop on a per-m^2 basis to obtain the cost penalty entered in the decision tree.

A feature of the decision tree tool is the accessibility of cost values for all crop mixes. This allows the designer to investigate the cost of non-optimal solutions which might have more appeal than the optimal solution for qualitative reasons. For the example shown in figure 2, increasing the crop variety by selecting the most optimal 4 crop solution over the 3 crop solution increases the cost by 18%. Also, if a designer preferred wheat over potatoes in the optimal crop mix of lettuce, potatoes, and Y (crops 1, 2, and 4), the decision tree shows an increase in cost of 14% for lettuce, wheat, and Y (crops 1, 3, and 4).

DESIGN OPTIMIZATION METHOD

An alternative to using the decision analysis method described above is to take a design optimization approach (refs. 15 and 16). One can then minimize the cost function while removing the assumption of equal crop growth areas. For example, we use a linear programming approach to solve the constrained optimization problem

$$\min_{\text{area}} \left\{ \sum_{i=1}^{N} (\text{cost})_i \, (\text{area})_i \right\}$$

Subject to the following constraints

$$\sum_{i=1}^{N} \left(\frac{H_2O \text{ transpired}}{\text{area}} \right)_i (\text{area})_i \geq H_2O \text{ transpiration requirement}$$

$$\sum_{i=1}^{N} \left(\frac{CO_2 \text{ removed}}{\text{area}} \right)_i (\text{area})_i \geq CO_2 \text{ removal requirement}$$

$$\sum_{i=1}^{N} \left(\frac{O_2 \text{ produced}}{\text{area}} \right)_i (\text{area})_i \geq O_2 \text{ production requirement}$$

$$\text{protein lower bound} \leq \sum_{i=1}^{N} \left(\frac{\text{protein produced}}{\text{area}} \right)_i (\text{area})_i \leq \text{protein upper bound}$$

$$\text{carbo. lower bound} \leq \sum_{i=1}^{N} \left(\frac{\text{carbohydrate produced}}{\text{area}} \right)_i (\text{area})_i \leq \text{carbo. upper bound}$$

$$\text{lipid lower bound} \leq \sum_{i=1}^{N} \left(\frac{\text{lipid produced}}{\text{area}}\right)_i (\text{area})_i \leq \text{lipid upper bound}$$

where i identifies the crop species and N is the total number of crops being considered. The objective is then to identify the crop mix which minimizes cost while meeting certain requirements for air and water regeneration as well as food production. One could easily modify the above formulation to include additional requirements, such as vitamin and mineral nutritional requirements, or to include additional constraints, such as physical constraints on the crop-growth areas due to rack-size limitations or edge-effect considerations.

This constrained optimization problem can be solved using standard linear programming techniques. We used a SIMPLEX algorithm, coded in FORTRAN on a MicroVax 3200 computer. The algorithm first identifies whether a feasible solution exists, then solves for the optimum solution and determines whether or not the solution is degenerate (i.e., an infinite number of solutions exist).

The optimization method has computational advantages, especially when a large number of crop species or nutritional requirements are being considered. The decision analysis method requires an exhaustive search since the cost of each possible solution must be calculated, while the optimization method uses search directions to quickly find the optimum solution. Also, standard methods exist for performing parameter sensitivity analyses for the linear programming formulation. Such analyses would be very useful for performing "what if" studies to investigate the effects of changing costs or productivities of the various crop species.

RESULTS

Table 5 shows the decision analysis output for the baseline case outlined in tables 1–3. For this case we have specified 100% of the requirements for oxygen, carbon dioxide, and carbohydrates to be fulfilled, as well as 40% of those for water, 25% of lipids, and 25% of protein. Results show three crops being selected (lettuce, potatoes, and Y) as the optimum mix, with a total area of 3.0 m^2 and total cost of 2.33. Results also show that in order to supply 100% of the carbohydrate requirement, oxygen, carbon dioxide, water, and protein are oversupplied, and more carbon dioxide is taken up than is necessary. In design optimization terminology, carbohydrates are the active constraint.

Table 6 shows the results of the design optimization technique for the same base set of constraints. Recall that this technique is not limited to equal areas for each species in the crop mix selected. This is reflected in the results, which in this case show three crops being selected (lettuce, Y, and soybeans), with a total area of 2.5 m^2 at a cost of 2.16. Examining the results, we see that the carbohydrate, water, and lipid requirements are active constraints.

The optimization technique can also be used to examine the optimal solution in the case where protein, carbohydrate, and lipid production all become active constraints. This is accomplished by setting the upper and lower bounds on these variables all equal to 100% of the requirements, thus forcing the optimization to choose a crop selection which produces a nutritionally balanced diet (no over production of protein, carbohydrates, or lipids). In the baseline case, no feasible solution exists.

Table 5. Decision analysis baseline results

Desicion Analysis Output

Total Crop Area [m2]	3.0
Number of plant species	3
Area planted per specie [m2]	1.0
Total power required [kW]	0.84
Total volume required [m3]	1.40
Total cost of plants	2.33

Species Selected

1	LETTUCE
2	POTATOES
3	Y
4	
5	

Life Support Requirments By Output Crop Mix

% Oxygen	171
% Carbon Dioxide	231
% Water	74
% Lipids	58
% Carbohydrates	100
% Protein	202

Table 6. Design optimization baseline results

Total cost = 2.1595
Total area = 2.5004 m^2

Area of crop #1 (lettuce)	=	0.0584	m^2
Area of crop #2 (potatoes)	=	0.0000	m^2
Area of crop #3 (wheat)	=	0.0000	m^2
Area of crop #4 (Y)	=	2.3549	m^2
Area of crop #5 (soybeans)	=	0.0870	m^2

CO_2 removed	= 2.1621	kg/day	(216.21	% of human reqt.)
O_2 produced	= 1.5724	kg/day	(187.19	% of human reqt.)
H_2O processed	= 12.5040	kg/day	(40.00	% of human reqt.)

Protein produced	= 24.48	g/day	(32.21	% of human reqt.)
Carbohydrate produced	= 633.00	g/day	(100.00	% of human reqt.)
Lipid produced	= 26.25	g/day	(25.00	% of human reqt.)

However, if crop X is substituted for crop Y a solution exists such that exactly 100% of the protein, carbohydrate, and lipid requirements are satisfied. In this example, lettuce, potatoes and crop X are selected, and carbon dioxide, oxygen, and water requirements are satisfied but are not active constraints.

Note that in the base case, we have set the lipid requirement to be satisfied by the plants to a fairly low level (25%). In the study of reference 4, it was found that the lowest total area (only nutritional needs were evaluated) resulted when no minimum percentage of fat was made available to the diet via plants. We have not found the lipid requirement to be an active constraint in our case, perhaps because we have constrained it to only a small degree. Since additional constraints have been added to the baseline case (and the crops to be considered have been changed), the cost increases to 3.0 requiring 4.8 m^2 of crop area.

In a study by McDonnell Douglas (ref. 4), it is found that the lowest total area (only nutritional needs are considered) results when no lipid production requirement is placed on the plants. In the baseline case of our study, the lipid requirement to be satisfied by the plants is set to a low level (25%). For this case the lipid requirement is not an active constraint. However, when the requirements for the three nutritional categories are increased to a level of 100%, lipids become the active constraint, which is consistent with the McDonnell Douglas study.

SENSITIVITIES

There are several ways in which sensitivities can be examined. Two approaches are demonstrated below.

From the results of the baseline case, it was determined that carbohydrates were an active constraint. With this in mind, we might like to see how sensitive our answers are to the specified carbohydrate requirement. For example, what happens when the carbohydrate fulfillment level is lowered to 50%? The decision analysis results show a 40% savings in cost and a 15% decrease in crop area using only soybeans and Y. With this new requirements specification, the active constraint shifted to water fulfillment. The design optimization method showed a 38% savings in cost and a 21% decrease in crop area. The active constraints remain carbohydrate and water fulfillment. This sensitivity analysis demonstrates that resupplying a portion of the carbohydrates from Earth might be preferred to requiring the plants to produce the entire requirement depending on resupply costs.

Another approach to analyzing sensitivities is to examine the effect on the results when plant performance data for a particular species are altered. As an example, the biomass production rate and transpiration rate were varied (doubled and halved) about nominal values. Table 7 lists the results of the two methods to each of these cases . This table shows that certain increases in plant performance parameters result in larger cost savings than others. This method could provide a tool for steering plant research, as well as addressing the balance between transpiration rate and plant biomass production.

Table 7. Parameter sensitivity analysis results

Crop Y		Transpiration rate $\left[\frac{kg}{m^2 d}\right]$		
		2.5	5.0 (nominal)	10.0
Biomass generation rate $\left[\frac{kg}{m^2 d}\right]$	0.35	DA cost: 2.45 area: 3.4 m^2 species: L,P OPT cost: 2.36 area: 3.50 m^2 species: L,S	DA cost: 2.45 area: 3.4 m^2 species: L,P OPT cost: 2.36 area: 3.50 m^2 species: L,S	DA cost: 2.42 area: 2.9 m^2 species: L,Y OPT cost: 2.24 area: 2.76 m^2 species: L,Y
	0.70 (nominal)	DA cost: 2.42 area: 3.3 m^2 species: L,Y,S OPT cost: 2.28 area: 2.98 m^2 species: Y,S	DA cost: 2.27 area: 3.1 m^2 species: L,Y,S OPT cost: 1.96 area: 2.34 m^2 species: Y,S	DA cost: 1.87 area: 2.3 m^2 species: L,Y OPT cost: 1.79 area: 2.17 m^2 species: L,Y
	1.40	DA cost: 1.73 area: 2.5 m^2 species: Y,S OPT cost: 1.56 area: 2.29 m^2 species: Y,S	DA cost: 1.41 area: 2.0 m^2 species: Y,S OPT cost: 1.40 area: 1.97 m^2 species: Y,S	DA cost: 1.19 area: 1.4 m^2 species: Y OPT cost: 1.06 area: 1.32 m^2 species: Y,S

LEGEND:

P = potato
L = lettuce
W = wheat
S = soybeans
Y = Y

DA = results from decision analysis
OPT = results from design optimization

CONCLUSIONS

1. The design optimization method clearly provides the most optimal crop selection of the two methods considered. The decision analysis method results are usually within 10% of the cost and total crop area of the design optimization results.

2. The advantages and disadvantages of both methods imply that the two methods are ideal companions to one another. The decision analysis method allows an interactive atmosphere with the user, facilitating experimentation with design specifications. A decision tree displays the cost of all crop mixes simultaneously. This allows the user to evaluate at a glance the cost of additional variety of preferred (more appetizing) crop species.

The design optimization method has computational advantages especially when the number of crops being considered or the number of nutritional (or other) constraints become large. It also ensures that the last 10% of cost and area savings will be provided by the specified crop mix, and it allows the user to further constrain the optimization problem as needed. A more rigorous sensitivity analysis approach could also be developed using this method.

3. There are limitations to this analysis. A significant limitation of the decision analysis method is the assumption of an equal area for each species in a crop mix. Both methods are limited because they do not allow the plant performance parameters to be simultaneously optimized (the transpiration rate/biomass generation rate trade-off, as well as other variables). No attempt is made to account for the compatibility of crop species if a common air space or nutrient delivery system is planned. Also, the power and volume of the processors required to support a plant system, including environment control, are not accounted for.

REFERENCES

1. MacElroy, R.; Smernoff, D.; and Rummel, J.: CELSS-Design, Development, and Use of a Ground-Based Plant Growth Module. NASA CP-2479, 1987.

2. Cullingford, H. and Schwartzkopf, S.: Conceptual Design for a Lunar-Base CELSS 20th International Conference on Environmental Systems. SAE 901278, July 1990.

3. Gustavino, S. and Mankamyer, M.: Application of Bioregenerative Subsystems to an ECLSS for a Manned Mars Sprint Mission. 19th International Conference on Environmental Systems, SAE 891504, July 1989.

4. Dyer, L. and Glover, G.: OPTDES Trade Study of Future CELSS Diet. McDonnell Douglas Space Systems Company Summer Intern Study, September 1990.

5. Dunne, L.: Nutrition Almanac. Nutrition Search, Inc, 1990.

6. PV Module Thermal Control System Trade Study Report. SSF Program Office, Reston, Virginia, Doc. No. SSS-E-39-R5, October 31, 1989.

7. Bilardo, V.: A Generic Trade Study Methodology for the System Analysis of Regenerative Life Support Systems. SAE Paper No. 911320, 21st International Conference on Environmental Systems, July 1991.

8. Wheeler, R. and Sager, J.: Carbon Dioxide and Water Exchange Rates by a Wheat Crop in NASA's Biomass Production Chamber: Results from an 86-Day Study (Jan - Apr 89), NASA TM-102788, 1990.

9. Henninger, D. and Edeen, M.: Regenerative Life Support System (RLSS) Test Bed Performance: Characterization of Plant Performance in a Closed, Controlled Atmosphere. 21st International Conference on Environmental Systems, SAE 911426, July 1991.

10. Tibbitts, T.; Bennett, S.; and Morrow, R.: Environmental and Cultural Considerations for Growth of Potatoes in CELSS. CELSS '89 Workshop, NASA TM-102277, 1989.

11. Tibbitts, T.; Bennett, S.; Morrow, R.; and Bula, R.: Utilization of White Potatoes in CELSS. 1988 COSPAR, NASA CP-10040, 1989.

12. Salisbury, F. and Bugbee, B.: Plant Productivity In Controlled Environments. HortSci., vol. 23, 1988, p. 293.

13. Salisbury, F. and Ross, C.: Plant Physiology, 3rd ed., Wadsworth Publishing Company, 1985.

14. McNamee, P. and Celona, J.: Decision Analysis for the Professional. The Scientific Press, 1987.

15. Hadley, G.: Linear Programming. Addison-Wesley, 1962.

16. Gass, S.: Linear Programming, Methods and Applications. McGraw-Hill, 1969.

BIOGRAPHIES

Ann McCormack works as a systems analyst in the Advanced Life Support Division at NASA Ames Research Center and has been working at Ames since 1987. She received a B.S. in mathematics in 1984 and an M.S. in mechanical engineering in 1987 from the University of New Hampshire, Durham, New Hampshire.

Cory Finn received a B.S. in chemical engineering from the University of Rochester, Rochester, New York in 1985 and a Ph.D. in chemical engineering from the University of Massachusetts, Amherst, Massachusetts in 1990. She has been at NASA Ames Research Center since that time working as a control systems engineer in the Advanced Life Support Division.

Betsy Dunsky is currently completing her Ph.D. in mechanical engineering at the University of California at Berkeley, Berkeley, California and received an M.S. in mechanical engineering from the same school in 1983. She received a B.S. in mechanical engineering from the State University of New York at Stony Brook, Stony Brook, New York in 1982. She works as a systems analyst in the Advanced Life Support Division at NASA Ames Research Center and has been working at Ames since 1984.

DEVELOPMENT OF A CHANGE MANAGEMENT SYSTEM

Cathy Bonifas Parks
Sterling Software, Inc.
Ames Research Center
Moffett Field, California

INTRODUCTION

The complexity and inter-dependence of software on a computer system can create a situation where a solution to one problem causes failures in dependent software. In the computer industry, software problems arise and are often solved with "quick and dirty" solutions. But in implementing these solutions, documentation about the solution or user notification of changes is often overlooked, and new problems are frequently introduced because of insufficient review or testing. These problems increase when numerous heterogeneous systems are involved. Because of this situation, a change management system plays an integral part in the maintenance of any multi-system computing environment. At the NASA Ames Advanced Computational Facility (ACF), the Online Change Management System (OCMS) was designed and developed to manage the changes being applied to its multi-vendor computing environment. This paper documents the research, design, and modifications that went into the development of this change management system (CMS).

RESEARCH INTO CHANGE MANAGEMENT SYSTEMS

Change management systems have been defined in as many ways as they have been named. Numerous articles document locally-developed and vendor-supplied software management packages and change management systems. Research into the requirements of a CMS revealed the following definitions.

An article describing "change control software" stated, "the primary purpose of a change control system is to impose management control over the application development environment without affecting productivity" (ref.1). The author proposed that a complete change control system should provide MIS organizations with source code change management, audit trails of the changes, synchronization between load modules and source, task and project reporting, management control over parallel development, and options for handling control and quality assurance groups (ref. 2).

Another article described "change management" as a means of ensuring accountability, stating, "It is the function of change management to control the implementation of the new system—to schedule the moment on which it is installed to ensure that all affected users are aware of the change and to control backout procedures" (ref. 3).

A more encompassing view, incorporating control of the complete configuration, was described as "configuration control." The author stated, "it should be possible to track source and object code,

load modules, test data, documentation, and so forth automatically, and to define all applications components" (ref. 4).

But, regardless of what the definition for change management is, or to what extent one feels it covers the total system configuration, there are basic components common to most change management systems. Each of these components plays an important role in the success of the CMS. The general components that are identified in the numerous articles on change management include:

- Software maintenance packages for developing, maintaining, and controlling code.
- Management forms and reports to record change requests and problems.
- Change review processes to reduce the number of "quick fixes" and to promote planning of the changes.
- Documentation and communication of the changes.
- Change implementation and backout procedures.

When selecting a change management system, it is imperative that the chosen package meets the needs of your environment; but the single most important feature to have in your system is "ease of use." The users must be willing to use the system in order for any change management system to be successful.

CHANGE MANAGEMENT SYSTEM REQUIREMENTS AT ACF

At the Advanced Computational Facility at NASA Ames Research Center, the need for a change management system was recognized, but because of the number of heterogeneous systems that were being maintained, and the small amount of software development that was being done, our needs appeared unique when comparing them to the needs addressed by most systems. The majority of changes that needed to be managed at the ACF were modifications to the site-controlled parameters and the configurations of two Cray supercomputers and connected Digital, Silicon Graphics, and Sun Systems. Prior to the implementation of a CMS, changes to these systems often affected our staff and users, but notifications about the changes were not being made. We also experienced problems in which changes to one area of a system affected other areas, but because of insufficient review of the changes, the effects were not noticed until the changes were implemented.

A recent article best defines the CMS requirements that the ACF had when the author described the "software configuration management" function as filling the "need for some organization to ensure that all parties know how to request a change, that a change is necessary, that all affected parties agree with the change, that all parties are informed of the impending change, and that there is a record of all changes made, who made them, when they were made, and why they were made" (ref. 5).

Similar to this definition of the software configuration management function, our primary requirement for a change management system was to provide notification of changes to the ACF staff and the system users. Other important requirements for this system included the need for review of the changes, completion of documentation about the change, and tracking the known problems identified in the various systems. Because of the small amount of software development, there was no need for a software maintenance package within our CMS.

DESIGNING A CHANGE MANAGEMENT SYSTEM

The first change management system for ACF was defined in July 1989. The stated goals of this system were to ensure that all parties were informed of changes and that the impacts of the changes were considered before changes were made. This CMS consisted of seven forms that were used to manage the system, including three forms to document the problem and solution surrounding the change, track the review of the change, and describe the impacts of the change and schedule its installation. Also included were three logs to provide management summaries of the open logs, approval status of the logs, and completed system changes. The final form was the change notification that was sent via e-mail to ACF staff members.

The Systems Group within ACF used this system for two months before it was expanded to include the rest of the staff. In August 1989, a survey was sent to the staff to determine whether the expectations for the CMS were being addressed. The responses received in this survey indicated that the system was too complicated, stating that the best way to ensure continued usage of this system was to simplify the design. As a result, the components of the CMS were reduced to include only three forms: the tracking form (figs. 1-3) which contained the problem, solution, and impacts of the change, as well as the review committee's approval status; the problem log (figs. 4-5) which was used to report the status of all logs on a weekly basis; and the e-mail notification that informed the staff of changes.

The survey also asked what features were required in the CMS. The majority of the responses indicated that the required features included the documentation of known problems, internal notification of changes, and the review of the changes. The components of the CMS handled these features.

The revised change management system was used within the ACF from August 1989 through May 1990. The procedure for using this system was as follows:

1. A problem or change request was reported by filling out a tracking form that included the problem description and any workarounds for the problem. This form was given a log number and assigned to an analyst.

2. When a solution was available, the solution portion of the tracking form was completed and the form was submitted to the review committee.

3. The review committee approved implementation of the change, or requested that additional work and/or notification be done before the change was implemented.

_____ PROBLEM ___ TASK TRACKING FORM

Log Number: _____ Contact: _____

Submitter: _____ Date Submitted: _____

Brief Description: _____

Full Description:

Initial Response: SPR or Vendor No.: _____

Solution:

Rev. 11/89 Page 1 of 2

Figure 1. Tracking form (side 1).

CHANGE NOTICE

Change Type: ____ None ____ Routine _____ Scheduled _____ Emergency

Reviewed By: _____

Impact Analysis:

Consequences of No Action:

COMMITTEE RESPONSE

Impact Analysis Response:

Change Management Committee Actions:

Initials/Date: _____ ___ Approved ___ Disapproved ___ Held
Initials/Date: _____ ___ Approved ___ Disapproved ___ Held
Initials/Date: _____ ___ Approved ___ Disapproved ___ Held
Initials/Date: _____ ___ Approved ___ Disapproved ___ Held

INSTALLATION AND MAIL NOTICE

Date/Time of Change: _____

Date of Mail Notice: _____

Rev. 11/89 Page 2 of 2

Figure 2. Tracking form (side 2).

Tracking Form

Definition of Fields:

Problem/Task: Identifies whether the log documents a problem or a task.

Log Number: Identifying number for the problem log.

Contact: Analyst assigned to resolve the documented problem.

Submitter: Person submitting the problem log.

Date Submitted: Date the log was submitted.

Brief Description: One line description of the problem.

Full Description: Detailed description of the problem.

Initial Response: Description of applied workaround or initial suggestion for a resolution for the problem.

SPR or Vendor No: Assigned vendor number if this is a vendor's problem.

Solution: Description of the problem solution.

Change Type: Type of change installed.

None	no change occurred.
Routine	pre-approved common change.
Scheduled	change which has been scheduled.
Emergency	critical change, pre-approval not required.

Reviewed By: Analyst who reviewed the problem solution.

Impact Analysis: Impacts the change will have on users and staff.

Consequences of No Action:
Consequences of not making the change.

Impact Analysis Response:
Further actions requested by the Review Committee.

Change Management Committee Actions:
Initials, date, and approval indication from the committee members.

Date/Time of Change: Date and time the change was installed.

Date of Mail Notice: Date the staff notification was sent.

Figure 3. Tracking form field descriptions.

PROBLEM LOG

Log No.	Submit Date	Contact	Status	Type/ Close Dt	Ref. No.	DESCRIPTION

(Date/Time of Report) Page 1

Figure 4. Problem log.

Problem Log

Definition of Fields:

Log No.	Log number from the Tracking Form.
Submit Date	Date the Tracking Form was submitted.
Contact	Analyst assigned to resolve the problem or task.
Status	Current status of problem or task. Statuses are: Received — Form has been received, but is not assigned. Assigned — Form has been assigned to an analyst. Active — Analyst is actively working on the problem. New — Analyst has a fix available for the problem; the response is in the change review process. Approved — Response has been approved, but it is not yet installed. Closed — Problem is closed.
Type/Close Dt.	Identifies the type of problem or task that is documented on the tracking form. The types are: 6-Project — Major system project. 5-Problem — System problem. 4-Task — Minor request or system enhancement. 3-Vendor — Problem reported to vendor. 2-Chng Req — Change is awaiting approval by committee. Date — Date the log was closed.
Ref. No.	Vendor log number for problems reported to the vendor.
Description	One line problem or task description from the Tracking Form.

Figure 5. Problem log field descriptions.

4. Upon approval of the change, an implementation date was set for the installation of the change.

5. After installation of the change, an e-mail notice was sent to the ACF staff to inform them of the change.

After the initial entry of problems into the CMS, the usage of this system fluctuated between 13 and 36 logs entered each month, with an average of 27 new logs per month. The peak months of usage coincided with memos to the staff emphasizing the importance of this system. The review process for the logs also fluctuated greatly. The committee initially met once a week to review proposed changes, but eventually each member individually reviewed the logs. Because of this process, review of a log could take from one day to one month, and numerous changes were implemented without review.

In May 1990, the CMS underwent a review of its effectiveness when a second survey was sent asking the staff to evaluate the CMS. The areas of "documentation of known problems" and "weekly reporting of CMS information" received the highest scores for the CMS features. Both of these categories received an average score of 7.0 on a scale of 1 (poor) to 10 (great). Internal notification of changes received a 6.6 score, but the category for "change review" received only a 5.3. The overall effectiveness of the CMS, when compared to the previous informal method of managing changes, was rated as 6.7, indicating that the CMS was superior to the old method. But the overwhelming endorsement of CMS was indicated by 100% of the users stating that this system should be continued.

Statistics obtained from the CMS logs showed that 337 problems and tasks were documented during the ten-month period. Of these, 298 logs were closed, with only 42% of them reviewed by the review committee prior to implementation. Of the reviewed logs, 11% had requests for additional action before implementation. Internal notices were issued for 43% of the closed logs.

Recommendations from the survey revealed that 43% of the respondents wanted online database features to ease the use of the system and enhance its capabilities, and 36% mentioned that the review process needed improvement.

DESIGNING AN ONLINE CHANGE MANAGEMENT SYSTEM

In December 1990, a design for an online CMS was completed, and in late April 1991, the paper CMS system was replaced by the Online Change Management System (OCMS). A total of 674 logs had been entered through the old CMS. All open logs were transferred to the new system.

The location for OCMS was specifically chosen to provide easy access for the users. The goals of OCMS included: ease-of-use; the capabilities to enter, transfer, update, comment, close, reopen, and display problem logs; the automatic notification to the OCMS users about new comments and log transfers via e-mail; a command to list recently changed logs; and an audit trail about entries to the logs. The review committee was no longer in effect; instead, each user had the responsibility of staying up-to-date on the information documented in the logs, and they had the capability of adding requests or information to any of the open logs. To accommodate both novice and experienced users, the OCMS provided command and menu-driven modes of operation. An administrator was assigned to maintain the system and to add and delete users of the system.

From May 1991 until mid-November 1991, 280 logs were entered on OCMS, averaging 40 logs per month. This represents a 48% increase over the previous CMS. Of these, 92 logs (33%) received additional comments, and 188 logs were closed.

The new OCMS is more widely accepted than the old system, and it has proven to be much easier to use. The process for entering a log (fig. 6) is to enter OCMS and respond to the prompts for the required information. A summary of the new log is displayed when all the information has been gathered. Figure 6 shows an example of the command mode of OCMS; figures 7 and 8 show an example of displaying a full log via the menu mode.

As with the previous CMS, we again reviewed how well we had addressed the goals for OCMS. Enhancement requests were solicited from the staff, and a second version of the OCMS was designed and released in November 1991.

OCMS Version 2 provided categories for the problem or task being documented, which allows for summarizing the types of problems we encounter. It also provided a capability to search for a string in the brief problem description. For the advanced users of this system, the command formats were enhanced to accept unique strings rather than full words as parameters. Further work is in progress to improve the editing capabilities on this system.

```
$ ocms -c enter

Starting new log.
Enter Log Category
   Valid Categories are:
      1)  Accounting     12) Libraries       22) Sys Problems
      2)  Backups        13) Mailer          23) Sys S/W Maint
      3)  Benchmarks     14) Networks        24) Tapes
      4)  CCF            15) NQS             25) TMX
      5)  Compilers      16) Ops Procedure   26) Training
      6)  Configuration  17) Other           27) ULTRIX
      7)  DMF            18) OWS             28) User Services
      8)  Documentation  19) Performance     29) Utilities
      9)  Hardware       20) Security        30) VMS
      10) In-house S/W   21) Sys Admin       31) Workstations
      11) IOS Problems

Enter Category Number: 1

Submitter:  bonifas   Status: Received    Category: Accounting
Date/Time Submitted is: Fri Dec  6 17:31:54 1991
Implementation Date:  none
Enter brief description:
<Brief problem description is entered here.       >
Enter full description or ctrl-f to include a file (terminate with a '.'):
<Full details of a problem are entered here.                              >
<.                                                                        >

Do you wish to (Commit/Abort/Edit) [Commit]: C
Should this be transferred to you (y/n):  n
Mailing to:  brosen
   99  (None)    Brief problem description is entered here.
Submitter:  bonifas   Status: Received    Category: Accounting
Date/Time Submitted is: Mon Nov  4 13:34:06 1991
Implementation Date: (none)
- - - - - - - - - - - - - - - - - - - - - - - - - - - - - - - - - - - - -
DESCRIPTION:

  Full details of a problem are entered here.
```

Figure 6. Log entry on OCMS.

```
$ ocms

                Welcome to the ACF
           Online Change Management System
                OCMS, Release 2.0


+-------------------------------------------------+
  Online Change Management System: Release 2.0
+-------------------------------------------------+
The Online Change Management System functions are as follows.
The OCMS command option for the function is listed in parentheses.
1)    Display information about a log (view)
2)    Enter a new log (enter)
3)    Transfer a log to a new owner (transfer)
4)    Add a comment to a log (comment)
5)    Add a planned solution to a log, but don't close it (solution)
6)    Schedule the implementation date for a log (schedule)
7)    Close a log (close)
8)    Reopen a closed log (reopen)
9)    Recategorize a log (category)

Enter option number (<CR> to exit): 1
Display log information.
   View display options are:
   -a analyst    Display logs owned by specified analyst
   -d date       Display logs updated since the specified date (MM/DD/YY)
   -k string     Display logs with string in the brief description.
   -p options    Print options:
                 a - audit trail            c - comments
                 d - full description       f - all options
                 g - general information    s - solution
   -s statuses   Display logs with specified statuses.  Options are:
                 r - received               a - assigned
                 s - scheduled              c - closed
   -u user       Displays logs submitted by specified user

   $ ocms -c view [-a analyst] [-d date] [-k string] [-p acdfgs]
                  [-s rasc] [-u user] [log1, ...]

Enter display options and log number[s]: -pf 1311
```

Figure 7. Menu display from OCMS.

```
 1311  cardo     Reported operand range error in OCMS during reopen.
Submitter:  cardo     Status: Closed      Category: In-house S/W
Date/Time Submitted is: Thu Dec  5 12:51:56 1991
Implementation Date: 12/05/91
- - - - - - - - - - - - - - - - - - - - - - - - - - - - - - - - - - - - -
DESCRIPTION:
  An operand range error was received during reopening of
  log 1305.
- - - - - - - - - - - - - - - - - - - - - - - - - - - - - - - - - - - - -
COMMENTS:
  ----------  Thu Dec  5 12:53:46 1991  Comment added by:  cardo
  Initial investigation shows that the core file produced contains
  a lot of invalid information, making it very difficult to obtain
  any information from it.  Also it appears that the error may have
  occurred during mail notifications of the transaction.

- - - - - - - - - - - - - - - - - - - - - - - - - - - - - - - - - - - - -
SOLUTION:
  A formatting problem was found in module reopenlog.c for ocms.
  An sprintf was using a string format for an integer field.  This
  caused the allocated buffer for the sprintf to be overrun and
  destroy some neighboring information.
  The original source line was:
      (void) sprintf(printmsg,"Log %s reopened.\n",lognumber);
  The new source line is:
      (void) sprintf(printmsg,"Log %d reopened.\n",lognumber);
  The same conditions were applied to the test ocms system in order
  to reproduce the problem.  The problem appears under some very
  specific conditions within OCMS which is probably why it was not
  detected during the test phases of OCMS.
  The problem has been corrected and a new version of ocms installed
  for use which corrects this problem.

Solution Reviewed by: Dan

- USER IMPACT:
  Users of OCMS will no longer encounter this problem.

- OPERATIONS IMPACT:
  None

- SYSTEM IMPACT:
  None
- - - - - - - - - - - - - - - - - - - - - - - - - - - - - - - - - - - - -
AUDIT:
  Thu Dec  5 12:53:28 1991  Log entered by:  cardo
  Thu Dec  5 12:55:36 1991  Comment added by:  cardo
  Thu Dec  5 15:20:31 1991  Solution added by:  cardo
  Thu Dec  5 15:20:43 1991  Schedule added by:  cardo
                            Implementation scheduled for 12/05/91
  Thu Dec  5 15:20:46 1991  Closed by:  cardo

----End of log 1311----
```

Figure 8. Full view of an OCMS log.

SUMMARY

As the usefulness of our change management system grows, we are also encountering new ways to utilize its features. Tracking tasks through the OCMS has helped in managing analysts' time. The information stored in the logs has been helpful in resolving new problems. And User Services continually use this information to keep abreast of the system changes that may affect the users.

The OCMS users continue to request new features. New requests include a host name, machine type, and level of criticality for each problem, multiple categories for a problem, and automatic notification to the problem submitter of comments added to a log. Management reports have also been requested from this system, in particular, reports that summarize categories of problems and the time it takes to resolve problems.

But, although we have provided a mechanism which addresses our primary goals (documentation of problems, review of changes, and notification of changes), the most difficult requirement for attaining these goals is ensuring that all users utilize this tool. Too often the documentation aspects of OCMS are avoided. As one author states,

> Moans and groans come as soon as that word is mentioned. That dreaded pain acts up in the lower posterior; the activity that is so easily put off until we have absolutely nothing else to do; the most boring part of a technical person's life—documentation. But it is one of the more important aspects of Change Management (ref. 6).

And similarly, providing an inviting, informative, and easy to use change management system is one of the most important challenges for a change management designer.

REFERENCES

1. Di Marcantonio, Joseph: Change Control Software Provides Comprehensive Methodology for Managing the Program Update Cycle. Technical Support, September 1988, p. 33.

2. Ibid., p. 35.

3. Hundley, Kim and Tootill, David: Change Management: Past, Present and Future. Technical Support, September 1988, p. 22.

4. Jander, Mary: Buyers' Guide/Change Control Software: Change Control Meets CASE. Computer Decisions, October 1988, p. 81.

5. Bersoff, Edward H. and Davis, Alan M.: Impacts of Life Cycle Models on Software Configuration Management. Communications of the ACM, August 1991, p. 105.

6. Krukowski, Ray: Building Change Control in the Network. Technical Support, December 1988, p. 42.

BIOGRAPHY

Cathy Parks is a systems analyst with Sterling Software, Inc. She has been working the past four years on the Supercomputing Capability Contract at the NASA Ames' Central Computer Facility. One of her projects on this contract was to design and develop a change management system to control the modifications being applied to the numerous systems maintained through this contract. Cathy has a bachelor's degree in Information Systems Management from the University of San Francisco, and has worked in the computer industry for fifteen years. Before coming to Sterling, she worked for Control Data Corporation and was involved in developing their world-wide call logging system and providing operating system support.

TRAINING FOR LIFE SCIENCE EXPERIMENTS IN SPACE AT THE NASA AMES RESEARCH CENTER

Annette T. Rodrigues and A. Christopher Maese
Ames Research Center
Moffett Field, California

SUMMARY

As this country prepares for exploration to other planets, the need to understand the affects of long duration exposure to microgravity is evident. The National Aeronautics and Space Administration (NASA) Ames Research Center's Space Life Sciences Payloads Office is responsible for a number of non-human life sciences payloads on NASA's Space Shuttle's Spacelab. Included in this responsibility is the training of those individuals who will be conducting the experiments during flight, the astronauts.

Preparing a crew to conduct such experiments requires training protocols that build on simple tasks. Once a defined degree of performance proficiency is met for each task, these tasks are combined to increase the complexity of the activities. As tasks are combined into in-flight operations, they are subjected to time constraints and the crew enhances their skills through repetition. The science objectives must be completely understood by the crew and are critical to the overall training program. Completion of the in-flight activities is proof of success. Because the crew is exposed to the background of early research and plans for post-flight analyses, they have a vested interest in the flight activities. The salient features of this training approach is that it allows for flexibility in implementation, consideration of individual differences, and a greater ability to retain experiment information. This training approach offers another effective alternative training tool to existing methodologies.

INTRODUCTION

The Space Life Sciences Payloads Office at NASA's Ames Research Center (ARC), is responsible for the development and operations of non-human Life Sciences research performed aboard the Space Shuttle. Experiment proposals are submitted to NASA by Investigators from the research community. Selected experiments are then developed by NASA for performance aboard the Space Shuttle. Once experiments are identified and manifested for a mission, the next important step is the training of flight crew to perform the experiments to be flown.

The objective of this paper is to describe the training approach used by the Ames Research Center Space Life Sciences Payloads Office to prepare payload crew for non-human life sciences experiments. Using a systems approach, the project office optimizes personnel and crew time within the constraints of mission schedules, equipment availability, and funding. What follows is a detailed description of the process used to train the crew, the documentation requirements, certification and

final validation of operation. This approach to crew training has been successful in training crews on Spacelab-3 and most recently on STS-40, the Spacelab Life Sciences-1 (SLS-1) Mission.

CREW TRAINING FLOW

In order to prepare crew members for successful performance of the in-flight science objectives and tasks for each payload, critical tasks must be separated and identified in such a manner as to distinguish the discrete skills and knowledge required to perform. Training activities are aligned with the experiment objectives. To facilitate training, an experiment is divided into experiment sessions, which are related to the experiment objectives identified in the experiment requirements documents. Each session is then divided into distinct training modules. Modules are further divided into procedures and then into the smallest operational elements, procedural steps (fig. 1).

Training activities for all crews assigned on Space Shuttle missions are developed such that the various procedural elements flow with the training components, specifically Mission Dependent Training. Crew training for space life sciences payloads is managed as part of the overall Mission Dependent Training.

Mission Dependent Training on Life Sciences Payloads is divided into timed phases: Orientation, Task, Phase, Project Integrated, Mission Integrated, and Proficiency Training. Every component of each experiment and associated hardware is subject to the same basic training template (see fig. 2). This approach provides an ideal working model as each successive training session builds knowledge gained from the previous training session until proficiency on the integrated payload procedures is achieved. What follows is a description of each component of the training process, and how it is integrated into the in-flight operations.

Orientation Training

As part of Orientation training, the crew gets briefed on all aspects of the in-flight activities, as well as pre- and post-flight ground activities. This is an opportunity for the crew to gain a full understanding of the overall objectives to be accomplished as part of the mission. The in-flight activities are justified to the crew, which gives them an opportunity to relate to the various aspects of our activities, and help them fully understand the ramifications of the successful performance of the hardware. The training may take place at Ames or in the Principal Investigator's (PIs) laboratory. In the case of SLS-1, the crew's orientation at Ames Research Center consisted of a briefing of our experiments and orientation to our complement of rack mounted hardware (i.e., Research Animal Holding Facility, General Purpose Work Station and Small Mass Measurement Instrument), other associated hardware, and the middeck stowed Animal Enclosure Modules. They also received experiment orientation at PIs' labs for the Jellyfish Experiment and the Cardiovascular animals. For SLS-1, approximately 47 training hours were accomplished for each crew member during this interval of training.

Task Training

During task training, the payload crew becomes proficient in all aspects of the experiment objectives through intensive and in-depth lectures on Experiment Unique Hardware (EUH), stowed items, discussion of procedures, and thorough hands-on training with specimen and available experiment hardware. Task training is often accomplished together with orientation training. Sometimes a training session is offered at two different times so that every crew member can be exposed to the same material. In this way, we are able to cross-train each payload crew member.

Phase Training

This portion of training is designed to allow the crew the opportunity to complete enough repetitions of the experiment so the crew member is able to complete the experiment procedures at a defined level of time proficiency. Training utilizes the experiment operating procedures, payload specific hardware, and stowage items. This training opportunity also provides the crew with a level of proficiency which would guarantee a meaningful participation in the Experiment Verification Test, scheduled during the next phase of training.

For SLS-1, the crew logged approximately 37 hours during this portion of the training.

Project Integrated Training

The objective of crew training during an Experiment Verification Test is to conduct project integrated training of the payload crew members. Crew members must perform all ARC in-flight activities while assisting in validation of the SLS-1 timeline. The crew must be trained ahead of time in the tasks necessary to support these various experiments. Although the crew is familiar with the payload, this test is usually the first time they combine the tasks into operational procedures using flight hardware and stowage items.

For the SLS-1 Mission the crew participation covered approximately 40 hours of the total 72 hour execute shift. Crew participation was scheduled such that the crew witnessed and participated in the major in-flight activities and received systems and malfunction training during hours outside of the EVT timelined events. The verification test allows for evaluation of the 1-G timeline and also allows validation of the in-flight procedures as written for the hardware configurations and science requirements known at the time.

Mission Integrated Training/Simulations

Mission Integrated Training/Simulations is two fold; it allows the crew to develop their proficiency to a level of performance where they can successfully perform all the payload activities within the mission timeline and also allows the Payload Operations Control Center (POCC) cadre and PED support the opportunity to rehearse in-flight ground protocols. It is similar to project

integrated training, but includes timeline performance of all mission experiments and other activities necessary to carry out the mission. This training occurs within a fully integrated spacelab mockup.

Locations for stowage hardware are finalized, locker foam is included, and the stowage hardware is integrated into the respective locations with the mockup. Procedure validation, designation of velcro mapping, and timelining are important elements of this phase of training. Flight documentation in various stages of development is normally used by the crew to support these simulations. In addition, the crew uses Spacelab and Orbiter equipment, consumes food to be supplied during flight, and dresses as they would during the actual flight.

During this phase, it is recommended that additional proficiency training be conducted on critical operations, this includes nominal as well as malfunction training.

The SLS-1 payload had the unique opportunity of participating in ten simulations with the POCC cadre. In addition 5 Joint Integrated Training/Simulations were scheduled with POCC Cadre at MSFC, mission control personnel at JSC, and the crew traveling between the spacelab mockup, the middeck mockup and the shuttle simulators. Each of these training opportunities simulates different start and stop times on the overall mission timeline.

DOCUMENTATION REQUIREMENTS

Working on a shuttle experiment involves a large number of people, working at different locations on a variety of activities. Crew training activities involve crew members, generally in Houston; mission management personnel, either at Johnson Space Center or Marshall Spaceflight Center; principal investigators, located throughout the United States, and project personnel and hardware, located at ARC. Publication and timely distribution of documentation are the most effective methods for coordinating information with personnel in multiple locations who engage in widely differing activities. Training documentation required for all ARC Space Life Sciences Payloads includes:

Crew Training Plan

This document describes in detail the content of the ARC training and how it will be conducted for a particular mission. It defines the number of hours required to achieve proficiency and subsequent flight performance. It describes the training approach and objectives. In addition, the project crew training plans will include appendices which address the following:

Experiment Summaries
Payload Training Requirements
(by level: Orientation/Task, Phase, Project Integrated, Mission Integrated, etc.)
Documentation Requirements Schedule
Flight Crew Training Schedule

The Crew Training Plan should be issued at the launch minus 24 to 18 month timeframe.

Milestones for Scheduling

When planning crew training, there are a number of milestones that must be accomplished before the training session can begin. Some are generic requirements and others are specific to the individual experiment or payload. These should be included in each project's sub-tier schedule for crew training. The following lists those generic milestones that are ordinarily included in a crew training sub-tier schedule:

Workbook/Familiarization Manuals Completed and/or Procedure update completed (include draft, review and signature cycle)
Room Logistics (Schedule conference rooms, labs or high bay)
Visitor Requirements
Public Information Office (PIO)/photo involvement
Training Agenda
Input from PI (for Orientation/Task Training)
To Crew
Final to Project Office
Hardware Readiness (Individual hardware items that are needed for training)
Readiness Reviews (1-2 weeks prior)
Training Session Dry Run (1 week prior)
Actual Training Sessions
Crew Debriefing after each training session
Project Debriefing

Familiarization Manual

This document provides background material that is useful for crew orientation. The manual summarizes the goals of the mission and describes each of the payload experiments and all associated hardware. Each manual is controlled under configuration management. This manual is usually distributed one month before the payload orientation session.

The basic format for a familiarization manual is as follows:

- Cover Page
- Table of Contents
- Background to particular mission
- Experiment Descriptions
- Experiment Hardware Descriptions – including labelled drawings and or photographs

Crew Training Workbook

A Crew Training Workbook is developed for each experiment or test to be flown. The workbook gives much more detail about each experiment than does the Familiarization Manual and is used by

the crew as an orientation of the in-flight procedures, as a reference during hands-on training and as a post-training refresher. Each workbook is assigned a control number, and subsequent revisions are made by the Crew Training Office. Workbooks are distributed 2-4 weeks prior to experiment task training.

The basic format for the workbook is as follows:

- Cover Page
- Forward Page – which includes the instructor's (principal investigator), address, phone and general introduction statements
- Table of Contents
- Acronyms and Abbreviations
- Applicable Documents
- Lesson Introduction – covers the reason for the experiment, background, past research, rationale, methodology, expected results, references, and summary of Experiment-Unique Equipment.
- Learning Material – the bulk of the workbook, includes in-flight procedures
- Appendices – may include applicable PI publications

Depending on the complexity of the experiments or the payload, it may be necessary to combine the Familiarization Manual with the Crew Training Workbook. In such cases, it will be called a Workbook/Familiarization Manual.

Procedures

There are two categories of procedures: (1) Ground Experiment Operating procedures which detail experiment tasks, and (2) Experiment Operating procedures which are performed in flight.

Ground Experiment Operating procedures are detailed experiment specific laboratory procedures which are learned during task training. They may be more detailed or may be the same as experiment operating procedures. They may include specific specimen handling practices, surgical operations, materials processing and operation of experiment unique flight hardware. They are defined by the PI and other members of the experiment team and are part of the experiment workbook. They will be provided to the crew with workbooks.

Experiment operating procedures are discipline (experiment) oriented; they are performed in-flight. They may be the same as a ground operating procedure or they may involve several integrated experiment procedures which utilize an animal. They may also involve common hardware.

Payload Flight Data File

A portion of the Payload Flight Data File (PFDF) is an outgrowth of the nominal in-flight procedures used in the training workbooks and is revised during and after each training session. It develops with the crew's experience on the various experiments, hardware items, etc. The crew

procedures are updated after each training session so that prior to Project Integrated training, the experiment procedures are converted to the PFDF format (the project's preliminary version). With each revision, the procedures are reduced from a detailed to a checklist format and requires input from the crew as they become more proficient in the experiments. The other portion of the PFDF consists of malfunction procedures. These procedures are also revised after being validated, whether through hardware verification or crew training. The nominal in-flight procedures, together with malfunction procedures, constitute a small portion of the PFDF. The PFDF consists of all documentation flown during a flight. This includes orbiter and payload nominal and malfunction procedures, reference documents and flight rules.

The by-products of Mission Dependant Training are documented in the following Payload Flight Data File documents:

Experiment Procedure Reference Book
Experiment Procedures Checklist
Stowage Book
Experiment Malfunction Procedures
Spacelab Photo/TV Checklist
Payload Systems Handbook
Payload Crew Activity Plan
Spacelab Activate/Deactivate Checklist

The final PFDF is a mission-produced document composed of project submittals.

CREW EVALUATION AND CERTIFICATION PROCESS

The evaluation and certification of crew members in the performance of experiment operations progresses through each training level in a building block fashion. The goal of training is to teach. The intent of crew evaluation is to identify areas where the training should be revised, improved or repeated. Each crew member has an important responsibility in this process. Evaluation and certification of crew proficiency in performing payload operations starts with the PI at the first level of training, moves on to the project level during phase and/or project integrated training and is finally completed by the mission manager after Joint Integrated Training Simulations (JITS).

Crew Evaluation

The following are suggested criteria to be used when evaluating crew proficiency:

1. Completion of all training documentation.

2. Completion of number of required training hours.

3. Demonstration of payload operations during task, phase, and project integrated training.

4. Demonstration that payload operations conform to predetermined timeframe.

5. Demonstration of understanding that experiment measurements and samples are in normal range.

6. Results of nominal, off-nominal, long duration, and joint integrated training simulations.

The PI is responsible for completion of a training report (see Appendix A) for each crew member following the completion of orientation/task training. Each crew member is also responsible for identifying additional training desired by completing questions 5 and 6 of the ARC Project Crew Evaluation form (see Appendix B).

IN-FLIGHT ACTIVITIES

After the crew supports the above training schedule, the fruits of their labor are witnessed as they conduct the in-flight activities on POCC console monitors and NASA Select television (figs. 3-9). The activities are generally performed as rehearsed during training, keeping the science constraints, flight rules, and hardware limitations in mind, adapting their skills and knowledge of the experiments to the zero-g environment. The actual results of the experiments is the validation of successful training.

CONCLUSION

While the project goals in support of a mission are generally assumed to be the delivery of hardware and its subsequent integration, an integral portion of flight development includes ensuring the prime operators of the experiments are fully versed in all its operations.

Effective crew training is crucial to the successful completion of in-space life sciences experiments. Ames Research Center has developed and utilized a training process that assures proper exposure of crew members to all aspects of experiment protocols and prepares them for proper implementation of these experiment protocols in space (ref. fig. 2).

The ability of the crew to perform the in-flight procedures, to respond to hardware anomalies, as trained, and to speak knowledgeably of the experiments at briefings can be considered the validation of a successful training program.

ACKNOWLEDGMENTS

The authors would like to thank Dr. M. Rhea Seddon, Dr. James P. Bagian, Dr. F. Andrew Gaffney, Dr. Millie Hughes-Fulford and Dr. Tamara Jernigan, the crew of STS-40 (Spacelab Life Sciences-1) for their support in the development of the Ames Research Center Payload Crew Training methodology described in this paper.

APPENDIX A

ARC PROJECT TRAINING REPORT

EXPERIMENT NAME/NO.: _____ DATE: _____

TYPE OF TRAINING: _____

TIME UTILIZED TO COMPLETE SESSION: _____

1. I certify that _____ has successfully completed the above training session.

2. PI Comments:

   a. Accomplishments during training:

   b. Tasks requiring additional practice/training:

   c. Recommendations for future training sessions.

_____ _____

Principal Investigator Date

ARC PROJECT CREW EVALUATION

EXPERIMENT NAME/NO.: _____ DATE: _____

TYPE OF TRAINING: _____

LOCATION OF TRAINING: _____

1. Was training documentation provided in sufficient time to allow for adequate preparation for training?

_____ Yes

_____ No; explain

2. Were training resources such as training documentation, procedures, hardware, and facilities adequate?

_____ Yes

_____ No; explain

3. Was time used efficiently during training?

_____ Yes

_____ No, explain

4. Was the time allocated for training:

_____ Too long: explain

_____ Correct

_____ To short; explain

ARC PROJECT CREW EVALUATION

5. Do you feel the training activities have prepared you to perform the required tasks?

_____ Yes

_____ No; explain

6. Identify any additions, deletions or modifications to training and/or training resources (hardware, procedures, facilities, etc.).

7. Other comments?

_____

Crew Signature (optional)

BIBLIOGRAPHY

1. Rodrigues, Annette T.: Crew Training Plan, Volume 1, General Crew Training. NASA Ames Research Center, Space Life Sciences Payloads Office controlled document, Sept. 15, 1989.

2. Dickey, Bernadette: Operational Manual for Payload Specialists Related Activities: Payload Specialists Training, Volume 1 Plan.

3. Kelly, Fred: America's Astronauts and Their Indestructible Spirit. TAB Books, 1986.

4. Johnson Space Flight Center Document #12819: Training Materials Development Handbook. Nov. 1978.

5. Johnson Space Flight Center Document #08969: Space Shuttle Crew Procedures. May 1976.

6. Johnson Space Flight Center Document #09958: Space Shuttle Flight Data File Preparation Standards. March 1991.

7. NASA Reference Publication 1059: STS and Associated Payloads: Glossary, Acronyms, and Abbreviations. 1982.

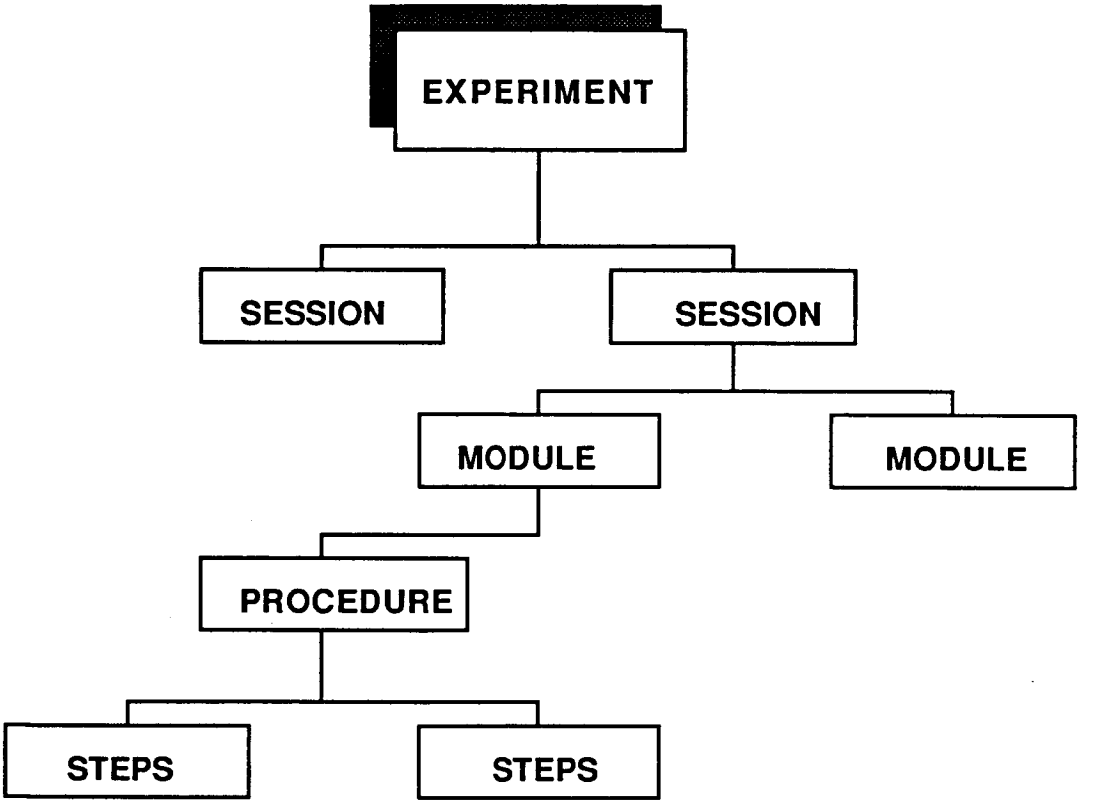

Figure 1. Experiment procedural elements.

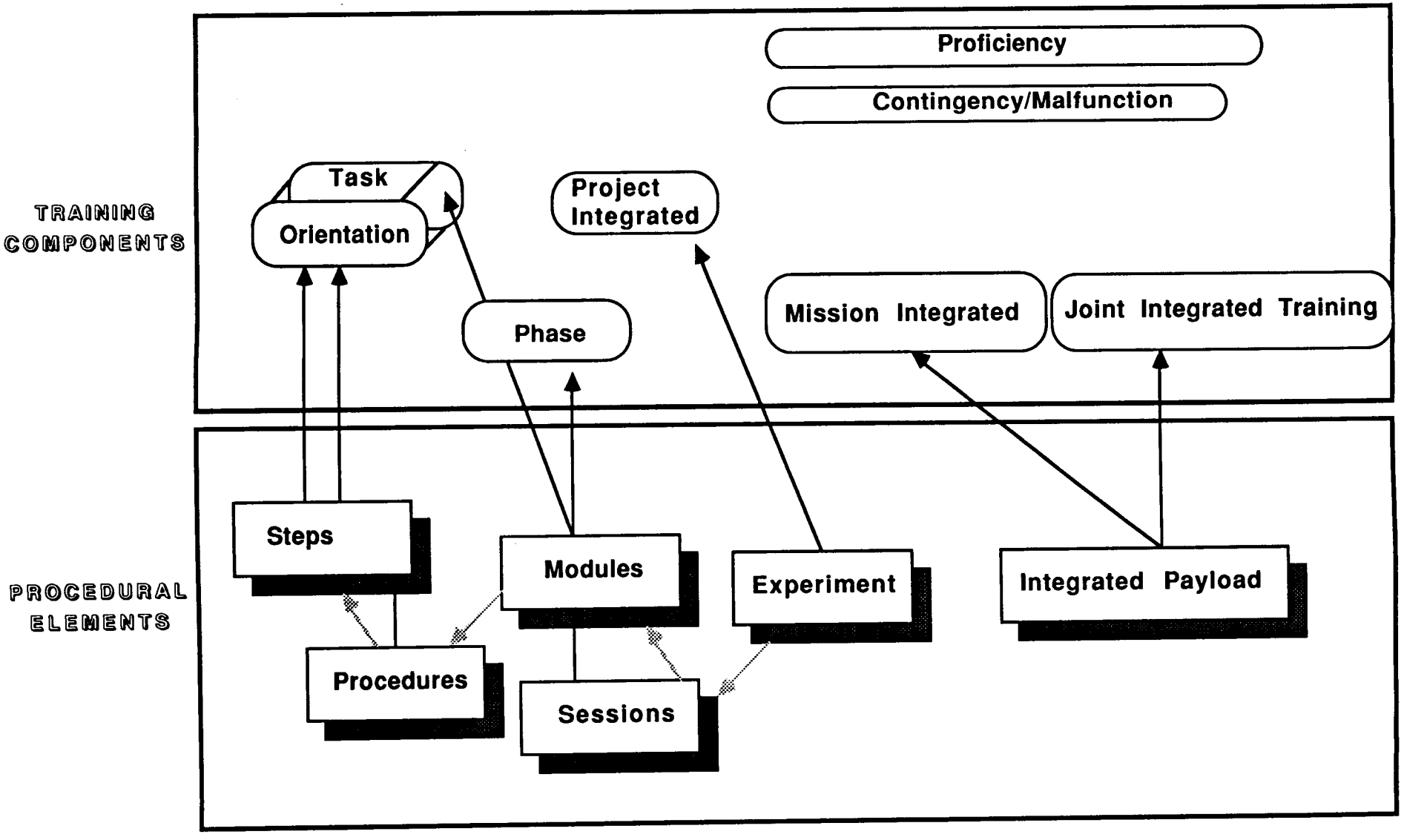

Figure 2. Crew training flow.

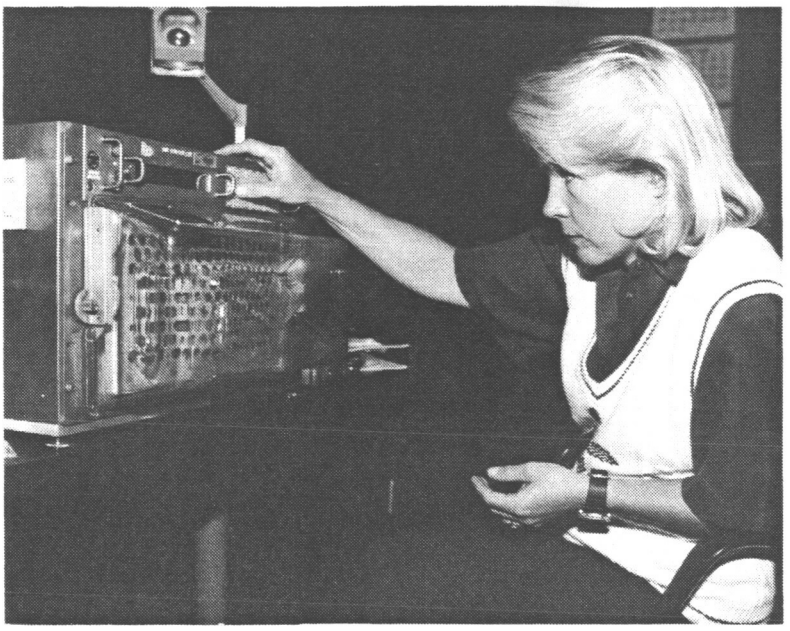

Figure 3. Mission Specialist Rhea Seddon during orientation training of small mass measurement instrument.

Figure 4. Payload Specialist Millie Hughes-Fulford during laboratory orientation training.

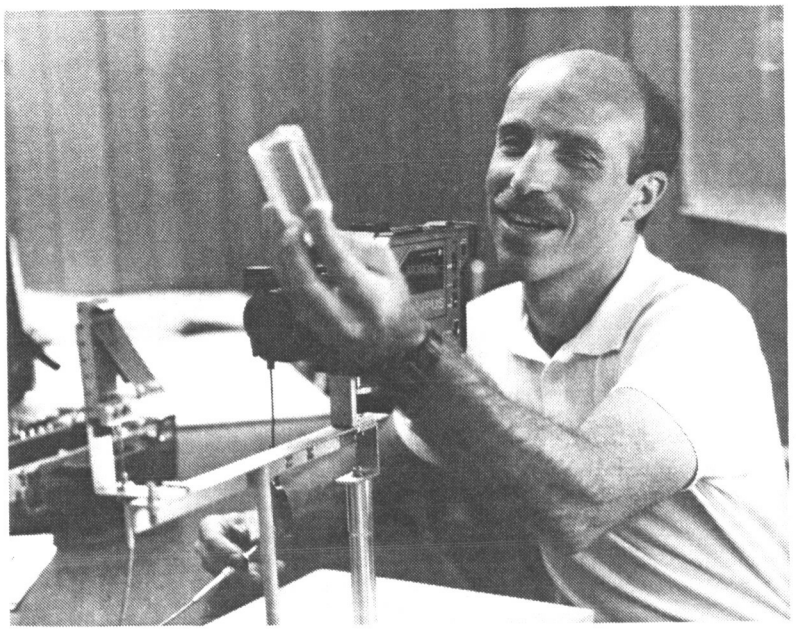

Figure 5. Mission Specialist Jim Bagian examining jellyfish specimen during jellyfish task training.

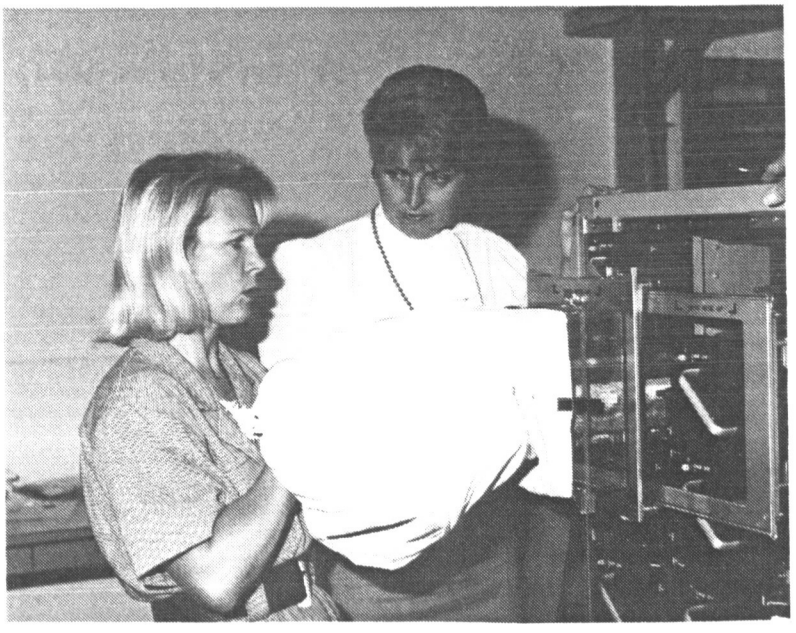

Figure 6. Mission Specialist Rhea Seddon and Payload Specialist Millie Hughes-Fulford during cage transfer phase training.

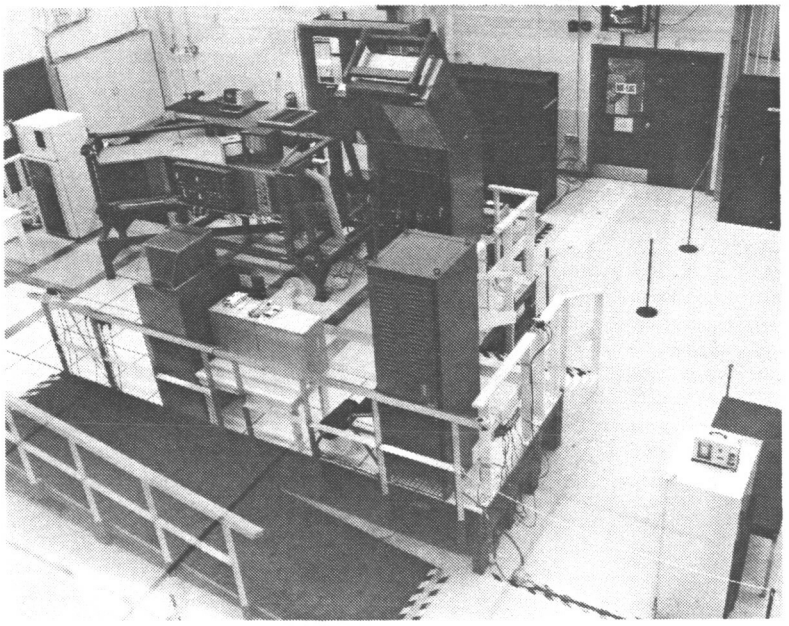

Figure 7. Project hardware configuration during payload experiment verification test.

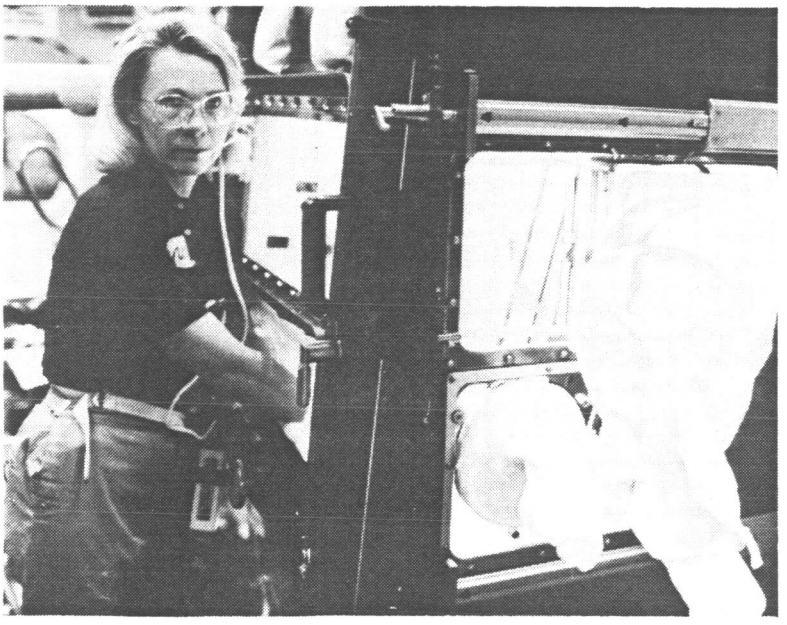

Figure 8. Ms. Rhea Seddon at general purpose workstation during EVT.

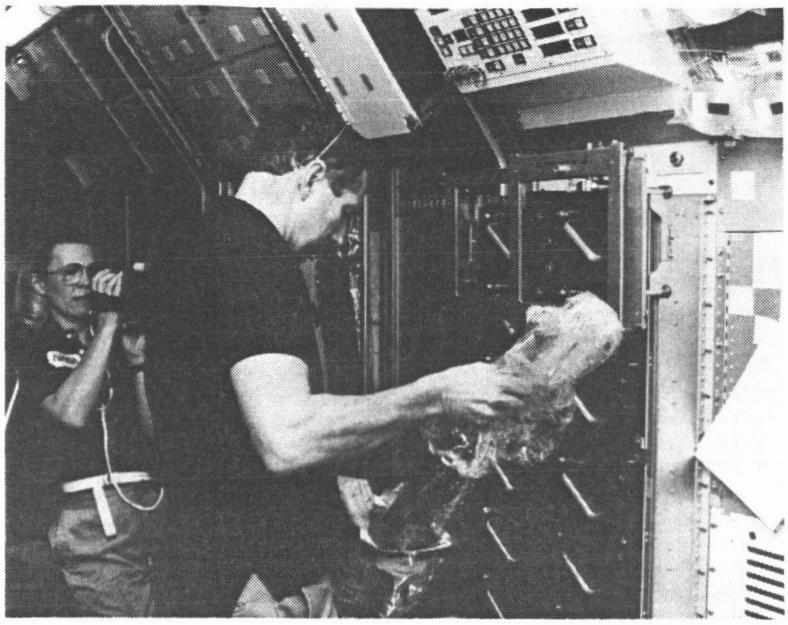

Figure 9. Payload Specialist Drew Gaffney and Mission Specialist Rhea Seddon doing cage transfer procedure during mission integrated simulation.

BIOGRAPHY

Annette T. Rodrigues started her Federal career with the Naval Radiological Defense Laboratory in 1968. Over the years she has acquired a vast array of experience in such areas as Government Procurement, Human Resources, Personnel Development, Spaceflight (experiment) Crew training and various Project Management functions. Her project experience at Ames Research Center has included work on the Biosatellite III and Spacelab Life Sciences Missions (SL-3, SLS-1, SL-J & SLS-2).

Currently Ms. Rodrigues is the staff assistant to the Center Deputy Director. In this capacity she serves as advisor and special assistant to the Deputy Director of the Center. As the Deputy Director's representative, she is responsible for the continuous review and analysis of institutional activities and policies. As the prime interface with the Deputy Director, she provides administrative advice and direction to his staff offices, including the offices of the Chief Counsel, Safety, Reliability, and Quality Assurance, Equal Opportunity and External Affairs.

Ms. Rodrigues received her BS degree in Business Administration from San Jose State University (1976) and an MS degree in Systems Sciences from University of Southern California (1987).

Christopher Maese graduated from the University of Santa Clara in 1980 with a B.S. in Biology, then earned an M.A. in Biology, specializing in physiology, from San Jose State University. Since 1988, he has worked in the Space Life Science Programs Office at Ames Research Center.

THE RHESUS MEASUREMENT SYSTEM: A NEW INSTRUMENT FOR SPACE RESEARCH

Julie E. Schonfeld and John W. Hines
Ames Research Center
Moffett Field, California

INTRODUCTION

The Rhesus Research Facility (RRF) is a research environment designed to study the effects of microgravity using rhesus primates as human surrogates. This experimental model allows investigators to study numerous aspects of microgravity exposure without compromising crew member activities. Currently, the RRF is slated for two missions to collect its data, the first mission is SLS-3, due to fly in late 1995. The RRF is a joint effort between the United States and France. The science and hardware portions of the project are being shared between the National Aeronautics and Space Administration (NASA) and France's Centre National D'Etudes Spatiales (CNES).

The RRF is composed of many different subsystems in order to acquire data, provide life support, environmental enrichment, computer facilities and measurement capabilities for two rhesus primates aboard a nominal sixteen day mission. One of these subsystems is the Rhesus Measurement System (RMS). The RMS is designed to obtain in-flight physiological measurements from sensors interfaced with the subject. The RMS will acquire, pre-process, and transfer the physiologic data to the Flight Data System (FDS) for relay to the ground during flight. The measurements which will be taken by the RMS during the first flight will be respiration, measured at two different sites; electromyogram (EMG) at three different sites; electroencephalogram (EEG); electrocardiogram (ECG); and body temperature. These measurements taken by the RMS will assist the research team in meeting the science objectives of the RRF project.

THE SCIENCE OBJECTIVES OF THE RRF

The science experiments of the project will be performed by a team of U.S. and French principal investigators (P.I.) studying the effects of microgravity in the following areas: behavior and motor performance; muscle and bone physiology; calcium homeostasis; immunology/microbiology; cardiopulmonary, regulatory, and neural physiology.

During the mission, the subject will occupy his daylight hours by performing tasks on the Psychomotor Test System (PTS). The PTS consists of a monitor, a joy stick, and a number of pre-programmed tasks that the subject performs. The tasks involve maneuvering a pellet through a maze, similar to that of several video games. Successful completion is rewarded with a food pellet. Behavior and motor performance will be evaluated through the use of the PTS and the Activity Video System (AVS). Basically, the AVS is a video camera and image processing system which will record the subject's actions during the flight. The scientists will integrate the data recorded from the PTS

and the AVS to study the primate's eye-hand motor skill, reaction time, perception and discrimination, target prediction, attention, memory, and ability to learn. These results will be compared to pre- and post-flight testing to determine how exposure to microgravity affected these characteristics.

Several aspects of muscle physiology will be studied. The research team will examine pre- and post-flight EMG patterns, using the AVS system to coordinate EMG activity with muscle movement. Muscle biopsy samples will be extracted pre- and post-flight and evaluated for biochemical changes due to microgravity exposure. The research team will examine muscle contractile protein alteration, myosin changes in muscle fibers, and ultrastructural remodelling of the muscle-tendon and muscle-nerve interfaces. The investigators will characterize the physiological mechanisms responsible for any observed changes due to microgravity.

To aid the research team, the RRF will be a closed biological system: all inputs and outputs will be quantified and qualified; food and water intake, electrolyte intake, urine output, and feces volume. Utilizing this closed system, the investigators will gain insight into calcium regulation, fluid and electrolyte shifts, hormonal responses, and temperature regulation.

Bone morphology studies will include pre- and post-flight bone biopsy samples, bone density measurements, and bone marrow samples. These observations will help determine if changes in bone calcium regulation (release/resorption) occur upon exposure to microgravity, and if so, whether these changes lead to modified bone cell activity and/or bone synthesis.

Fluid, electrolyte, and hormonal shifts are known to occur in human subjects upon exposure to microgravity within the cardiopulmonary system. The RRF will collect data on heart rate, pulmonary gas exchange kinetics, respiration rate, tidal volume and fluid volume shifts via ECG and abdominal and thoracic respiration. This information will allow investigators to quantify the magnitude of regulatory changes within the cardiopulmonary system.

Within the environment on the space shuttle, it is not possible to completely separate the life support systems of the animals and the astronauts. Therefore, it is necessary to assess the cross contamination of micro-organisms between the humans and the animal subjects, and any subsequent immune response. Cultures will be collected from both groups and susceptibility to antibiotics will be assessed as well as lymphocyte proliferation. Modification of intestinal microflora and fermentation will also be studied as a part of the immunology-microbiology discipline.

Space Adaptation Syndrome (SAS) is a problem encountered by many astronauts and may affect the ability of man to inhabit space for any significant length of time. The RRF will examine ECG and EEG data, correlated with PTS and AVS activity, to study the neurophysiological responses and potential mechanisms associated with SAS.

THE RHESUS MEASUREMENT SYSTEM

The RMS has several different components. Functionally, the RMS is composed of sensors, which interface to the subject; the Respitrace subsystem, which interfaces directly with the respiration sensors; the biotelemetry subsystem; the signal conditioning unit, a digital sampling and

memory storage unit, and a power supply module. The biotelemetry subsystem is a receiver for an implanted transmitter which measures ECG and deep body temperature. The biopotential signal sensors for EEG and EMG interface directly to the signal conditioners.

Physically, the system is comprised of four different units: the Biotelemetry subsystem, the Respitrace subsystem, the Animal Analog Signal Conditioner, and the Power Supply Module. The configuration of the RMS can be seen in figure 1.

The Biotelemetry subsystem, referred to as Experiment Unique Equipment-1 (EUE-1), is one unit. The subsystem consists of a receiver, EUE-1, and the implanted transmitter. This transmitter contains the sensors which measure ECG and body temperature. ECG is measured with bio-potential leads attached across the heart. Body temperature is measured with a thermocouple. These readings are then modulated on to bursts of a 455 KHz signal which is then demodulated into the different signals and passed on the AASC for final signal conditioning. Because of the low power implanted transmitter, the receiver must be located close to the subject. Therefore, EUE-1 is mounted under the primate's left armrest.

The Respitrace Subsystem consists of EUE-2, and the respiration sensors, called the Respibands. The Respitrace utilizes inductance plethysmography to measure volume shifts in different parts of the body. This is implemented by the two Respibands, which are used to measure the respiration rate of the primate, and additional circuitry. The two Respibands, one placed around the thoracic region and the other on the abdominal region, are composed of a wire sewn into an elastic band in a zig-zag fashion. The bands each act as a single turn inductor which, when expanded and contracted, cause a change in inductance proportional to the circumference changes caused by respiration. Each inductor completes a phase-lock-loop oscillator circuit, creating a frequency shift proportional to the inductance change. A frequency to voltage conversion circuit then produces a voltage output analogous to the inductance change. The outputs of the Respitrace are further conditioned by a card located within the AASC. EUE-2 must also be close to the subject because it is connected to the Respibands. The unit mounts underneath the right armrest of the primate's chair.

The AASC houses the signal conditioning cards, the digital system, and two power cards. This unit has been the most complicated piece of the RMS to develop. While the AASC will provide 8 channels of data during its first mission, it is designed to accommodate up to 16 channels. The AASC is configured into 7 signal conditioner cards, 3 digital system cards and 2 power cards mounted into a single backplane. Because of a $180 \times 240 \times 70$ cm envelope enclosure restriction, surface mounted components have been used in the design. The AASC is mounted on the wall behind the rhesus compartment. The signal conditioners must be located fairly close to the low level signals it receives in order to reduce noise induced on the lines. Table 1 gives the characteristics of all the cards in the AASC.

The signal conditioner cards in the AASC filter the signals into appropriate bandwidths and scale them to a 0-5 Volt signal. There is one signal conditioner card for each physiological signal except the respiration measurement, which has a dual respiration signal conditioning card. The signal conditioner cards also contain calibration circuitry to allow for in-flight calibration of the circuits and to optimize measurements for each particular subject. The AASC has been designed as a modular system. Signal conditioner cards are interchangeable. The modular design allows new signal

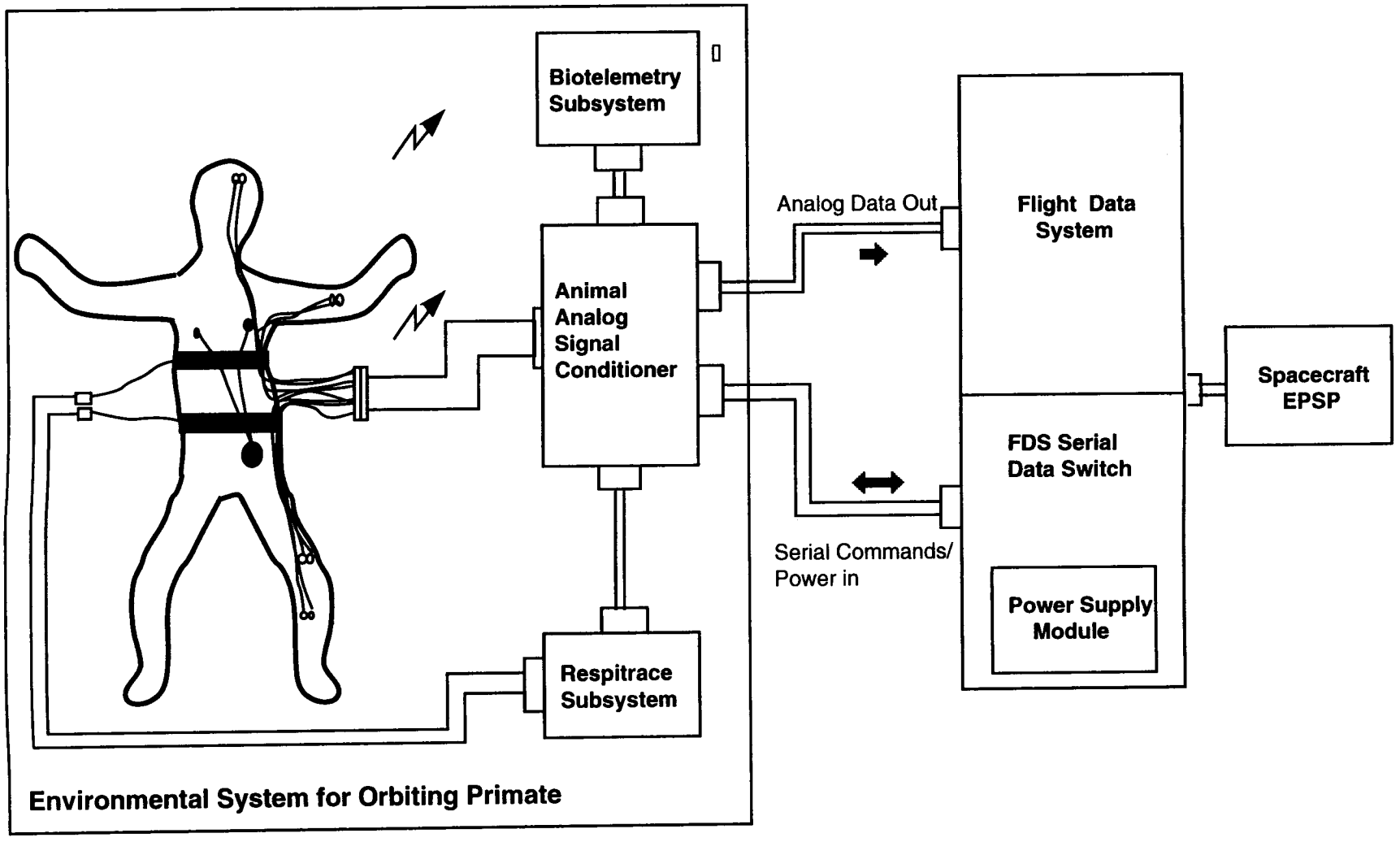

Figure 1. RMS Block and Interconnect Diagram.

Table 1. AASC board characteristics

Board	Input level (V)	Gain range	Offset range (V)	Filter range (Hz)
EMG	.1 - 10 mV	400 to 40,000	2.5 nominal	2 to 1000
EEG	.01 - 10 mV	400 to 40,000	2.5 nominal	1 to 100
TEMP	0 - 1 V	0 to 100	2.5 nominal	Low pass 1 Hz
ECG	1 V P-P	1,2,5,10,20, 50, 100	2.5 nominal	0.05 to 100
Dual RESP	1 V P-P	1,2,5,10,20,50, 100	2.5 nominal	Low pass 10 Hz
PWR Cond	± 8.5 V	N/A	N/A	N/A
PWR ISO	± 8.5 V	N/A	N/A	N/A
Micro-controller	68HC11 Microcontroller, provides parallel control ports to cards: 8 ch., 8 bit A/D converter, RS-232 Serial Communications Port			
Micro-peripheral	Provides control for the memory plus battery backup for memory			
Memory	≥ 2 Mbytes 8 bit SRAM Memory			

conditioner cards to replace the originals so that new measurements can be collected in future flights without a complete redesign of the instrument. Also, this allows the hardware to be used for ground-based research.

The power cards and the digital system cards are fixed in the AASC. The first power conditioner card further regulates the output of the Power Supply Module and routes it to the power isolation card. The power isolation card prevents a shock hazard to the subject by generating a floating power supply for the biopotential signals (EEG and EMG) which are directly connected to the biopotential signal conditioning cards. To prevent shock originating from direct short circuits to the isolation power card, there is a high input impedance between the probes and the signal conditioning card, which severely restricts current flow.

The digital system provides the AASC with the ability to acquire and store data during the ascent and descent phase of the flight. During that time, power supplied to non-critical hardware in the shuttle must be kept to a minimum. The Flight Data System requires much more power than the RMS alone; therefore, during those phases the RMS must store the data. The data will be down-loaded to the FDS in flight when it comes on line. The digital system consists of a microcontroller card, a memory card containing at least 2 megabytes of memory, and a memory controller card.

The digital system gives the AASC considerable flexibility. Through the software stored in the microcontroller card, the system has the capability to adjust gains, offsets, and sample rates and provide a calibration and operate mode for each different signal. Because of the limited memory due to size constraints, different sampling scenarios have been developed. These scenarios are outlined in table 2. These scenarios allow the research team to optimize the data available to them during ascent and descent. In EEG and EMG, with a bandwidth of 1000 Hz, there is much information to be gained at a high sampling rate. However, to do so would require large chunks of memory. The compromise is to sample high fidelity data for 10 seconds of each minute on two channels of EMG, and 1 minute out of every 2 hours on the other EMG channel.

Table 2. RMS Digital System Sampling Scenario

Parameter	Ascent Duty cycle	Ascent sample rate (Hz)	Descent Duty cycle	Descent sample rate (Hz)
ECG	N/A		N/A	
Heart rate	60 sec		.2	
Body temp	60 sec		.2	
EMG1	50 sec/6 min	50	50 sec/8 min	50
	10 sec/6 min	1000	10 sec/8 min	1000
EMG2	50 sec/6 min	50	50 sec/8 min	50
	10 sec/6 min	1000	10 sec/8 min	1000
EMG3	N/A		1 min/2 min	50
	1 min/2 hr	2000	1 min/2 hr	2000
EEG	(Undecided)			
Respiration (abdominal)	1 min/3 min	20	1 min/2 min	20
Respiration (thoracic)	1 min/3 min	20	1 min/2 min	20

The Power Supply Module (PSM) is the fourth element of the RMS. The PSM receives power in the form of +28 Volts from the Shuttle's Experimental Power Switching Panel (EPSP). Utilizing DC to DC converters, it then converts it to the ±8.5 volts necessary to power the AASC. As required by Shuttle, the PSM has a large inductor on the front end to smooth voltage transients up to twice the nominal value of the supply. The Power Supply Module, which does not require close proximity to the AASC, is mounted in a separate rack.

FLIGHT HARDWARE REQUIREMENTS

In addition to the electrical requirements, the hardware must prove to be rugged and safe in order to be certified for flight on the Shuttle. The primary requirement is that the hardware must not compromise the safety of the crew or the study subjects. Further, the hardware must be able to withstand moderate vibration, possible pressurization and depressurization, and temperature fluctuations without flying apart or exploding. Materials used in the instrument must not offgas chemicals into the

shuttle environment and must not be flammable. The system must not radiate electromagnetic interference (EMI) which might disrupt Shuttle systems. A secondary requirement is that, subject to all these conditions, the hardware must function properly. Electrical components must have the highest reliability available and mechanical components must maintain their integrity.

The system, therefore, is subject to rigorous analysis and testing regimes to verify it is qualified for flight on Shuttle. Analyses are performed to show it will withstand pressurization and to show a sufficient number and size of fasteners are used to mount components. The vibration and EMI tests performed on the hardware demonstrate that the RMS will not come apart and it will not interfere with other Shuttle systems. Materials used in the system must have been individually evaluated for suitability in space are rated non-toxic, particularly with regards to flammability and offgassing in non-metallic parts. Since the RMS utilizes surface mounted components, a relatively new flight hardware technology, the electrical components will face card level testing before flight. The cards will be subject to temperature cycling and vibration tests. This is in addition to the normal qualification testing sequence.

Another important requirement of the RRF is that it not contaminate the crew cabin with animal odors or particles. The RMS fulfills this requirement, because the AASC mounts on a surface which is an interface between the animal's chamber, the Environmental System for Orbiting Primate (ESOP), and the crew cabin. Thus, the AASC is attached with a gasket that provides an airtight seal. The integrity of the seal is tested for a specific leak rate. The interface gasket on the AASC also supplies a continuous electrical connection to the ESOP thereby providing a complete EMI shield.

The RRF has also developed a "power contract" with the shuttle limiting the maximum power the RRF may consume at all times during the mission. Power on the shuttle is limited and therefore, is doled out carefully, particularly during ascent and descent. The RMS has been allocated 20 Watts for the duration of the mission. The use of low power and CMOS surface mounted circuitry provides the RMS with a tremendous advantage in being able to accomplish the science objectives of the RRF well under this power restriction.

THE FUTURE

The RMS was designed to support the science objectives of the Rhesus Research Facility, but the system's capabilities extend beyond this mission. The surface mounted components utilized in the RMS will continue to pave the way for future flight hardware design, especially given the size and power restrictions on the Shuttle. The configuration of the RMS also allows the incorporation of hybrid technology which would further expand its capabilities. With instrumentation being so costly to develop, it is well worth our efforts to design hardware which can be used over again. With its versatile design, the RMS can implement new measurements accommodating many different kinds of science research, both ground-based as well as in space.

BIOGRAPHIES

Julie Schonfeld has been at Ames Research Center for one year in the Electronic Systems Branch. She is currently serving as the Deputy Project Manager, Systems Engineer for the Rhesus Measurement System project. Previously, Ms. Schonfeld worked at Kennedy Space Center in the Design Engineering, Instrumentation Section. There, her projects included the Hazardous Gas Detection System, both primary and back-up, and the Solid Rocket Booster Inadvertent Ignition Detection System. Ms. Schonfeld received a B.S. in Electrical Engineering from the University of Central Florida is currently working on an M.S. in Electrical Engineering at Santa Clara University.

John Hines is manager of the Sensors 2000! (S2K!) Program, an Advanced Biosensor Technology Development initiative within the Electronic Systems Branch at Ames Research Center. In addition to the S2k! Program, Mr. Hines is Project Manager for the Rhesus Measurement System, the Cosmos '92 US/Russian Bioinstrumentation System, and several ground-based sensor and instrumentation projects. Prior to those activities, Mr. Hines was a Major in the US Air Force assigned as Deputy Chief of the Information Processing Technology Branch in the Avionics Laboratory at Wright-Patterson AFB, Ohio. Previously to that, he was Manager of the NASA-Ames Cardiovascular Research Laboratory. Mr. Hines has a B.S. in Electrical Engineering from Tuskegee University and a M.S. in EE/Biomedical Engineering from Stanford University. Mr. Hines has over 17 years of combined NASA/Air Force service.

ON THE ISOLATION OF HALOPHILIC MICROORGANISMS FROM SALT DEPOSITS OF GREAT GEOLOGICAL AGE

Helga Stan-Lotter[1,2] and Ewald Denner[2]
[1]Ames Research Center, Moffett Field, California
[2]Institute of Microbiology and Genetics, University of Vienna, Vienna, Austria

SUMMARY

From salt sediments of Triassic or Permian age from various locations in the world halophilic microorganisms were isolated. Molecular characteristics of several of the isolates suggested they belong to the archaebacteriae. One group appears to represent novel strains; several properties of one such isolate, strain BIp, are described here.

The existence of viable microorganisms in ancient sediments would have great implications with respect to our notions on evolution, the search for life in extraterrestrial environments and the long-term survival of functional biological structures. Of crucial importance is thus the question if these microorganisms existed in the salt since the time of deposition or invaded at some later date. Some suggestions to address these issues experimentally are discussed.

INTRODUCTION

In all parts of the world salt deposits are found which originate from early periods of the geological history of the Earth. The major such halogenic epochs occurred during the Paleozoic period (Zharkov, 1981). Particularly large sediments were deposited during the Permian and Triassic era, that is, 280 to 195 million of years before present. Microscopic examinations revealed the presence of bacteria in thin sections or dissolved rock salt samples (see Sonnenfeld, 1984 for references). Rather sensational were the claims about thirty years ago that bacteria from Permian or older salt sediments had been brought back to life (Dombrowski, 1963; Reiser and Tasch, 1960). Other workers could not confirm these findings (Bien and Schwartz, 1965). Recently, extremely halophilic bacteria were isolated from an English salt mine, whose deposition appears to have occurred during the Triassic period (Arthurton, 1973). The rock salt samples had been collected right after blasting, and care was taken to exclude any extraneous microbial contamination (Norton, 1988, 1989). Other halophilic bacteria were isolated from a Permian age bedded salt deposit located in New Mexico (R.Vreeland, personal communication). We were able to cultivate halophilic bacteria from rock salt which was obtained from an Austrian salt mine, also of the Permian period. A preliminary characterization of isolates from the English as well as the Austrian salt mines with respect to their antibiotic sensitivity, ATPase enzymes and cellular proteins has been described (Stan-Lotter *et al.*, manuscript submitted for publication). The bacterial isolates fell into two classes; one, which resembled known bacterial strains and one, which did not. Extremely halophilic bacteria belong to the archaebacteria, a group of microorganisms thought to have diverged early from the main line of prokaryotic evolution (Woese, 1987). A comparison of known archaebacteria with similar isolates from ancient sediments might provide a time scale for mutational events, since the bacteria, which were included in the salt

sediments, have not evolved for a few hundred million years, in contrast to all other living organisms. The significance of viable organisms from paleozoic times would, besides evolution, extend to other areas of scientific study, for instance, to the search for extraterrestrial life. If it can be proven that bacteria remain viable in a dry state for very long periods, it would be feasible to look for remnants of such life forms in sedimentary formations on other planets, e.g., on Mars.

Here we extend the description of properties of one of the novel isolates, strain BIp, and discuss strategies to determine the age of the microorganisms isolated from rock salt of paleozoic origin.

MATERIAL AND METHODS

Bacteria and Culture Conditions

Samples of rock salt, with varying contents of clay, were obtained from the salt mine in Bad Ischl, Austria. Pieces of about 2 g were dipped in ethanol and flamed. Then they were transferred to 50 ml of sterile complex medium (M2 medium) that was 20% with respect to NaCl and whose pH was 7.4 (Tomlinson and Hochstein, 1976) and incubated at 37 °C with shaking. After about 4 weeks samples of the cultures were streaked on plates containing M2 medium which was solidified by the addition of 2% agar. Colonies appeared after three to four weeks and were purified further by repeated spreading on solid M2 medium. One isolate with pink pigmentation was picked for further characterization and will be referred to as BIp. For some experiments a culture medium with a pH of about 9.5 was used (Tindall *et al.*, 1980). Growth in liquid culture was monitored with a Klett-Summerson colorimeter with a red (No. 66) filter. The following archaebacterial type strains were obtained from the Deutsche Sammlung für Mikroorganismen (DSM): *Halococcus morrhuae* DSM 1307, *Hc. morrhuae* DSM 1309, *Natronococcus occultus*, *Natronobacterium magadii*, *Nb. gregoryi*, *Nb. pharaonis*. *Halobacterium saccharovorum* (ATCC 29252), *Hb. halobium*, *Haloferax denitrificans* and *Hf. vallismortis* were obtained from Dr. L.I.Hochstein, NASA Ames Research Center.

Antibiotic Sensitivity

Paper disks impregnated with the particular antibiotics were placed on agar plates, which contained 20 ml of solid M2 medium and on which 200 µl of liquid culture had been spread. Zones of inhibition around the disks were recorded after 7 days of incubation at 37 °C. Antibiotics were from Sigma Chemical Company.

Biochemical Tests

Catalase activity was determined by placing a drop of a 3% H_2O_2 solution on a lawn of bacteria. The formation of gas bubbles indicated a positive reaction. Oxidase was detected by spotting a loopful of bacterial culture on a paper strip containing N,N-dimethyl-1,4-phenylendiammoniumchlorid and naphthol. Blue coloration revealed the presence of the enzyme.

Gel Electrophoresis

Sodium dodecyl sulfate (SDS) gel electrophoresis of whole cell proteins was performed as described previously (Stan-Lotter *et al.*, 1989) using the gel system of Laemmli (1970). Isoelectric focussing (IEF) was done in a pH range of 2.5 to 5.0 and 3 to10, respectively, as described for halobacteria (Stan-Lotter *et al.*, 1989). Ampholytes were from Pharmacia-LKB.

Light Microscopy

Cells were examined with a Leitz Diaplan microscope using phase contrast. Photographs were taken with Ilford film PAN F.

RESULTS

Isolation and Growth Characteristics

Numerous colony types on agar plates were isolated from samples of rock salt, many of them showing pink or red pigmentation. Some of the isolates from an English and an Austrian salt mine, respectively, were similar, but not identical, to classified archaebacteria (Stan-Lotter *et al.*, submitted for publication). Other isolates as represented by strain BIp did not show obvious similarities to known bacteria. These might be novel isolates of potential great interest. The criteria for the characterization of strains included sensitivity towards antibiotics, possession of certain enzymes such as a membrane ATPase and properties of whole cell proteins. In the case of one isolate from the English salt mine, lipid analysis was performed and showed the typical archaebacterial diphytanyl-diether (Norton, 1988). More detailed data are, however, necessary to decide upon the novelty of bacterial strains.

BIp grew with a generation time of about 24 h at 37 °C in liquid M2 medium (pH 7.4) with shaking. It reached the stationary growth phase at about 150 Klett units. Similar growth characteristics were observed when BIp was cultivated in medium of pH 9.5. Cells from liquid cultures were coccoid and often growing in tetrads or, particularly in older cultures, in large clusters (see fig. 1). Growth on solid medium was as irregular colonies of pink pigmentation; older colonies turned to a brownish color.

Biochemical Characteristics

Table 1 shows the sensitivity of BIp towards several antibiotics. Growth was strongly inhibited by anisomycin, bacitracin and novobiocin. Moderate sensitivity of BIp was observed against chloramphenicol and tetracyclin. No inhibition of growth occurred with ampicillin, nalidixic acid and streptomycin. These results were generally consistent with previous studies of antibiotic sensitivities of archaebacteria (Hilpert *et al.*, 1981). BIp was catalase positive and oxidase positive.

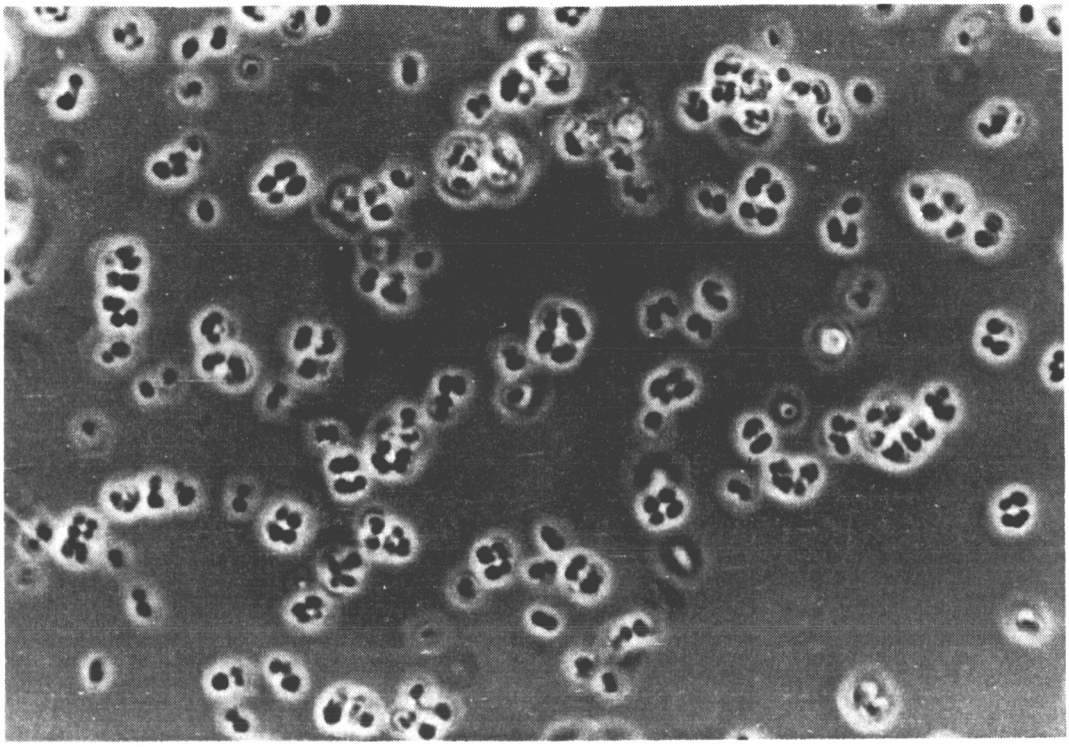

Figure 1. Phase-contrast photomicrograph of strain BIp, x 3550.

Table 1. Effect of antibiotics on growth of strain BIp.

	Concentration (μg per disk)	Sensitivity
Ampicillin	40	- *
Anisomycin	50	+++
Bacitracin	40	+++
Chloramphenicol	40	+
Nalidixic acid	40	-
Novobiocin	40	+++
Streptomycin	40	-
Tetracyclin	40	++

*-, no inhibition; +, ++, +++, zone of inhibition $\leq$ 1 mm, $\leq$ 3 mm, > 10 mm, respectively.

Gel Electrophoresis of Whole Cell Proteins

SDS gel electrophoresis of whole cell proteins is a rapid method for distinguishing bacterial species (Jackman, 1985). We have used this method to identify wild type strains and mutants of halobacteria (Stan-Lotter *et al.*, manuscript in preparation). Strain BIp showed a unique protein

pattern following SDS gel electrophoresis which did not resemble that of any of the halobacterial type strains which we tested (data not shown). In particular, none of the known coccoid archaebacterial strains (*Halococcus* , *Natronococcus*) were similar to BIp. The protein patterns of strain BIp were identical, whether the strain was grown at pH 7.4 or pH 9.5.

Extremely halophilic bacteria are known to possess almost exclusively acidic proteins (Reistad, 1970), with isoelectric points ranging between pH 3.6 and 5.0 (Stan-Lotter *et al.*, 1989). On isoelectric focusing gels, strain BIp showed acidic proteins between pH 3.8 and 4.5. The overall protein pattern on IEF gels was again different from that of any of the archaebacterial type strains (not shown).

DISCUSSION

Several properties of strain BIp which are described here suggested that it is an archaebacterium. The sensitivity towards antibiotics (table 1) was similar to that of other archaebacteria and its whole cell proteins were acidic, as is the case for proteins from all halophilic archaebacteria. Its rather slow growth is similar to that of other halophilic archaebacteria, particularly *Halococcus* (Staley *et al.*, 1989). However, none of the two types of coccoid aerobic archaebacterial isolates known to date, *Halococcus* and *Natronococcus* , showed similarities to BIp with respect to cell protein patterns and pigmentation. In addition, the wide growth range of BIp , from pH 7.4 to 9.5, is unlike that of other coccoid archaebacteria. A clear distinction of archaebacteria from eubacteria and among archaebacterial strains can be made by sequencing nucleic acids, e.g. 16 S rRNA (Woese, 1987) and by the analysis of lipids (Ross et al., 1985). These methods are in progress with strain BIp. In summary, BIp probably belongs to the halophilic archaebacteria and might represent a novel isolate.

From several different locations of salt sediments of great geological age halophilic microorganisms have now been isolated. The question arises if these bacteria were deposited at the time of sedimentation. Alternatively, they may have entered the salt sediments at some later date, or, thirdly, they may represent present-day bacterial contaminants which were introduced during handling of the samples. If the first scenario is correct, these organisms would provide a unique repository of biomolecules, which was not changed by mutational events experienced by all other living organisms. Many evolutionary problems could be addressed by the study of such ancient bacteria. Moreover, the possibility of long term survival of bacteria would have to be taken into consideration when looking for extraterrestrial forms of life. In lunar soil, minerals such as halite (NaCl) and sylvite (KCl) have been detected (Ashikmina *et al.*, 1978); on Mars, surface features were seen which suggested the presence of a liquid, probably water, at some earlier period of its history (Carr, 1987). Thus, the possibility of "halophilic life" in extraterrestrial environments might be realistic and should be worth of further exploration.

Direct determination of the age of microorganisms from rock salt is not easy because of the scarcity of organic material in the samples and the lack of suitable isotope dating methods. An indirect method is the analysis of pollen and spores from extinct plants, which has been performed with Austrian salt sediments (Klaus, 1974) and revealed a Permian origin of the rock salt. However, the possibility that the bacteria in the same sediment entered at a later time by unknown processes cannot be excluded at present. Here, geological investigations would be necessary which could prove

that the salt sediments consist of primary crystals, which have not been extensively altered during later times. The third possibilty mentioned above, contamination with present-day halophilic microorganisms, can be excluded with proper isolation techniques, such as flaming the salt samples and/or treatment with bactericidal agents. In addition, halophilic archaebacteria are, in the experience of most laboratories, not likely to occur as air- or dust-borne contaminants, due to their complex nutritional requirements.

A different approach to the problem of long term survival of halophilic microorganisms was taken by Norton and Grant (1988), who showed that cells remained viable after at least six months of storage in fluid inclusions of salt crystals. This type of experiment could be extended to include crystallization and storage of bacteria-containing brines under conditions, e.g., atmospheric composition, temperature etc., which are thought to prevail on Mars.

ACKNOWLEDGMENT

We thank Dr. L. I. Hochstein, NASA Ames Research Center, and Dr. W. Lubitz, University of Vienna, for laboratory space. This work was supported by NASA Cooperative Agreement NCC2-578 while H. Stan-Lotter was a Principal Investigator with the SETI Institute.

REFERENCES

Arthurton, R. S.: Sedimentology, vol. 20, 1973, pp. 143-160.

Ashikmina, N. A.; Gorshkov, A. I.; Mokhov, I. A.; and Obronov, V. G.: Dokl.Akad. Nauk SSSR, vol. 243, 1978, pp. 1258-1260.

Bien, E. and Schwartz, W.: Z. Allg. Mikrobiol., vol. 5,1 965, pp. 185-205.

Carr, M. H.: Nature, vol. 326, 1987, pp. 30-35.

Dombrowski, H. J.: Ann. New York Acad. Sci., vol. 108, 1963, pp. 477-484.

Hilpert, R.; Winter, J.; Hammes, W.; and Kandler, O.: Zbl. Bakt. Hyg., I.Abt. Orig. C 2, 1981, pp. 11-20.

Jackman, P. J. H. in: Chemical Methods of Bacterial Systematics (M. Goodfellow and D. Minnikin, eds.), 1985, pp. 115-139. Academic Press, London.

Klaus, W.: (1974) Carinthia III, 164/Jahrg. vol. 84, 1974, pp. 79-85, Klagenfurt.

Laemmli, U. K., Nature, vol. 227, 1970, pp. 680-685.

Norton, C. F.: Abstr. I-84, Annu. Meetg. Am. Soc. Microbiol., ASM, Washington, 1988.

Norton, C. F.: Abstr. I-108, Annu. Meetg. Am. Soc. Microbiol., ASM, Washington, 1989.

Norton, C. F. and Grant, W. D.: J. Gen. Microbiol., vol. 134, 1988, pp. 1365-1373.

Reiser, R. and Tasch, P.: (1960) Trans. Kansas Acad. Sci., vol. 60, 1960, pp. 31-34.

Reistad, R.: Arch. Mikrobiol., vol. 71, 1970, pp. 353-360.

Ross, H. N. M.; Grant, W. D.; and Harris, J. E.: In Chemical Methods in Bacterial Systematics (Goodfellow, M. and Minnekin, D. E., eds.), Acad. Press, London, New York, 1985.

Sonnenfeld, P.: Brines and Evaporites. Academic Press, Orlando, Florida, 1984.

Stan-Lotter, H.; Lang, F. J., Jr.; and Hochstein, L. I.: Appl. Theoret. Electroph., vol. 1, 1989, pp. 147-153.

Staley, J. T.; Bryant, M. P.; Pfennig, N.; and Holt, J. G.: Bergey's Manual of Systematic Bacteriology, vol. 3. Willams and Wilkins, Baltimore, 1989.

Tindall, B. J.; Mills, A. A.; and Grant, W. D.: J. Gen. Microbiol., vol. 116, 1980, pp. 257-260.

Tomlinson, G. A. and Hochstein, L. I.: Can. J. Microbiol., vol. 22, 1976, pp. 587-591.

Woese, C. R.: Microbiol. Rev., vol. 51, 1987, pp. 221-271.

Zharkov, M. A.: History of Paleozoic Salt Accumulation. Springer Verlag, Berlin, Heidelberg, New York, 1981.

BIOGRAPHY

Helga Stan-Lotter holds a M.Sc. degree in Microbiology and a Ph.D. degree in Science, both from the Technical University of Munich, Germany. Postdoctoral studies were on bacterial membrane pore proteins at the University of Calgary, Alberta, Canada. She then obtained a faculty position as research associate at the University of Vancouver, Canada, working on microbial bioenergetics. Under an NRC associateship she joined the laboratory of L. Hochstein at Ames Research Center, where she is now a Principal Investigator with the SETI Institute. Research interests are the evolution of bioenergetics and archaebacteria from salt sediments. She also holds teaching appointments in Microbiology at the University of Vienna, Austria.

COMPUTATIONAL FLOW PREDICTIONS FOR HYPERSONIC DRAG DEVICES

Susan Tokarcik and Ethiraj Venkatapathy
Eloret Institute
Palo Alto, California

SUMMARY

The effectiveness of two types of hypersonic decelerators is examined: mechanically deployable flares and inflatable ballutes. Computational fluid dynamics (CFD) is used to predict the flowfield around a solid rocket motor (SRM) with a deployed decelerator.The computations are performed with an ideal gas solver using an effective specific heat ratio of 1.15. The results from the ideal gas solver are compared to computational results from a thermo-chemical nonequilibrium solver. The surface pressure coefficient, the drag, and the extent of the compression corner separation zone predicted by the ideal gas solver compare well with those predicted by the nonequilibrium solver. The ideal gas solver is computationally inexpensive and is shown to be well suited for preliminary design studies. The computed solutions are used to determine the size and shape of the decelerator that are required to achieve a drag coefficient of 5. Heat transfer rates to the SRM and the decelerators are predicted to estimate the amount of thermal protection required.

NOMENCLATURE

A	reference area, $A = \pi R_{case}^2$
C_D	drag coefficient, $C_D = D/(q_\infty A)$
C_H	heat transfer coefficient, $C_H = q_w / (0.5\rho_\infty U_\infty^3)$
M	total mass, kg
q_∞	freestream dynamic pressure, N/m^2
q_w	wall heat transfer rate, W/cm^2
R_{case}	radius of SRM casing
U_∞	freestream velocity, m/s
β	ballistic coefficient, $\beta = M/(C_D A)$, kg/m^2
δ	flare angle or initial angle of ballute
γ	specific heat ratio, c_p/c_v
ρ_∞	freestream density, kg/m^3

INTRODUCTION

The Aeroassist Flight Experiment (AFE) is designed to provided information which is needed to design a full scale Aeroassist Space Transfer Vehicle (ASTV). The ASTV will be used to transfer payload from high Earth orbits, lunar bases, and planetary missions to low Earth orbit (LEO). In order to enter LEO the ASTV will enter Earth's upper atmosphere and use aerobraking to attain the

necessary velocity depletion. It will then fly back out of the upper atmosphere and enter LEO. Because the ASTVs will operate at very high altitudes, the flow about the ASTV may be in thermo-chemical nonequilibrium. These conditions cannot be adequately simulated in ground based facilities. Therefore a flight experiment, the AFE, is required.

The AFE is a subscale ASTV. The AFE would fly a representative ASTV trajectory in order to collect the desired flight data. The AFE would be deployed from the Space Shuttle. Then a solid-propellant rocket motor (SRM) is fired to accelerated the AFE. When the desired entry velocity for the test is attained, the SRM casing is jettisoned from the AFE, and the AFE continues on to perform an aerobraking maneuver. This scenario is shown in figure 1.

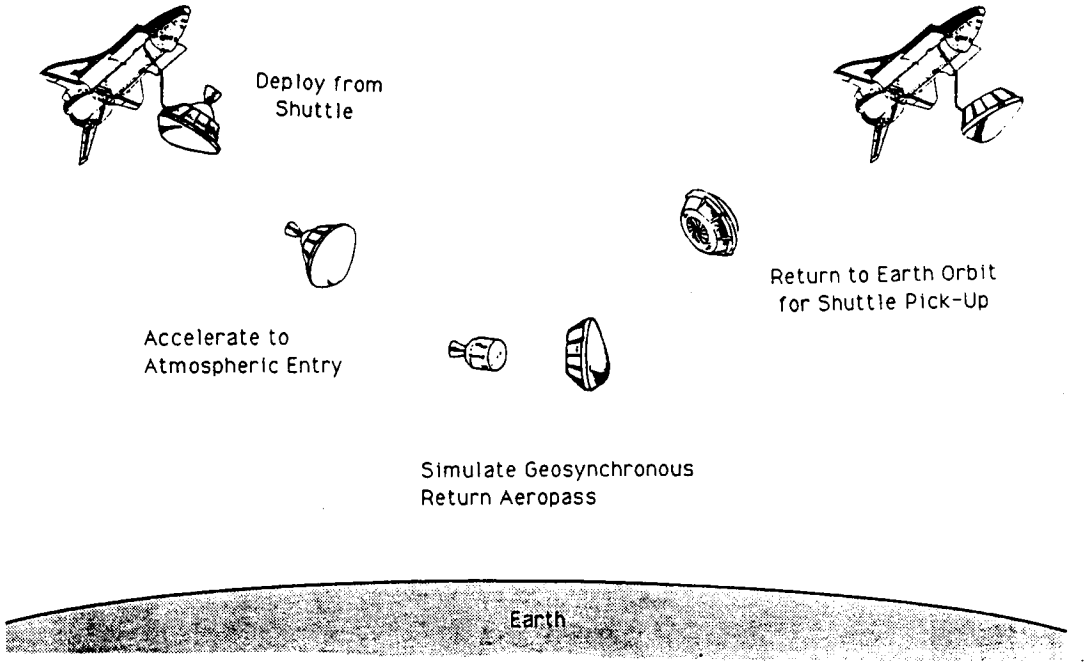

Figure 1. AFE mission (NASA I-87-9597).

The SRM casing jettisoned from the AFE is large enough that it will not entirely burn up during entry. To protect human beings from this falling debris, it is required that the SRM casing drop in to the water at least 300 miles from any large land mass (ref. 1). In order to determine approximately where the SRM casing will land, it is necessary to know where it begins its descent into the atmosphere. If the SRM casing initially skips out of the atmosphere before being captured, it is very difficult to predict where and when it will be captured and where it will finally land. As recently as April 1991, the seriousness of such a problem was brought to light when a large piece of debris from a Soviet space station fell into a populated area of Argentina.

Whether or not the SRM casing will skip out is determined by its ballistic coefficient, $\beta = M/(C_D A)$. The reference area, A, used to calculate C_D is the same as that used to calculate β. Therefore, β is altered by changing the total mass of a body or the total drag produced by a body. Increasing the drag, hence lowering β, will cause a body to lose momentum more quickly. This will cause the body's atmospheric trajectory to become steeper. Increasing the mass of a body, hence

increasing β, will tend to cause the body to decelerate more slowly and to maintain a shallower trajectory longer. It is this shallow trajectory that can cause a body to skip out.

The calculated trajectories for a range of ballistic coefficients is shown in figure 2 (ref. 2). The ballistic coefficient of the SRM casing is approximately 112 kg/m^2. As can be seen in figure 2, a body with a β of 112 has a high probability of skipping out before being captured by the atmosphere. Also shown in figure 2 is a range of acceptable ballistic coefficients. A ballistic coefficient of 49 kg/m^2 will assure that skip out does not occur. In order to lower β, either the weight of the SRM casing must be lowered or the drag must be increased. Since the minimum weight of the SRM casing is predetermined by the needs of the AFE mission, it cannot be adjusted to lower β. Therefore, the drag must be increased. The C_D of the SRM casing alone is predicted to be approximately 1.56. By increasing the C_D to around 5, a β of 49 or less can be attained. The additional drag needed can be produced by attaching a drag enhancement device to the SRM casing to increase the total pressure drag.

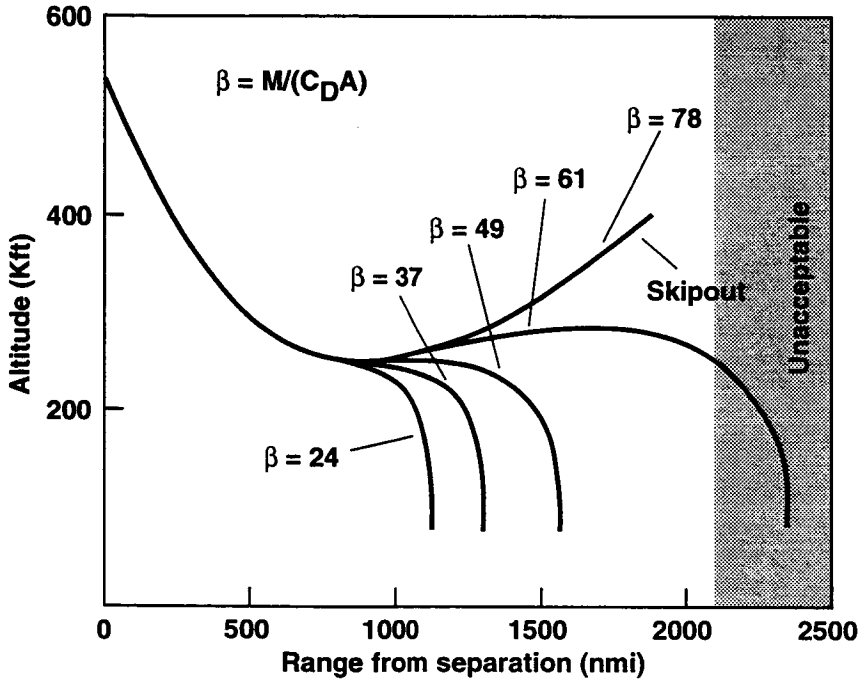

Figure 2. Ballistic entry trajectories (ref. 2).

The use of high speed and hypersonic drag brakes, has been investigated for many years and many different configurations have been proposed. Among these drag devices were attached or tethered ballutes (ref. 3). A ballute is a combination balloon parachute and is inflated using ram air pressure or an on board pressure source. Also investigated were rigid flares, spoilers, and spikes that are mechanically deployed (ref. 4). A flare is attached around the entire vehicle while one or more spoilers can be deployed intermittently around the vehicle. Most recently, a ballute decelerator has been examined computationally (ref. 2). Most of the research done thus far for hypersonic decelerators has been applicable to high performance reentry vehicles or Apollo capsule recovery, payload

recovery, and booster payload collision avoidance. However, none of this research takes into account the real gas effects encountered at the altitudes and speeds experienced by the SRM casing.

A number of considerations must be taken into account when choosing a viable decelerator configuration. These considerations include high heating rates, ease of decelerator deployment, stability of the SRM/decelerator configuration, and, ultimately, how much drag the decelerator can produce. After examining several of the above configurations, it was decide that a ballute attached to the rear of the SRM casing or a flare attached in the same manner would most likely be the best suited for this mission (ref. 1). This conclusion was reached for the following reasons. First, a ballute attached to the rear of the SRM casing or a conical flare attached in the same way would tend to be a more stable configuration. Also, since the flare is mechanically deployed, tumbling would not affect the flare deployment. If an on board pressure source is used to inflate the ballute, tumbling would not affect the ballute deployment. The amount of drag produced by the conical flare and the ballute must be predicted in order to determine the size of the drag device needed to produce the desired increase in drag. Also the heat transfer rates to these drag devices needs to be estimated in order to determine whether existing materials could be used for thermal protection.

NUMERICAL METHODS

Thermo-Chemical Nonequilibrium Solver

The actual configuration for the SRM casing is shown in figure 3(a). Shown in figure 3(b) is the modified SRM configuration, with an attached flare decelerator, used in the numerical computations. The model for the ballute is shown in figure 3(c). The outer ring of the SRM casing shown in figure 3(a) is neglected in the models used for numerical computations. Neglecting the ring is possible because it will be contained within the large separated region of the flow. Because of this, the ring is not important when calculating the total drag. Therefore, the ring is neglected in the computational analysis.

All flowfield calculations assumed axisymmetric flow. The freestream conditions for the computations correspond to the peak heating trajectory point (ref. 1). These conditions are given in table 1. Because of the high altitude and the high speed of the SRM trajectory, the flowfield around the SRM casing may be in thermo-chemical nonequilibrium. This flowfield was solved for by using a thermo-chemical nonequilibrium code developed by Palmer. This code is an explicit, finite-difference, shock-capturing algorithm that used flux-vector splitting to solve the thin layer Navier-Stokes equations in a time marching fashion (ref. 5). The algorithm incorporated a finite rate chemistry model consisting of 10 species and a fully coupled two temperature thermal nonequilibrium model of Park (ref. 6). This code has been validated using experimental and computational data. The experimental data included ballistic range, shock tunnel, and flight data. The computational results have been compared against values from a thermo-chemical nonequilibrium solver developed by Candler. This code also solved the thin layer Navier-Stokes equations but used a finite volume, fully coupled, implicit technique that used Gauss-Seidel line relaxation (ref. 7). It also incorporated a multi-temperature thermal nonequilibrium model. However, the nonequilibrium codes are very costly to run, requiring 3 to 4 hours of CPU time on a CRAY-2 for the cases considered in this work. Therefore, they are not well suited for producing results for multiple configurations as was required here.

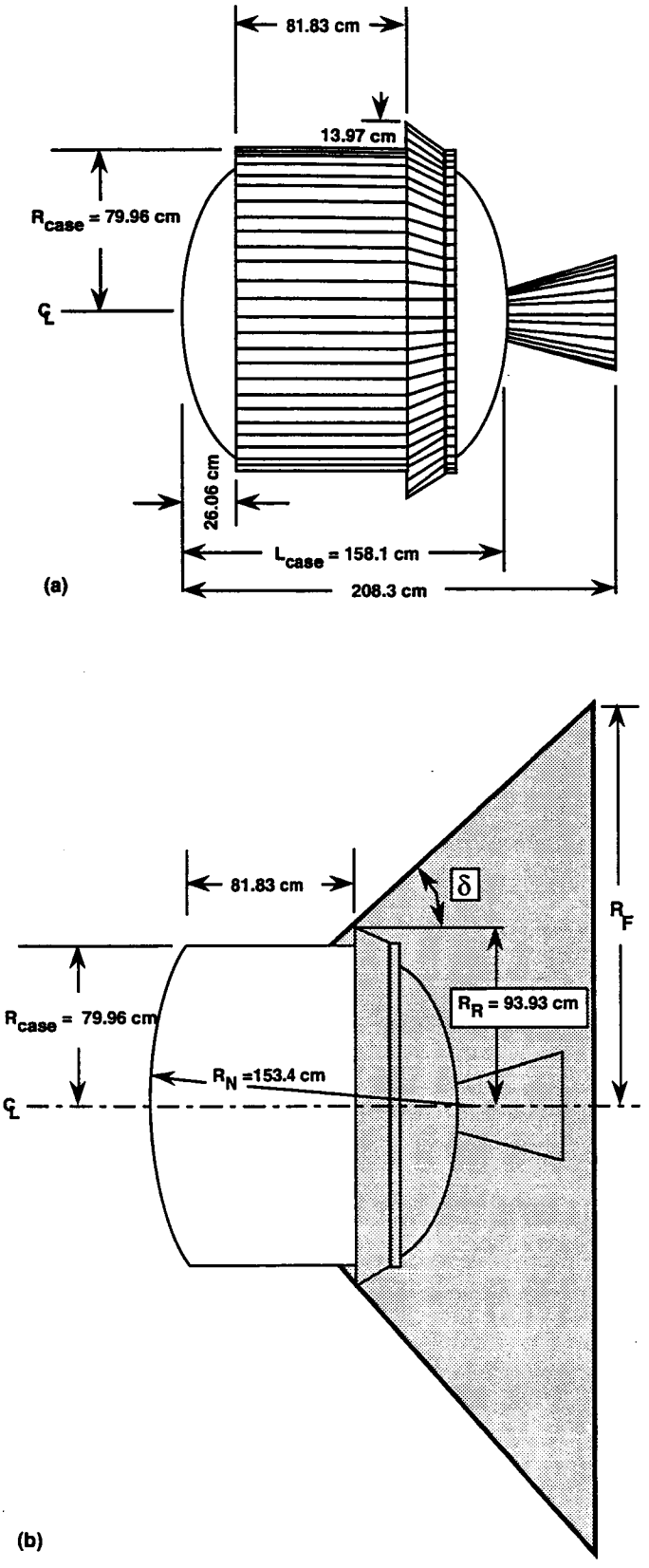

Figure 3. SRM model. (a) Configuration, (b) model for computation with flare.

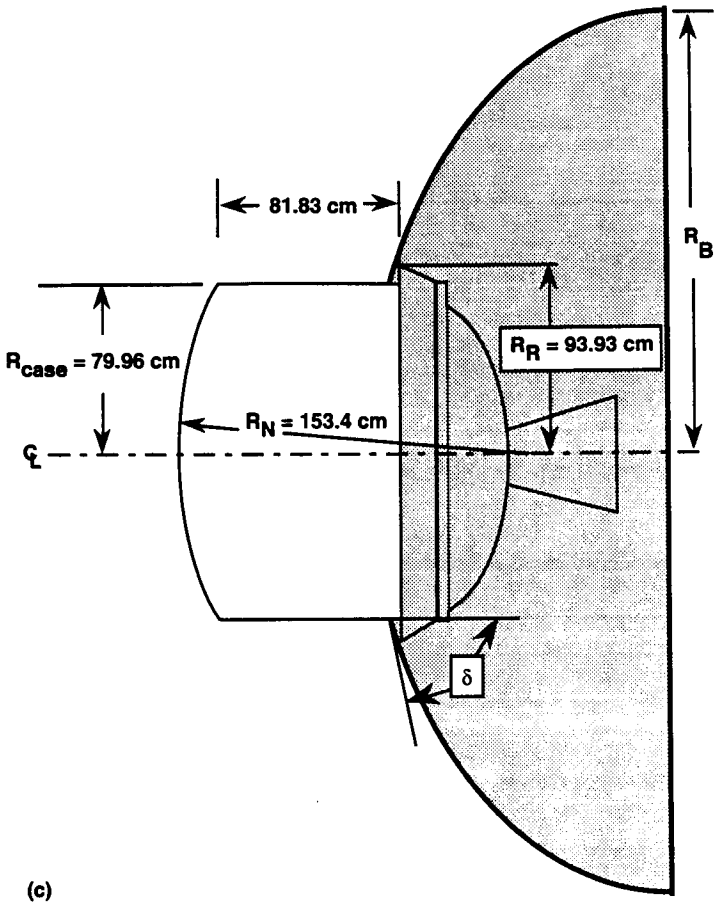

Figure 3. Concluded. (c) Model for computations with ballute.

Table 1. Freestream conditions

altitude	76,250 m
velocity	9,126 m/s
density	3.6087×10^{-5} kg/m^3
pressure	2.0674 N/m^2
temperature	199.6 K
Reynolds No.	22,370 /meter

Effective γ Ideal Gas Solver

In order to calculate solutions in a timely manner, a perfect gas version of the thermo-chemical nonequilibrium code developed by Candler was used. An effective specific heat ratio, γ, was used in the ideal gas solver in an effort to simulate the real gas nature of the flowfield. This technique has been used successfully to predict drag and moment coefficients produced by a body in a real gas flowfield (ref. 8). The choice of effective γ was based on a solution produced by Palmer's thermo-chemical nonequilibrium solver. Further explanation of the procedure used to choose an effective γ

is given in the next section. The ideal gas solver has been validated against experimental data for spheres, sphere cones, and sharp nosed cones at a variety of hypersonic speeds (ref. 7). The ideal gas solver is very robust and requires only 10 to 15 minutes of CPU time on a CRAY-2 for the same conditions that were used in the nonequilibrium code.

A schematic of the expected flow features of the SRM casing with a conical flare decelerator is shown in figure 4. Shown in this figure is the strong outer blunt body shock produced by the nose of the SRM casing. Then there is a strong expansion region around the shoulder of the SRM casing. The juncture of the SRM casing and the decelerator forms a compression corner. The hypersonic flow in this region cannot negotiate this corner and separates. A shock forms at the upstream edge of the separated region. Further downstream, this shock interacts with the blunt body shock off the nose of the SRM. The peak pressure and heat transfer rate for the drag device occur in the vicinity of this shock-shock interaction. The two shocks then coalesce to form an oblique shock.

While both the nonequilibrium solver and the perfect gas solver have been used extensively for hypersonic blunt body flows, until now neither has been used to study flows with large separated regions such as that shown in figure 4. The prediction of this separated region is important since the size of the region will affect the amount of drag produced by the decelerator.

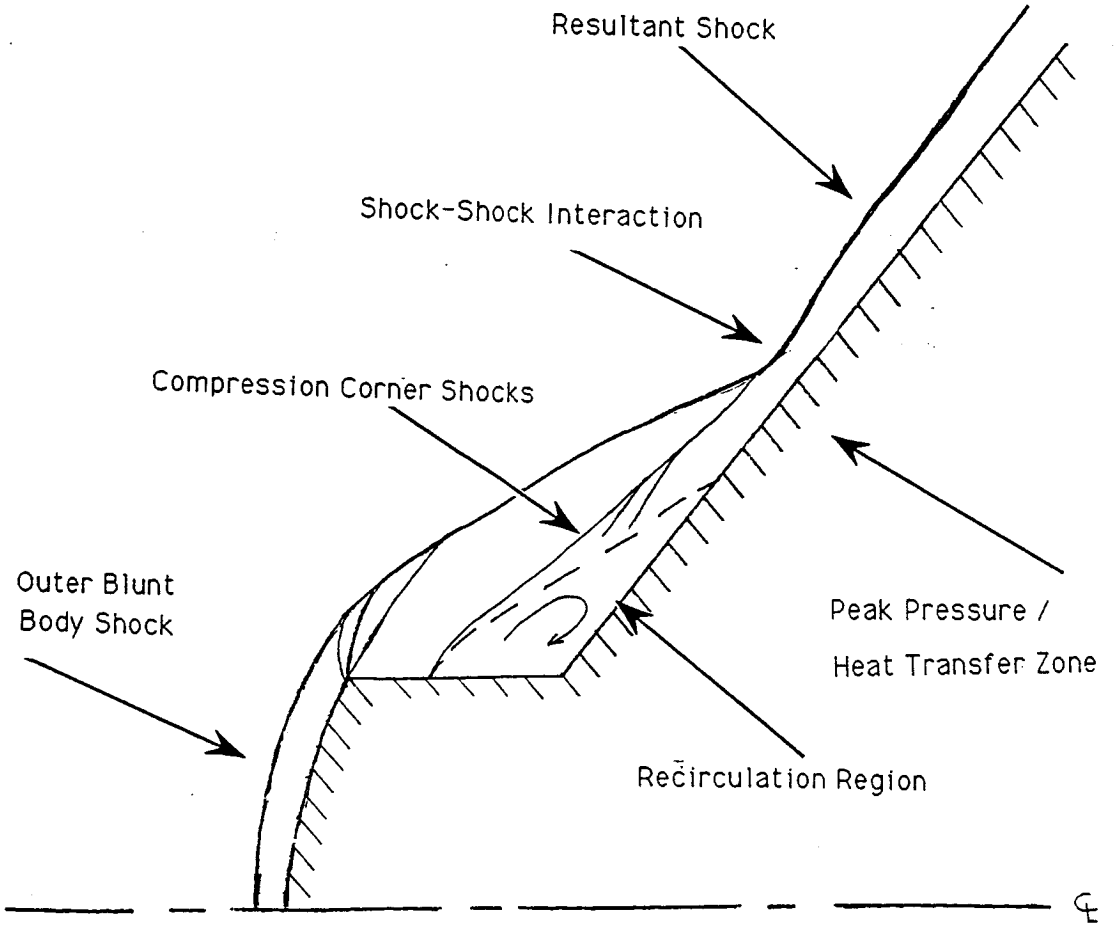

Figure 4. Flow schematic for SRM and flare.

COMPUTATIONAL RESULTS AND ANALYSIS

2-D Compression Corner Simulation

The region where the the SRM casing and the decelerator join forms a compression corner. The hypersonic flow coming into this compression region cannot negotiate the corner made by the SRM/decelerator juncture, and the flow separates. In order to confirm that this type of flow can be predicted with reasonable accuracy using the available solvers, a comparison is made with experimental results for a two-dimensional compression corner (ref. 9). The experimental flow was laminar until the reattachment region where transition was suspected to have occurred. The experimental case used for comparison was a compression corner with a 15° corner angle at Mach 10 with a 100°K constant temperature surface. The experiment was performed in air with $\gamma = 1.4$. The freestream conditions were as follows: $T_\infty = 50°$ K, $P_\infty = 294.5$ Pa, $Re_L = 2.3 \times 10^6$ where L is the length of the flat plate portion of the model, L = 0.25 m. The solution computed using the ideal gas solver with $\gamma = 1.4$ is compared to the experimental schlieren photograph in figures 5(a) and 5(b). In figures 6 and 7, C_P and C_H are compared with experimental results. In figure 6, the modest pressure rise at about X/L = 0.82 indicates the separation point. This is followed by a plateau typical of laminar separation (ref. 9). Then, in the reattachment region, the pressure rises rapidly and over-shoots the constant downstream value. The pressure over-shoot occurs in the reattachment region and is a common feature in high Mach number separated flows (ref. 10). This over-shoot is caused by the interference between the separation and reattachment shock waves. The computational results are able to predict the pressure overshoot in the reattachment region. The overshoot predicted by the computations is somewhat less than that found by experiment. The discrepancy could be due to turbulent transition taking place in this area. The differences in peak pressure are acceptable and any impact on the decelerator calculations will not be significant. The computed C_P in the separated region compared well with experimental values. The size of the separated region and the value of the pressure within the separated region agreed with that found experimentally.

Heat transfer data are shown in figure 7. The experimental data show that heat transfer rates decrease slowly along the upstream portion of the flat plate. The separation point is indicated by the sharp decrease in heat transfer rate. The heat transfer rate reaches a minimum within the separated

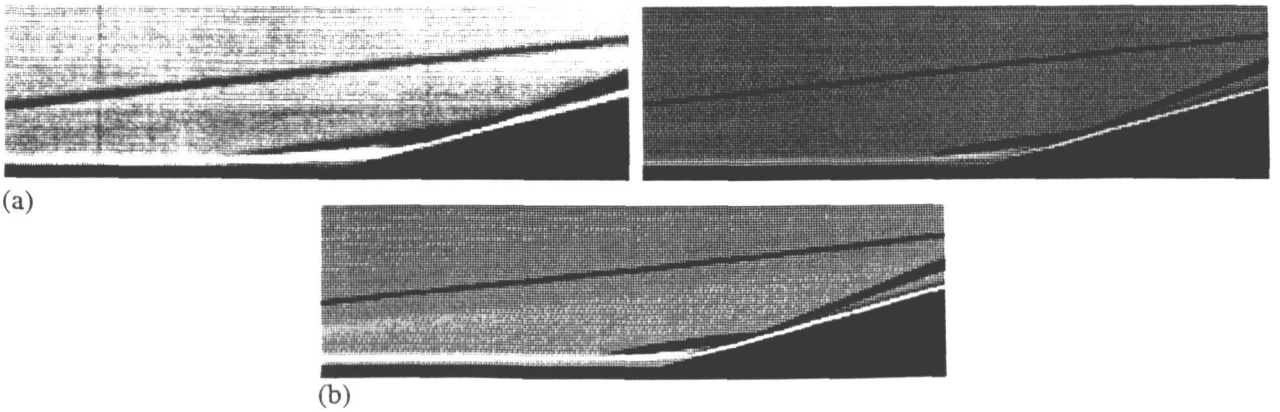

(a)

(b)

Figure 5. (a) Schlieren of 2-D compression corner (ref. 9), (b) calculated Schlieren of computational solution.

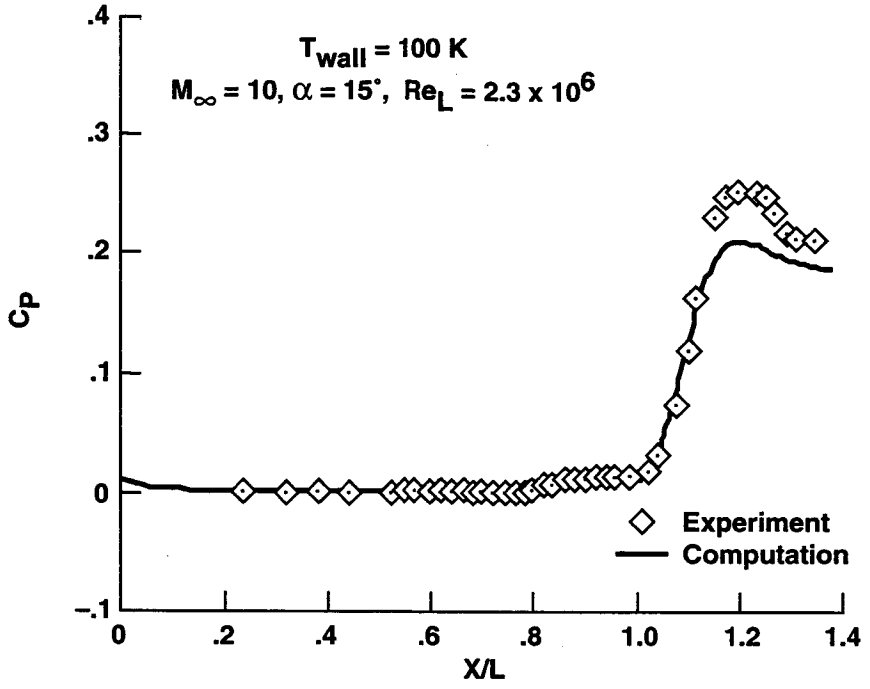

Figure 6. Pressure coefficient for 2-D compression corner.

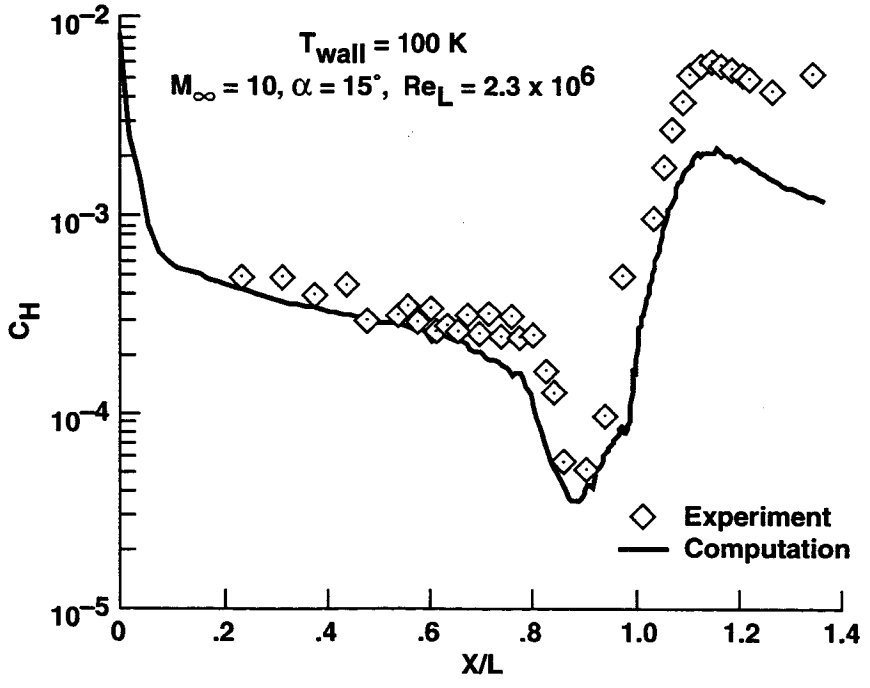

Figure 7. Heat transfer rates for 2-D compression corner.

region and then increases rapidly in the reattachment region. The trend of the computed heat transfer rates compares well with the experiment. The size and location of the separated region, inferred by the rapid drop and then rapid rise in heat transfer, is adequately predicted by the computational methods. The computed heat transfer rates reach a peak in the reattachment region but fall short of the experimental peak value. However, the agreement is adequate for preliminary design purposes. The higher heat transfer rates found by the experiment may be due to transition taking place in the reattachment region.

SRM/DECELERATOR SIMULATIONS

Although the flowfield around the SRM/decelerator will be dominated by real gas effects, the pressure field can be simulated using a perfect gas with an effective γ. The value of the effective γ that is chosen depends on the particular conditions under consideration. In a hypervelocity flow of a diatomic gas, high temperatures cause the molecules to dissociate into atoms, and the available modes of energy decrease from five to three, namely translational energy in three dimensions. Decreasing the available energy modes will increase the value of γ until the theoretical limit of 5\3 is reached. However, the high temperatures also cause the molecules to become vibrationally excited. This increases the number of energy modes and thus decreases γ. For a highly nonequilibrium flowfield, vibrational energy modes are excited, but the molecules do not have time to dissociate into atoms. So the chemical dissociation effects are swamped by the thermal effects, and the value of γ drops below the perfect gas value of 1.4. Flowfields which are dominated by real gas effects may have a value of γ around 1.1.

The pressure field can be simulated with a perfect gas solution because the pressure is only loosely coupled to the thermo-chemistry of the flow. Instead it is much more dependent on the fluid dynamics of the flow. It was shown earlier that the blunt body flow and the compression corner flow for the SRM/decelerator can be calculated with reasonable accuracy. Therefore, with the proper choice for the value of effective γ, the pressure field for this flow can be calculated reasonably well.

To be able to choose an appropriate effective γ either a computational solution which takes into account the real gas thermo-chemistry or experimental data for the flight conditions in question is needed.Since no experimental data exists for the present configuration, the nonequilibrium code is used to generate the real gas flowfield around the SRM/decelerator configuration. The nonequilibrium code is used to determine the shock shape and standoff distance associated with the real gas flow. The shock shape and standoff distance determine the pressure field of the flow. A series of effective γs was tried in the ideal gas solver in the effort to reproduce the real gas shock shape and standoff distance. The resulting drag curves for various γs is shown in figure 8. This figure shows that an effective γ of 1.15 does a good job of reproducing the surface pressure field.

Pressure contours of the entire flowfield are shown in figure 9. The pressure contours computed by the real gas solver for an SRM with a 50° flare are shown in figure 9(a). Figure 9(b) shows the pressure contours computed by the ideal gas solver with an effective γ of 1.15 for the same configuration. Figures 9 and 10 show that an effective γ of 1.15 does a very good job of reproducing the pressure field of the real gas flow.

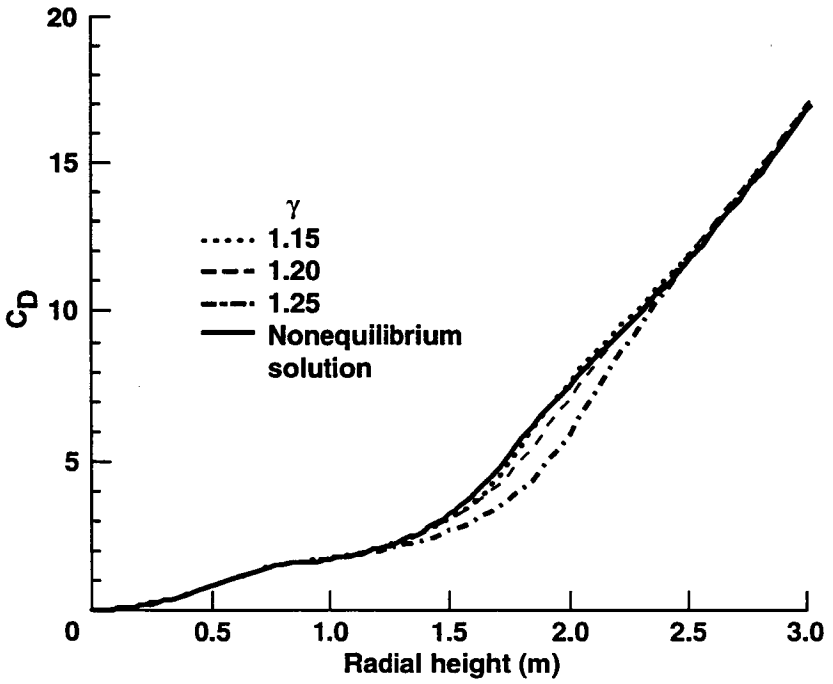

Figure 8. Drag coefficient for variable γ and real gas solution.

The pressure contours shown in figure 9 can be compared to the schematic of the expected flow features shown in figure 4. The pressure contours clearly show the blunt body shock formed by the nose of the SRM casing. The shock formed at the separation point is seen as a moderately large gradient in pressure just downstream of the SRM shoulder expansion. The separation shock interacts with the bow shock creating a high pressure region about half way up the flare. The two shocks merge in the interaction region to form an oblique shock. The extent of the separation region can be inferred from the pressure contours as the region of nearly constant pressure at the base of the SRM casing. A better idea of the separated region can be made by looking at velocity vectors. Figure 10 shows an expanded view of the SRM/decelerator corner region. The velocity vectors clearly show that a large portion of the SRM casing and the flare are contained within the separated region.

Computations for Conical Flare Decelerators

With an appropriate value of γ, the perfect gas code was used to study the flare and ballute drag devices. The decelerator must increase the drag of the SRM casing such that $\beta = 49$ Kg/m^2 or less is achieved. This condition corresponds to producing a C_D of about 5.

The first decelerator concept that was examined was the conical flare. A schematic of the flow-field produced by this type of configuration is shown in figure 4. The schematic was drawn for a flare angle of 50°. The angle of the flare influenced the size of the separated region and also the shape and strength of the shock in the downstream region. The size of the separated region affects the efficiency of the flare. If no separation occurs, the entire length of the flare is utilized as a compression surface. If a separation region exists, that portion of the flare within the separated region is

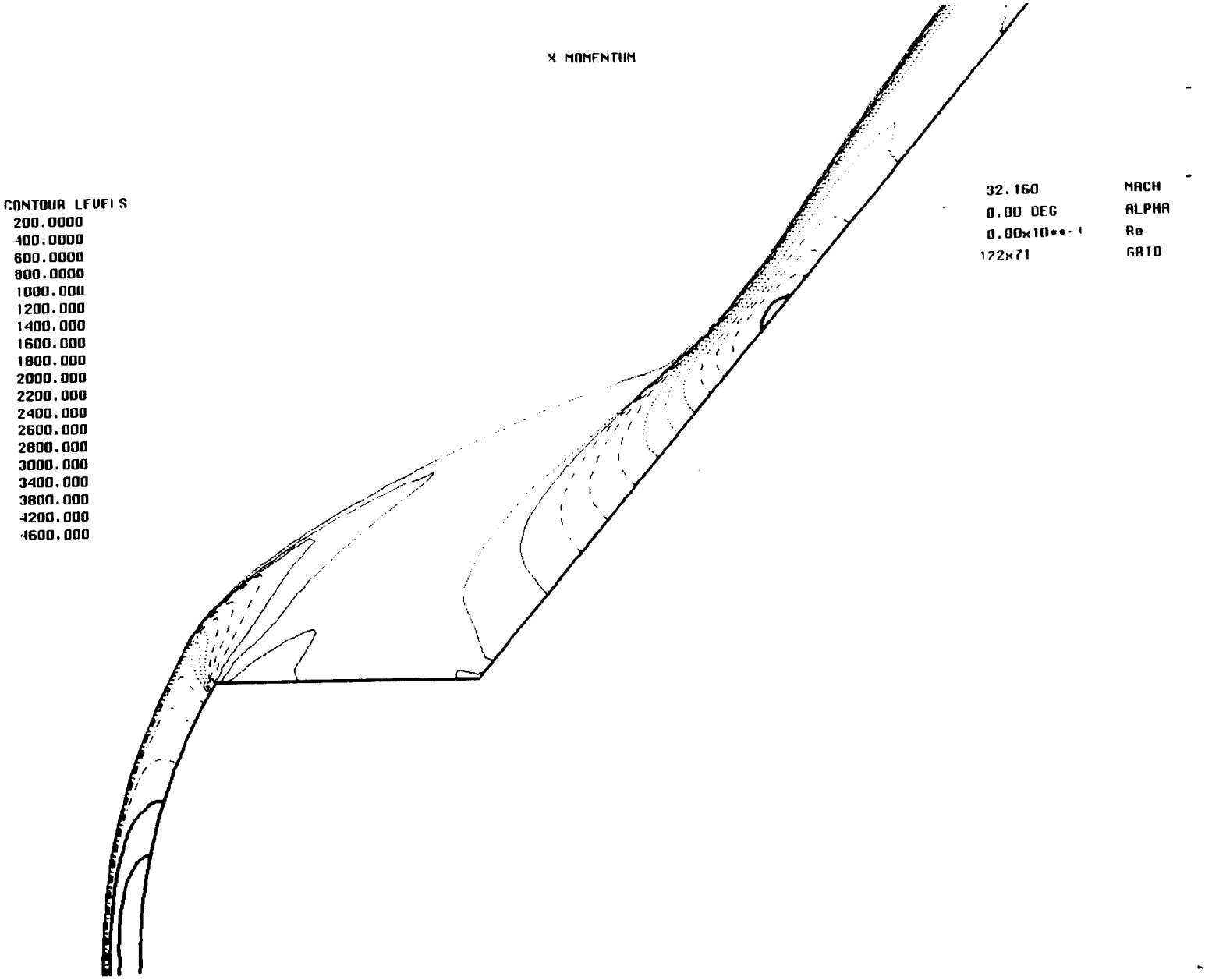

Figure 9. Pressure contours. (a) Real gas solution.

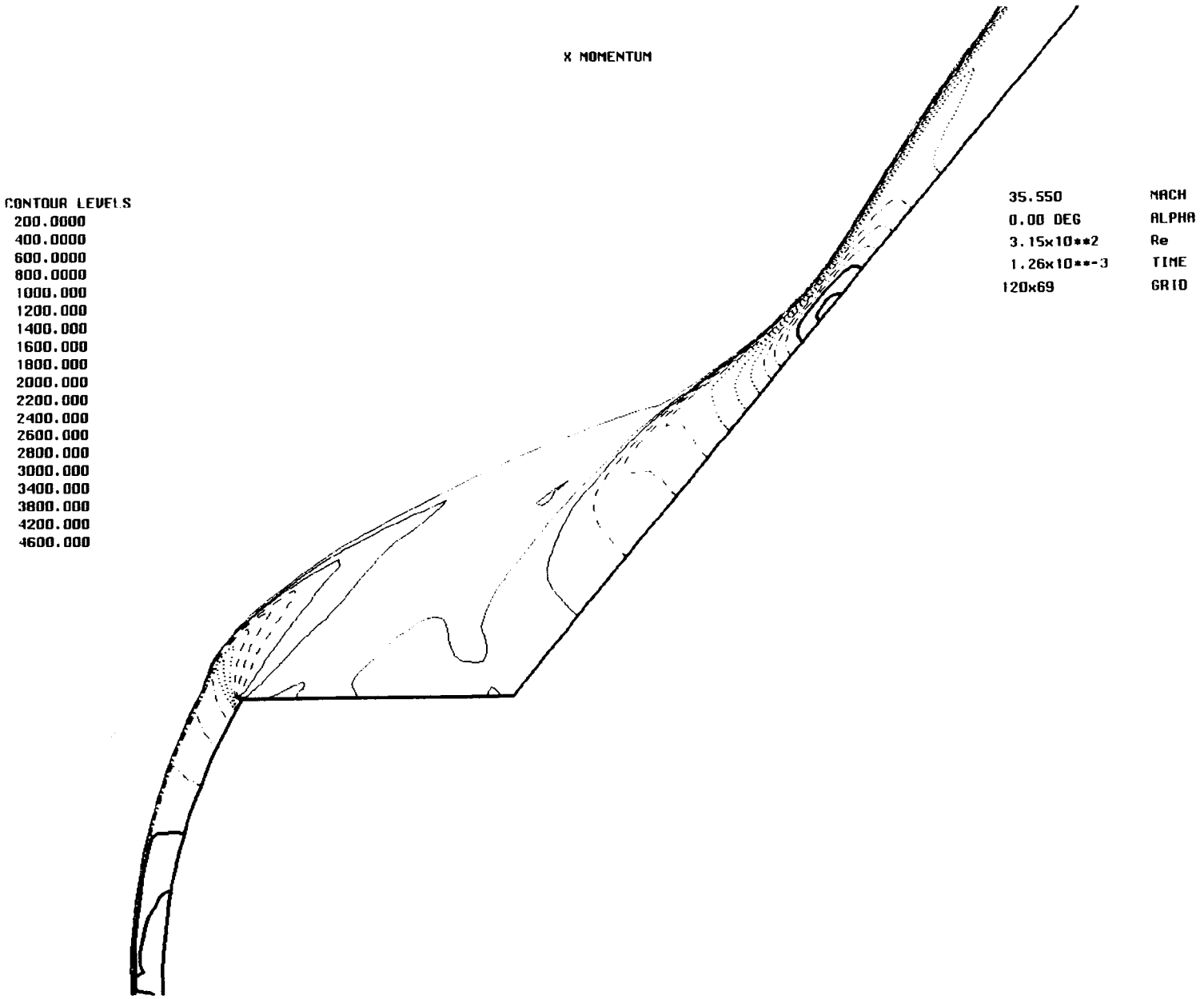

Figure 9. Concluded. (b) $\gamma = 1.15$.

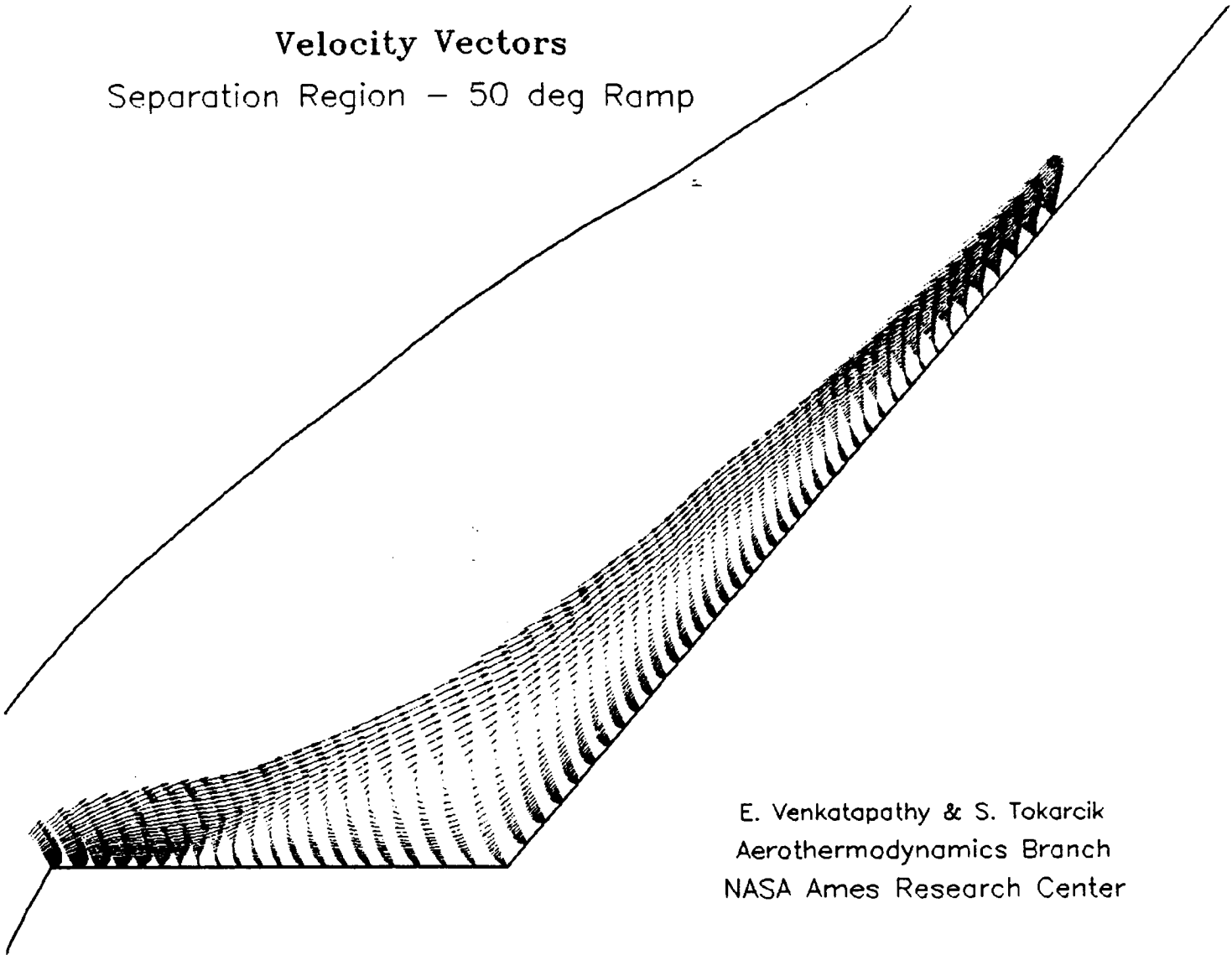

Figure 10. Velocity vectors – separation region 50° flare with $\gamma = 1.15$.

lost as a compression surface. The strength of the shock produced by the flare also affects the efficiency of the decelerator. A strong shock produces a greater pressure rise than a weak shock and therefore a greater increase in drag. Also, for larger flare angles, a greater portion of the pressure force vector acting on the body is directed in the axial, or drag, direction. Therefore, more drag is produced for the same distribution of surface pressure.

Pressure contours for three flare angles, 40°, 50°, and 60°, were computed. The results for the 50° flare are shown in figure 9(b). The 40° and 60° cases are shown in figures 11(a) and 11(b). A very small separation region was produced by the 40° flare, and a relatively weak downstream shock was formed. The peak pressure on the flare for this case was considerably lower than at the SRM nose stagnation point. The 50° flare produced a larger separated region and a stronger resulting oblique shock. The peak pressure produced by this flare was on the order of that produced in the

SRM nose region. As the flare angle was increased to 60° the character of the downstream shock changed. A very large separated region was produced encompassing almost the entire SRM casing downstream of the expansion shoulder. But more importantly, the downstream shock changed from a weak oblique shock to a strong blunt shock. The peak pressure on the flare occurs in the area where the strong shock is located. This pressure was much higher than the SRM nose stagnation point pressure. The C_D produced by the 40°, 50°, and 60° flares is shown in figure 12 . As can be seen in this figure, the desired C_D of 5 can be achieved by any of these flares with the proper choice ramp length.

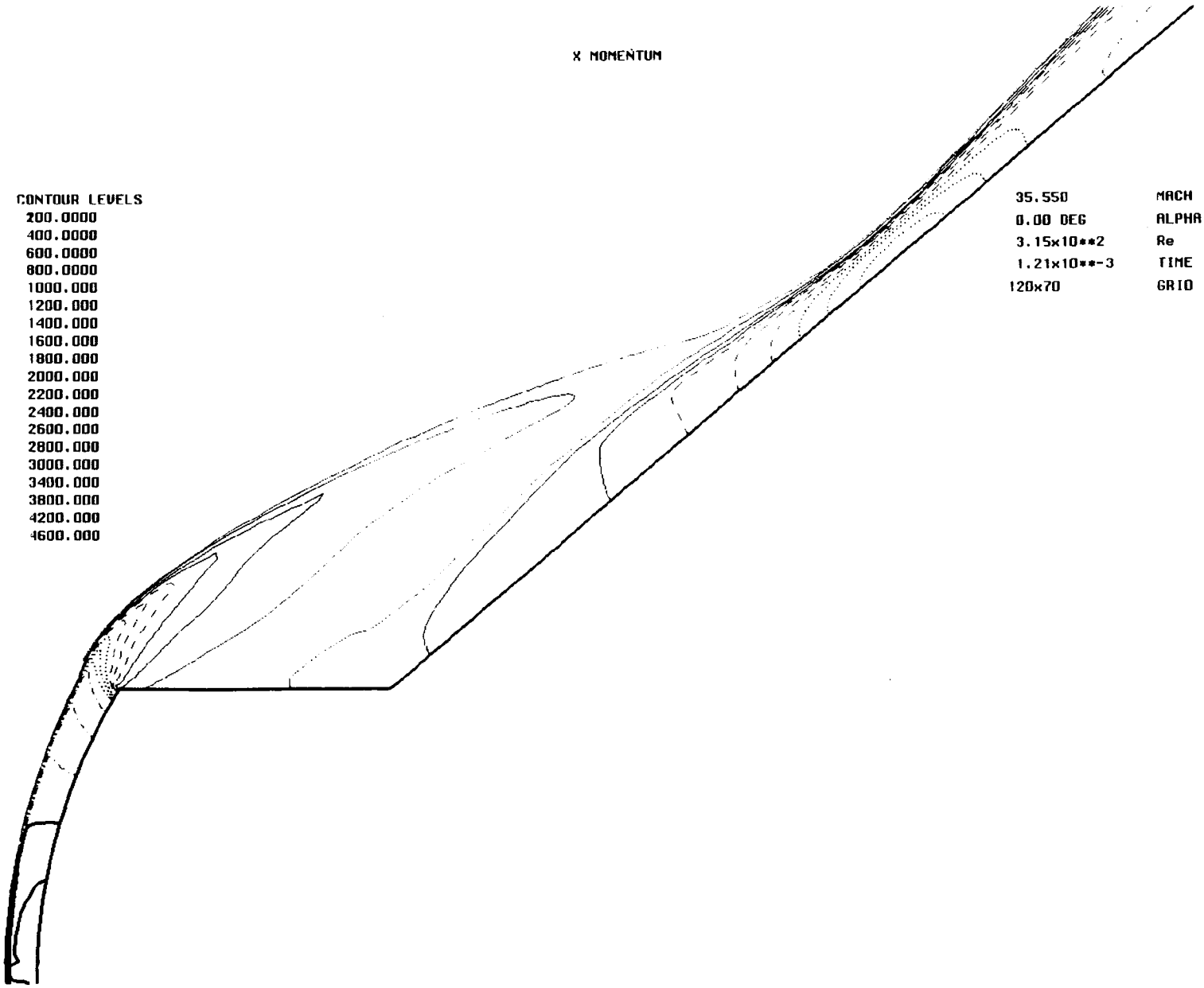

Figure 11. Pressure contours. (a) 40° flare.

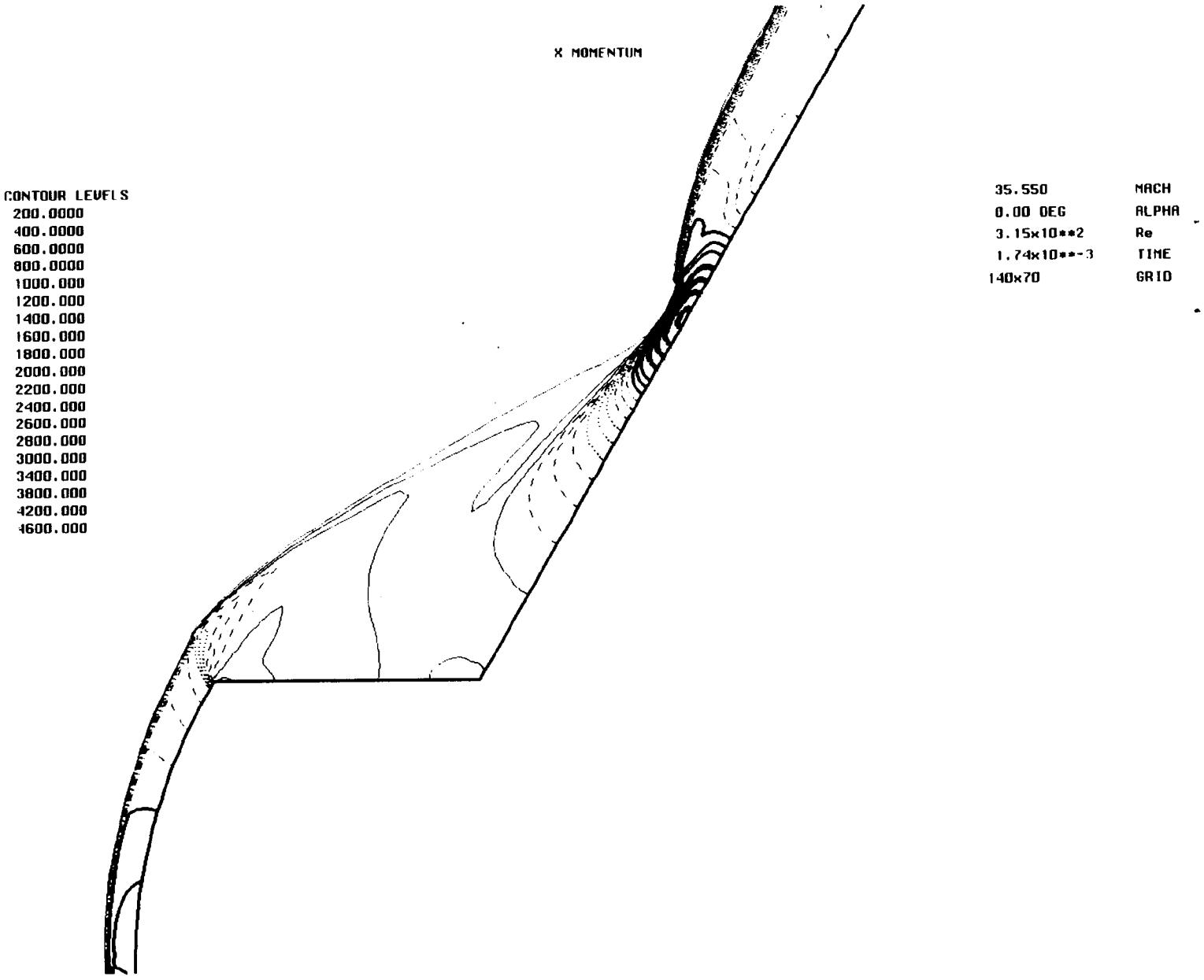

Figure 11. Concluded. (b) 60° flare.

The computed heat transfer rates for the flare decelerators are shown in figure 13 . The rise in surface heat transfer rate seen at 0.9 m along the surface was due to the thinning of the boundary layer as the flow expanded around the shoulder of the SRM casing. The peak in heat transfer rate to the flare was due to the bow shock, produced by the nose of the SRM, interacting with the shock produced by the decelerator. The peak in heat transfer rate corresponds to the peak pressure on the flare. This region of peak pressure can be seen in the pressure contours shown in figure 11. The peak in heat transfer rate on the flare was of particular importance because, for a ballistic coefficient of 49, the decelerator must survive for approximately 150 seconds to ensure atmospheric capture.

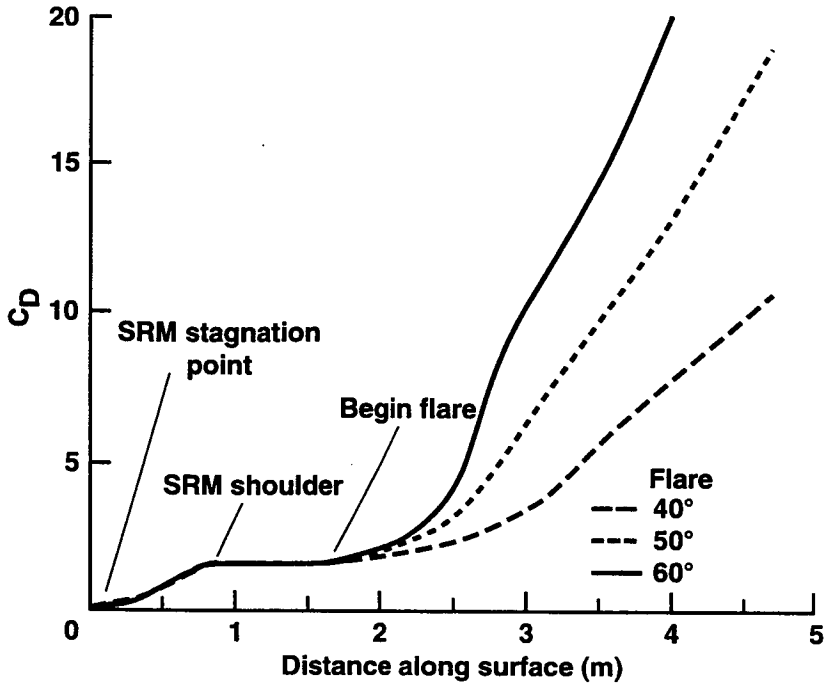

Figure 12. Drag coefficient for flare.

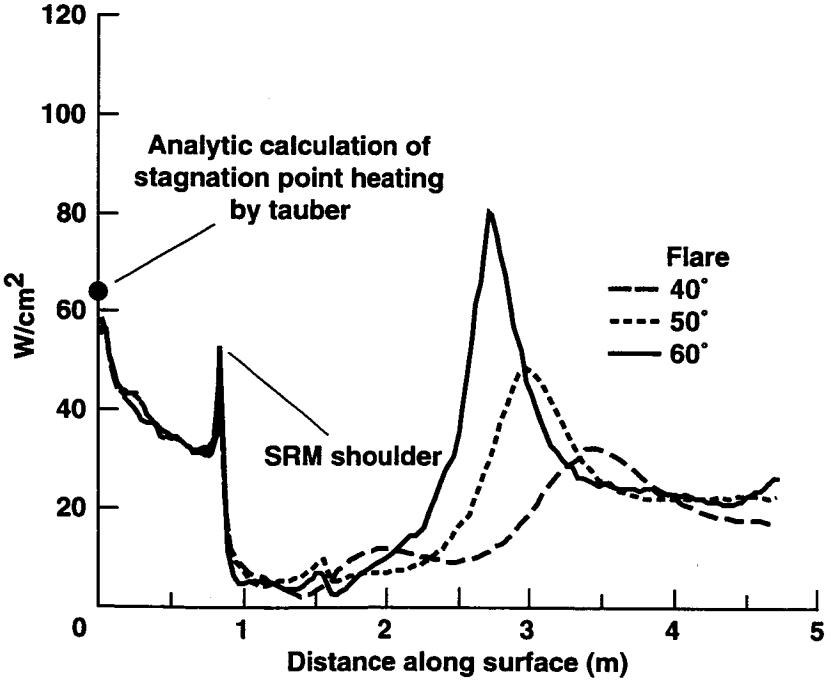

Figure 13. Heat transfer rates for flare.

While the 40° flare has a low heat transfer rate, figure 13, it must have a greater length than the 50° or 60° flares in order to achieve the desired C_D, figure 12. Therefore, an additional mass penalty must be accepted. The 60° flare can achieve the desired drag with a relatively short length, but it

must also endure a significantly higher heat transfer rate than the other configurations. This brings the survivability of the 60° flare into question. The 50° flare achieved a C_D of 5 with a length only 20% larger then the 60° case. Furthermore, the 50° flare had a peak heat transfer rate similar to that found at the stagnation point and shoulder of the SRM casing which was considerably lower than for the 60° flare. An analytical check of the SRM stagnation point heating rate was performed by Tauber using reference 10. This point, shown in figure 13, is only 8% higher than that calculated by the perfect gas solver.

Computations for Ballute Decelerators

The next type of drag device that was examined was the ballute. The ballutes studied here are ellipsoidal in shape. The ballutes were attached to the SRM casing with initial angles that varied between $\delta = 70°$ and $\delta = 80°$. The ballute produced a bow shock wave that interacted with the bow shock off the nose of the SRM casing. This is in contrast to a flare drag device which generally produced a weaker oblique shock. The interaction of the SRM nose shock and the ballute shock created a high pressure region on the surface of the ballute. Downstream of this region the pressure dropped off as the flow expanded around the aft portion of the ballute. The flow in the region where the ballute attached to the SRM casing was again largely separated causing a large region of nearly constant pressure.

Pressure contours shown in figure 14 are for three ballute shapes. The ballutes attached to the SRM casing with initial angles of 70°, 75°, and 80°. Increasing initial angle implies increasing ballute size. The pressure contours for the 70° ballute show a separation shock formed just downstream of the SRM expansion shoulder. This shock interacted with the blunt nose shock, but only a modest pressure increase was realized. The pressure contours for the 75° ballute show that the nearly constant pressure separated region has enlarged. The 75° ballute formed a stronger blunt shock than the 70° ballute. This shock interacted with the bow shock off the nose and produced a small region of high pressure. The pressure contours for the 80° ballute also show a very large separated region, but a stronger shock was produced by this ballute. The interaction of the nose bow shock and the ballute bow shock produced an area of peak pressure that is considerably higher than for the 75° ballute. Also the size of the high pressure region on the surface of the 80° ballute was almost twice that for the 75° ballute.

The C_D produced by these three shapes is shown in figure 15. For the problem considered here, a C_D of around 5 was required. As can be seen in figure 15 , a 75° ballute would produced the desired drag. But also note that an 80° ballute produced a C_D as high as 10 with only a modest increase in size.

Heat transfer rates for these three cases are shown in figure 16. What is important to note here is that for the 75° ballute, which produced the desired amount of additional C_D, the maximum heat transfer rate was less than that found at the stagnation point of the SRM casing. Also, for the 80° ballute case which produced a very high C_D, the maximum heating rate was on the order of that found at the stagnation point of the SRM casing.

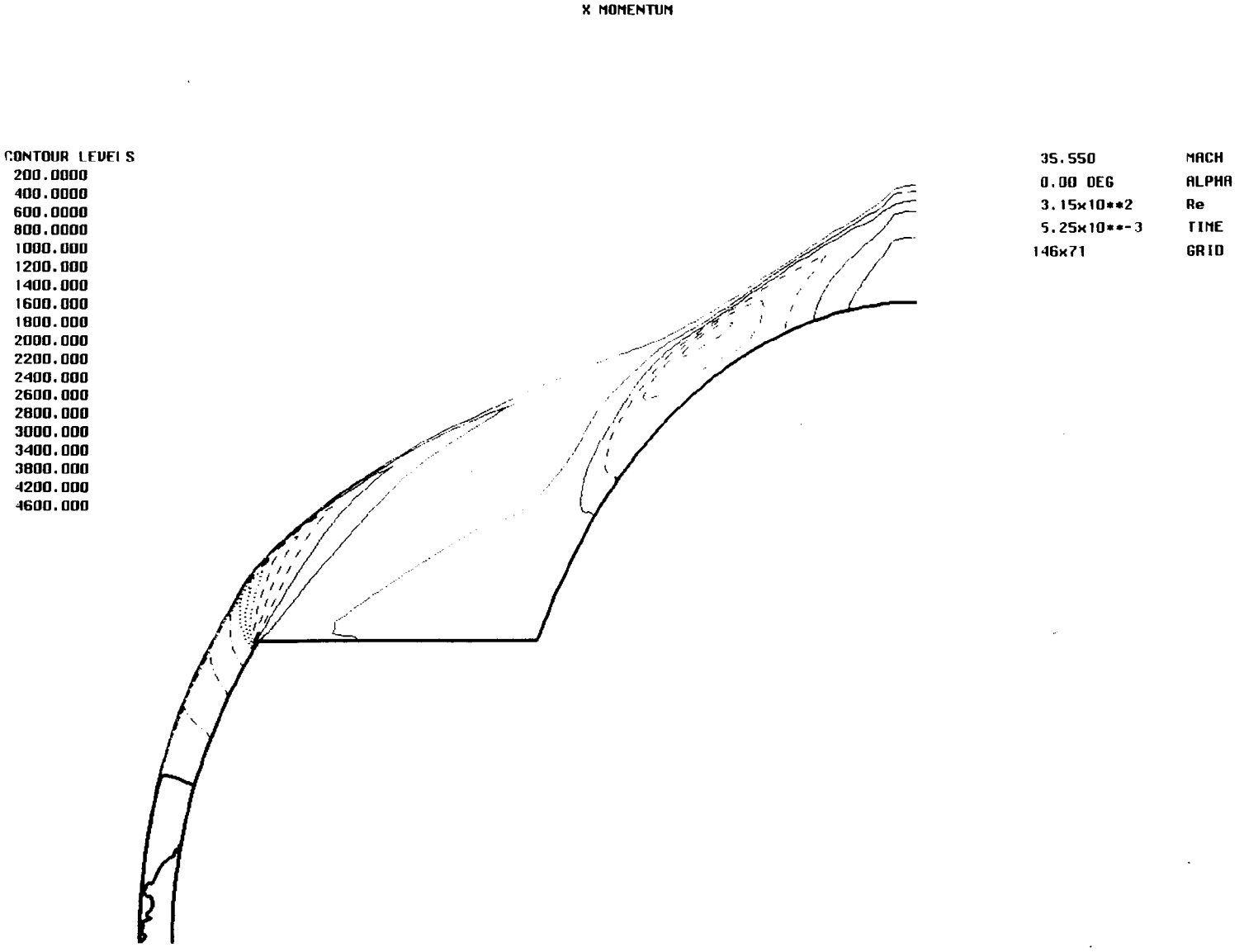

Figure 14. Pressure contours. (a) 70° ballute.

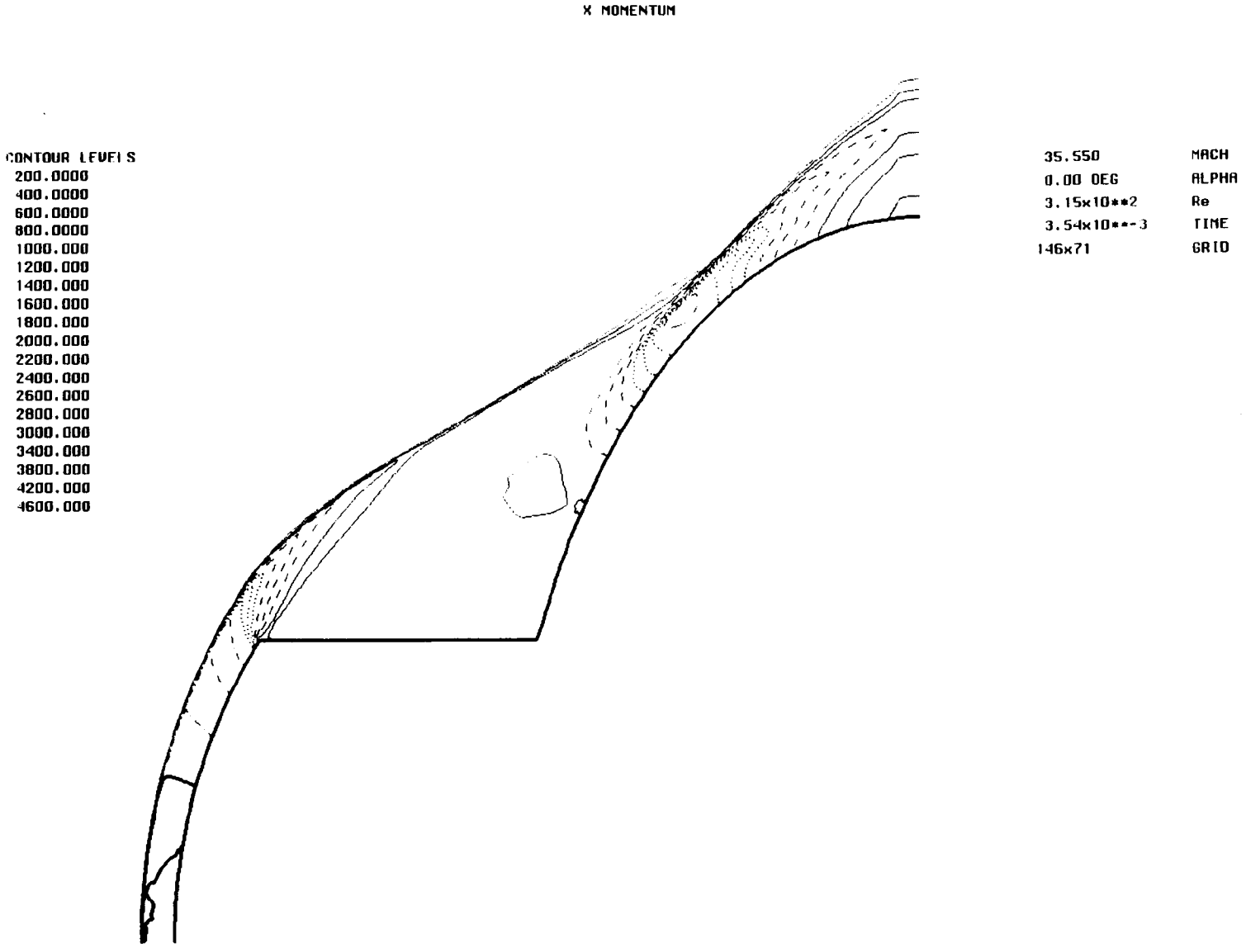

Figure 14. Continued. (b) 75° ballute.

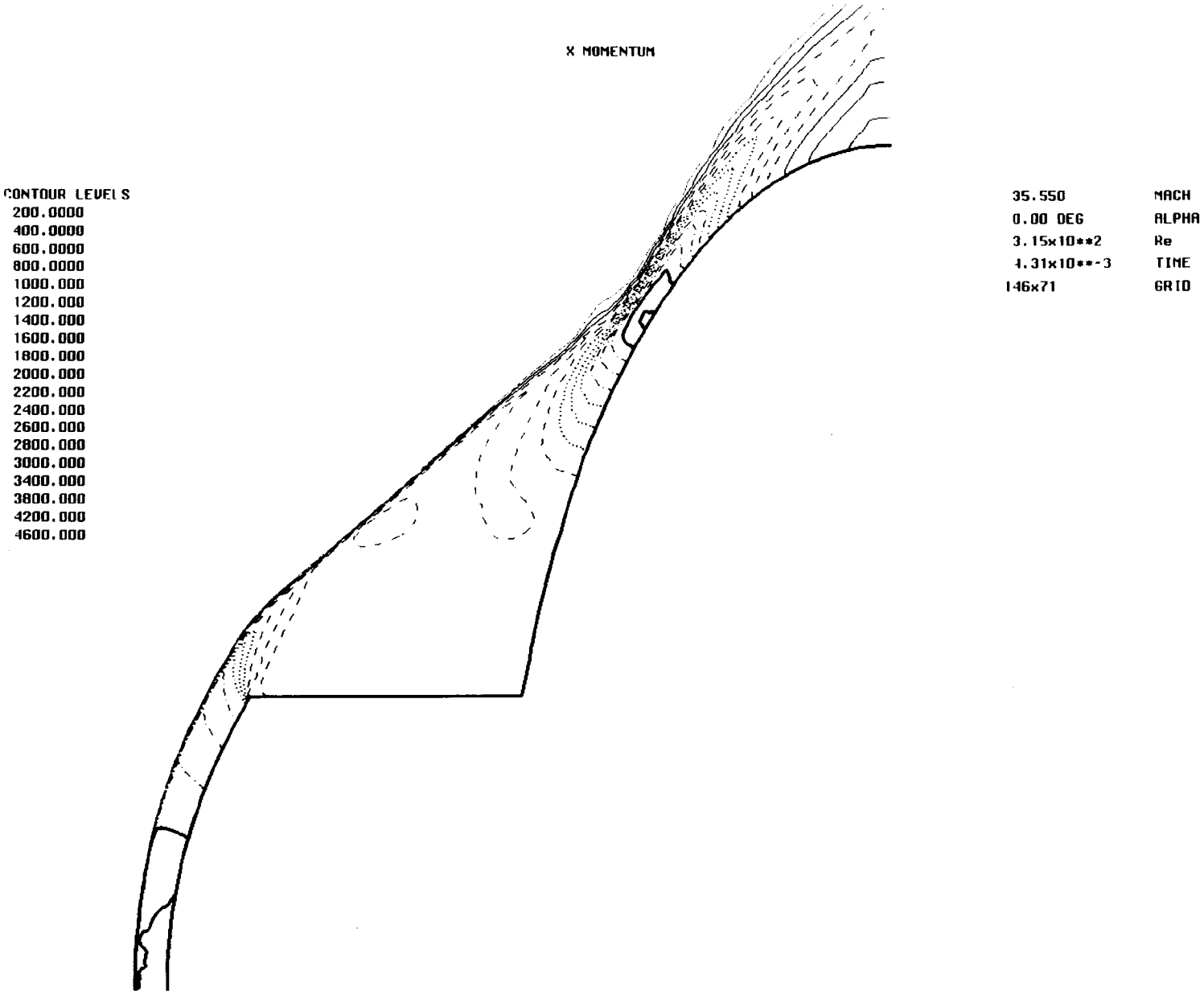

Figure 14. Concluded. (c) 80° ballute.

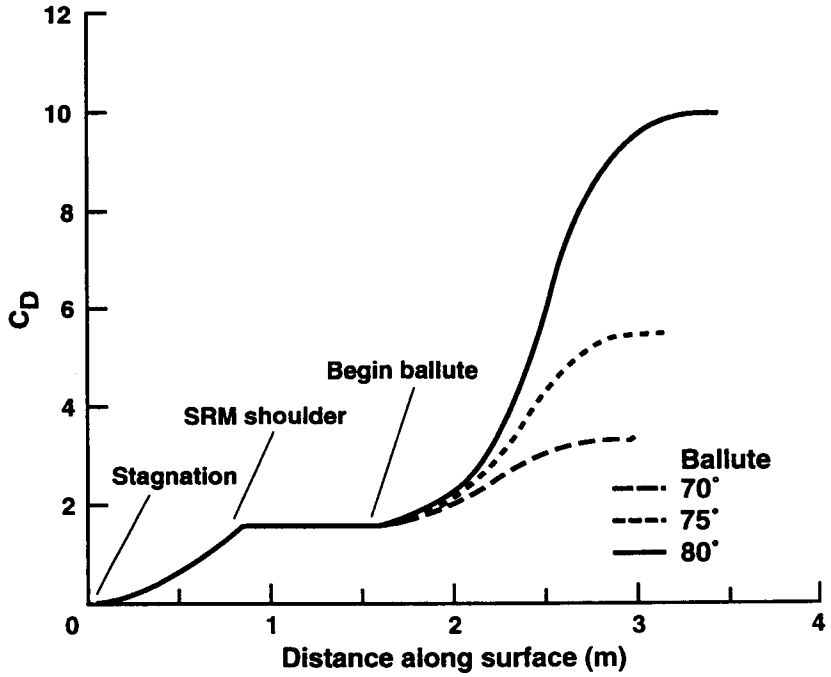

Figure 15. Drag coefficient for ballute.

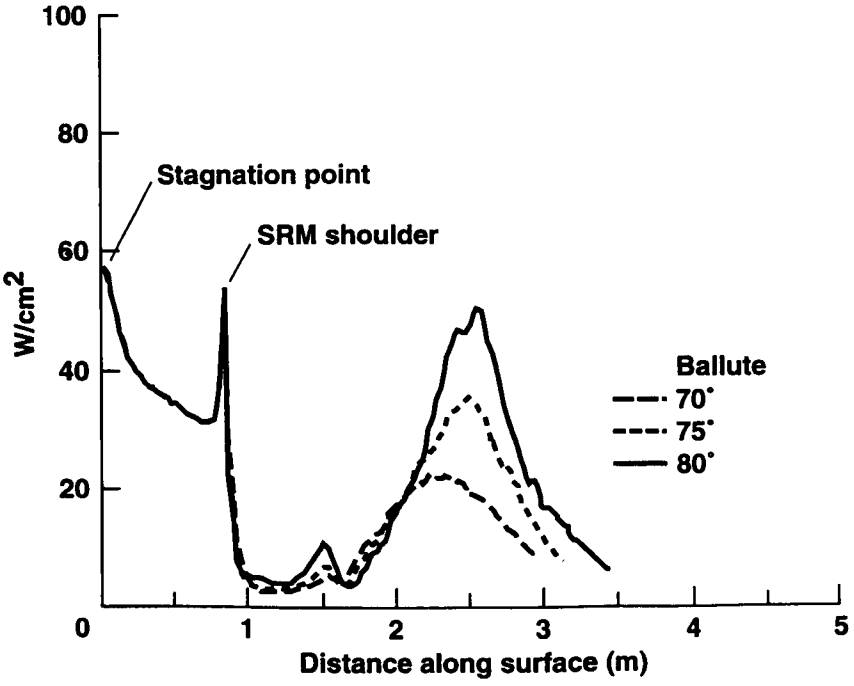

Figure 16. Heat transfer rats for ballute.

A similar type of ballute design was investigated by Wang and Shih (ref. 2). The ballute discussed in reference 2 had a circular cross section. The peak heat transfer rate predicted for the circular cross section ballute was about twice as high as that predicted for the ellipsoidal shapes examined here. Wang and Shih found that a number of existing materials could provide suitable thermal protection for their ballute design. Since neither the heating rates for the flared decelerators nor those for the ballutes exceed those anticipated by Wang and Shih, it is assumed that the same type of thermal protection can be used for the decelerator designs discussed here.

DISCUSSIONS

Comparisons of C_D and heat transfer rates for the flared decelerator and the ballute are shown in figures 17 and 18, respectively. As is indicated in these figures, the ballute is capable of producing a larger amount of drag than the flare for the same amount of heat transfer. Note, however, that the C_D produced by the ballute reaches an asymptotic value, while that for the flare increases linearly as the length of the flare is increased. There are several other considerations which must be addressed before deciding what design is more suited for the SRM mission. First, because the ballute is inflated, it is possible for it to deform in regions of high pressure such as that produced by the shock-shock interaction discussed earlier. These local deformations may cause the SRM/ballute configuration to behave in an unsteady manner. To avoid this problem, the internal pressure of the ballute could be made high enough to make the ballute geometrically stiff. The maximum pressure on the external surface of the 80° ballute was 0.04 atm. Because the maximum external pressure is low, the ballute could be inflated to an internal pressure substantially higher than the maximum external pressure. This would make the ballute essentially stiff. Since the flare decelerator is made of rigid members, local deformations should not be a problem.

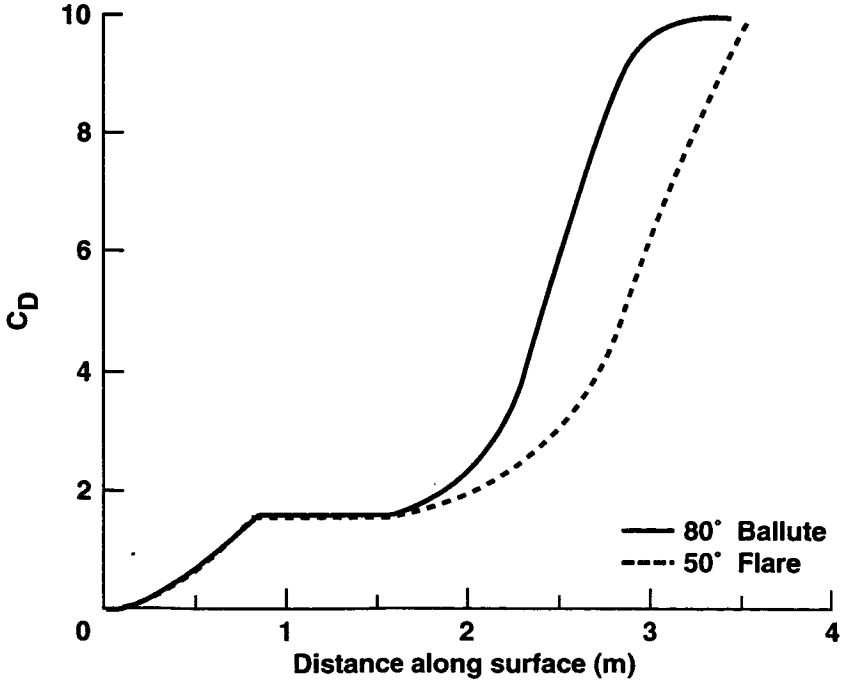

Figure 17. Drag coefficient comparison.

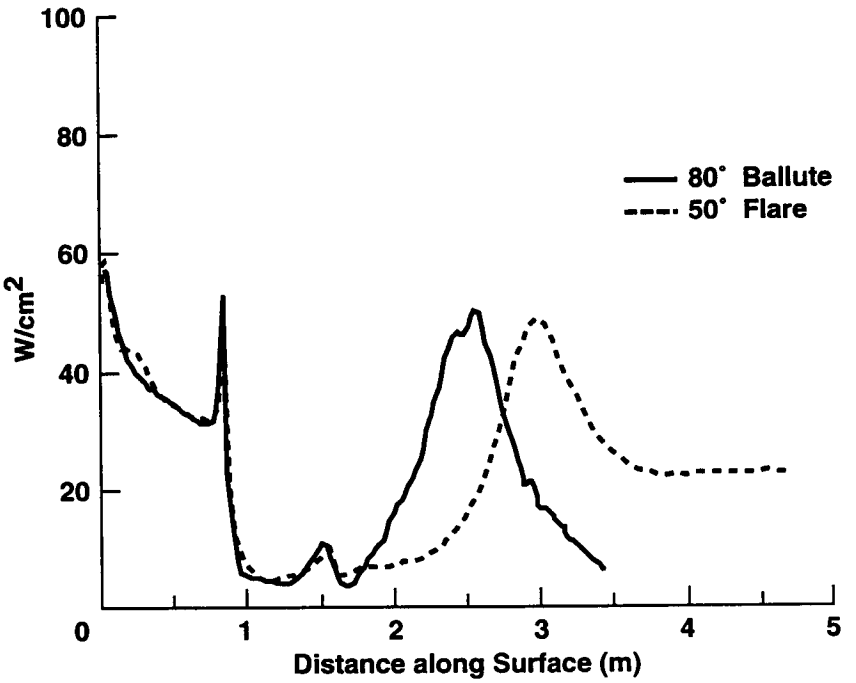

Figure 18. Heat transfer rate comparison.

For both the flare and the ballute, the base flow region is not computed. It is likely that the base flow will be unsteady and turbulent. However, the pressure in the base flow region will be very low, so the total drag will not be affected. The heat transfer rates in the base flow region are also expected to be considerably lower than the peak heating rates in the forbody (ref. 11).

Turbulence is neglected in the flowfield computations for the SRM/decelerator. The Reynolds number of the flow is sufficiently low, 2.2×10^4/m, to assume that the flow is laminar. Furthermore, it has been shown that turbulence tends to decrease the size of a separation region for a 2-D compression corner (ref. 9). A reduction in the size of the separated region would cause the amount of drag produced by the decelerator to increase. Therefore, by omitting turbulence, the computations would tend to under predict the drag produced by a decelerator, which is acceptable for design studies. However, if transition did occur, the heat transfer rates in the turbulent region would be higher than if the flow had remained laminar.

It is likely that the SRM/decelerator will not immediately steady out to a zero angle of attack orientation. Instead it will probably go through a transition stage where it will experience a range of orientations at non-zero angles of attack. The peak pressure and heat transfer rates experienced by the decelerators at non-zero angles of attack can be anticipated by looking at zero angle of attack solutions with flare angles larger that the nominal flare angle. For instance, the peak pressure and heat transfer rates experienced by a 50° flare at 10° angle of attack can be estimated by looking at the axisymmetric solution for the 60° flare, figure 11(b). Therefore, by examining higher flare angle solutions, the maximum pressure and heat transfer rates that the decelerator must endure during its mission can be estimated.

The ballute and the flare have both desirable and undesirable characteristics as drag decelerators. For instance, the ballute produces a large total drag increase with a relatively low heat transfer rate. However, the efficiency of the ballute is compromised by the large separated region caused by the high angle compression corner. Also, as the flow expands around the downstream end of the ballute the drag increase levels off until it is zero. So the rear end of the ballute, where the local surface is along the freestream direction, does very little to increase the total drag. Since the flare does not have a downstream expansion region, the drag increases linearly with the length of the flare. However, for high flare angles, the heat transfer rates are very high. And for lower flare angles, the length of the flare required to achieve the desired drag increase becomes large. Although the separated regions created by the flares tend to be smaller than for the ballutes, the flares still suffer significant losses due to the separation.

It seems likely that a combination of the flare and ballute geometries could be constructed to take advantage of the desirable characteristics of the separate geometries. An optimization procedure could be performed to produce a geometry that minimizes the separation region, maximizes the total drag increase, and minimizes the maximum heat transfer rate to the decelerator. An optimization study of this sort would be expensive and time consuming in experimental facilities. It would be too costly to perform this sort of study computationally with a full thermo-chemical nonequilibrium solver. However, the computational method used here is very well suited for optimization studies. The computational procedure has about a 10 minute turn around time for each new design, and this time could be considerably reduced with a judicious choice of initial conditions. Furthermore, this procedure could be used to conduct similar design studies for geometries other than hypersonic decelerators. As long as the fluid dynamics are similar and either experimental results for shock shape or CFD results, which take into account real gas effects, for shock shape are available, an appropriate value for effective γ can be chosen. With an appropriate choice of effective γ, the ideal gas code can be used to efficiently study a wide range of vehicle designs.

CONCLUSIONS

This work has shown that, aerodynamically, either the flared decelerator or the ballute decelerator can be used to produce a SRM/decelerator configuration with $\beta = 49$ Kg/m^2 to assure that no atmospheric skip out occurs. The ballute can produce a higher drag increase than the flare for the same amount of surface area and for similar peak heating rates. The heat transfer rates computed for the decelerators can be used to estimate the amount of thermal protection needed to assure decelerator survival for the necessary amount of time.

Employing an ideal gas formulation with an effective γ to compute the pressure field and estimate the heat transfer rates of a hypersonic flowfield with real gas effects has been shown to be successful for preliminary design purposes. The effective γ procedure requires only 5% of the CPU time needed for a full thermo-chemical nonequilibrium solution making this procedure ideal for design studies of this nature.

REFERENCES

1. Aero-Assist Flight Experiment System Requirement Document. MSFC-RQMT-1439-B, NASA Marshall Flight Center, June 1990.

2. Wang, J. A. and Shih, K. C.: Numerical Studies on Inflatable Ballute as an Aerodynamic Decelerator for a Solid Rocket Motor Hypersonic Reentry. AIAA Paper 91-0841, April 1991.

3. Alexander, W.: Summary of the Development Status of Attached Inflatable Decelerators. AIAA Paper 68-929, Sept. 1968.

4. Wyborny, W. and Kabelitz, H.: Comparison of Hypersonic Aerodynamic Deceleration Systems Based on Gun Tunnel Investigations. AIAA Paper 70-1174, Sept. 1970.

5. Palmer, G.: The Development of an Explicit Thermo-Chemical Nonequilibrium Algorithm and Its Application to Compute Three Dimensional AFE Flowfields. AIAA Paper 89-1701, June 1989.

6. Park, C.: Assessment of Two Temperature Kinetic Model for Ionizing Air. AIAA Paper 87-1574, Honolulu, HA, 1987.

7. Candler, G.: The Computation of Weakly Ionized Hypersonic Flows in Thermo-Chemical Nonequilibrium. Ph.D. Dissertation, Stanford University, Palo Alto, CA, 1988.

8. Yates, L. A. and Venkatapathy, E.: Trim Angle Measurements in Free-Flight Facilities. AIAA Paper 91-1632, June 1991.

9. Delery, J. and Coet, M.-C.: Experiments on Shock-Wave/Boundary-Layer Interactions Produced by Two-Dimensional Ramps and Three-Dimensional Obstacles. Workshop on Hypersonic Flows for Reentry Problems, Antibes, France, Jan. 22-26, 1990.

10. Marvin, J. G. and Deiwert, G. S.: Convective Heat Transfer in Planetary Gases. NASA TR R-244, July 1965.

11. Venkatapathy, E. and Feiereisen, W.: Computational Analysis of Plume Induced Separation. AIAA Paper 91-0711, Jan. 1991.

BIOGRAPHY

Susan A. Tokarcik attended the University of Maryland from 1984 to 1988 where she pursued a B.S. in aerospace engineering. During this time she was employed at NASA Goddard through a University of Maryland grant. At Goddard she worked in the geophysics branch as a computer programmer. She also spent one semester and a summer session working as a co-op student at Boeing Helicopter Company in Philadelphia, PA. She continued on at the University of Maryland and received an M.S. in aerospace engineering, specializing in hypersonic aerodynamics, in 1990. While in graduate school, she spent two summers as a visiting student at NASA Ames in the aerothermodynamics branch (RTAC). When she finished her M.S., she was hired by Eloret Institute and now continues her work with RTAC.

TEST MODEL DESIGNS FOR ADVANCED REFRACTORY CERAMIC MATERIALS

Huy Kim Tran
Ames Research Center
Moffett Field, California

SUMMARY

The next generation of space vehicles will be subjected to severe aerothermal loads and will require an improved thermal protection system (TPS) and other advanced vehicle components. In order to ensure the satisfactory performance of these newly developed materials and components, testing is to be performed in environments similar to space flight. The designs and fabrication of the test models should be fairly simple but still accomplish test objectives. In the Advanced Refractory Ceramic Materials test series, the models and model holders will need to withstand the required heat fluxes of 340 to 817 W/cm^2 or surface temperatures in the range of 2700 K to 3000 K. The model holders should provide one dimensional (1-D) heat transfer to the samples and the appropriate flow field without compromising the primary test objectives. The optical properties such as the effective emissivity, catalytic efficiency coefficients, thermal properties and mass loss measurements are also taken into consideration in the design process. Therefore, it is the intent of this paper to demonstrate the design schemes for different models and model holders that would accommodate the test requirements and ensure the safe operation in a typical arc jet facility.

INTRODUCTION

Future space vehicles such as the National Aerospace Plane (NASP), Mars and Lunar return vehicles , and other planetary probes reentering the earth atmosphere at hypersonic speed, will require an adequate Thermal Protection System (TPS). Thus, development of such TPS requires new research programs for high temperature heat shields. Recently, a program called Advanced Refractory Ceramic Materials has been initiated at Ames to develop and search for new materials for future space vehicles. A series of high temperature materials such as zirconium diboride and hafnium diboride were tested in the Ames 60MW plasma arc-jet facility. Preliminary results showed that the diboride materials are promising candidates for high temperature heat shields (ref. 1). One of the limiting aspects of the test series is that the samples were too small for any thermal, optical property and recession rate measurements. Consequently, in order to further characterize these new materials, more testing is required. Therefore, a second phase of arc-jet testing is initiated which requires new model and model holder designs. The model designs for the phase II arc jet test will accomplish the following objectives.

1. Study the scaling effect (larger sample size) on the thermal performance of materials such as mass loss measurement, recession rate, thermal shock, and thermal stress.

2. Measure the effective emissivity, catalytic efficiency coefficients and thermal conductivity.

3. Observe the geometry effects, i.e., material directional effects, on thermal performance materials applications.

Model design for arc jet testing requires some basic understanding of the high temperature supersonic flow in wind tunnels and heat transfer. These basic concepts are essential in determining the model size, geometry, and instrumentation options that will satisfy the test objectives. The next section gives a brief description of a typical arc jet facility and its capabilities followed by the essential considerations in the model designing process. Simple heat transfer equations are outlined to assist the designer in determining the overall model size and geometry. It also points out other factors which affect the final model configuration. Based on the above considerations, the next section describes the chosen model designs for the phase II arc-jet tests . A coupon sample model is used to investigate the scaling effect and to obtain thermal and optical measurements. Leading edge and nose tip models are designed to explore the geometry effects as well as the possibilities of new applications for diboride material.

DESCRIPTION OF THE AMES 60 MW ARC JET FACILITY

The Ames 60MW Interactive Heating Facility (IHF) is used to simulate earth re-entry flight conditions of space vehicles. It is a plasma arc blow-down type supersonic wind tunnel where the test gas is heated by electrical power using the 8-cm constricted arc heater (fig. 1). After leaving the arc heater column, the highly energized gas is supersonically expanded by a convergent-divergent nozzle and is discharged into an evacuated test chamber where the test article is located. The temperature, velocity and pressure of the test gas can be varied to simulate atmospheric re-entry for the space vehicle by using different nozzle exit areas of the divergent nozzle section. The stream can attain enthalpy up to 56 MJ/Kg and velocity up to Mach 8.

DESIGN CONSIDERATIONS

When a supersonic stream flows over a blunt body, a wedge or a compression corner, a shock wave is created. This is caused by a large change in density, pressure, temperature, velocity, etc. across an extremely thin region of the shock layer. In the arc jet facility, the flow is not only supersonic in the test section but the gas itself is highly energized. The kinetic energy of the gas in the free stream is converted into internal energy that results in a very high temperature shock layer near the surface. This phenomenon is referred as the aerodynamic heating effect.

The aerodynamic heating effect can be understood by simply considering that the kinetic energy in the free stream is converted into internal energy and radiant energy at the shock . Part of this energy is being used to heat the air which causes the increase in temperature across the shock and the other portion goes into heating the body. At the surface, the energy in the shock layer is transferred to the body by conduction. For a blunt body, a detached strong shock is generated and a portion of the energy in the shock layer is conducted to the body while the remainder is convected downstream past the body (fig. 2(a)). For a slender body with a sharp nose, e.g., NASP, the shock is oblique and nearly attached at the nose or leading edge. In this case, nearly all of the internal energy is conducted to the body at the nose tip and leading edge (fig. 2(b)).

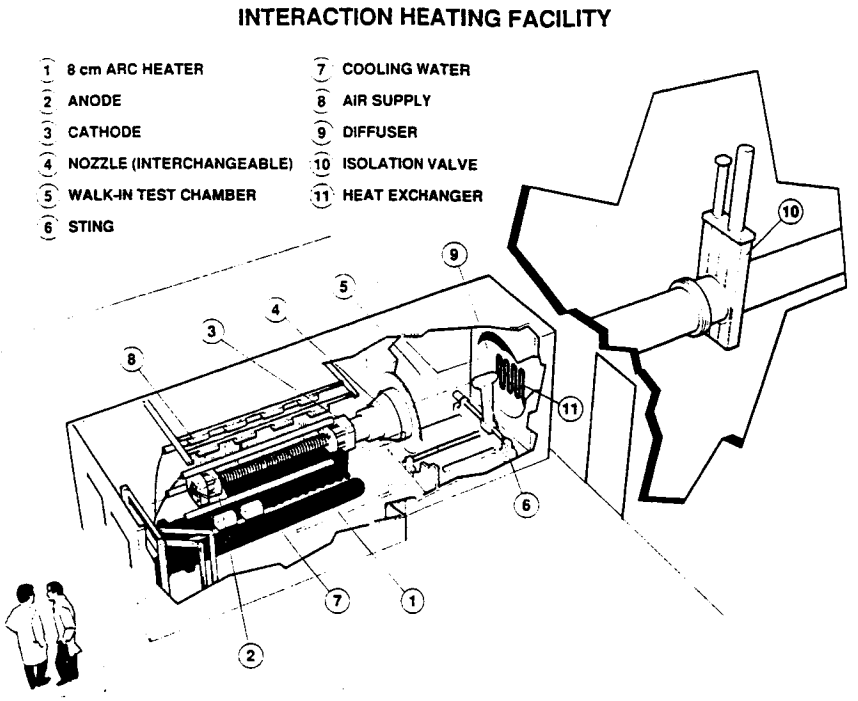

Figure 1. Schematic of Ames 60 MW interactive heating facility.

The primary design parameters for the arc jet model are the nose radius and final geometry. These parameters are affected by the imposed heat flux, stream enthalpy and flow field requirement. The section below describes the methodology in determining the model overall configuration for a given flight condition.

MODEL SCALE (NOSE RADIUS CALCULATION)

It is essential to determine the actual cold wall heat flux on model surface which includes both geometry and surface chemistry effects. The flow field and shock shape are also dictated by the body's shape. Therefore, the nose radius calculation is based on the given corrected cold wall heat flux or surface temperature in the following manner.

a. Cold wall heat flux known

If the heat flux is known, the radius of the test model can be calculated by considering the following:

The convective heat transfer rate at the stagnation surface of a spherical nose can be empirically written as (ref. 2)

$$\dot{q}_{conv} = \rho_e u_e C_h (H_r - h_w) \tag{1}$$

Note that there is little if any radiation flux in these arc jet tests. This equation emphasizes the difference in enthalpy as the "driving potential" for aerodynamic heating where h_w is wall enthalpy. H_r is

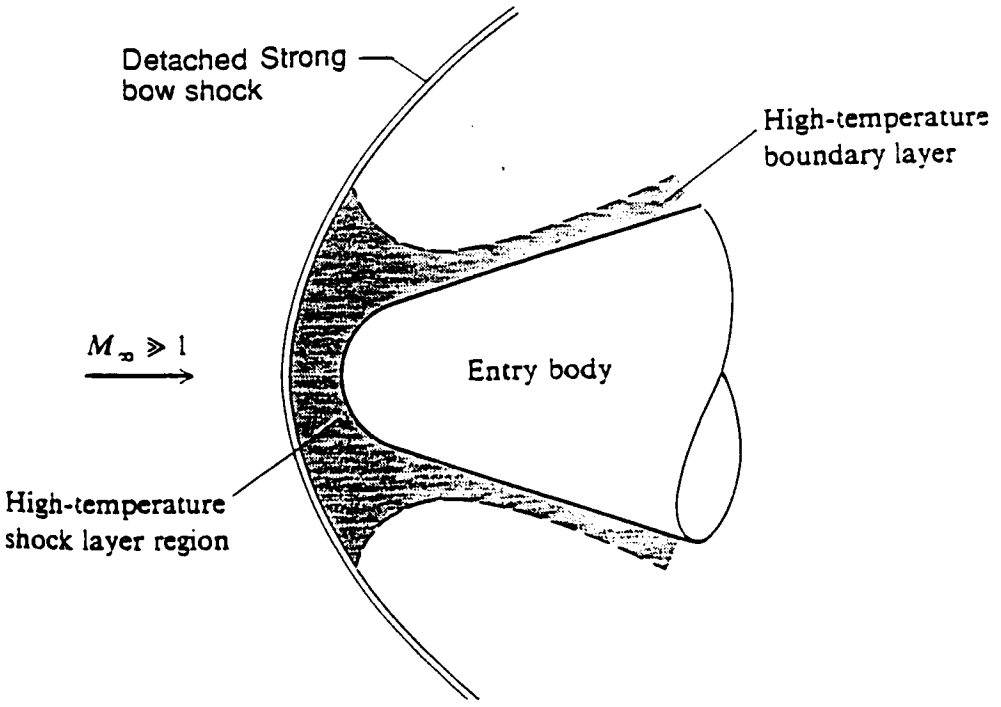

a) Detached Shock Wave on a Blunt Body (Ref. 2)

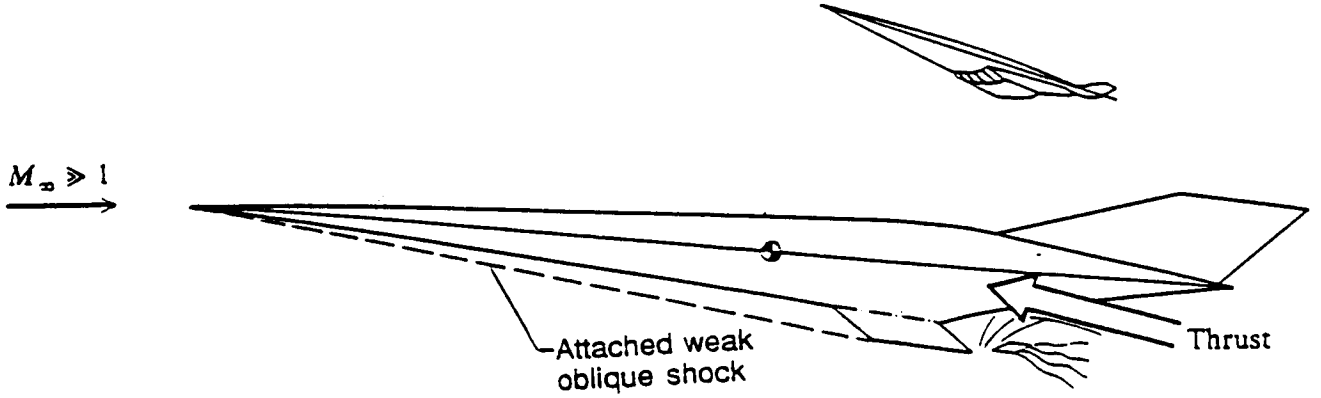

b) Attached Shock Wave on a Slender Body; e.g., NASP. (Ref. 2)

Figure 2. Flow field and shock shape of typical entry bodies.

the recovery enthalpy (i.e., total enthalpy near the shock), C_h is the heat transfer coefficient, and ρ_e and u_e are the boundary layer edge density and velocity, respectively. Equation (1) can be simplified to give

$$\dot{q}_{conv} = C\sqrt{\frac{P_{t_2}}{R}}\,(H_r - h_w) \tag{2}$$

Equation (2) is often referred to as a simplified Fay-Riddell expression (ref. 3). The nose radius of a hemispherical body at a given flight condition can therefore be approximated by

$$R_{hemi} = \left(\frac{C(H_r - h_w)}{\dot{q}_{conv}} \right)^2 P_{t_2} \tag{3}$$

where P_{t_2} is stagnation pressure(in PASCAL); R is the nose radius of a sphere (in cm), $\dot{q}_{conv}$ is in W/cm^2 and C is a proportionality constant and is taken to be 0.3531. The wall enthalpy, h_w, is often neglected for cold wall heat flux and H_r is the free stream recovery enthalpy in MJ/kg.

To obtain the effective radius in other geometries such as a flat face cylinder, a correction factor, f, is used. This factor is obtained from the ratio of heat flux on different model geometry to that on a hemisphere. For a flat face cylinder, f is taken to be 0.53-0.57 (ref. 4).

$$R_{eff} = f\, R_{hemi} \tag{4}$$

b. Surface temperature known

In some instances, the surface temperature becomes more important because of the uncertainty in heat flux calculation due to surface chemistry effects or there is an upper use limit temperature. In this case, the convective heat flux in equation (2) can be calculated by using the Stefan-Boltzmann equation and assume that the given temperature is the radiative equilibrium temperature.

The Stefan-Boltzmann equation is

$$\dot{q}_{conv} = \dot{q}_{eq\ rad} = \sigma \varepsilon T_{eq}^4 \tag{5}$$

where

$\dot{q}_{eq\ rad}$ is the equilibrium radiative heat flux in W/cm^2
σ is the Boltzmann constant and equal to 5.669E–12 $W/cm^2–K^4$
ε is the emissivity.

Surface chemistry or wall catalysis is another important consideration in calculating the surface convective heat flux. It is defined as the recombination rate of dissociated species at the surface. For a fully catalytic surface such as a metal, the recombination rate is very large; i.e., the mass fractions at the wall are their equilibrium values at the local pressure and temperature at the wall. At partially catalytic surfaces, the recombination rate is finite; i.e., there is a gradient of mass fraction at the wall. Finally, when there is no recombination at the surface, it is said to be a non-catalytic surface (e.g., oxides). Surface catalysis is not well understood because of the complex physical nature of gas-surface interaction. Consequently, to simplify the model design process, the surface is assumed to be either fully catalytic or non-catalytic. Past experience and study indicate that the aerodynamic heating of a fully catalytic surface is about a factor of two more than that on the non-catalytic surface (ref. 2).

MODEL DESIGNS

1. Coupon sample arc jet model:

In the Advanced Refractory Ceramic Material phase I arc jet test, a series of heat fluxes were imposed on the test samples. The results indicated that the upper limit heat flux for the reusability of diboride material is about 340 W/cm^2. The surface of the diborides is also considered to be fully catalytic. This heat flux occurred at a corresponding enthalpy of 27.9 MJ/Kg and stagnation pressure of 1.013E-06 PASCAL. This test condition is also similar to that was used in late 1960s and 1970s arc jet testing at ManLab (ref. 1). Thus, in phase II testing, the similar test conditions are used in model scaling calculations.

A flat face cylinder is chosen for model geometry for several reasons. First, the temperature and pressure gradient across the surface are small which result a uniform heating distribution across a large portion of sample surface. This, in effect, allows an accurate measurement for recession rates and thus a better characterization of material thermal performance. Secondly, for optical property measurements such as the emissivity and radiative flux for catalysis calculations, the model surface has to be large enough so that there is a sufficient reflected area for sensor detection. Thus, using equation (3) and taking the instrumentation constraints and facility operating limitation into consideration, the allowable radius for a spherical model is 8.478 cm for heat flux of 340 W/cm^2. From equation (4), the radius of a flat face cylinder is calculated to be about 5.08 cm.

Figure 3 shows the schematic of the coupon sample model assembly. To study the scaling effect and measure the optical properties, the radius on the coupon sample for phase II testing is three times as long as that of phase I. In order to accurately measure the recession rate and mass loss, the heat transfer needs to be one dimensional, i.e., no side heating around the model. Unlike the hemisphere geometry, the peak heating on a flat face cylinder does not occur at stagnation point but rather at the corner region. It has been shown that the edge heating effect occurs at about 0.75 of X/R ratio where X is the distance from the sample center to the edge (ref. 4). To eliminate the edge heating effect and provide a uniform heating distribution on the sample surface, a high density (POCO PGSC-1) graphite ring with a thick wall (1.40 cm) is used. Several layers of Grafoil are used to insulate the sample from the graphite ring so that the heat transfer to the test sample is one dimensional. This particular graphite ring can accommodate a 3.556 cm radius and 0.635 cm thick coupon sample.

An adiabatic wall condition is needed to further ensure the 1-D heat transfer requirement. This is achieved by placing a zirconia reflector plate between the back face of test sample and the holder . The length of the graphite ring can be determined by using an one-dimensional Fourier equation for heat conduction (ref. 7):

$$\dot{q}_{cond} = \dot{q}_{conv} = -K\frac{\partial T}{\partial x} = -K\frac{\Delta T}{\Delta x} = -K\frac{T_2 - T_1}{L} \qquad (6)$$

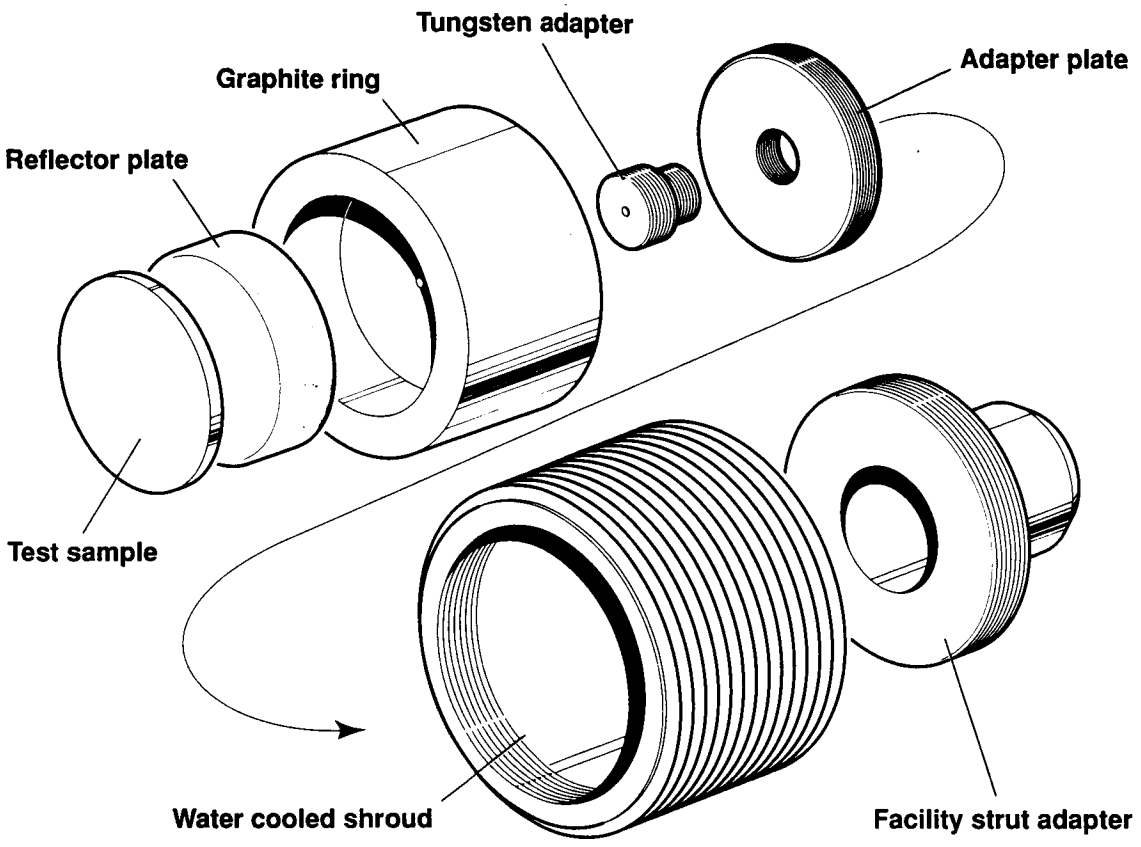

Figure 3. Isometric view of coupon sample model.

where

K is the thermal conductivity of holder material, W/cm^2–K
T_2 is the surface temperature, K
T_1 is the desired interface temperature, K
L is length of the holder, cm

The graphite ring is connected to the water cooled shroud by a two-end threaded tungsten adapter. The shroud conducts most of the heat from the graphite away and prevent the melting of the facility water cooled strut. In a oxidizing environment such as that in the arc jet facility where the free stream consists of 21% oxygen, the use of tungsten is not recommended due to its high oxidation reaction rate. However, if it is protected by other material that is oxidized more rapidly such as graphite, tungsten can be used to withstand the high temperature application.

The installation of surface thermocouples in the diboride material is extremely difficult due to its high mechanical strength. It was decided that the surface temperature could be obtained by placing one thermocouple at 0.081 cm from the sample's surface. The back face temperature is monitored by installing a thermocouple at the contact surface between the reflector place and sample. The thermal conductivity and effective emissivity can be calculated by using these temperature results along with the corrected black body temperatures from pyrometers.

C-3.

The effective emissivity can be calculated by using the Stefan-Boltzmann equation (ref. 7);

$$\sigma\varepsilon_b T_b^4 = \sigma\varepsilon_{eff} T_s^4 \tag{7}$$

where

σ is the Boltzmann constant
ε_b is the emissivity = 1.0 for a blackbody
ε_{eff} is the effective emissivity of the material
T_b is the corrected black body temperature from the pyrometer, K
T_s is the surface temperature from the thermocouple, K
Thus, the emissivity of the material, ε_{eff}, can be calculated by

$$\varepsilon_{eff} = \left(\frac{T_b^4}{T_s^4}\right)\varepsilon_b \tag{8}$$

2. Leading edge arc jet model

The third objective of this test series is to investigate geometry effects and materials applications. It is believed that the diborides can be used as reusable material for leading edge application for future hypersonic vehicles. In fact, the diboride materials were used to construct the leading edges and nose tip for the Air Force FDL-5A lifting body program (ref. 6). The results were not encouraging due to thermal stress problems. In recent years, the manufacturing process has been improved, so it is reasonable to re-evaluate the performance of diborides as a potential material for leading edge configurations. The leading edge radius chosen for the arc jet model is 0.953 cm. This value is based on the the full scale dimension of the leading edges radius of the NASP (ref. 8).

Figure 4 shows the exploded view of components of the leading edge model for the Advanced Refractory Ceramic Materials phase II arc jet test. The design consists of two removal end caps, main body and back plate. Each end cap is aligned with the main body by two guide pins and attached by two machine screws. The leading edge is held by the end caps with two tungsten pins. The main body is insulated from the high temperature leading edge by the grafoil.

The contours applied on the main body and radius on the end caps are the design's main features which minimize the shock impingement from the oblique portion of the bow shock. Another important feature in the leading edge model is the attachment between the back plate and main body. The back plate is in contact with the leading edge assembly only at the attachment areas where the screws are located. This minimizes the heat transfer from the body to the plate and takes advantage of cooling by convection. The whole assembly is then mounted on the facility water cooled strut. Notice there is no additional cooling shroud placed in between the test model and facility strut. This is due to the considerable drop in heat flux at locations away from the stagnation point. The test conditions imposed on the leading edge model are similar to those of NASP flight conditions. In this case, the imposed heat fluxes range from 260 to 817 W/cm^2 and the enthalpy is in the range of 18.6 MJ/Kg.

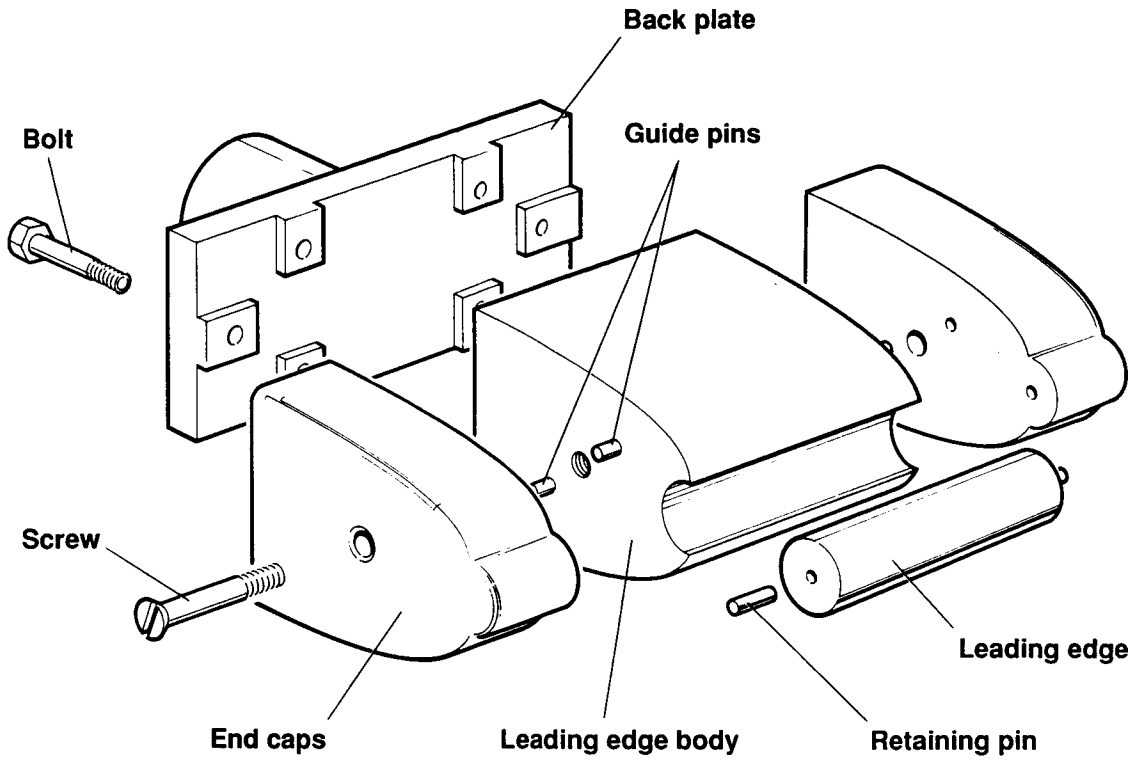

Figure 4. Isometric view of leading edge model.

3. Nose tip model

The use of diboride materials for nose tip applications is also being considered, in particular for the Pegasus SWERVE (Sandia Winged Energetic Reentry Vehicle Experiment) program. The test model consists of a nose tip and a skirt made of diboride material, a graphite sleeve and a tungsten strut. These components shown in figure 5 are assembled into a slender cone with a small blunt nose tip that is similar to the SWERVE configuration. The test model is then mounted on a water cooled cone shroud (not shown) which is installed on the facility model support system. The flare in the skirt and sleeve is used to deflect the attached shock to prevent flow impingement which might result in melting of the facility strut.

The purpose of designing this model is to study the thermal performance of the diboride materials in a high heat flux and very low Reynold's number flow regime. Because of the small radius, the nose tip model will experience rarefied or non-equilibrium flow. Mass loss measurements are taken at post test, and the recession rate is evaluated by using the high speed motion picture film.

CONCLUSION

It is shown that the size and geometry of an arc jet test model can be calculated by using simple heat transfer equations. The flow field requirement and shock shape are also important factors in selecting the final model geometry. If the model radius is too small, a rarefied flow regime results, which has a more severe effect on the thermal performance of materials. The model however needs

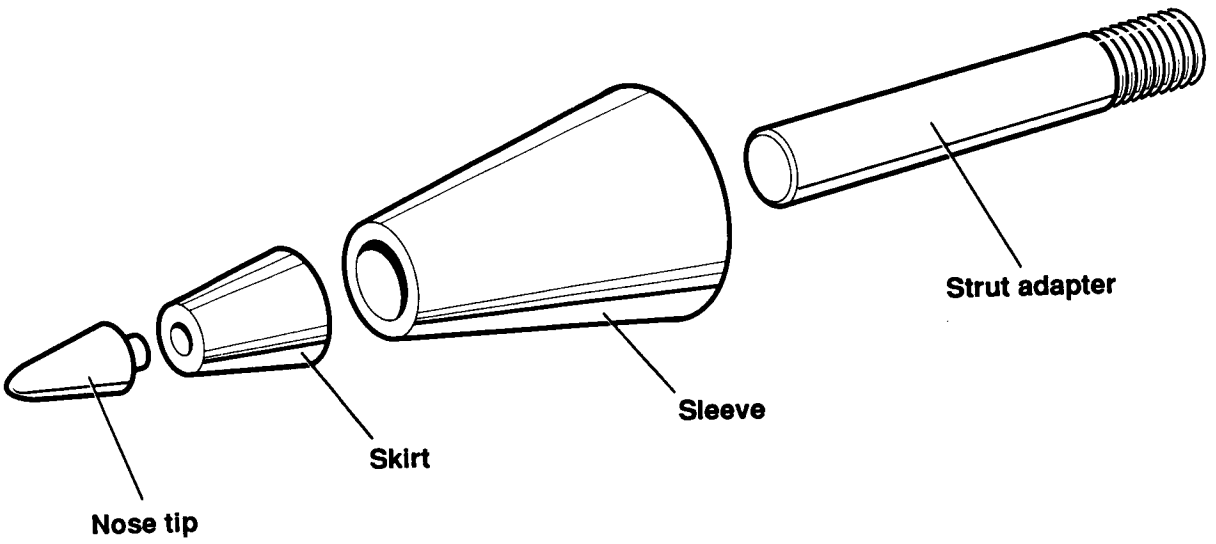

Figure 5. Isometric view of nose tip model.

to be large enough if optical and thermal property measurements are to be obtained. In the Advanced Refractory Ceramic Materials phase II arc jet tests, three model assemblies are designed to satisfy the test objectives. The coupon sample model increases the sample size from 1.27 cm in phase I to 3.56 cm in diameter in phase II. Its holder is designed to provide 1-D heat transfer to the sample and adequate protection for facility hardware. Leading edge and nose tip models are designed to fulfill a third test objective of determining geometry effects on material performance. These models and holders are used to study material performance in a rarefied flow regime and to ascertain possible applications for future hypersonic vehicles.

ACKNOWLEDGMENTS

The author would like to express her thanks to Dr. W. D. Henline for his invaluable suggestions on technical aspects of this paper and to Mr. M. Smith for his contributions in the leading edge model design.

REFERENCES

1. Rasky, D. J.; Bull, J. D.; and Tran, H. K.: Ablation Response of Advance Refractory Composites. Advanced Ceramics Association, 15th Annual Conference on Composites, Materials & Structures, Restricted Session, Cocoa Beach, Florida, Jan. 1991.

2. Anderson, J. D., Jr.: Hypersonic and High Temperature Gas Dynamics . McGraw Hill, Inc., 1989, pp. 248.

3. Fay, J. A. and Riddell, F. R.: Theory of Stagnation Point Heat Transfer in Dissociated Air. Journal of the Aeronautical Sciences, vol. 25, no.2, Feb. 1958, pp. 73-85.

4. Zoby, E. V. and Sullivan, E. M.: Effects of Corner Radius on Stagnation-Point Velocity Gradients on Blunt Axisymmetric Bodies. NASA TM-X-1067.

5. Smith, A. M. O. and Clutter, D. W.: Machine Calculation of Compressible Boundary Layers. AIAA J., vol. 3, no. 4, April 1965, pp.639-647.

6. Strauss, E. L.: Ceramic Nose Cap and Leading Edges for High Performance Weapon Systems. Tech. Report No. AFFDl-TR-72-19, Air Force Flight Dynamics Laboratory, Wright-Patterson Air Force Base, OH, April 1972.

7. Holman, J. P.: Heat Transfer, 7th Edition, McGraw Hill Inc., 1990.

8. Goldstein, H. E.; Cagliostro, D.; and Smith, M.: Spinning Leading Edge Concept for NASP. First National Aerospace Plane Technology Symposium, May 20-22, 1986.

BIOGRAPHY

Huy Kim Tran:

My family and I left Vietnam in 1979 in a small fishing boat and spent the next year and a half in the refugee camp in Indonesia waiting for the admission to the United States of America. We arrived in Woonsocket, South Dakota in spring 1981 and moved to California during that summer. I attended De Anza Junior College and transferred to San Jose State University (SJSU) several years later. I started working at Ames 1982 as an intern through Foothill-De Anza Internship Program, and continued on as a student assistant at different locations at Ames throughout my college years. I received a Bachelor of Science degree in Materials Engineering in 1987 and a Master of Science degree in Mechanical Engineering in 1990; both from SJSU. Presently, I am working in the Thermal Protection Branch as a research scientist. I am the lead engineer in a new project entitled Light Weight Ablators and am also the test/design engineer for the Advanced Refractory Ceramic Materials program and the NASP-Government Work Package 95, Internal Insulation Development.

THE CROP GROWTH RESEARCH CHAMBER

Kimberly Wagenbach
Ames Research Center
Moffett Field, California

INTRODUCTION

In order to support humans on a Lunar base or a mission to Mars, the essential elements for life support, namely water, food, and oxygen, must be supplied. The Controlled Ecological Life Support System (CELSS) program defines a regenerative life support system which supplies these elements with a minimum of resupply and waste. The primary goal of the CELSS program is to provide the major components of life support in a closed system which operates with stability and efficiency. The conceptual diagram of a CELSS is shown in figure 1. The figure focuses on the four major components of the closed system, (1) biomass production or plants, (2) food processing, (3) humans, and (4) waste processing, and how materials and gases flow from one component to another. The next step of identifying and meeting the detailed requirements of the CELSS system will be accomplished through scientific experimentation and technology development in space and on the ground.

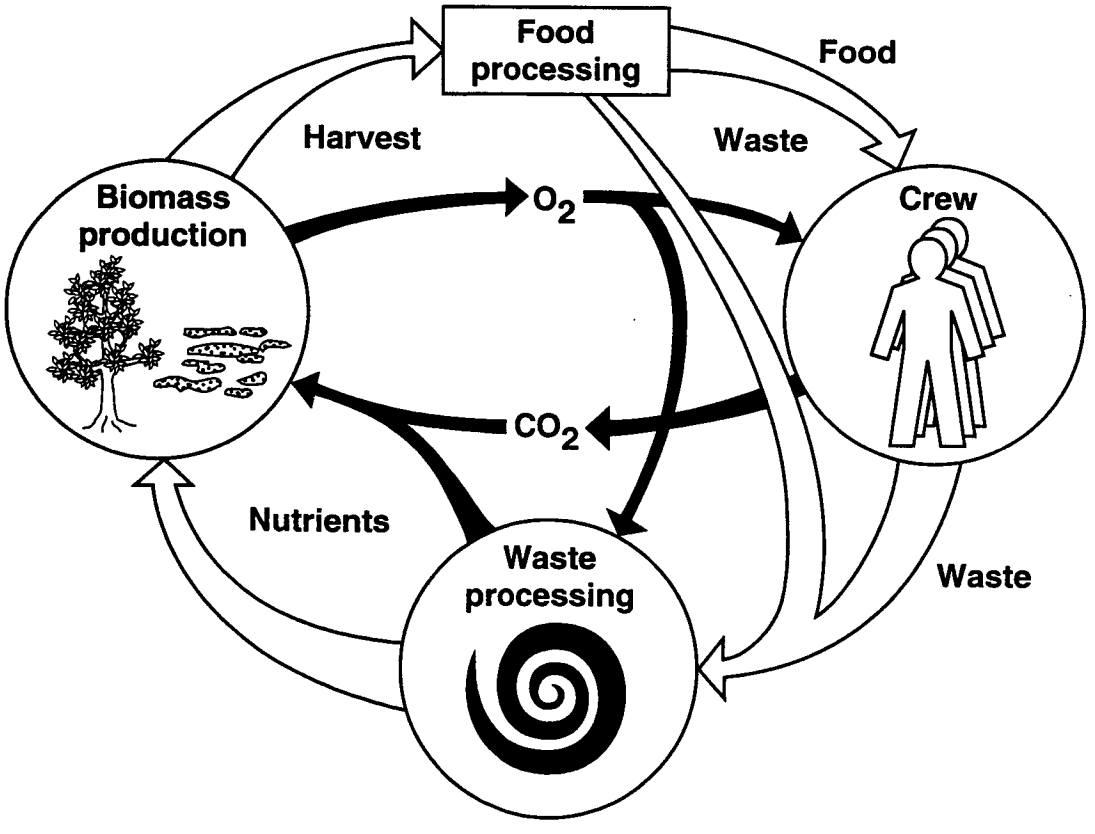

Figure 1. Conceptual diagram of a CELSS.

The Crop Growth Research Chamber (CGRC) has been defined by CELSS principal investigators and science advisory panels as a necessary ground-based tool in the development of a regenerative life support system (refs. 1 and 2). The focus of CGRC research will be on the biomass production component of the CELSS system.

The ground-based Crop Growth Research Chamber is for the study of plant growth and development under stringently controlled environments isolated from the external environment. The chamber has importance in three areas of CELSS activities: (1) crop research, (2) system control and integration, and (3) flight hardware design and experimentation. The laboratory size of the Crop Growth Research Chamber will be small enough to allow duplication of the unit, conduct of controlled experiments, and replication of experiments, but large enough to provide information representative of larger plant communities. Experiments will focus on plant growth in a wide variety of environments and the effects of those environments on plant production of food, water, oxygen, toxins and microbes. To study these effects in a closed system, tight control of the environment is necessary.

CROP GROWTH RESEARCH CHAMBER DESCRIPTION

The CGRC is a closed (sealed) controlled environment system designed for the growth of a community of crop plants with separate, recirculating atmospheric and nutrient delivery systems. In the CGRC, various combinations of environmental factors can be selected and the influence on biomass, food, water, and oxygen production of crop plants investigated. Also, measurement of plant produced toxins and microbial activity will be performed to determine if control of these elements will be necessary in a CELSS. Strict environmental control, closure or sealing of the system, and conservation of mass in the system are essential to measure the effects of various environments on crop production rates.

The CGRC is unique in that it will provide environmental control of more parameters over wider ranges and with higher accuracies than any other closed plant growth chamber. It will also take the next step in gas control by monitoring and selectively removing constituent gases as necessary to maintain setpoints. Table 1 details the CGRC control variables, their ranges and accuracies.

As shown under the physical specifications, the maximum allowable leak rate is extremely low. It can be achieved theoretically, however, the challenge occurs when purchasing off-the-shelf components such as motors, heaters, and compressors to maintain this level of closure. Also, the ratio of the growing volume to the total air volume is required to be at least 30%. This requirement stems from the necessity to measure toxins produced by the plants. If the growing volume is much smaller than 30% of the total air volume, small amounts of toxins produced by the plants will be diluted and may not be measurable.

A simplified block diagram of the CGRC is shown in figure 2. Each system is shown as a block and will be described in the following paragraphs. The sealed portion, commonly called the chamber, includes the growing volume, the ducting, and the air-conditioning system. The other systems are located external to the chamber and are interfaced to the chamber through ports located

Table 1: Design parameters table 2

Physical specifications	Limits	
1. Closure		
a. Leak Rate	< 0.5% of total CGRC air volume day^{-1}	
2. Size		
a. Total Air Volume	15 m^3	
b. Growing Volume	> 30% of total CGRC air volume	
c. Growing Area	≈ 2.0 m^2	
Environmental Control	**Control Range**	**Control Accuracy**
1. Shoot Zone		
a. **Air Temperature**	**15-40°C**	**±1°C**
b. Air Pressure	±108 kPa (absolute)	±1.6 kPa
c. **Relative Humidity**	**35-90%**	**±3% RH**
d. Air Composition		
Nitrogen	750-950 mmol mol^{-1}	±1.6-2.7 mmol mol^{-1}[a]
Oxygen	50-250 mmol mol^{-1}	±1.5-2.5 mmol mol^{-1}[a]
Carbon Dioxide	25-50k µmol mol^{-1}	± 5-500 µmol mol^{-1}[a]
e. **Air Velocity**	**0.3-1.0 m s^{-1}**	**±10%**
f. **Photosynthetic Photon Flux**	**0%, 30%-100%**	**±15%**
2. Nutrient Solution in Hydroponic Reservoir		
a. Temperature	15-40°C	±1°C
b. pH	4.0-8.0	±0.1 units
c. Conductivity	50-500 mS m^{-1}	±10 mS m^{-1}
d. Oxygen Concentration	5-20 µmol mol^{-1}	±0.5 µmol mol^{-1}

[a]Measured accuracy.

Tested using the Engineering Development Unit

on the chamber walls. Even though these systems are physically external to the chamber, they maintain closure.

The growing volume includes the shoot zone where the plant shoots grow, the root zone where the plant roots grow in a hydroponic solution, and the subroot zone where the hydroponic nutrient delivery system piping is housed. The shoot zone and the root zone are separated with a medium located at the base of the plant stem, providing isolation of the shoot from the root environment. Both environments must be maintained independent of the other; the goal is to have no movement or migration of materials between the environments except for what is conducted through the plants which are continuous between the environments. Separation of the shoot zone from the root zone is necessary for accurate measurement of plant transpiration, carbon dioxide uptake, oxygen production, and toxin production in the shoot zone, and microbial monitoring and nutrient usage in the root zone. Environmental parameters controlled in the growing volume include air temperature, chamber pressure, relative humidity, air composition, air velocity, and lighting (photosynthetic photon flux).

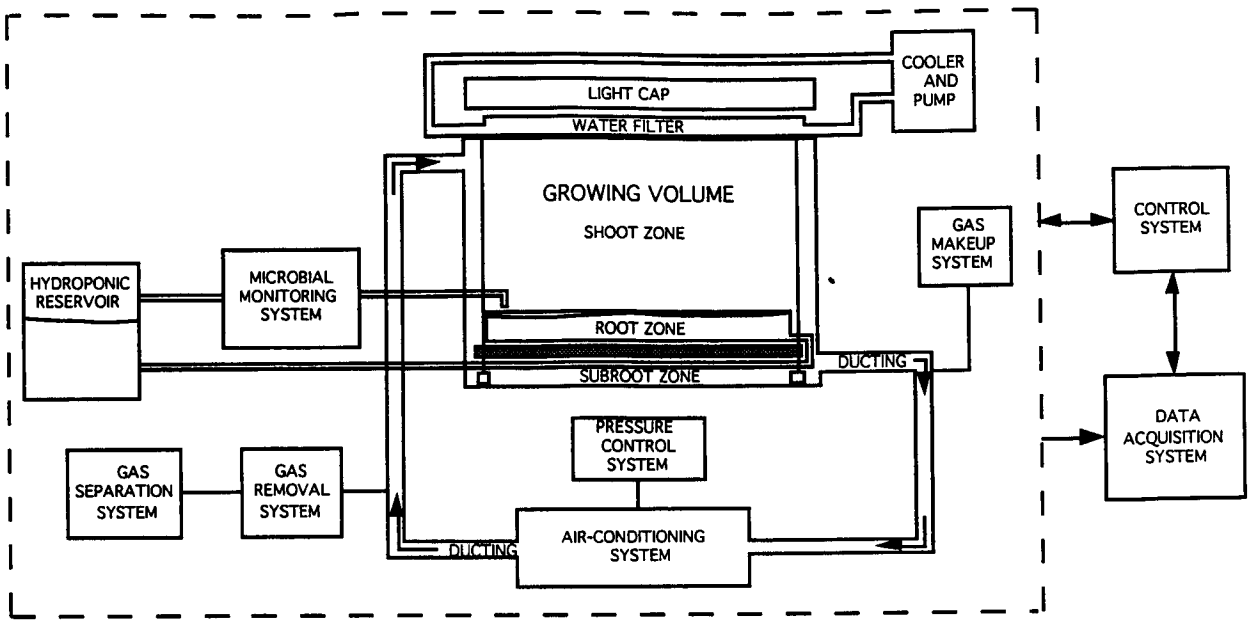

Figure 2. The crop growth research chamber block diagram.

Parameters controlled in the hydroponic reservoir which feeds up to 3 different nutrient solutions to the root zone are solution temperature, pH, conductivity, and oxygen concentration.

The air from the growing volume is transported through the ducting to the air-conditioning system which controls temperature, relative humidity, and velocity. The pressure control system port is located in the air-conditioning system and upstream of the gas removal and separation systems, to allow any air that enters the airstream from the pressure control system to be conditioned prior to entering the growing volume.

The light cap houses sixteen, 1000 watt, high-pressure sodium lamps which provide photosynthetically active radiation (wavelength = 400-700 nanometers) required for photosynthesis. The water filter located directly below the lamps consists of temperature controlled water flowing on the glass ceiling of the chamber. The water and glass filter out the longwave radiation to reduce the heat input to the chamber and to maximize the percentage of energy input that is photosynthetically active. A hood covering the light cap is required to prevent extraneous light from entering the chamber since only radiation from the overhead lamps can enter the chamber.

The gas makeup, removal and separation systems control the levels of nitrogen, carbon dioxide and oxygen within the chamber by selectively removing or injecting constituent gases. The gases removed and injected are quantified in order to determine how much of each gas is consumed or produced by a particular crop under pre-determined environments.

The hydroponic reservoir contains the nutrient solution which is fed to 10 plant trays located in the root zone. Three different solutions will be available to feed to the 10 trays to allow for random testing of various nutrient solutions. The control of the solutions' compositions is automated and recorded to determine the uptake rates of various chemicals by the plants.

The control and data acquisition systems allow for control of all the parameters listed in table 1 as is shown by the dotted lines encompassing the systems in figure 2. Measurements made within the chamber will serve as feedback to the control system and as scientific data that will be further utilized in calculations and manipulations to investigate trends in the various parameters.

Not only is the design of each separate system technically challenging, but the integration and control of the system as a whole makes the CGRC the first of its kind.

ENGINEERING DEVELOPMENT UNIT

A Science Advisory Review for the Crop Growth Research Chamber (CGRC) was held in February 1990 to review the preliminary designs. Due to discussions and concerns regarding the CGRC's air-conditioning system design and the need for control system hardware and software experimentation, it was decided to build an Engineering Development Unit (EDU). The main purpose for building the EDU was to test the hardware and software necessary to control temperature and relative humidity within the wide ranges and high accuracies listed in table 1. Therefore, the EDU includes only the air-conditioning system and control components necessary to control temperature and relative humidity. Closure was not a goal of the EDU, although steps were taken so closure could be simulated in order to accurately assess control.

A simplified diagram of the EDU is shown in figure 3. The variable speed fan is required to control the air velocity inside the chamber from 0.3 to 1.0 m s^{-1} ± 10%, as measured from the top plane of the plant canopy. The dampers determine the amount of airflow that is partitioned through the coil and through the bypass. They are controlled by the linear actuators. Most of the air flows through the bypass in cases when the plants are small and do not transpire heavily enough to require dehumidification of the air. In cases when the plants are large and transpire substantial amounts of water, most of the air is passed through the coil for dehumidification. The electric heater provides reheat for points on the envelope in which too much heat is extracted by the coil in order to obtain the correct relative humidity.

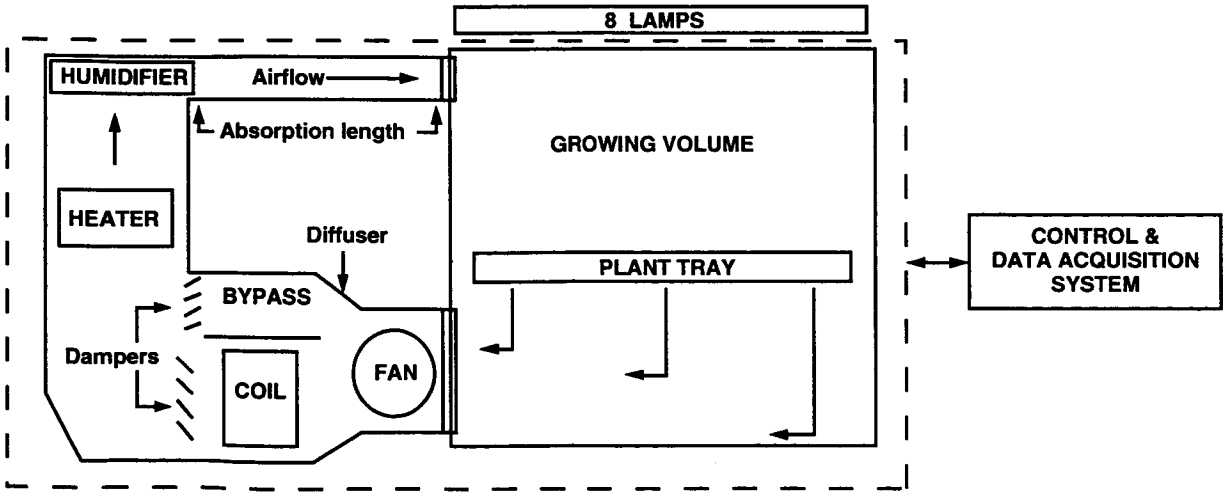

Figure 3. Engineering development unit block diagram.

To develop a better understanding of the the temperature and relative humidity control requirements, see figure 4. The slashed portion of the graph highlights the minimum air temperature attainable due to the minimum water temperature delivered by the water chiller, which cools the water entering the cooling coil. The shaded portion of the graph shows the temperatures and relative humidities not achievable due to the characteristics of the cooling coil. What makes achieving the required range so challenging is the use of off-the-shelf components which are designed to control temperature and relative humidity over very small ranges and with low accuracies. For example, temperature control required for a building's air-conditioning system is typically 20-26 °C with no set control accuracy, except to note that the system should reheat when the temperature drops below 20 °C. And relative humidity control for a building is normally 50% ±10% RH (ref. 5). Therefore, trying to use off-the-shelf components to attain ranges and accuracies for which they were never designed is difficult. Also, temperature and relative humidity are dependent upon each other. For example, a change in air temperature with a given specific humidity will cause a change in relative humidity as shown on a psychrometric chart (ref. 4). These realities become even more challenging when controlling temperature and relative humidity in a closed environment.

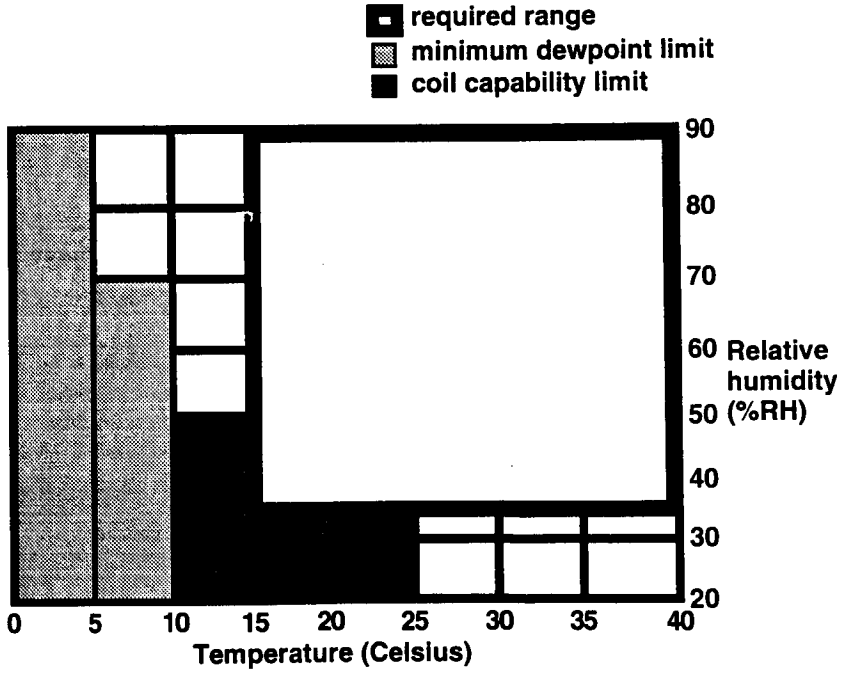

Figure 4. Envelope for control of temperature and relative humidity.

The five goals of the EDU are listed below.

1. Perform hardware performance evaluations of the air-conditioning (AC) components to ensure that they are sized properly and function according to the manufacturers' specifications. The AC components include the fan, the coil, the actuators which control the dampers, the heater, the humidifier, the water chiller, and the mixing valve which controls the water temperature entering the coil.

2. Evaluate the operation and placement of sensors to provide for accurate and reliable feedback information.

3. Evaluate the computer system, both the software and input/output hardware, to determine suitability for the final CGRC.

4. Develop a working control scheme for temperature and relative humidity control over the required range shown in figure 4.

5. Perform tests to determine if and how the AC system volume can be reduced.

The results obtained from the testing of the EDU are summarized in the following text.

1. Hardware performance evaluation

Most of the hardware performed as expected and according to the manufacturer's specifications. The components that differed from the manufacturer's specifications and from the project's expectations are detailed below.

The variable speed fan is required to control the air velocity inside the chamber from 0.3 to 1.0 m s^{-1} ± 10%, as measured from the top plane of the plant canopy. The fan was able to perform these requirements and can actually produce air speeds lower than 0.3 m s^{-1}, however, the lowest air velocity measurable with the flow sensors is 0.3 m s^{-1}.

The dampers, controlled by linear actuators, manipulate the amount of airflow through the coil and through the bypass to control temperature. The range of airflows available through the coil vs. damper positions were tested and determined if linear. The airflow with respect to damper position is linear only when the actuators are working in the 10% to 50% range. Tables reflecting this data were stored in the computer and are used to generate the proper actuator command to produce the required airflow necessary for temperature control.

The heater does not have the capacity to reach the high temperature points for which it was intended because the energy input to the EDU is much smaller than anticipated. Specifically, the heat input from the lamps is only 1 kwatt as compared to the 6 kwatts expected. The heater had to compensate for both the heat that the lamps were expected to provide and the heat lost due to leaks in order to test the control algorithm for the final CGRC, which is expected to have 6 kwatts of energy input from the lamps. Therefore, the heater had insufficient capacity to reach the high temperatures. Since it is expected that the CGRC will have 6 kwatts of energy input from the lamps due to closure, the heater's capacity will be sufficient to reach the high temperature points.

2. Sensor evaluation

Temperature, humidity, air velocity, and photosynthetic photon flux (PPF) are measured using a variety of sensors. Only problems associated with temperature and humidity measurements were experienced. The thermocouples initially used for temperature feedback, accurate to 1 °C, were replaced with resistance temperature detectors (RTD's), accurate to 0.2 °C. This allowed for much

tighter control. Also, the RTD's located inside the chamber are shielded and aspirated to negate any effects from the overhead lamps. Chilled mirror sensors are the most accurate for measuring the dew point to obtain relative humidity. However, since the air swirls within the chamber, even under the plant tray, the readings from the chilled mirror were unstable and could not be used for control. Therefore, Vaisala® temperature (measured with an RTD) and relative humidity sensors are used to provide feedback from the chamber and at set locations in the ducting. The Vaisala® sensors, calibrated at the factory with a chilled mirror sensor, are very stable and accurate. They are sturdy, easily mounted and easily integrated with the computer system. The Vaisala sensor located inside the chamber is also shielded and aspirated to negate any effects from the overhead lamps.

3. Control system software and hardware evaluation

A process control system software package was used on an IBM PC compatible and worked well for this application. It was simple to develop and experiment with various control algorithms because of its intuitive graphical format. The input/output hardware which processed feedback information from the sensors and sent it to the computer via one twisted, shielded cable also worked very well. Both the software package and the input/output hardware will be used on the CGRC.

4. Control scheme development for temperature and relative humidity control

The first control scheme tested was a complex control algorithm developed from a mathematical model of the EDU on $Matrix_x$®, a controls modeling and simulation software package. In testing this control scheme it was noted that actual control could be accomplished with a more simple, straightforward control scheme. The simple control scheme actually controlled temperature and relative humidity better than the complex algorithm and was easier to manipulate. This control scheme, shown in figure 5, consists of two proportional, integral, derivative (PID) loops. One PID controls the damper positions for temperature control and the other PID sets the mixing valve position for humidity control. For humidity control, a nested loop was necessary to effectively control the temperature of the water entering the coil, therefore feedback of the temperature of the water entering the coil was fed to another PID. In conclusion, the AC design, control hardware, and control software proved successful in meeting the goals of the CGRC Requirements Specification for control of temperature and relative humidity (ref. 3).

Control was established for over 90% of the required range shown in figure 4 to within 1 °C and 3% RH. Some high humidity, high temperature points on the envelope in the upper right hand corner of the graph are not obtainable due to the leak rate of the EDU. The heater and the humidifier cannot keep up with the leak rate at the high levels. It is expected that these points will be achieved in the CGRC due to closure. Some low humidities and low temperatures on the bottom, left portion of the graph cannot be achieved due to the chiller and coil characteristics. The chiller must cool water travelling through the coil to a minimum of 8 °C in order reach these points. The 120 foot long pipeline from the chiller to the coil is insulated to minimize heat gains, however, the water entering the coil is 10 °C at its coldest. Therefore, some of the lower temperatures and relative humidities cannot be reached and will not be achieved in the CGRC. Some high humidity points, located along the 90% relative humidity line, could not be reached in the EDU. These points could not be reached due to the leak rate, the lack of plant transpiration (because plants were not grown in the EDU), and the lower

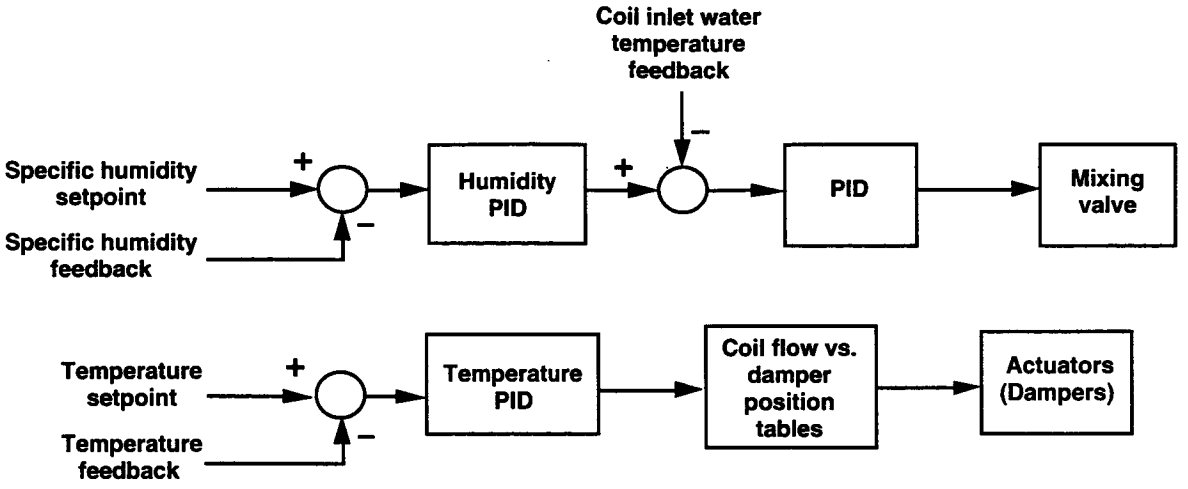

Figure 5. The EDU control scheme block diagram.

level of heat input from the lamps than expected. It is anticipated that these points will be achieved in the CGRC due to closure.

5. AC volume reduction

The two main drivers behind the volume of the AC system are the coil size and humidifier absorption length. The coil area is large to prevent air from traveling too fast across the coil such that condensed water flies off into the ducting. The scientists require that no water flies off the coil because gases that are being measured can dissolve in that water. The humidifier absorption length was determined from the manufacturer's recommendation to allow for complete absorption of the steam into the air before it enters the chamber. Steam is not allowed to enter the chamber due to plant stress and to eliminate water droplets in which gases could dissolve. Tests were conducted to determine if the coil area could be reduced and if the humidifier absorption length could be shortened, while maintaining the same level of control.

Tests concluded that reduction in the area of the coil can possibly be achieved by increasing its length, thus maintaining the total energy removal capacity of the coil. Decreasing the area of the coil will decrease the diffuser outlet area and the diffuser length, therefore decreasing the AC system volume. Further analysis will determine exactly how much the coil face area can be reduced. Identifying the location of the actual absorption of the steam along the duct proved that the humidifier absorption length may also be reduced without allowing steam to enter the chamber.

FUTURE WORK

Results from the testing of the EDU are currently being applied to the final designs of the air-conditioning system. Detailed designs of the chamber are almost complete and preliminary designs of the hydroponic, pressure control and gas control systems are underway. Testing of the pressure

control system and the oxygen removal system, part of the gas control system, will occur over the next few months. Also, a model of the EDU which was created to develop control schemes for temperature and relative humidity control is being expanded to include the other systems in the CGRC.

CONCLUSION

Since the CGRC is the first of its kind, it was necessary to build an EDU in order to gain experience in designs never before tried. Testing of the EDU allowed design engineers to gain experience with the air-conditioning hardware and sensors, and enabled the development of a working control scheme for temperature and relative humidity control. It also provided added confidence in the possibility of shrinking the size of the cooling coil and reducing the humidifier absorption length. All of this knowledge gained will make the CGRC a better research tool for the study of plant growth in a closed environment.

REFERENCES

1. Tremor, John W.; and McElroy, Robert D.: Report of the First Planning Workshop for CELSS Flight Experimentation. NASA CP-10020, Mar. 1987.

2. McElroy, Robert D.; Smernoff, David T.; and Rommel, John D.: Controlled Ecological Life Support Systems Design, Development, and Use of a Ground-Based Plant-Growth Module. NASA CP-2479.

3. Crop Growth Research Chamber Requirements Specification. NASA Document A939-8901-XR1 (1989).

4. Assignments of Psychrometric Problems for Pocket-Computers, M.S. Audi, Proc. of the 1985 International Symposium on Moisture Humidity, Washington, D.C., April 15-18, 1985.

5. ASRAE Handbook, 1989 Fundamentals, American Society of Heating Refrigerating and Air-Conditioning Engineers, Inc.

® Mention of a trademark, proprietary product, or vendor does not constitute a guarantee or warranty of the product, and does not imply its approval to the exclusion of other products or vendors that may also be suitable.

BIOGRAPHY

Kimberly Wagenbach received her Bachelors of Science in Electrical Engineering (BSEE) in 1983 and her Masters in Business Administration (MBA) in 1988 from the University of Santa Clara. She began her work at NASA Ames Research Center in 1983 on the Frog Embryology Experiment, a life sciences experiment which will fly aboard the Shuttle's spacelab. Ms. Wagenbach has worked on a variety of life sciences experiments, control systems to support aircraft, and more recently, has worked on projects in the advanced life support arena. Currently, she is the Engineering Project Manager for the Crop Growth Research Chamber Project. Also, Ms. Wagenbach is a member of the Ames Speaker's Bureau and an Ames college recruiter.

MEETING THE CHALLENGE OF MANNED LUNAR AND MARTIAN EXPLORATION

Rebecca C. Williamson
Ames Research Center
Moffett Field, California

As the U.S. space program plans for a return to the Lunar surface and ultimately for a mission to Mars, space suits and portable life support systems will have to keep pace to meet the exploration mission requirements. The systems currently in use with the Shuttle program will not be adequate for exploration on the Martian surface or for extensive exploration and work on the Lunar surface. Currently, there are too many unknowns regarding locomotion and work physiology in reduced gravity to accurately design advanced suits and life support systems for routine extravehicular activity (EVA). It would be unwise and costly to arbitrarily develop new designs without first studying how the human body moves and works in these environments. This paper discusses the current state of the art of EVA space suit and portable life support system (PLSS) design, and how this compares to the requirements for suit and PLSS design to meet the needs of advanced exploration missions. Current research underway in the Extravehicular Systems Branch at Ames Research Center aimed at advanced system design will be highlighted.

THE CURRENT HARDWARE

Although it is satisfactory for the current Shuttle program, the space suit presently used on the Space Shuttle will not be adequate for future advanced missions. The Shuttle suit operates at 4.3 pounds per square inch (psi) internal pressure, requiring an extended decompression profile to allow the EVA astronauts to go from a 14.7 psi craft to a 4.3 psi EVA suit. The Shuttle pressure is first lowered to 10.2 psi for 24 hours before the planned EVA. The EVA crew then breathes pure oxygen for 45 minutes prior to embarking on the EVA. Even after this extensive preparation a significant bends risk on the order of 5% still exists. In addition, the lowered cabin pressure can cause overheating of the air-cooled electronic systems on the shuttle.

The Shuttle suit also requires a great deal of effort to flex the joints because the suit does not maintain a constant volume. When a joint is flexed and then held in a fixed position, the astronaut must contract his/her muscles isometrically to keep the joint flexed. This extra effort can lead to local muscle fatigue early in an EVA.

The extravehicular mobility unit (EMU) is not designed to be space-based since it is not easily maintained nor is it as rugged as would be required for frequent use. It is certified for only 3 uses and then it must be torn down completely and overhauled. These maintenance requirements virtually exclude both the Shuttle suit and EMU from being used for advanced missions.

There are currently two prototype suits developed for 0-gravity (g) EVA use on the Space Station as well as other microgravity situations. Ames Research Center developed the AX-5 and Johnson

Space Center developed the MK III. Both suits operate at 8.3 psi. If used in a 1 atmosphere (atm) base or cabin, these suits minimize prebreath time. These suits were designed for 0-g operations, however, rather than for walking or other planetary surface operations.

REQUIREMENTS FOR ADVANCED HARDWARE

Although there are elements which we know little about, there are some general parameters of advanced suit and PLSS design that can be used in developing advanced concepts. Ideally, advanced design concepts should improve the work capability of the EVA astronaut thereby increasing the amount of productive labor per EVA hour. An advanced suit should also maximize productivity while minimizing fatigue. One way to accomplish this is to minimize both the dynamic and static suit joint flexure forces. The suit mobility joints must also be designed to allow the degrees of freedom and range of motion required to perform the EVA tasks. Emphasis on comfort will be much more important for advanced missions because extravehicular operations have the potential of being much more routine and of longer duration. Designs which were tolerable for short missions with infrequent EVAs won't be acceptable for longer ones.

An advanced suit should also have the correct ratio of suit pressure to base or cabin pressure in order to eliminate pre-breathe and to decrease the bends risk. An advanced concept suit designed to operate at, or very near, cabin or base pressure could eliminate pre-breathe problems. A suit that can operate well at 9 or 10 psi would be ideal if the cabin or base pressure is 14.7 psi.

The remoteness and duration of a Mars mission will require every element of the mission be optimized for function, reliability and efficiency. Logistical problems such as how much support system mass must be launched to maintain the suit/PLSS must be addressed. The weight and volume of the unit could be minimized by efficient packaging. In addition, an advanced suit/PLSS unit must also be easily maintained. If Lunar exploration is to become more routine than what was done in the Apollo program, a new life support system will have to support more physically taxing work and be more efficient at removing metabolic heat quickly and effectively. Research into metabolic rates achieved with varying levels of EVA work may help us to understand what types of heat removal rates a future PLSS would have to provide.

The biomechanical and physiological assumptions about how an advanced concept suit and PLSS must perform need to be confirmed by experiment. Research must be performed and the results compared with mission requirements for extravehicular operations.

CURRENT EXPERIMENTS UNDERWAY AT AMES RESEARCH CENTER

One question that needs to be addressed with regard to an advanced concept PLSS is how to effectively and efficiently maintain thermal comfort throughout an extended orbital EVA. Currently, when more warmth or cooling is needed within the suit, the astronaut controls the action of the liquid cooling garment (LCG) by manually adjusting a knob on the suit. This takes away from an astronaut's work time and it is also inefficient. Operational experience with the current EVA system shows the astronaut's heat balance is poorly controlled, resulting in some areas of their body being

warm while they are simultaneously cold in other areas. Studies show that both skin temperature and internal body temperature may be important indicators of the state of thermal comfort (refs. 1 and 4). Another study purports that a linear relationship exists between skin temperature and metabolic rate and that a linear relationship also exists between the evaporation of sweat and metabolic rate (ref. 3). Therefore it's possible that an advanced heat balance system could "read" an astronaut's metabolic rate by way of some non-invasive sensor and then automatically change its cooling function without the astronaut having to do anything but continue his/her work. This could lead to not only greater overall thermal comfort and a more stable heat balance but it would also allow longer EVA sessions with less chance of astronaut fatigue due to over or under cooling.

In order to pursue this thermal comfort question as well as attempt to simulate the metabolic cost of orbital EVA, a set of experiments was designed to simulate orbital EVA and to quantify the physiological cost of the activity (ref. 12). Using three male subjects, exercise experiments were performed on a unique upper body arm crank device (figs. 1 and 2). The device provides four degrees of freedom of movement: roll, pitch, yaw, and a linear motion aligned with the spine. The bench on which the subject lies is supported by a gimballed shaft. The subject's body weight is counterbalanced by weights at the opposite end of the shaft. Thus, when the shaft is in the unlocked position (the actual EVA simulation situation), the subject reacts all forces at the feet which are secured in foot restraints that do not move relative to the ground. The device can also be used in the locked position in which the shaft remains immobile and the subject does not have to counterbalance himself using his feet.

The first series of experiments which were recently completed were designed to correlate this new exercise technique and to demonstrate its utility as a 0-g EVA work simulation device. Five

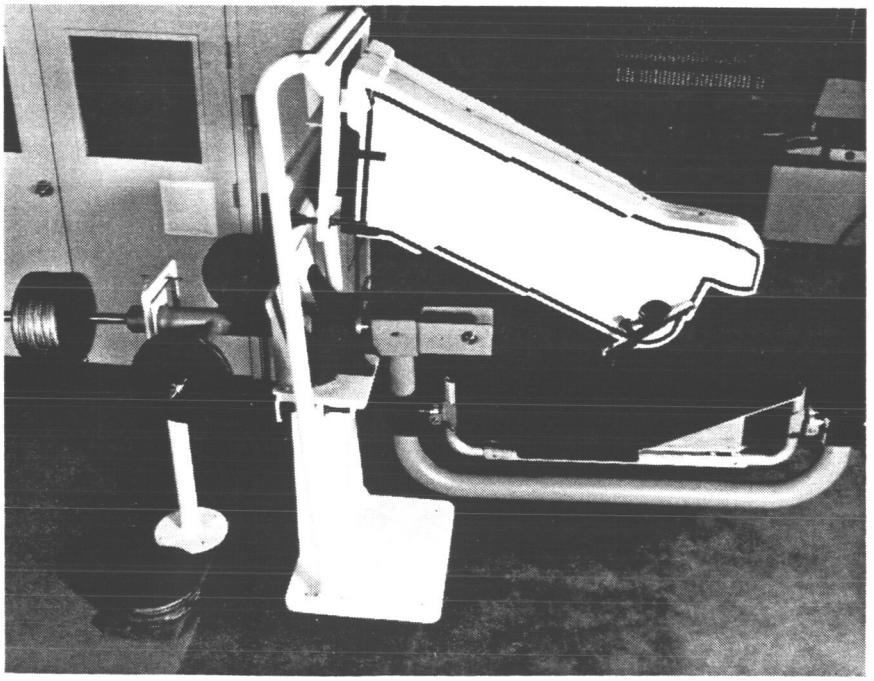

Figure 1. The extravehicular activity simulation device located at Ames Research Center.

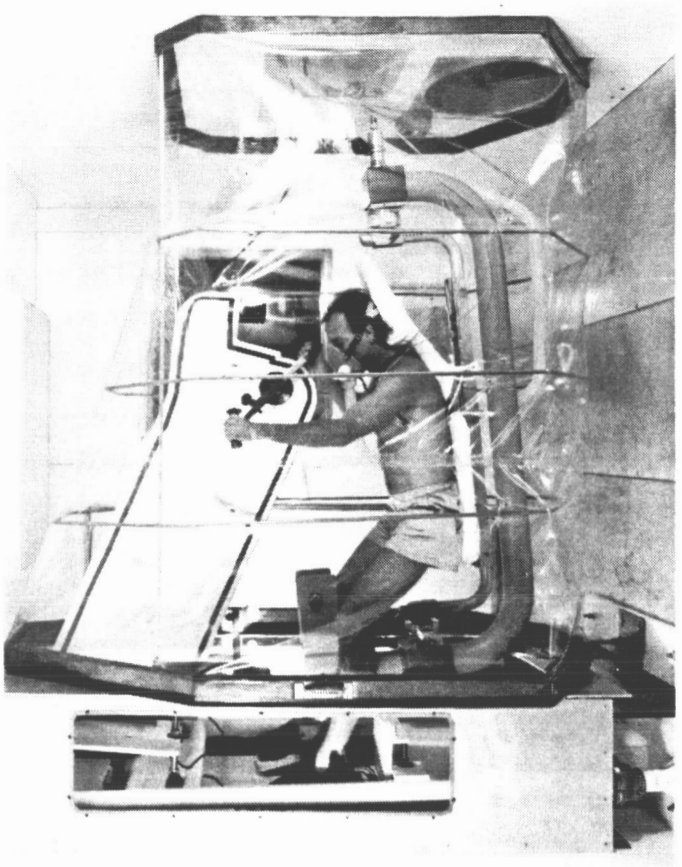

Figure 2. The extravehicular activity simulation device housed in its environmentally controlled chamber.

exercise protocols were used: (1) a low level constant workload (25 watt work output); (2) a moderate level constant workload (65 watt work output); (3) a high level constant workload (100 watt work output); (4) a transient workload; and (5) a maximum output protocol in which the subject cranked as hard as he could for 1 minute after a five minute warm up. For these initial tests, subjects were dressed in exercise shorts with no cooling system. First, a control situation was implemented in which subjects sat upright in front of the ergometer and performed the various protocols to correlate this exercise device with other upright arm crank research. Preliminary findings on oxygen uptake are comparable to other studies utilizing upright arm crank exercise (refs. 2, 7, and 10) (fig. 3). The subjects were then put on the device in the supine position and did all protocols at least three times in both a locked and unlocked position. Subjects came to the lab 2 or 3 times per week and performed 1 protocol per session until all test situations were completed. Subjects performed identical work protocols in both the locked position and unlocked position in order for the investigators to observe the metabolic rate and other physiological parameters when isometric lower body stabilization forces had to be performed by the subject.

Results from these experiments are currently being reduced and analyzed but preliminary findings suggest the average metabolic rate reached in three of the protocols, the low constant workload, the moderate constant workload, and the transient workload, most closely mirror the average

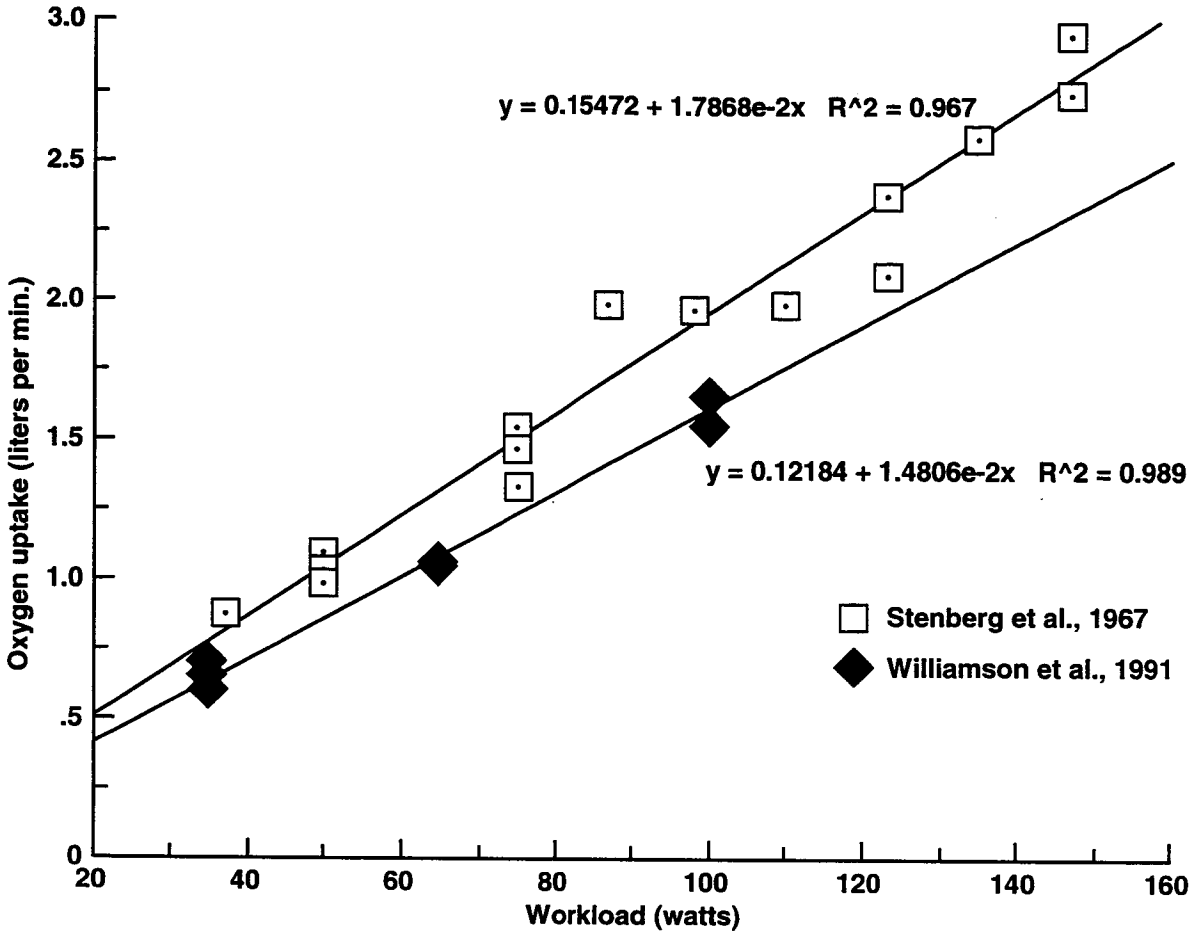

Figure 3. Comparison of oxygen uptake between two seated upright arm crank ergometry studies. In Williamson et al., (ref. 12), 3 male subjects exercised at 35, 65, and 100 watt constant work outputs. In Stenberg et al., (ref. 7), 6 male subjects exercised at various constant workloads from 1-4 sessions each.

metabolic load of actual EVAs (refs. 5, 8, and 9) (table 1). This suggests the exercise protocols may not only replicate the generic muscular movements of an average EVA (i.e., dynamic upper body work combined with isometric lower body work), but that the metabolic loads on the subject may be quite similar to that of EVA astronauts. Although the higher constant workload protocol elicited higher average metabolic costs than those thought to occur during orbital EVA, these data will indicate the upper limits that must be understood in order to build a controller capable of keeping an astronaut comfortable during short periods of hard work.

Once data analysis is finished, experiment findings will be submitted in the form of a formal journal article. In addition, another set of similar exercise experiments with a larger subject pool will be conducted to reconfirm the data. After analyzing data from these follow-on experiments, a prototype controller will be developed. Exercise experiments with subjects wearing the prototype controller will then be conducted to provide more information on how heat balance and thermal comfort during an EVA can be manipulated by a control system.

Table 1. Comparison of metabolic rates on actual mission EVAs (refs. 5, 8, and 9) and a simulated EVA study performed at Ames Research Center (ref. 12).

*ACTUAL EVA METABOLIC RATES FROM VARIOUS PROGRAMS**		
Program	Mean rate for entire program (kcal/hour)	Range of rates for entire EVAs (kcal/hour)
Apollo		
1/6-g	235	197-302
0-g	151	117-504
Skylab	238	145-330
Shuttle	197	152-275

*METABOLIC RATES FROM SIMULATED EVA STUDY (SUPINE UNLOCKED POSITION) AT AMES RESEARCH CENTER***		
Exercise protocol	Mean rate for entire test***(kcal/hour)	Range for entire test***(kcal/hour)
Low (constant 35 watt output)	154	32-401
Moderate (constant 65 watt output)	219	24-654
High (constant 100 watt output)	352	34-849
Transient	225	44-676

*Three methods were used to estimate real-time metabolic rates:
1. Heart rate
2. Oxygen usage (computed from the decrease in oxygen bottle pressure per unit time).
3. Difference in temperatures of the coolant water flowing into and out from the LCG.
**Standard laboratory method of measuring oxygen consumption/carbon dioxide production with gas analyers was used.
***Excluding 2 minute warm up at beginning of tests.

Another factor that must also be understood to optimize an advanced suit and PLSS is an understanding of both the allowable load carrying limits and acceptable perturbations to the center of gravity (c.g.) in simulated planetary surface EVAs. This will provide guidance as to how much a PLSS can weigh and how/where the load of the unit should optimally be placed relative to the astronaut's body. In the Martian environment of 3/8-g, the weight of the unit is especially significant as is the placement of the PLSS upon the suit. A unit that is too heavy or that has the PLSS placed in such a way as to hinder the astronaut's activity would make EVAs difficult and possibly dangerous.

A set of experiments is currently being performed to assess the effect of reduced gravity levels on various measures of work performance in human load-carrying capability during planetary EVA (ref. 11). Tasks such as walking, kneeling down from and returning to an upright posture, lifting boxes of graduated weights, and positioning boxes at various locations while the subject's c.g. has been displaced from normal are activities of interest to the investigator in order to observe how load placement affects astronaut movement and productivity.

The first round of these experiments was conducted on the KC-135 aircraft at NASA Johnson Space Center. During 2 days of testing, 50 Martian and 95 Lunar parabolas were flown. Five male subjects wore a Variable Load Positioning Backpack (VLPB) which placed a 50 pound load at one of two extreme locations: high on the back, at the location of the current shuttle PLSS c.g.; or low on the front torso, at the same horizontal distance from the body's centerline as the high back location but at the vertical height of the normal body c.g. Subjects performed several lifting, positioning, and treadmill walking tasks with the load in the two different locations. All tests were also videotaped for biomechanical motion analysis. After the flights, subjects answered questionnaires regarding comfort, difficulty, stability, and control for each task and load position. Further experiments will be conducted at the Ames Neutral Buoyancy Test Facility (NBTF) where additional measurements of oxygen consumption, carbon dioxide production, heart rate, foot to treadmill contact forces, joint movement ranges, and body segment trajectories will be taken in order to further investigate these issues. Once data have been analyzed, an analytical biomechanical model will be developed to provide a more thorough understanding of the role of reduced gravity in human load carrying and optimal load placement. Results from this study are expected to have significant effect on the design of future planetary EVA suits and PLSS design/placement by giving design engineers new information on optimal load placement and suit structure.

Modeling the biomechanics and mobility of humans performing simple planetary locomotion is a third area that needs investigation in order to drive advanced suit design. Identifying gait, transition speed, and oxygen consumption during locomotion is a critical first step in the understanding of human performance in partial gravity. Quantifying workloads encountered and the energy cost of planetary locomotion will help define oxygen consumption and carbon dioxide production requirements for planetary life support systems.

Newman and colleagues recently completed a study investigating the biomechanics and energetics of locomotion in reduced gravity environments (ref. 6). The study took place at the Ames NBTF. Six subjects (4 male, 2 female) were used in this study. Each subject completed six experimental sessions. One session was a 1-g control experiment with the subject exercising on the treadmill outside the NBTF. The remaining five sessions took place underwater in the NBTF with the subjects breathing through modified commercial diving gear (fig. 4). Partial gravity loads were provided by

an adjustable loading harness on the subjects which distributed lead weights ranging from 0% to 100% of their dry body weight. The subject's body-segment masses and inertial properties determined the amount of weight required to simulate partial gravity loading. Weights were distributed on five regions and balanced across the mass center of the left lower leg, right lower leg, left thigh, right thigh, and torso. Five gravity conditions were simulated: 0-g, 1/6-g, 3/8-g, 2/3-g, and approximately full body loading (90-100%). Subjects walked at three speeds: 0.5 meters per second (m/s), 1.5 m/s, and 2.3 m/s during each of the experimental sessions.

Vertical ground reaction forces were measured during each session while oxygen consumption, carbon dioxide production, and heart rate were sampled. Video data were recorded and manually analyzed by a computer program to encode the limb position. The data revealed a significant ($p < 0.5$) reduction in peak ground reaction force with a decrease in gravity level at all speeds. Stride frequency measurements indicated a general trend toward a loping gait as gravity level decreased. For locomotion at 1.5 m/s and 2.3 m/s, the plot of average stride frequency versus gravity depicted a non-linear reduction in stride frequency as gravity level decreased, while there was no significant difference in foot contact time for various gravity levels. This suggests that the aerial phase (time between toe-off and ground contact of the opposite foot) is significantly longer for partial gravity locomotion because the contact time does not vary with gravity level while the stride frequency

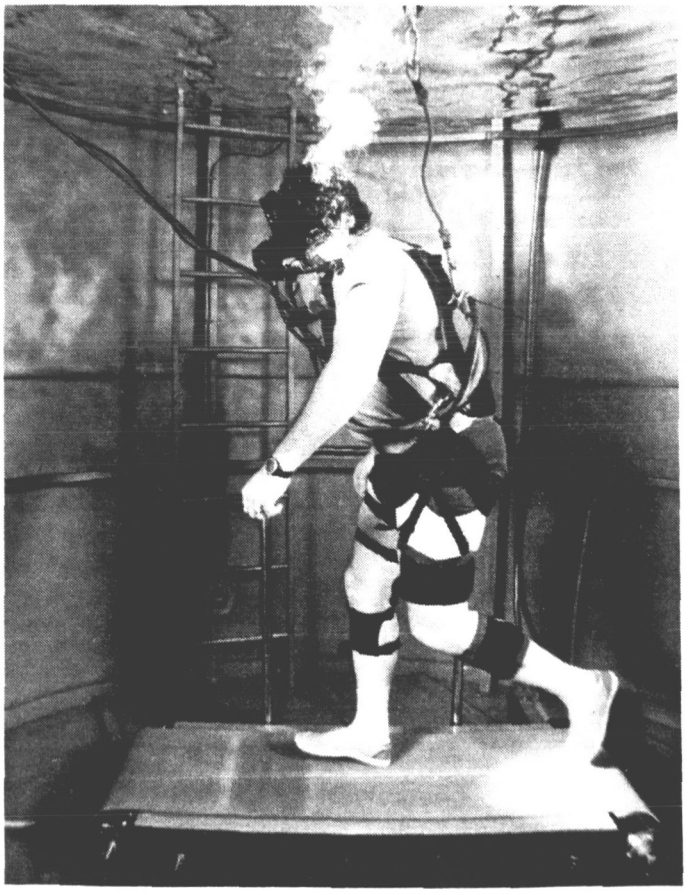

Figure 4. The underwater treadmill at Ames Research Center.

decreases. The extended aerial phase, or reduction in number of strides per minute, is typical of a loping gait in which the subject's ground reaction force is greater than the pull of gravity; the subject essentially propels himself/herself into an aerial trajectory for a few seconds during locomotion.

There was a reduction in oxygen uptake as gravity was decreased from the 1-g level. For locomotion at 1.5 m/s and 2.3 m/s, a continuous decrease in heart rate was seen with decreasing gravity level. However, for locomotion at 0.5 m/s, the results indicated an *increase* in heart rate. This suggests that at low speeds, and low levels of gravity, proportionately more energy is expended in stability and posture control than in locomotion itself. Interestingly, for locomotion at 0.5 m/s during the Martian simulation (3/8-g) subjects commented that this level was the "optimal and most comfortable" of all the partial gravity levels. Newman contends that the g-level threshold for humans being able to locomote in a typical "terrestrial" upright posture using their legs effectively for movement needs to be defined through future experimentation.

These three studies help fill a void in the knowledge on human locomotion and work capability for the entire range of gravity between microgravity (0-g) and 1-g and could, when combined with data from similar future studies, provide substantial information to space suit designers on how the human body moves through space in reduced gravity environments and the energy requirements associated with this movement. By studying how the human body most effectively works in these environments, we will learn not only how to fabricate life support systems that will support such work in space but we will also learn how to keep our astronauts safe. By understanding human physiological limits, we can more adequately plan EVA schedules and planetary activities and extend our exploration capabilities immeasurably.

REFERENCES

1. Allnut, M. F. and Allan, J. R.: The effects of core temperature elevation and thermal sensation of performance. Ergonomics, vol. 16, 1973, pp. 189-197.

2. Bergh, U.; Kanstrup, I. L.; and Ekblom, B.: Maximal oxygen uptake during exercise with various combinations of arm and leg work. J. Appl. Physiol., vol. 41, no.2, 1976, pp. 191-196.

3. Fanger, P. O.: Thermal comfort: analysis and application in environmental engineering. Copenhagen: Danish Technical Press, 1970, as cited in Human Performance Physiology and Environmental Medicine at Terrestrial Extremes, K. Pandolf, M. Sawka, and R. Gonsalez, Eds. Benchmark Press, Inc. 1988.

4. Gagge, A. P. and Hardy, J. D.: Thermal radiation exchange of the human by partitional calorimetry. Am. J. Physiol., vol. 23, 1967, pp. 248-258.

5. Horrigan, D. J. and Waligora, J. M.: Overview of crew member energy expenditure during shuttle flight 61-B EASE/ACCESS task performance. NASA N88-10882, 1986.

6. Newman, D. J.; Alexander, H. L.; and Webbon, B. W.: Energetics and mechanics for partial gravity locomotion. In review, for J. Aviat., Space, and Environ. Med., 1991.

7. Stenberg, J.; Astrand, P. O.; Ekblom, B.; Royce, J.; and Saltin, B.: Hemodynamic response to work with different muscle groups, sitting and supine. J. Appl. Physiol., vol. 22, no. 1, 1967, pp. 61-70.

8. Waligora, J. M. and Horrigan, D. J.: Metabolic cost of extravehicular activities. NASA N77-33818, 1977.

9. Waligora, J. M. and Horrigan, D. J.: Metabolism and heat dissipation during Apollo EVA periods. In Biomedical Results of Apollo (NASA SP-368), 1975.

10. Washburn, R. A. and Seals, D. R.: Peak oxygen uptake during arm cranking for men and women. J. Appl. Physiol., vol. 56, no. 4, 1984, pp. 954-957.

11. Wickman, L.: Personal communication, November 1991.

12. Williamson, R. C.; Sharer, P. J.; and Webbon, B. W.: Metabolic responses to simulated zero-g extravehicular activity. In progress, 1991.

BIOGRAPHY

Rebecca C. Williamson, M.S., works with the Extravehicular Systems Branch of the Advanced Life Support Division under subcontract to Sterling Software, Inc. Having expertise in human responses to exercise and human exercise testing, she was hired as a consultant in 1988 to design and develop a human exercise protocol to simulate orbital extravehicular activity and run experiments to assess the physiological cost of the activity. Future research will include additional in-depth study into the metabolic requirements for advanced life support systems. Orbital EVA research has been the main focus of Ms. Williamson's research efforts at Ames, however, she has also participated in AX-5 testing and range-of-motion studies and consults with Branch engineers on biomechanics and human physiology issues relating to advanced life support system development.

INTERFEROGRAMS, SCHLIEREN, AND SHADOWGRAPHS CONSTRUCTED FROM REAL- AND IDEAL-GAS, TWO- AND THREE-DIMENSIONAL COMPUTED FLOWFIELDS

Leslie A. Yates
Eloret Institute
Palo Alto, California

SUMMARY

The construction of interferograms, schlieren, and shadowgraphs from computed flowfield solutions permits one-to-one comparisons of computed and experimental results. A method for constructing these images from both ideal- and real-gas, two- and three-dimensional computed flowfields is described. The computational grids can be structured or unstructured, and multiple grids are an option. Constructed images are shown for several types of computed flows including nozzle, wake, and reacting flows; comparisons to experimental images are also shown. In addition, the sensitivity of these images to errors in the flowfield solution is demonstrated, and the constructed images can be used to identify problem areas in the computations.

INTRODUCTION

The development of techniques for comparing computed flowfield solutions with experimental interferograms, schlieren, and shadowgraphs is vital for validation of ideal- and real-gas computational fluid dynamics (CFD) codes. Infinite- and finite-fringe interferograms can be transformed into density fields only for two-dimensional (2-D) and axially symmetric non-reacting flows. In experimental schlieren and shadowgraphs, several flow features including shocks, shear layers, and expansion fans are recorded. When flow solutions are compared to these images, contour plots for only one plane of data, usually the symmetry plane, are typically used. If the flow is three dimensional or the model is free to roll, no single computational plane provides all the information necessary for realistic comparisons to experimental images.

The information required for the construction of interferograms, schlieren, and shadowgraphs is contained in the flowfield solutions. By developing routines to evaluate and integrate appropriate functions of the refractive index (n), direct comparisons of computed and experimental results can be made. Constructed interferograms provide the basis for quantitative comparisons of line integrals of n for reacting flows and the integrated density for non-reacting flows. With constructed schlieren and shadowgraphs, the computed and experimental locations of shocks, shear layers, expansion fans, separation, and reattachment can be compared. Constructed schlieren can also be used to compare signs of line integrals of the gradient of n.

In this paper, CISS (Constructed Interferograms, Schlieren, and Shadowgraphs) is described. CISS is software that constructs images from ideal- and real-gas, 2-D, axially symmetric, and 3-D computed flowfield solutions. The computational grids can be structured or unstructured, and

multiple grids are an option. Results are shown for several types of flowfields, and the effects of grid resolution and solution convergence are discussed. Comparisons to experimental images are also included.

CONSTRUCTING NUMERICAL INTERFEROGRAMS, SCHLIEREN, AND SHADOWGRAPHS

Construction of interferograms, schlieren, and shadowgraphs from flowfield solutions requires three steps: (1) identifying and evaluating the appropriate functions of *n*, (2) integrating these functions along lines of sight, and (3) post-processing the integrals to give the desired images. In this section, these three processes will be described.

Functions of the Refractive Index used in Constructing Images

As light passes through the flowfield, the phase shift and angle of deflection are obtained by integrating functions of the refractive index along lines of sight. For ideal and non-reacting gases, the refractive index is simply

$$n = 1 + \kappa\rho$$

where κ is the appropriate Gladstone-Dale constant for the gas and ρ is the density. For both equilibrium and nonequilibrium real-gas computations, the species mass fractions vary throughout the flow, and the refractive index is given by the sum of the contribution from each gas (ref. 1),

$$n = 1 + \sum_i \kappa_i \rho_i$$

Here, κ_i is the Gladstone-Dale constant and ρ_i is the partial density for the ith species.

Interferograms measure the phase shift between reference and object beams caused by variations in the refractive index throughout the flowfield. When calculating interferograms from computational flowfields, the phase shift is obtained by integrating

$$f(n) = \frac{2\pi}{\lambda}(n - n_0)$$

along a line of sight. Here, n_0 is the refractive index of the undisturbed flow and λ is the wavelength of the light.

Schlieren are created in the laboratory by passing collimated light through the flowfield, focusing this light to a finite-sized point, using a knife edge to block out a portion of the light, and then re-focusing the remaining light onto an image plane (fig. 1). The amount of light blocked by the

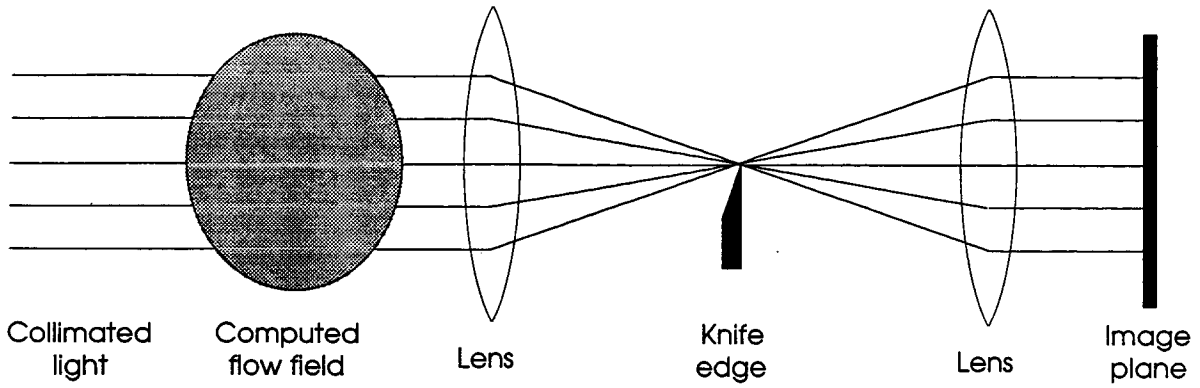

Figure 1. Schematic for constructing schlieren.

knife edge is proportional to the angular deflection of the light; the deflection is caused by gradients in the refractive index. The incremental change in the angular deflection at any point in the flowfield is

$$\delta\varepsilon_x = f(n) = \frac{1}{n}\frac{\partial n}{\partial x} \quad \text{and} \quad \delta\varepsilon_y = f(n) = \frac{1}{n}\frac{\partial n}{\partial y}$$

Integrating these functions through the flowfield solution gives the total angular deflections, ε_x and ε_y.

In shadowgraphs, the image plane is not focused in the flowfield, but at some distance from it, and the dark and light regions are caused by the concentration and divergence of light. In many text books (e.g., refs. 2 and 3), the function used for constructing shadowgraphs is the line integral of the second derivative of the refractive index. In CISS, the function used for constructing shadowgraphs has been chosen to be equal to that used for schlieren. At the exit of the computational flowfield, the angular deflection is known. If the distance to the image plane is also known, then the location on the image plane where the deflected light falls is known. The shadowgraph is constructed by adding the contribution of the deflected light beams at each point on the image plane. Using this method, the thickness of the dark and bright regions is partially controlled by the position of the image plane. This dependency of the dark and bright regions on the image plane's position is observed in experimental shadowgraphs.

Integration Scheme

Tracing the actual light path as it bends through the computational flowfield and integrating the appropriate function of the refractive index along this path is computationally expensive. The resources required for producing constructed images can be reduced by approximating the light's path by a straight line perpendicular to the image plane. For regions of the flow without shocks, this approximation should have a minimal effect on the constructed images. In shock regions, the index

of refraction changes rapidly, and the approximation may introduce errors; however, these errors are in many cases on the order of or smaller than the solution and experimental errors.

This approximation minimizes the need for search routines, and interferograms, schlieren, and shadowgraphs can be constructed without any ray tracing. For instance, consider an image defined by an M × N array of light 'cells.' The value of the integral for the m,n element of the array is given by

$$A_{m,n} = \int_0^z f\left[n(x_m, y_n, \zeta)\right] d\zeta$$

where the image plane is located at z and (x_m, y_n) are the x,y-coordinates of the light cell at the m,n location in the array. The integration path can be broken into several segments

$$A_{m,n} = \sum_{i=1}^{N} \int_{z_i}^{z_{i+1}} f\left[n(x_m, y_n, \zeta)\right] d\zeta$$

In this expression, the line of integration enters the ith computational cell at z_i and exits it at z_{i+1} (fig. 2). In the actual solution procedure, no ray tracing of the line of integration through the flowfield is necessary. By assuming minimal deflection of the light through the flowfield and approximating the light's path by a straight line, the contribution of each computational cell to the line integral can be found independently, and the order of evaluation and summation has no effect on the final result. Therefore, for each computational cell, the integrals

$$\int_{z_i}^{z_{i+1}} f\left[n(x_m, y_n, \zeta)\right] d\zeta$$

are evaluated for every x_m, y_n that fall within the cell, and the value of the integral is added to the appropriate location on the image plane.

The test for determining if the point x_m, y_n falls within the computational cell is as follows. First, to minimize the number of tests required, the maximum and minimum x and y values for the computational cell are found. Then the surfaces of the computational cell are described by triangles, and for each triangle, three cross products are formed:

$$\left(\vec{x}_1 - \vec{x}_{mn}\right) \times \left(\vec{x}_1 - \vec{x}_2\right)$$

$$\left(\vec{x}_2 - \vec{x}_{mn}\right) \times \left(\vec{x}_2 - \vec{x}_3\right)$$

$$\left(\vec{x}_3 - \vec{x}_{mn}\right) \times \left(\vec{x}_3 - \vec{x}_1\right)$$

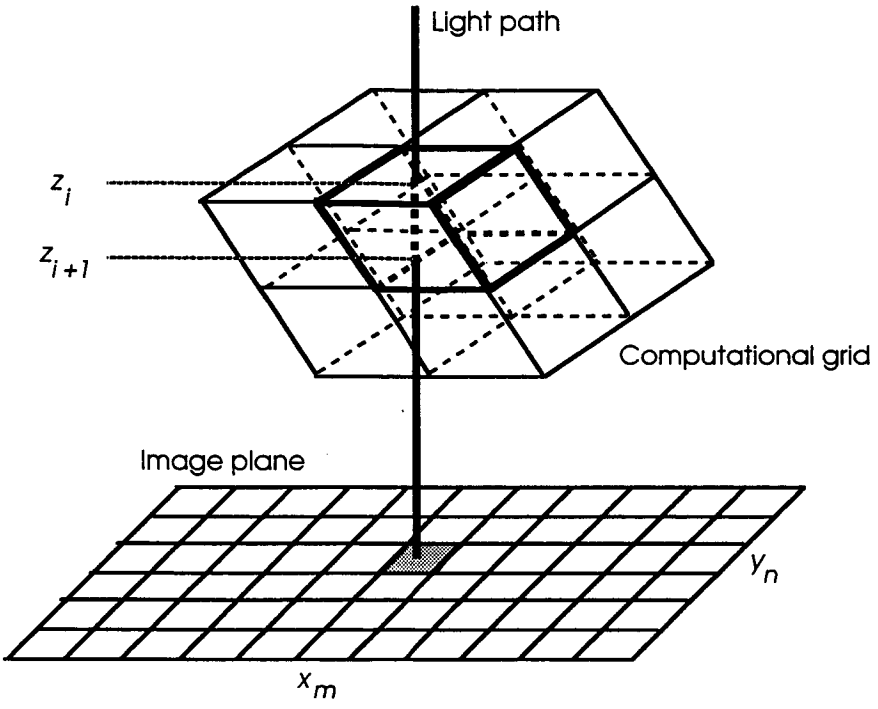

Figure 2. Schematic for integration process.

In these equations, $\vec{x}_{mn}$ gives the position of the light cell, and $\vec{x}_1$, $\vec{x}_2$, and $\vec{x}_3$ are the projections onto the image plane of the vertices of the triangle. Testing is performed only for the x_m and y_n that lie within the minimum and maximum x and y values for the computational cell. The sign for all three cross products is the same if and only if the point lies within the triangle, and the triangular surfaces through which the line of integration enters and exits the computational cell can be determined. Once these surfaces are determined, interpolated values for z_i, z_{i+1}, $f(x_m, y_n, z_i)$, and $f(x_m, y_n, z_{i+1})$ at the entrance and exit are obtained, and the line integral is evaluated. In CISS, three functions of the refractive index are integrated simultaneously: $n - 1$, $(1/n)\partial n/\partial x$, and $(1/n)\partial n/\partial y$.

Construction of the Images

For infinite-fringe interferograms, the image intensity is simply proportional to the sine of the phase shift ϕ:

$$\phi = \frac{2\pi}{\lambda} \int_0^z (n - n_0)\, d\zeta$$

For finite-fringe interferograms, an additional phase is added:

$$\delta\phi = k_x x + k_y y$$

and the spacing and orientation of the freestream fringes are determined by k_x and k_y.

For schlieren, the intensity is a function of the angular deflection. As an example, consider a horizontal knife edge (fig. 1) and a rectangular section of the initial light source with height h. As the rectangular section of the light source passes through the flowfield, it is deflected and exits the flow at an angle. When the light exiting from the flowfield is then focussed to a finite-sized dot at the plane of the knife edge, the rectangular element has a height of h', and it has been deflected vertically by $\kappa\varepsilon_y$; κ is a function of the distance between the flowfield and the knife edge. There is also a horizontal deflection; however, it is unimportant in this case. If the horizontal knife edge is placed at the center of the plane, the ratio of light not blocked by the knife edge to the amount of the original light is

$$0 \qquad \text{for} \qquad \frac{\kappa\varepsilon_y}{h'} \le -\frac{1}{2}$$

$$1 \qquad \text{for} \qquad \frac{\kappa\varepsilon_y}{h'} \ge \frac{1}{2}$$

$$\frac{1}{2} + \frac{\kappa\varepsilon_x}{h'} \qquad \text{for} \qquad -\frac{1}{2} < \frac{\kappa\varepsilon_y}{h'} < \frac{1}{2}$$

The intensity patterns in the schlieren are proportional to the square of this ratio.

As mentioned previously, shadowgraphs are not constructed in CISS from line integrals of second derivatives of the refractive index. Instead they are given by variations in the intensity caused by the deflection of the light. The location and size of a square element of light after it passes through the flowfield is determined by the deflection of light sources that define the corners of the element. The total angular deflection for these light sources is a function of the angle at which the light exits the flowfield; that is, shadowgraphs are also governed by ε_x and ε_y. The deflected square element is then projected onto the image plane, and the amplitude of the electric field at each i,j-element in the image plane is increased by

$$\Delta E_{ij} = E_o \frac{B_f \cap A_{ij}}{B_i}$$

Here, E_o is the amplitude of the initial field, $B_f \cap A_{ij}$ is the area of the intersection of the deflected element with the i,j-element of the image plane, and B_i is the initial area of the deflected element. The intensity pattern observed in the shadowgraph is proportional to the square of the E_{ij}'s.

The time requirements for constructing these images from simulated flowfields are linearly proportional to the grid size and the number of pixels defining the image. For 2-D flowfields, the image construction takes only a few seconds on a CRAY-YMP. For 3-D images defined by 400,000 pixels, construction using flowfield solutions with 250,000 grid points takes a few minutes.

CONSTRUCTED IMAGES

Representative images are shown in this section for several types of hypersonic flows including ramp, nozzle, reacting, and blunt-body flows. In figure 3, constructed and experimental schlieren are shown for a 2-D, 15° compression corner; a horizontal knife edge was used for both the schlieren. The shocks, shear layers, and separation region observed in the experimental schlieren are simulated by the constructed schlieren. The dark regions in the constructed schlieren are caused by rapid increases in density across the computed shocks, and they correspond to dark regions in the experimental schlieren. The light regions in both the constructed and experimental schlieren are identified with shear layers, and they are caused by density gradients near the surface. These shear layers lift off the surface when separation occurs, and the extent of the computed and experimental separation regions can be compared. The sharpness of the features in the constructed schlieren can be further improved by using grid adaptation to reduce solution errors.

In figure 4, constructed and experimental shadowgraphs for a generic, National Aerospace Space Plane (NASP) nozzle configuration, the Single Expansion Ramp Nozzle (SERN), are shown. Both the freestream and nozzle flows are supersonic. The flowfield solution in figure 4(a) is a 2-D, ideal-gas simulation at the symmetry plane; the solution in figure 4(b) is 3-D (ref. 6). The interaction of the external flow with the nozzle plume is complicated, and all the main features observed in the experimental shadowgraph are captured in the constructed shadowgraphs. These features include the leading edge shock, separation from the nozzle, and the shocks, shear layers, and expansion fans caused by the interaction of the nozzle plume with the freestream. As with the schlieren, dark and light regions in the constructed shadowgraph correspond to dark and light regions in the experimental shadowgraph; however, in the shadowgraphs, each shock is described by the combination of a dark and light line. In the two constructed shadowgraphs, the effects of grid resolution and solution errors can be seen. The grids in the two 2-D solutions are very fine, and the constructed shadowgraph closely resembles the experimental shadowgraph. For the 3-D solution, although multiple grids were used, the gridding was much coarser than that used for the 2-D solutions. The shocks, shear layers, and expansion fans were not as well resolved in the 3-D flowfield solution and, hence, are much more diffuse in the shadowgraph.

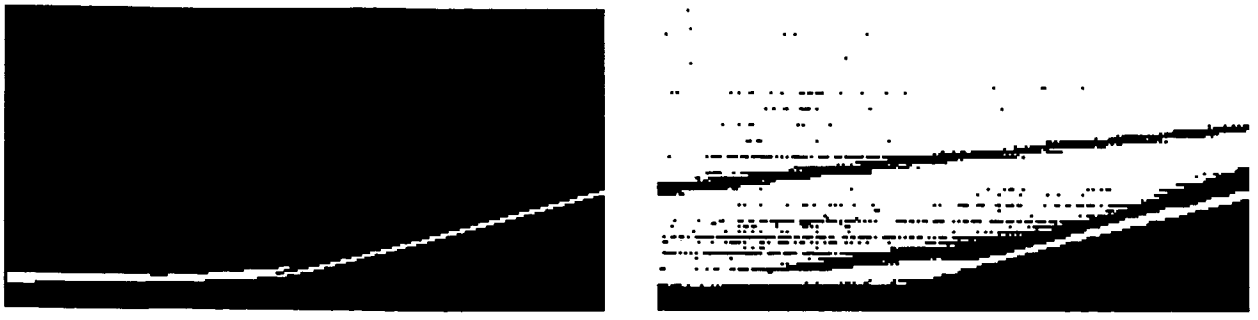

Constructed schlieren Experimental schlieren

Figure 3. Constructed and experimental schlieren for a two-dimensional compression corner. Flow solution: Tokarcik et al. (ref. 4); experiment: Delery and Coet (ref. 5).

a) 2-D solution b) 3-D solution c) Experiment

Figure 4. Constructed and experimental shadowgraphs for SERN. Two-dimensional flow solution and experiment: Ruffin et al. (ref. 6).

The solutions in figures 3 and 4 are ideal-gas computations, and the refractive index is simply given by a constant times the density. For reacting flows, the refractive index is a function of the gas species. In figure 5, a constructed shadowgraph is shown for an axially-symmetric, real-gas, flowfield solution for a ballistic range shot of a hemisphere cylinder in a combustible mixture (refs. 7 and 8). Also shown is an experimental shadowgraph (ref. 9). This flow is very complex, and many of the features observed in the shadowgraph are three dimensional and difficult to identify in contour plots. In the constructed shadowgraph most if not all of the features in the experimental shadowgraph are captured, and the computations and experiment can be compared on a one-to-one basis. The ability to construct shadowgraphs facilitates the comparison of computed and experimental results, especially for very complicated flows.

In figure 6, a constructed and experimental infinite-fringe interferogram is shown for a ballistic range test of the Aeroassist Flight Experiment (AFE). The flowfield simulations were performed using an ideal-gas CFD solver (ref. 10); the grid was adapted to the flowfield solution using SAGE (ref. 11). A one-to-one comparison of the two interferograms is not possible; the flowfield solution is for a model with no yaw, the experimental model did yaw. However, there are similarities. The constructed and experimental interferograms both show similar light and dark patterns, and the number of fringe shifts are comparable. The location of the fringes provides information concerning the computed and experimental integrated index of refraction.

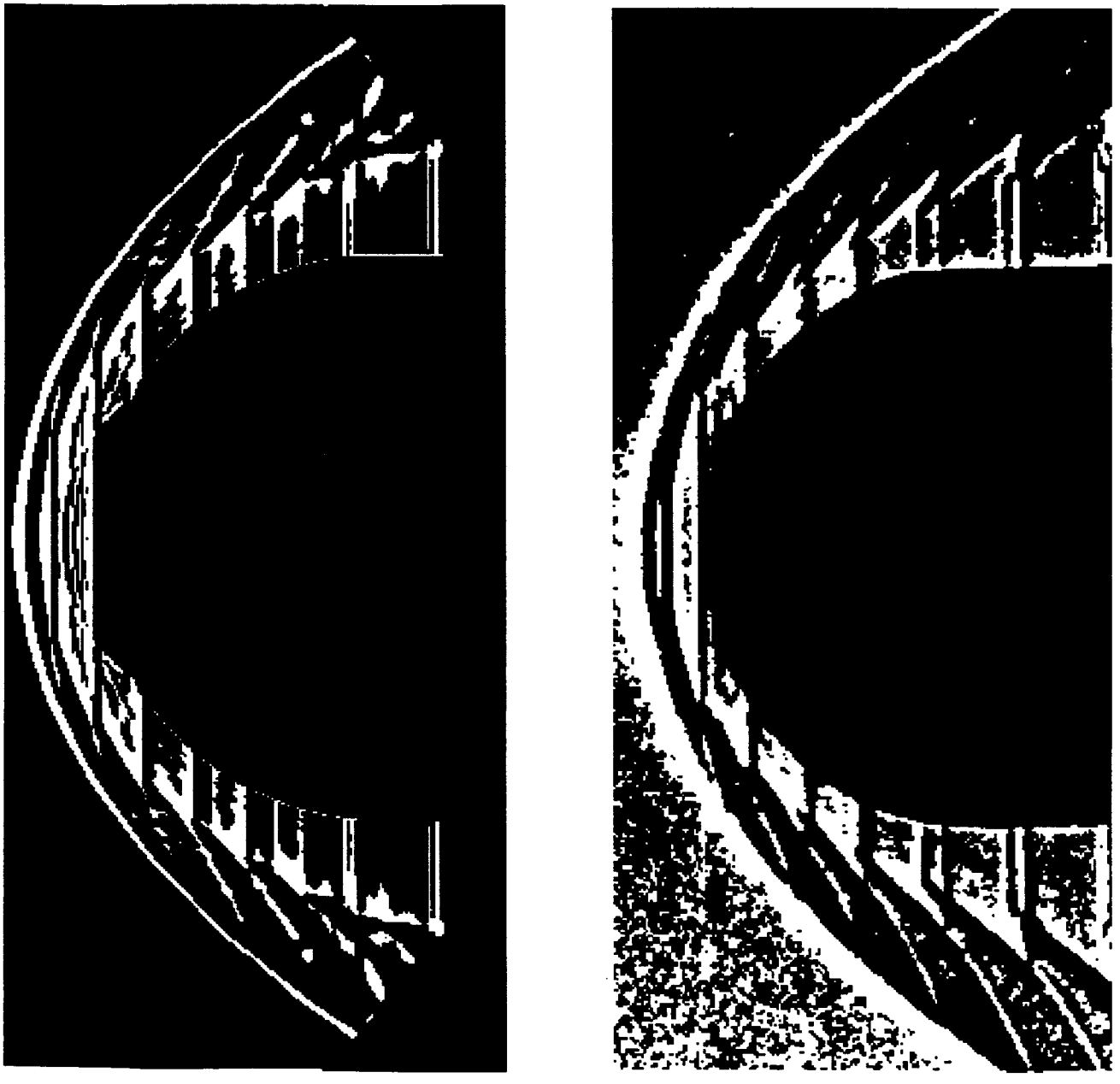

Constructed shadowgraph

Experimental shadowgraph

Figure 5. Constructed and experimental shadowgraphs for a hemisphere-cylinder in a combustible mixture. Flowfield solution: G. Wilson (refs. 7 and 8); experiment: Lehr (ref. 9).

Constructed interferogram Experimental interferogram

Figure 6. Constructed and experimental infinite-fringe interferograms for an AFE model. Three-dimensional flowfield solution: E. Venkatapathy et al. (ref. 10); experiment performed at NASA Ames Research Center's ballistic range.

CONCLUDING REMARKS

The construction of interferograms, schlieren, and shadowgraphs from 2-D and 3-D flowfield solutions permits one-to-one comparisons of CFD and experimental results. Experimental interferograms provide quantitative information for integrals of the refractive index and density. This information can be used to verify 3-D flowfield solutions only when line of sight integrals are computed and interferograms are constructed from the flowfield solutions. The positions of shocks and shear layers are easily obtained from experimental schlieren and shadowgraphs. When contour plots are used to locate shocks and shear layers, interpretation of the contour lines is required. Furthermore, the 3-D nature of the flow is not shown. In constructed schlieren and shadowgraphs, the shocks and shear layers are defined by the same intensity variations as in the experimental images. Hence, comparison of the positions of these flow features can easily be made. In addition, 3-D effects are included in the construction.

CISS has proven its capability in constructing interferograms, schlieren, and shadowgraphs from a variety of ideal- and real-gas, 2-D, axially symmetric, and 3-D flowfield solutions. For the examples shown here, the constructed and experimental images are very similar. However, the quality of the flowfield solution does affect the quality of the constructed images. Insufficient or improperly placed grid points can cause spreading of shocks and shear layers in the constructed images. CISS not only provides an excellent tool for comparing flowfield solutions with experiment, it can be used to identify problem areas in the flowfield solutions.

ACKNOWLEDGMENTS

Support for L. A. Yates was provided by NASA Grant NCC2-583.

REFERENCES

1. Ben-Dor, G.; Whitten, B. T.; and Glass, I. I.: Evaluation of Perfect and Imperfect-Gas Interferograms by Computer. Int. J. Heat and Fluid Flow, vol. 1, no. 2, 1979, pp. 77-91.

2. Shapiro, A. H.: The Dynamics and Thermodynamics of Compressible Flow, vol. 1, The Ronald Press Company, New York, 1953.

3. Liepmann, H. W. and Roshko, A.: Elements of Gasdynamics, John Wiley and Sons, New York, 1957.

4. Tokarcik, S.; Venkatapathy, E.; Candler, G.; and Palmer, G.: Computational Flow Predictions for Hypersonic Drag Devices. AIAA Paper 91-3303, Sept. 1991.

5. Delery, J. and Coet, M. C.: Experiments on Shock-Wave/Boundary-Layer Interactions Produced by Two-Dimensional Ramps and Three-Dimensional Obstacles. Workshop on Hypersonic Flows for Reentry Problems, Antibes, France, Jan. 1990.

6. Ruffin, S. M.; Venkatapathy, E.; Lee, S. H.; Keener, E. R.; and Spaid, F.: Single Expansion Ramp Nozzle Simulations. AIAA Paper 92-0387, Jan. 1992.

7. Wilson, G. J.: Computation of Steady and Unsteady Hydrogen-Air Combustion over Hypervelocity Blunt Bodies. Ph.D. dissertation, Stanford University, Dec. 1991.

8. Wilson, G. J. and Sussman, M. A.: Computation of Oscillating Shock-Induced Combustion Observed in Ballistic-Range Experiments," Presented at the Fourth International Conference on Numerical Combustion, St. Petersburg, Florida, Dec. 1991.

9. Lehr, H. F.: Experiments on Shock-Induced Combustion. Astronautica Acta, vol. 17, 1972, pp. 589-597.

10. Venkatapathy, E.; Palmer, G.; and Prabhu, D.: AFE Base Flow Computations. AIAA Paper 91-1372, June 1991.

11. Davies, C. B. and Venkatapathy, E.: The Multi-Dimensional Self-Adaptive Grid Code, SAGE. NASA TM-103905, 1992.

BIOGRAPHY

Leslie A. Yates, Ph.D., received her B.A. (1976) in Physics from New College in Sarasota, Florida. After graduate studies in Physics and Mathematics at the State University of New York at Stony Brook, she returned to Florida and obtained her M.S. and Ph.D. in Aeronautical Engineering from the University of Florida. She spent two years as a Research Associate with the National Research Council and is presently a research engineer at the Eloret Institute. Her research activities have included aerodynamics, vortical flows, and image processing.